TITLE OF THE PROJECT: OPTIMAGRID SOE2/P2/E322

GT < 3 >: Implementation of micro-grids with high penetration of renewable energies

DELIVERABLE < 9 >: Simulation of mini-grids with high penetration of renewable energies

DELIVERABLE < 10 >: Simulation of mini-grids with energy storage systems to manage energy

ABSTRACT

Once several case studies were defined in GT2, an analysis of different scenarios has been developed in GT3. Within this deliverable, the focus is on the maximum renewable energy acceptable in an industrial area with and without energy storage systems. For that, different simulations are carried out with the background of the case studies defined in GT2. Using renewable resources availability data and load profiles from the different industrial estates selected in GT2, several configurations of micro-grids have been simulated with specific software such as HOMER or others.

In a first step, micro-grids are based only on renewables and the grid, without energy storage systems, and the aim is to determine the maximum percentage of load satisfied by renewables. In a second step, energy storage systems are added to the micro-grids (architecture) to increase the manageability of the whole system and therefore, to increase the share of renewable energies integrated in the mini-grids.

Some sensitivity analyses have been carried out as well in order to determine the impact of some parameters in the performance of the micro-grids. The main results are collected in this report as well as the conclusions of the study.

CONTENTS

1 Port of Bayonne....12

1.1 Analysis of the renewable resources in the harbour of Bayonne....12
  1.1.1 Wind resources....12
  1.1.2 Solar resources....17
  1.1.3 Conclusions....19
1.2 Design of system with Homer....20
  1.2.1 Design with renewable technologies....20
  1.2.2 Design with renewable technology and the storage systems....31
  1.2.3 Conclusions....33
1.3 Modelling....33
  1.3.1 Eurostag modelling....33
1.4 Emulation of a wind turbine for the ENERGEA microgrid....37
1.5 Simulations....38
  1.5.1 Electrical infrastructure description....38
  1.5.2 Simulation with renewable resources....39
  1.5.3 Conclusion....42
1.6 Results of the study....43

2 Walqa Technology Park....44

2.1 Installation description....44
  2.1.1 Wind generation installation....44
  2.1.2 Photovoltaic installation....45
  2.1.3 Interconnection center....47
2.2 Introduction of the system in HOMER program....49
  2.2.1 Introduction to HOMER....49
  2.2.2 Mode of use of HOMER....49
  2.2.3 Case study introduction with energy storage....49
  2.2.4 Case study introduction without energy storage....55
2.3 Results and analysis with energy storage....55
2.4 Results and analysis without energy storage....57
2.5 Sensitivity analysis....58
  2.5.1 Data introduction....58
  2.5.2 Results....61
2.6 Sensitivity analysis without energy storage system....62
  2.6.1 Data introduction....62

2.6.2 Results ... 62

3 Landaben industrial area ... 63

3.1 Introduction ... 63
3.2 Power demand profile ... 63
3.3 Simulations without energy storage ... 65
3.3.1 Model construction ... 65
3.3.2 Results of the simulations ... 65
3.3.3 Wind + Biomass combined system ... 68
3.3.4 Photovoltaic + Hydro combined system ... 69
3.3.5 PV + Wind + Hydro + Biomass combined system ... 70
3.4 Simulations with energy storage ... 72
3.4.1 Model construction ... 72
3.4.2 Results of the simulations ... 73
3.5 Conclusion ... 76

4 Valdabra pumping station ... 77

4.1 Description of the modelled areas ... 77
4.1.1 Real Case: Rural microgrid for irrigation pumping ... 77
4.1.2 Generic case: Industrial area with small workshops and industrial stores 77
4.1.3 Consumption profiles ... 77
4.2 Simulation models ... 79
4.2.1 Comparison of HOGA and HOMER ... 79
4.2.2 Operational simulation with Matlab/Simulink® ... 80
4.2.3 Planning simulation with GAMS ... 86
4.3 Simulation results with HOMER and HOGA ... 90
4.3.1 Model Configuration ... 90
4.3.2 Simulation Scenarios ... 91
4.3.3 Results of 4 scenarios ... 91
4.3.4 Results sensitivity analysis ... 93
4.3.5 Conclusions from HOMER and HOGA ... 94
4.4 Simulation results with Matlab/Simulink® ... 95
4.4.1 Simulation Parameters ... 96
4.4.2 Statistical results: P Control ... 98
4.4.3 Statistical results: Q Control ... 105
4.4.4 Statistical results of SOC ... 107
4.4.5 Conclusions from Simulink simulation ... 109
4.5 Simulation results with GAMS ... 110

4.5.1 Cost of energy (COE) and system cost 110
4.5.2 Line losses 111
4.5.3 Installed power and generated energy 112
4.5.4 Conclusions 113

5 Huelva chemical park 115

5.1 Case without energy storage 115
5.1.1 Introduction 115
5.1.2 Electric demand description 115
5.1.3 Renewable energy sources 116
5.1.4 Simulations 117
5.2 Case with energy storage 122
5.2.1 Introduction 122
5.2.2 Simulations 122

6 Conclusions 125

LIST OF FIGURES

Fig. 1.1. Temporal series of the wind speed for the 2012 January 7 2012 12
Fig. 1.2. Temporal series of the wind speed on several days of January 2012 13
Fig. 1.3. Monthly data of the wind speed (*max* : maximum of month ; *daily high* : maximal daily average of month ; *mean* : average of monthly, *daily low* :minimale daily average of month ; *min* : minimum of mois) 13
Fig. 1.4. Temporal daily series of the wind speed by month 14
Fig. 1.5. PDF (Probability Density Function) of data of wind speed 14
Fig. 1.6. Location of the anemometer THIES on the crane 14 15
Fig. 1.7. Location of anemometre JRI on the crane 12 15
Fig. 1.8: Frequency comparison between CENER data (Vent_2011) and Crane14 data (VitesseVentGR14) 16
Fig. 1.9: Box plot comparison between CENER data (Vent_2011…) and Crane14 data (VitesseVentGR14..) 16
Fig. 1.10: Numerical comparisons comparison between CENER data (Vent_2011…) and Crane14 data (VitesseVentGR14..) 16
Fig. 1.11. Temporal series of the sun for May 30th 17
Fig. 1.12. Temporal series of the sun on several days for May 17
Fig. 1.13. Monthly data of solar illumination (*max* : maximum of month ; *daily high* : maximal daily average of month ; *mean* : average of monthly, *daily low* :minimale daily average of month ; *min* : minimum of mois) 18
Fig. 1.14. Temporal series of daily illumination per month 18
Fig. 1.15. PDF (*Probability Density Function*) of data of solar illumination 19
Fig. 1.16: PDF (*Probability Density Function*) of solar irradiation in 2011 19
Fig. 1.17. Configuration of electricity consumption in the port of Tarnos with HOMER 20
Fig. 1.18. Configuration of representation of the first wind turbine in the harbour zone of Tarnos with HOMER 21
Fig. 1.19. Configuration of representation of the second wind turbine in the harbour zone of Tarnos with HOMER .. 22
Fig. 1.20. Configuration of representation of solar panel in the harbour zone of Tarnos with HOMER 22
Fig. 1.21. Configuration of the electricity grid EDF and exchanges of energy of the harbour zone of Tarnos with HOMER 23
Fig. 1.22. Price of purchases of electricity of origin PV in France 24
Fig. 1.23. Configuration of converters associated to panels PV 25
Fig. 1.24. Configuration of economy part of report 25
Fig. 1.25. Configuration of electric system management in general 26
Fig. 1.26. Result of calculation with the electrical grid for the port containing only panels PV 27
Fig. 1.27. Résultats *électriques* de la simulation avec le réseau contenant des panneaux PV de 2.000 kW 28
Fig. 1.28. Electric results of simulation with the electrical grid containing panels PV of 400 kW 28
Fig. 1.29. Results of calculation with the electrical grid of the port containing only wind turbines 29
Fig. 1.30. Electric Result for a configuration with 10 wind turbines PGE 25 29
Fig. 1.31. Electric result for configuration with 5 wind turbines PGE 25 30
Fig. 1.32. Results of calculation with the electrical grid in the port containing wind turbines and panels PV 30
Fig. 1.33. Electric result of configuration with 3 wind turbine PGE 25 and 200 kW of panel PV 31
Fig. 1.34. Summary of the costs associated with the configuration with 3 wind turbines PGE 25 and 200 kW of panels PV 31
Fig. 1.35. Costs of system of type Redox's storage 33
Fig. 1.36. Mechanical torque vs wind speed. 34
Fig. 1.37. General description of the photovoltaic model. 35
Fig. 1.38. EneR-GEA microgrid illustration 37
Fig. 1.39: Harbor grid model in EUROSTAG 39

Fig. 1.40: HOMER micro-grid configuration 39
Fig. 1.41: Harbour micro-grid with wind turbine and PV panels 40
Fig. 1.42: Active, reactive and apparent power of crane 12 40
Fig. 1.43: EUROSTAG® simulation load profile of the crane 12 41
Fig. 1.44: Solar Irradiation, PV active power and total active power 41
Fig. 1.45: Wind speed, Wind Turbine active power and total active 42
Fig. 2.1. Wind turbines. 44
Fig. 2.2. Wind turbine locations in Walqa Technological Park. 45
Fig. 2.3. Fixed installation in parking canopies of Walqa Technological Park. 46
Fig. 2.4. DEGUER solar trackers and behind MECASOLAR solar tracker. 46
Fig. 2.5. ADES solar tracker. 47
Fig. 2.6. Diagram of the Project ITHER. 47
Fig. 2.7. Locations of distribution centers and evacuation. 48
Fig. 2.8. Line diagram of the installation. 48
Fig. 2.9. Introduction of solar radiation data. 49
Fig. 2.10. PV system data. 50
Fig. 2.11. Wind data in Walqa Technological Park. 50
Fig. 2.12. Wind installation in Walqa Technological Park. 51
Fig. 2.13. Wind farm data. 51
Fig. 2.14. Photovoltaic converters data. 52
Fig. 2.15. Defining the electrolizer. 52
Fig. 2.16. Hydrogen storage system. 53
Fig. 2.17. Electric consumption in Walqa Technological Park. 54
Fig. 2.18. Defining power capacity Exchange with the grid. 54
Fig. 2.19. Cost of purchase and sale of electric energy. 55
Fig. 2.20. Walqa Technological Park microgrid. 55
Fig. 2.21. Electric simulation results. 56
Fig. 2.22. Walqa Technological Park microgrid without energy storage. 57
Fig. 2.23. Electric simulation results. 57
Fig. 2.24. Different powers of PV for the optimization exercise. 58
Fig. 2.25. Wind farm sizes to be considered in the optimization. 58
Fig. 2.26. Fuel cell powers to evaluate. 59
Fig. 2.27. Electrolizers power for the optimization study. 59
Fig. 2.28. Hydrogen storage system sizes for the optimization study. 60
Fig. 2.29. Converters for the optimization study. 60
Fig. 2.30. Electric simulation results of optimization system 61
Fig. 2.31. Electric simulation results of optimization system 62
Fig. 3.1. View of Landaben industrial area 63
Fig. 3.2. Result of the synthetically generated annual electrical demand profile 63
Fig. 3.3. Share of hours corresponding to the different tariffs 64
Fig. 3.4. General diagram of the model 65
Fig. 3.5. Graphic of the annual generation of the renewable technologies 67
Fig. 3.6. Electricity production in the Wind+Biomass case 68
Fig. 3.7. Detail of a week in the Wind+Biomass case 68
Fig. 3.8. Electricity production in the PV+Hydro case 69
Fig. 3.9. Detail of a week in the PV+Hydro case 69

Fig. 3.10. Net Present Cost of each part of the system in the 4-renewables case 70
Fig. 3.11. Electricity production in the 4-renewables case 70
Fig. 3.12. Duration curve of electricity purchased from the grid in the 4-renewables case 71
Fig. 3.13. Excess electricity generated in the 4-renewables case 71
Fig. 3.14. General diagram of the model 72
Fig. 3.15. Operation of the biomass power plant in isolated mode 73
Fig. 3.16. State of charge of VRB in isolated mode 74
Fig. 3.17. Diagram of the excess electricity generated 74
Fig. 3.18. Detail of energy management through storage 75
Fig. 3.19. Electricity purchased from the grid in each month 75
Fig. 4.1. Microgrid structure of assumed industrial area of 100 kW total mean power. 77
Fig. 4.2. Demand profile of AC and DC pumps of case 1 (up) and AC load of industrial area of case 2 (below). 78
Fig. 4.3. Box plot of Seasonal load profile of the pumping station, given per unit. 78
Fig. 4.4. DMap of hourly load given per unit of the pumping station (up) and industrial area (below), ... 79
Fig. 4.5. Schema of the simulation model with active (P) and reactive (Q) power control of a grid-connected System with battery energy storage.. 80
Fig. 4.6. Example of a daily program of charge and discharge of the battery storage system. 82
Fig. 4.7. Example of reduced charge/discharge applying the limits of the present case. 86
Fig. 4.8. DMap of demand (left) and mean profiles of 2 clusters (right). 87
Fig. 4.9. Demand cluster 1 with low demand (left) and cluster 2 with high demand (right). 88
Fig. 4.10. DMap of wind generation (left) and mean profiles of 6 clusters (right). 88
Fig. 4.11. DMap of solar generation (left) and mean profiles of 5 clusters (right). 89
Fig. 4.12. DMap of electricity Prices (left) and 3 different daily profiles (right). 89
Fig. 4.13. Time series created from 70 cluster combinations for demand (above), renewable generation (middle) and electricity price (below). 90
Fig. 4.14. System configuration in HOMER; Case 1: Valdabra irrigation pumping station (left) and Case 2: Industrial area (right). 90
Fig. 4.15. System configuration of Valdabra irrigation pumping station in HOGA. 91
Fig. 4.16. Result of sensitivity analysis upon PV cost and electricity price from the grid, with reduction of battery capital cost of 75%; Installed PV power in kWp is superimposed. 93
Fig. 4.17. COE in €/kWh as a result of sensitivity analysis upon PV cost and electricity price from the grid, assuming a reduction of battery capital cost of 75%. 94
Fig. 4.18. Power distribution density (left) and cumulative (right) at PCC compared to original demand Pload, above case A (100 kW battery) and below case B (200 kW battery), without DG. 99
Fig. 4.19. Power distribution density (above) and cumulative (below) at PCC compared to original demand Pload minus DG, for only PV (left), only wind (center) and wind and solar PV (right). 99
Fig. 4.20. Power distribution density (left) and cumulative (right) of Pload at PCC for no DG (black), 250 kW wind (blue), 250 kW PV (yellow) and 250 kW wind + 250 kW PV (red). 100
Fig. 4.21. Power distribution density (above) and cumulative (below) at PCC for the three control strategies, for no DG (black), only wind (blue), only PV (yellow) and wind and solar PV (red). 101
Fig. 4.22. Two typical sequences (48h each) of active power demand under different control scenarios compared to Pload, left: typical activity, right: high activity. 103
Fig. 4.23. Two typical sequences (48h each) of active power demand under different control scenarios comparing four levels of DG penetration, left: typical activity, right: high activity. 104
Fig. 4.24. Cumulative distribution of power factors of original demand FPload. 107

Fig. 4.25. Cumulative distribution of power factors for the three control strategies and battery sizes A: 100 kW and B: 200 kW. 107
Fig. 4.26. Cumulative distribution of the state of charge (SOC) of the battery storage system for all simulation scenarios. 108
Fig. 4.27. Changes in the cost of energy during the planning period. 111
Fig. 4.28. Evolution of annual grid installation and operation cost by elements for case A with energy export (left) and case B without energy export (right). 111
Fig. 4.29. Line losses as a percentage of total demand plus exported energy. 112
Fig. 4.30. Installed power by technology for case A with energy export (left) and case B without energy export (right). 112
Fig. 4.31. Annual energy generates by each technology for case A with energy export (left) and case B without energy export (right). 113
Fig. 4.32. Renewable excess energy generation and storage losses as a percentage of total demand plus exported energy. 113
Fig. 5.1. Wind speed distribution. 116
Fig. 5.2. Gamesa G80 power curve. 117
Fig. 5.3. Isofoton I-106 Photovoltaic panel intensity-voltage curve 117
Fig. 5.4. Percentage of hours when demand is covered versus level of demand. Case 1. 120
Fig. 5.5. Excess and defect of electric energy during a year. Case 1. 100 % storage system. 123
Fig. 5.6. Excess and defect of electric energy during a year. Case 2. 100 % storage system. 124

LIST OF TABLES

Table 1.1. Wind Turbine model parameters 34
Table 1.2. Photovoltaic model parameters 36
Table 1.3. Other photovoltaic model parameters. 37
Table 2.1. Wind turbine characteristics in Walqa Technological Park. 44
Table 2.2. Wind turbines characteristics. 45
Table 2.3. Characteristics of Photovoltaic installation. 45
Table 2.4. Technologies of photovoltaic electric power generation. 46
Table 2.5. Solar tracking technologies. 47
Table 3.1. Electricity price for the simulations 64
Table 3.2. Equivalent emissions for the Spanish electricity grid 64
Table 3.3. Results of the simulations for the different options presented 66
Table 3.4. Electricity production in the Wind+Biomass case 68
Table 3.5. Electricity production in the PV+Hydro case 69
Table 3.6. Electricity production in the 4-renewables case 71
Table 3.7. Balance of electricity with and without energy storage 73
Table 4.1. Structure of output file of the Simulink model. 81
Table 4.2. Parameters of control strategy 1 (peak shaving), accessible through a dedicated Simulink mask. 82
Table 4.3. Parameters of control scenario 2 (daily program), accessible through a dedicated Simulink mask. 83
Table 4.4. Model parameters of the converter (accessible through a dedicated Simulink mask). 84
Table 4.5. Parameters of the battery model (accessible through a dedicated Simulink mask). 86
Table 4.6. Overview of the effect of limiting the number of days per combinations. 87
Table 4.7. Scenarios for different PV and Battery costs. 91
Table 4.8. System configurations proposed by HOMER and HOGA for case 1 (Pumping Station). 92
Table 4.9. System configurations proposed by HOMER and HOGA for case 2 (Industrial area). 92
Table 4.10. Control parameters for strategy 1 (peak shaving). 96
Table 4.11. Control parameters for strategy 2 (hourly program). 96
Table 4.12. Calculation of active power limits at PCC are from limits from strategy 1. 96
Table 4.13. Control parameters for strategy 3 (smoothing). 96
Table 4.14. Converter Model parameters. 97
Table 4.15. Battery model parameters. 97
Table 4.16. Summary and codification of the different simulation options. 97
Table 4.17. Statistical indicators of the impact of active power control. 98
Table 4.18. Statistical indicators of the impact of active power control. 100
Table 4.19. Peak demand relative to the original value (without battery and P control). 101
Table 4.20. Peak generation relative to the original value (without battery and P control). 102
Table 4.21. Statistical indicators of the impact of reactive power control, without DG. 105
Table 4.22. Statistical indicators of the impact of reactive power control. 106
Table 4.23. Statistical indicators of the state of charge (SOC) of the battery system under different scenarios of distributed generation (DG) and control strategies. 109
Table 5.1. Monthly electric demand. 115
Table 5.2. Monthly solar insolation. 116
Table 5.3. Percentage of electric demand covered by renewable sources. Case 1. 100% demand. 118
Table 5.4. Percentage of electric demand covered by renewable sources. Case 1. 50% demand. 119
Table 5.5. Percentage of electric demand covered by renewable sources. Case 1. 10% demand. 119

Table 5.6. Percentage of electric demand covered by renewable sources. Case 2. 100% demand............................ 120
Table 5.7. Percentage of electric demand covered by renewable sources. Case 2. 50% demand.............................. 121
Table 5.8. Percentage of electric demand covered by renewable sources. Case 2. 10% demand.............................. 121
Table 5.9. Percentage of electric demand covered by renewable sources. Case 1. 100% storage system.................. 122
Table 5.10. Percentage of electric demand covered by renewable sources. Case 2. 100% storage system. 123

1 PORT OF BAYONNE

1.1 Analysis of the renewable resources in the harbour of Bayonne

Given its geographic location, two types of renewable resources are interesting for the harbor of Bayonne: the wind and solar resource. This resources are studied here.

The hydraulic and marine resources could be important for start studies of installation of recovery of energy (hydraulics and waves). Being given the low maturity of these technologies, it wasn't decided to study these resources but rather of examine the wind and solar resources.

The data for the wind and solar resources presented afterward were supplied by respectively the research center on the Renewable energies CENER situated in Navarre and AICIA situated in Andalusia.

1.1.1 Wind resources

We can see this data for every month of year and for the total of year in the last column. We can see that the annual average of wind speed is about 5,3 m/s with a max speed of 28 m/s. This maximal speed is reached in January. Globally, the regimes of wind are more powerful for the winter and more low for the summer. For example the maximal daily averages in November-February exceed 10 m/s, while in July-August not exceeds 7 m/s. The monthly averages of November and in January-March are over 6 m/s. The monthly averages in July-August not exceed 4 m/s.

The Fig. 1.1 illustrates the temporal data of the wind speed by January 7th. We see a daily variation, with globally more low speeds of wind in the morning and bigger in the afternoon. This wind speed data comes from the CENER model and are evaluated for a height of 50 m compared to the sea level.

The Fig. 1.2 illustrates the temporal data of the wind speed estimated on the site of Tarnos from 4 a 10 January. We can see again daily variations, but the low and powerful winds don't correspond at the same part of the day. For this period, the wind speed was on average around 6 m/s, with peaks almost 10 m/s.

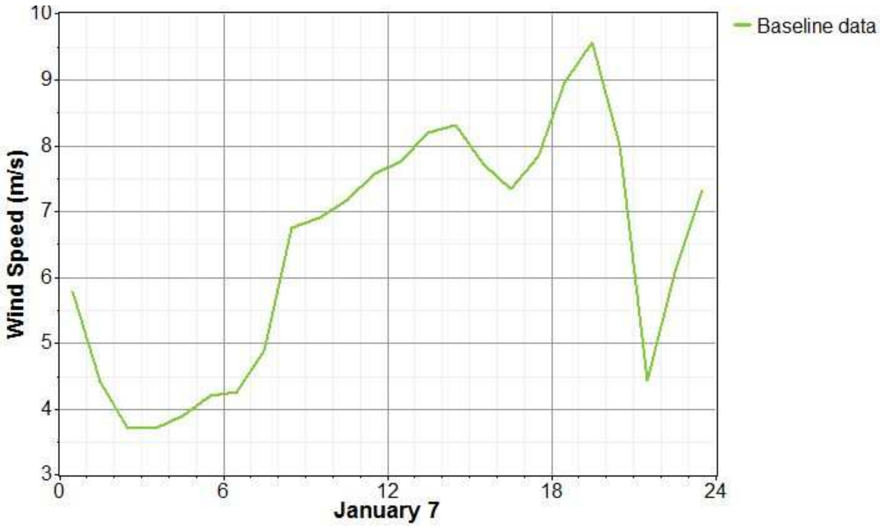

Fig. 1.1. Temporal series of the wind speed for the 2012 January 7 2012

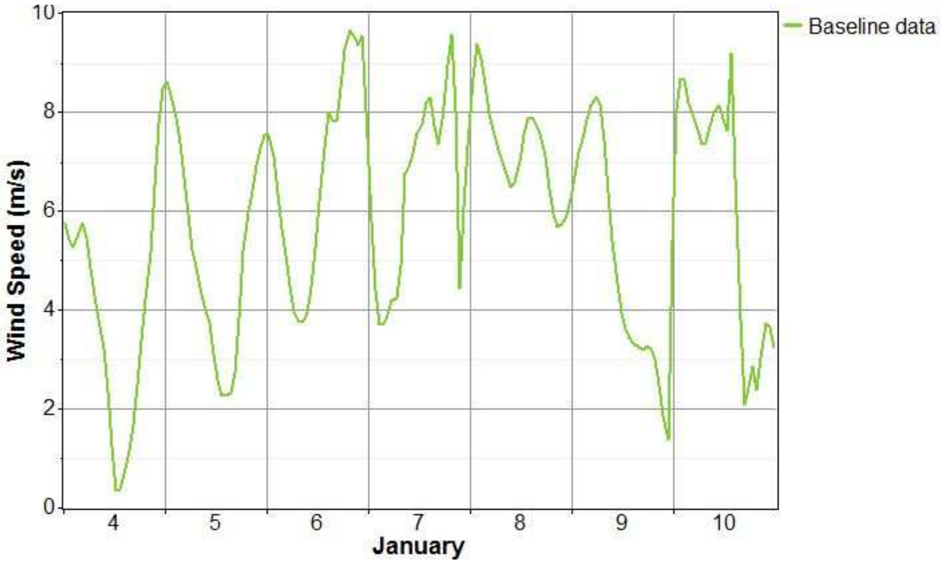

Fig. 1.2. Temporal series of the wind speed on several days of January 2012

The Fig. 1.3 shows monthly statistical data of the wind speed. Max means the maximum of the month and min the minimum of the month. We can see this data for every month of year and for the total of year in the last column.

We can see that the annual average of wind speed is about 5,3 m/s with a max speed of 28 m/s. This maximal speed is reached in January. Globally, the regimes of wind are more powerful for the winter and more low for the summer. For example the maximal daily averages in November-February exceed 10 m/s, while in July-August not exceeds 7 m/s. The monthly averages of November and in January-March are over 6 m/s. The monthly averages in July-August not exceed 4 m/s.

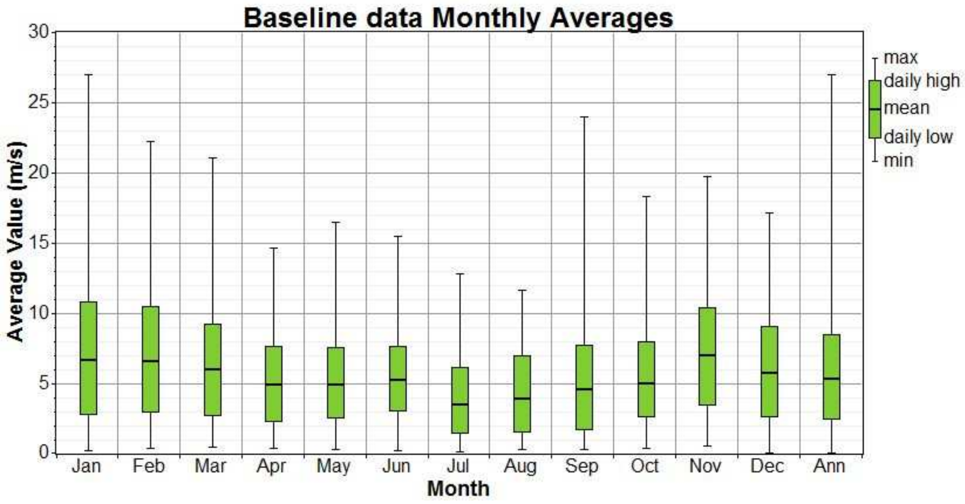

Fig. 1.3. Monthly data of the wind speed (*max* : maximum of month ; *daily high* : maximal daily average of month ; *mean* : average of monthly, *daily low* :minimale daily average of month ; *min* : minimum of mois)

These results are complementary with the electric consumption in the port, which is more important in winter (see report on the first part of study).

The Fig. 1.4 illustrates average daily data for every month. This Figure confirms analyses realized previously. On average, the differences of speed of wind aren't significant for the same day. It's in January, February and in November when we find the biggest averages and in July and in August when we find the smallest averages.

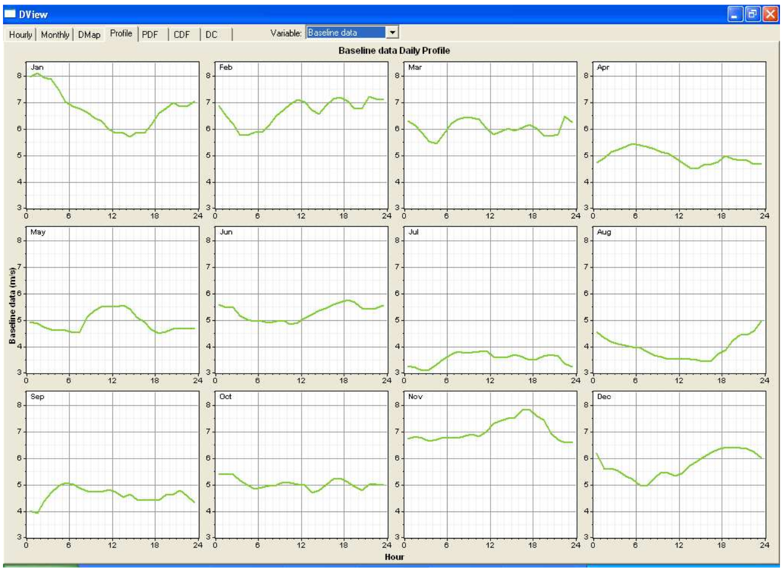

Fig. 1.4. Temporal daily series of the wind speed by month

The Fig. 1.5 shows the Probability Density Function (PDF) of the estimated wind speed on site.

We can see that the probability that speed of wind is between 4 and 5 m/s is more than 14 %. It's more than 13 % for wind speeds between 3 and 4 m/s, more than 12 % for wind speeds between 5 and 6 m/s and less than 12 % for wind speeds between 2 and 3 m/s. The probability for the other speeds of wind decrease significantly. The probability for a wind speed between 6 and 7 m/s is almost 10 %.

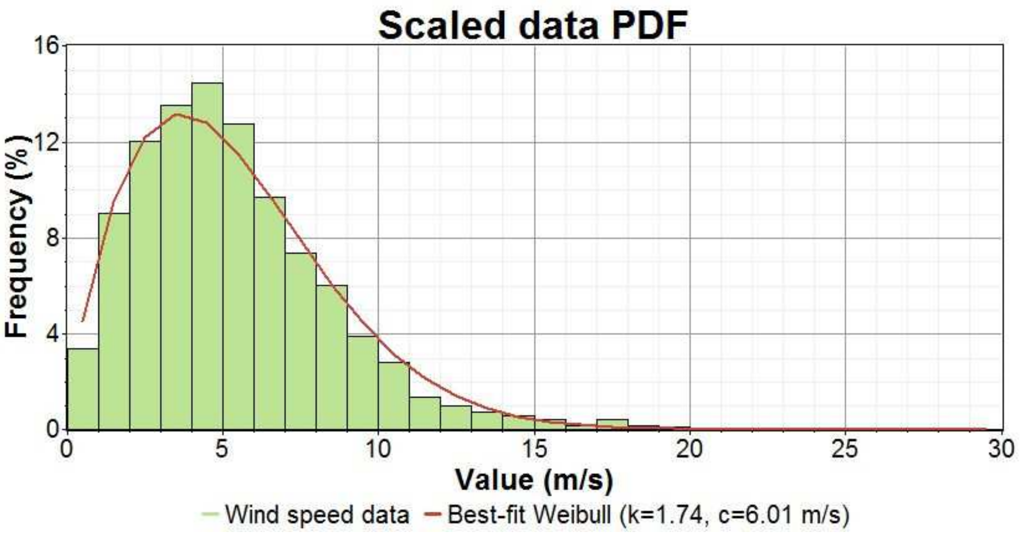

Fig. 1.5. PDF (Probability Density Function) of data of wind speed

At the beginning of the project, the aim was to use wind speed datas from anemometers installed on cranes. The idea was to use cranes as matt of measure to avoid installation of matt of measure for different reasons (cost, administratives elements…). The Fig. 1.6 shows the location of an anemometer THIES on the crane n°14. The Fig. 1.7 shows the location of an anemometer JRI on the crane n°12. Anemometers are situated at heights of 40 m.

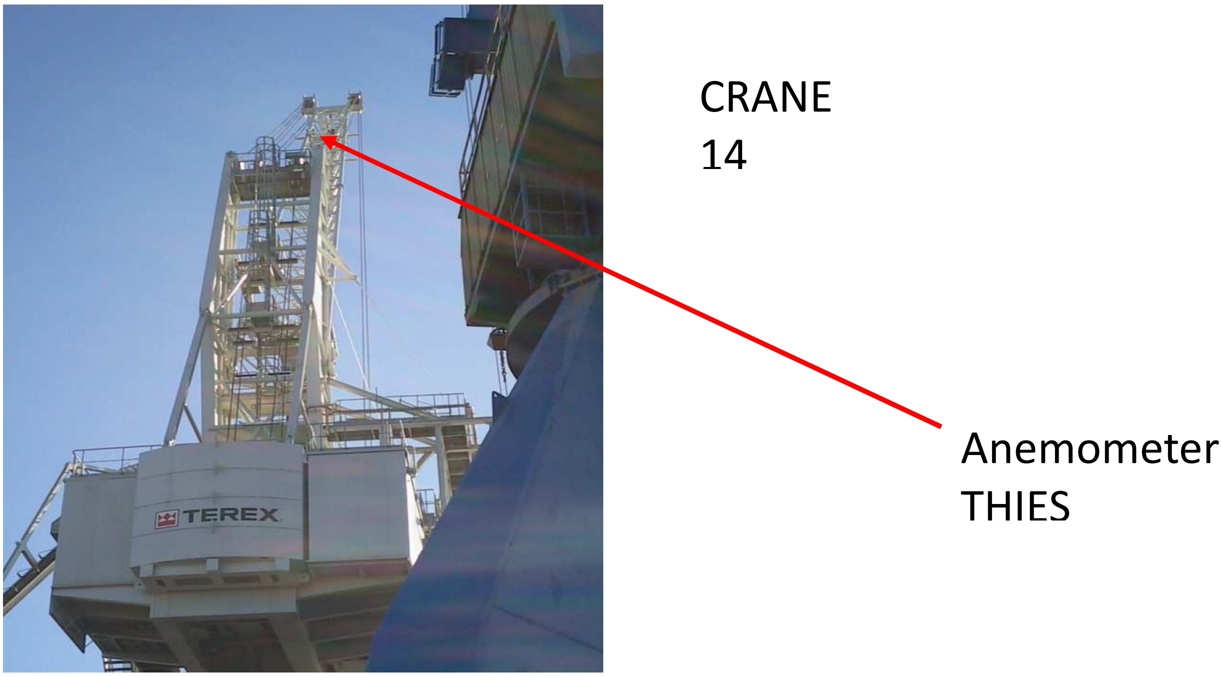

Fig. 1.6. Location of the anemometer THIES on the crane 14

Fig. 1.7. Location of anemometre JRI on the crane 12

1.1.1.1 Data comparisons

The obtained data from the anemometers are not of big quality. Firtsly, the cranes moves and affect anemometers data acquisition. But, the biggest problem is the hole in the datas. The data are taken only from end of September 2011 to February 2012. The sampling frequency is of 1 minute. The more interesting data are from the crane 14 du to the height of anemometer and also because the crane was rarely used. This quantity of data is not sufficien for the study done for GT3. In comparison, the wind speed data given by the CENER concerns a decade of data.

This lack of data in quality and quantity can't be used for the moment for the study. With more data in quality and quantity, it will be possible to extrapolate using for example neural network tools.

However, to have a global idea the Fig. 1.8 and Fig. 1.9 illustrates a comparison.

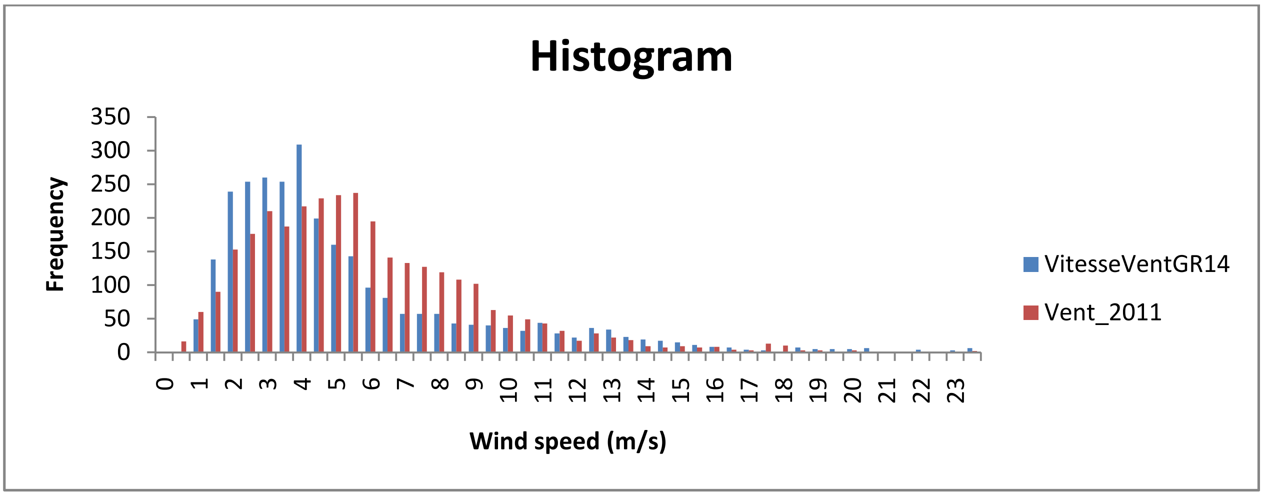

Fig. 1.8: Frequency comparison between CENER data (Vent_2011) and Crane14 data (VitesseVentGR14)

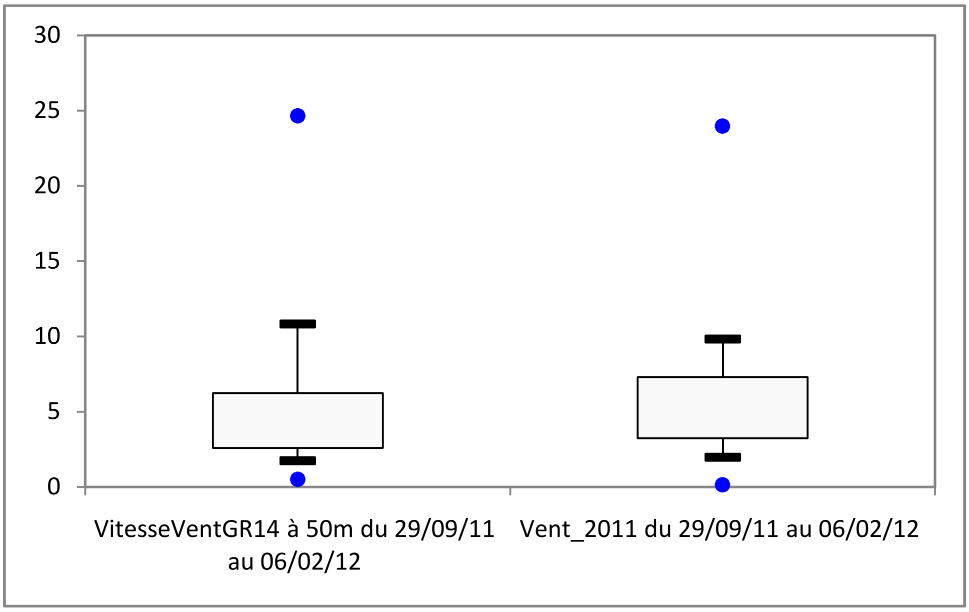

Fig. 1.9: Box plot comparison between CENER data (Vent_2011…) and Crane14 data (VitesseVentGR14..)

The Fig. 1.10 shows in condensate way the data comparison.

	VitesseVentGR14 à 50m du 29/09/11 au 06/02/12	Vent_2011 du 29/09/11 au 06/02/12
minimum	0,5	0,1
maximum	24,6	24
moyenne	5,1	5,6
écart type	3,8	3,3

Fig. 1.10: Numerical comparisons comparison between CENER data (Vent_2011…) and Crane14 data (VitesseVentGR14..)

We don't enter in data quality discussion, but the principal idea to retain is that the CENER data are not far from real data (not cleaned data) and the real wind speed is lower of approximately 10% from the CENER data.

According with data analyses the measured data by the anemometers are not reliable, and for the study only CENER datas are used.

1.1.2 Solar resources

The data of solar illumination were supplied by the AICIA situated in Andalucia, and concernes the port of Bayonne.

The Fig. 1.11 illustrates the solar illumination obtained on May 30th. We can see that this illumination increases the morning, with a maximum around midday, then decreases the afternoon. The maximal illumination is about 0,75 kW/m^2.

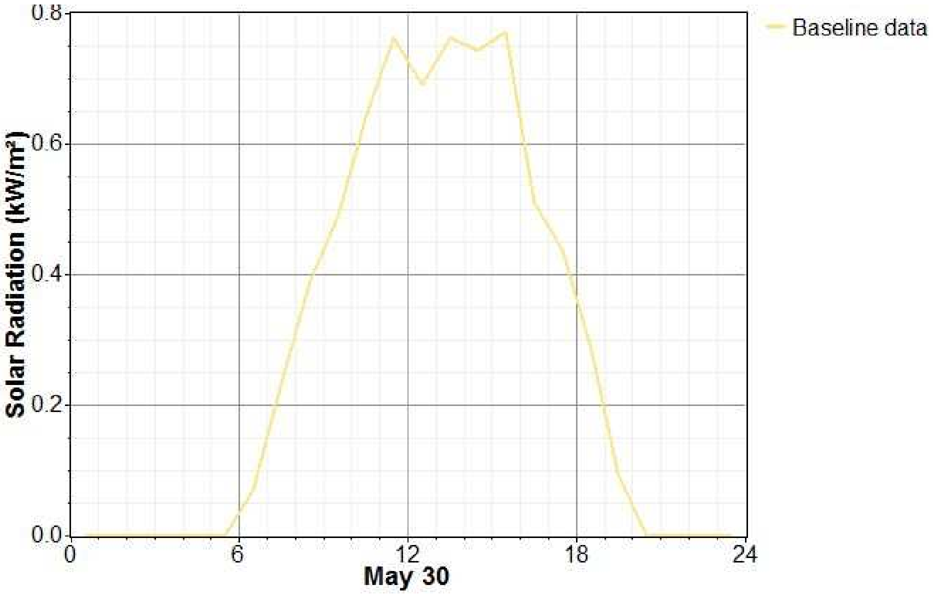

Fig. 1.11. Temporal series of the sun for May 30th

The Fig. 1.12 shows temporal data of the illumination from May 27th to June 2nd. We can see that, contrary at the speed of wind, the profile of the variation of this illumination is almost identical every day. It's logical because the illumination varies with the solar cycle. The small differences between some days can be understandable by occasional cloud.

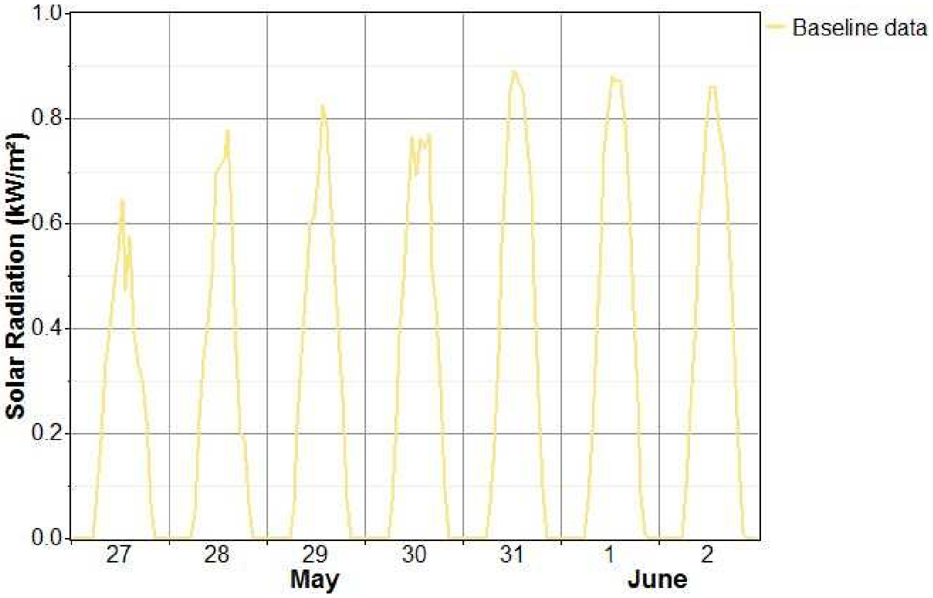

Fig. 1.12. Temporal series of the sun on several days for May

The Fig. 1.13 illustrates monthly statistical data of the solar illumination. Daily high represents the maximal daily average of the month. Daily low represents the minimal daily average of the month. We find these data for every month of the year, and all the year in the last column.

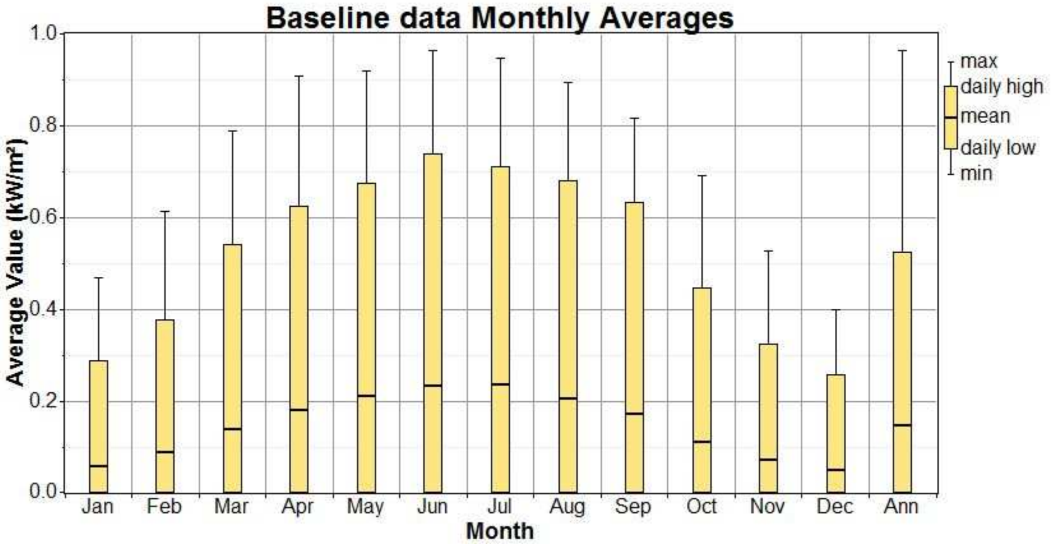

Fig. 1.13. Monthly data of solar illumination (*max* : maximum of month ; *daily high* : maximal daily average of month ; *mean* : average of monthly, *daily low* :minimale daily average of month ; *min* : minimum of mois)

Contrary at the speed of wind, the illumination is more important in summer. These resources are complementary compared with the wind resources. The annual evolution of the solar illumination is more regular that the wind evolution. There are an average monthly illumination about 0,23 kW / m2 in June-July and 0,05 kW / m2 in December-January. The annual average is 0,15 kW / m2.

The Fig. 1.14 shows the daily average data a month. We can see that the intensity of the illumination varies. The daily average profile is very different, for every month, compared with the wind speed.

This has a significant impact on the management for a smartgrid which contains an important quantity of solar energy PV. Indeed, the curve of daily electric consumption does not follow the variation of solar energy. The daily profile of the wind speed is more interesting from a point of view of the conduct of the electricity smartgrid because it's smoother. For compensate the abrupt variations of the solar energy, a system of storage can be indispensable, especially if the quantity of solar energy in the smartgrid is significant.

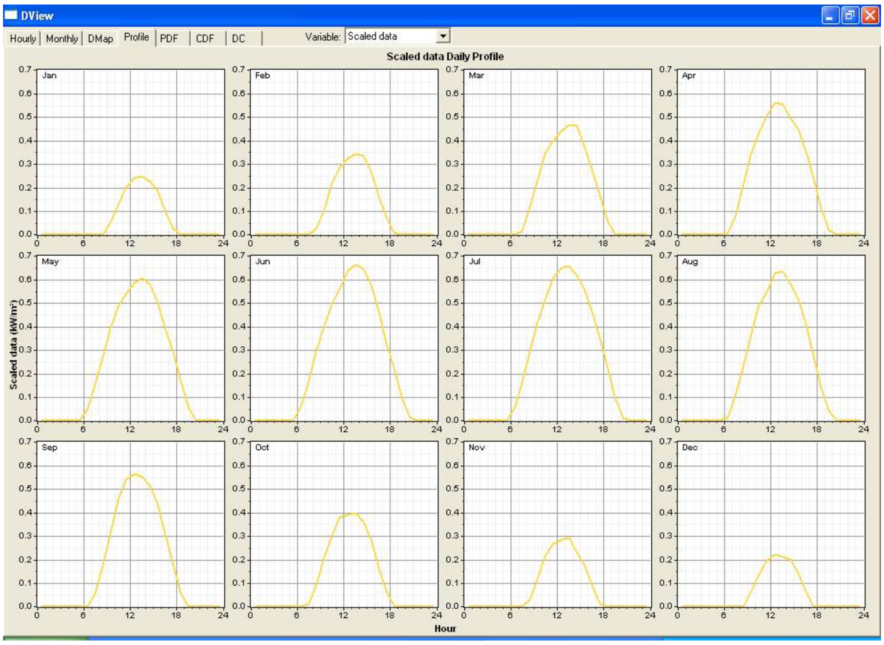

Fig. 1.14. Temporal series of daily illumination per month

The Fig. 1.15 illustrates the percentage of chances so that the illumination has a certain value. We can see in this figure that there is almost 55 % of chances so that the illumination is between 0 and 0,025 kW / m2. Then, the other possible slots of illumination are almost the same lucky to occur.

This enormous difference between the first scale-bar and the others is understandable by the night, when there isn't illumination. The Fig. 1.16 presents the PFD for only diurnal data and the median is about 0.24 W/m^2 with a mean of 0.29 W/m^2.

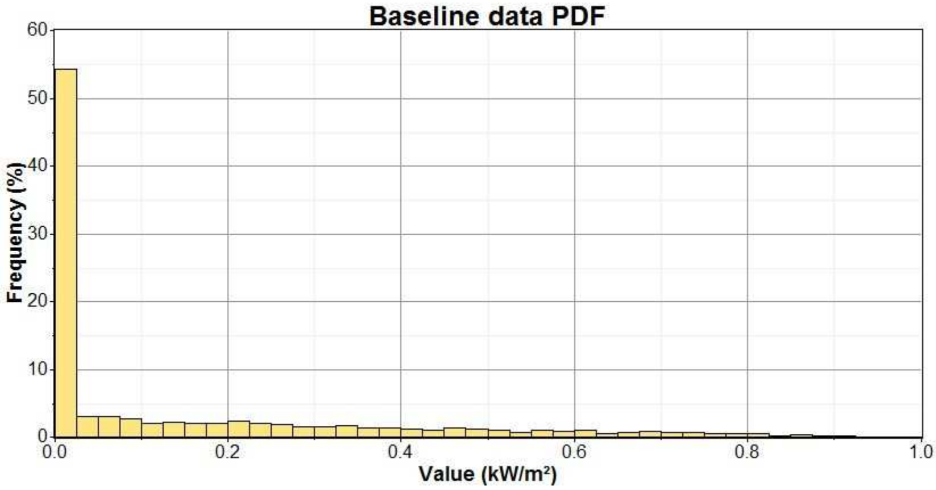

Fig. 1.15. PDF (*Probability Density Function*) of data of solar illumination

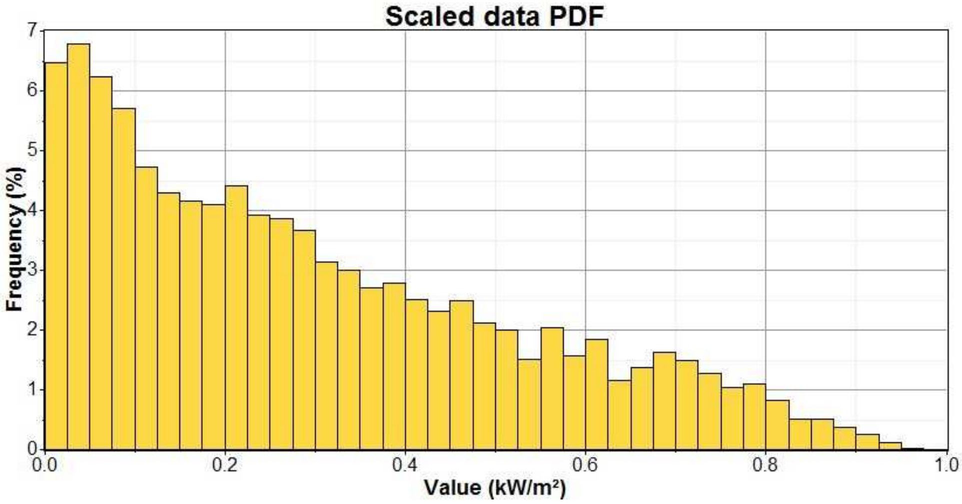

Fig. 1.16: PDF (*Probability Density Function*) of solar irradiation in 2011

1.1.3 Conclusions

The main conclusions for the wind resources are:

- The annual average speed of wind with a height of 50 m compared with the sea level on the site of Tarnos is 5,35 m/s;
- The wind is more powerful in winter than in summer;
- This resource is complementary with the curve of annual consumption of the site of Tarnos.

For the solar resources, the mean conclusions are:

- The annual average solar illumination is 0,15 kW / m^2;
- The solar potential is more important in summer than in winter. The annual evolution is very regular. This resource is complementary compared with the wind potential;

- The daily variation of illumination is important. It’s problematic from the point of view of the smartgrid control, and can lead to use storage systems, according to the quantity of solar energy in the smartgrid.

1.2 Design of system with Homer

Several studies of sizing of generators based on renewable resources and systems of energy storage devices are described in this chapter. Many parameters influence these technico-economic studies: the resources potential , the cost of used renewable sources, the price of purchase of the electricity produced by these sources, the price of purchase for electricity of the main elctrical grid, financial transactions etc. …

Two main studies are realized. The first is for the installation of renewable sources (concretely of wind turbines and PV panels, in the harbour zone of Tarnos. The second is interested in the contribution of a system of storage with an economic point of view.

1.2.1 Design with renewable technologies

As mentioned earlier, many parameters influence the system’s design. Here, this sizing is realized with the software HOMER. Before analyzing the results of the calculations of optimization realized by HOMER, a description of the configuration of every component is given in the following sub-sections.

1.2.1.1 Configuration of charge

The configuration of electric consumption for the site of Tarnos is illustrated on the Fig. 1.17. This configuration is based on the real consumption measured on cranes .

The data selected for a month show that there is a daily energy consumption (423 kWh) with a peak of power consumption of 134 kW. Concerning the energy consumed every day, a scale-up is realized, indicating that is in average equal to 1.217 kWh / d. This figure corresponds to the sum of the consumptions of the invoice EDF in 2009 (348.075 kWh for cranes and 95.989 kWh for workshops, offices and cloakrooms), divided by the number of days in the year.

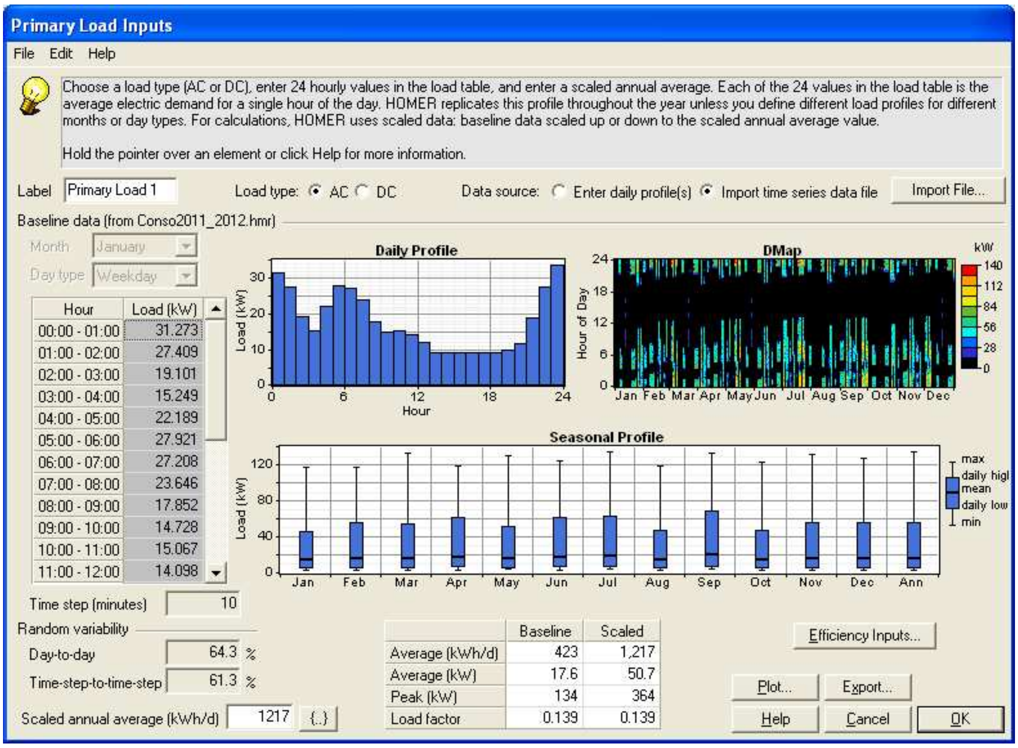

Choose a load type (AC or DC), enter 24 hourly values in the load table, and enter a scaled annual average. Each of the 24 values in the load table is the average electric demand for a single hour of the day. HOMER replicates this profile throughout the year unless you define different load profiles for different months or day types. For calculations, HOMER uses scaled data: baseline data scaled up or down to the scaled annual average value.

Hold the pointer over an element or click Help for more information.

Label: Primary Load 1
Load type: ● AC ○ DC
Data source: ○ Enter daily profile(s) ● Import time series data file

Baseline data (from Conso2011_2012.hmr)
Month: January
Day type: Weekday

Hour	Load (kW)
00:00 - 01:00	31.273
01:00 - 02:00	27.409
02:00 - 03:00	19.101
03:00 - 04:00	15.249
04:00 - 05:00	22.189
05:00 - 06:00	27.921
06:00 - 07:00	27.208
07:00 - 08:00	23.646
08:00 - 09:00	17.852
09:00 - 10:00	14.728
10:00 - 11:00	15.067
11:00 - 12:00	14.098

Time step (minutes): 10
Random variability
Day-to-day: 64.3 %
Time-step-to-time-step: 61.3 %
Scaled annual average (kWh/d): 1217

	Baseline	Scaled
Average (kWh/d)	423	1,217
Average (kW)	17.6	50.7
Peak (kW)	134	364
Load factor	0.139	0.139

Fig. 1.17. Configuration of electricity consumption in the port of Tarnos with HOMER

The profile of consumption shows that this one occurs in particular about midnight and at about 6 am. This profile has its importance because the price for the purchase of electricity supplied by EDF depends of slots provide (see later sub-section). This profile would also be significant if we want to consume the whole of production of the renewable sources in the port.

1.2.1.2 *Configuration of wind turbine*

The configuration of the wind sources is illustrated on the Fig. 1.18. The type of technology chosen in first was a wind generator AOC 15/50 proposed in the software HOMER. It's a wind generator AC (65 kW). It's necessary to note that the height of the hub is situated at 25 m, which is the middle of the height where was measured the speed of wind (see previous chapter). The price of the wind generator is 265.000 $ and the costs of functioning and maintenance are $6.000 / year. These figures were found with Internet. The price is raised compared with a wind generator of major power which costs approximately 1 € by kW.

The Figure indicates the curve of power of the wind generator, which shows that the nominal speed of wind is about 15 m/s, that is a very important speed with compared with the potential of the site.

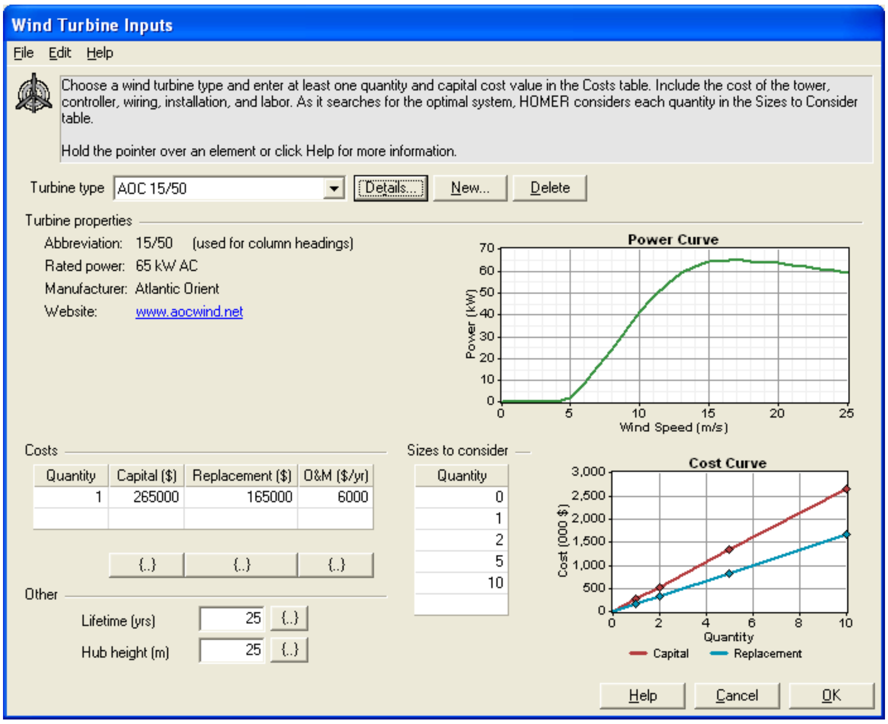

Choose a wind turbine type and enter at least one quantity and capital cost value in the Costs table. Include the cost of the tower, controller, wiring, installation, and labor. As it searches for the optimal system, HOMER considers each quantity in the Sizes to Consider table.

Hold the pointer over an element or click Help for more information.

Turbine type: AOC 15/50

Turbine properties

Abbreviation: 15/50 (used for column headings)
Rated power: 65 kW AC
Manufacturer: Atlantic Orient
Website: www.aocwind.net

Costs

Quantity	Capital ($)	Replacement ($)	O&M ($/yr)
1	265000	165000	6000

Sizes to consider

Quantity
0
1
2
5
10

Other

Lifetime (yrs): 25
Hub height (m): 25

Fig. 1.18. Configuration of representation of the first wind turbine in the harbour zone of Tarnos with HOMER

That is why another wind turbine is added for the design. 5 different configurations of wind turbine quantities were chosen for the simulation: 0, 1, 2, 5 and 10.

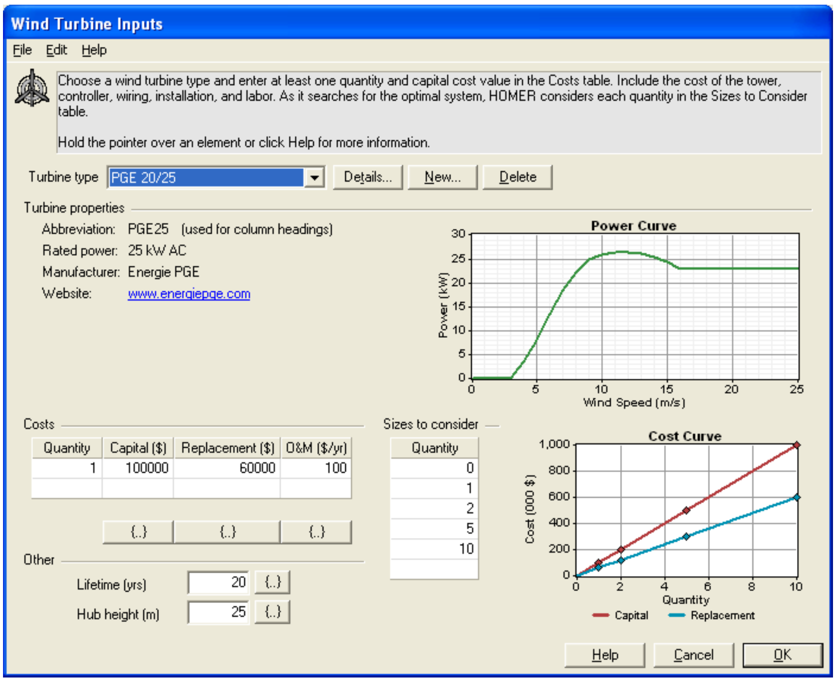
Wind Turbine Inputs

Choose a wind turbine type and enter at least one quantity and capital cost value in the Costs table. Include the cost of the tower, controller, wiring, installation, and labor. As it searches for the optimal system, HOMER considers each quantity in the Sizes to Consider table.

Hold the pointer over an element or click Help for more information.

Turbine type: PGE 20/25

Turbine properties
Abbreviation: PGE25 (used for column headings)
Rated power: 25 kW AC
Manufacturer: Energie PGE
Website: www.energiepge.com

Costs

Quantity	Capital ($)	Replacement ($)	O&M ($/yr)
1	100000	60000	100

Sizes to consider

Quantity
0
1
2
5
10

Other
Lifetime (yrs): 20
Hub height (m): 25

Fig. 1.19. Configuration of representation of the second wind turbine in the harbour zone of Tarnos with HOMER

The wind turbine presented in Fig. 1.19 is also in the software HOMER. It's the PGE 20/25. According to Internet at the address http://www.icrepq.com/icrepq'12/230-surianu.pdf, the price for the wind turbine is 100.000 $ and the costs of functioning and maintenance are $100 / year (very low, big difference compared with the previous wind turbine).

We can see that the curve of power is more interesting than the previous wind generator, because the nominal speed of the wind is 9 m/s. This wind turbine is also more adapted for the site of Tarnos.

5 different configurations of wind turbine quantities were considered for the simulation: 0, 1, 2, 5 and 10.

1.2.1.3 *Configuration of PV panels*

The configuration of the photovoltaic panels is illustrated in the Fig. 1.20.

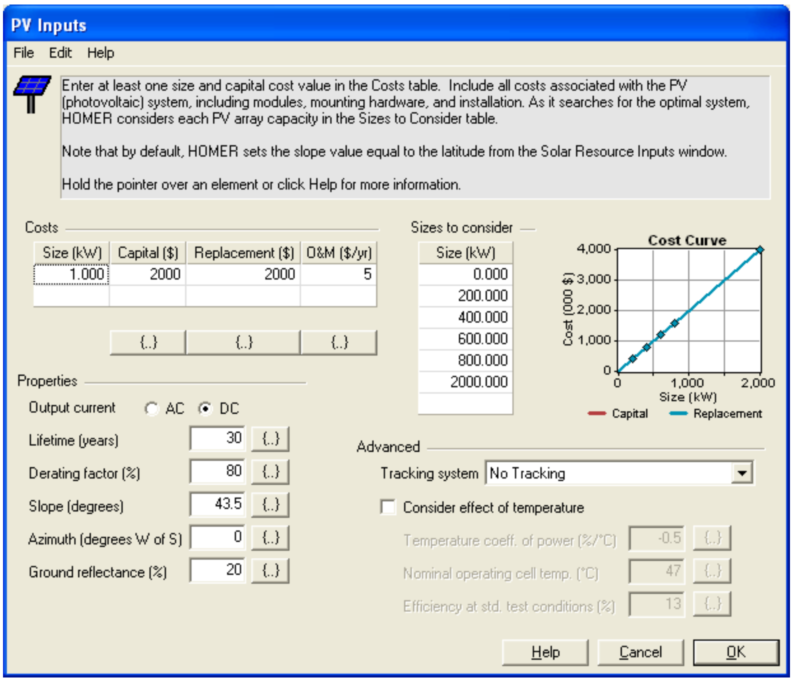
PV Inputs

Enter at least one size and capital cost value in the Costs table. Include all costs associated with the PV (photovoltaic) system, including modules, mounting hardware, and installation. As it searches for the optimal system, HOMER considers each PV array capacity in the Sizes to Consider table.

Note that by default, HOMER sets the slope value equal to the latitude from the Solar Resource Inputs window.

Hold the pointer over an element or click Help for more information.

Costs

Size (kW)	Capital ($)	Replacement ($)	O&M ($/yr)
1.000	2000	2000	5

Sizes to consider

Size (kW)
0.000
200.000
400.000
600.000
800.000
2000.000

Properties
Output current ○ AC ● DC
Lifetime (years): 30
Derating factor (%): 80
Slope (degrees): 43.5
Azimuth (degrees W of S): 0
Ground reflectance (%): 20

Advanced
Tracking system: No Tracking
☐ Consider effect of temperature
Temperature coeff. of power (%/°C): -0.5
Nominal operating cell temp. (°C): 47
Efficiency at std. test conditions (%): 13

Fig. 1.20. Configuration of representation of solar panel in the harbour zone of Tarnos with HOMER

The price for a panel PV of 1 kW is 2.000 $. The costs of operation and maintenance are estimated at 5$ / year. They were given by the research center CENER. No system of tracking is considered. The life cycle considered of panel is about 30 years.

Four different sizes of panels have been designed with HOMER: 0, 200, 400, 600, 800 and 2.000 kW.

1.2.1.4 Configuration of electricity grid EDF

The configuration of electricity grid is illustred in the Fig. 1.21.

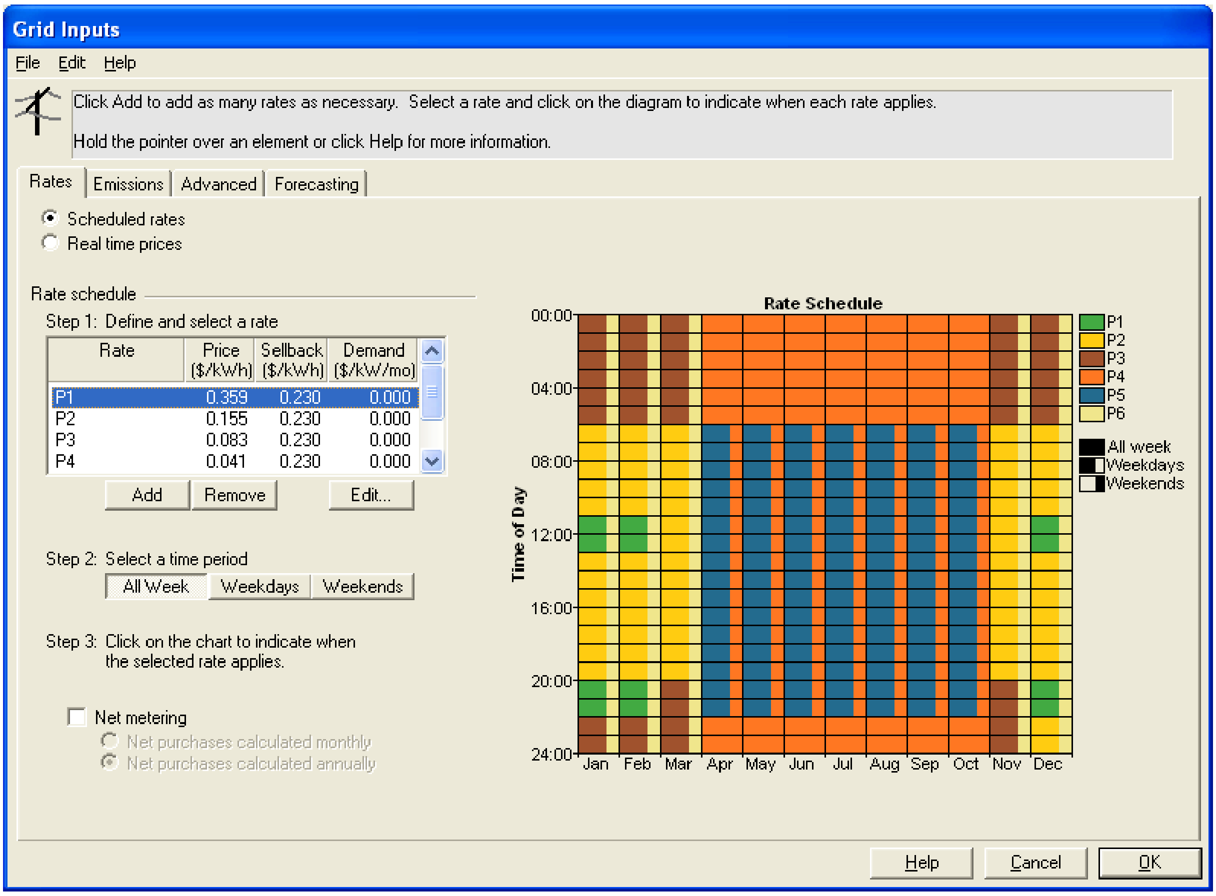

Click Add to add as many rates as necessary. Select a rate and click on the diagram to indicate when each rate applies.

Hold the pointer over an element or click Help for more information.

● Scheduled rates
○ Real time prices

Rate schedule

Step 1: Define and select a rate

Rate	Price ($/kWh)	Sellback ($/kWh)	Demand ($/kW/mo)
P1	0.359	0.230	0.000
P2	0.155	0.230	0.000
P3	0.083	0.230	0.000
P4	0.041	0.230	0.000

Step 2: Select a time period

Step 3: Click on the chart to indicate when the selected rate applies.

☐ Net metering
○ Net purchases calculated monthly
● Net purchases calculated annually

Fig. 1.21. Configuration of the electricity grid EDF and exchanges of energy of the harbour zone of Tarnos with HOMER

The tariff grid indicates the conditions of exchanges of electrical energy with the port. The price lists of electricity supplied by EDF contain 6 different section and correspond to a contract of type "yellow price list".

Price lists are: P1=0,3594 $/kWh, P2=0,1555 $/ kWh, P3=0,0826 $/ kWh, P4=0,0409 $ / kWh, P5=0,0675 $/ kWh, P6=0,083 $ / kWh. From an economic point of view, the best is to consume between 10 pm and 6 am in the morning in summer (price list P4), and the worst is to consume between 11 am and 1 pm or between 8 pm and 10 pm the winter (price list P1).

We also have the possibility to introduce the price list of repurchase of electricity by EDF of the energy produced in the port. The inconvenience is that this price list in HOMER cannot be associated with the type of source (required for a real repurchase by EDF). The regulations associate various price lists with the various sources. Another problem is that no price list is defined by the regulation for stored energy.

The Fig. 1.22 gives the price of purchases of electricity for the PV in France according to several parameters. We can see that these price lists fall gradually in the time. The price list considered for the port is 10,79 c€ / kWh (that is approximately 13,27 c$ / kWh) which corresponds at the category " Every type of installation ", for installations with a power superior to 400 kWc, and at a period of installation between 01/04/2012 and the 30/06/2012.

We can see that a new problem appears for the design. This price list is not valid for installations with a lower power. The software doesn't allow to associate the power PV with a different price list.

As regards the price lists of repurchase of electricity of wind origin, information can be found in the Order of November 17th, 2008 who fix the purchasing terms of the electricity produced by the installations using the mechanical energy of the wind (see at http://fee.asso.fr/tout_savoir_sur_l_energie_eolienne/aspects_economiques/le_tarif_d_ obligation_d_achat). It's difficult to specify a price list for small wind turbine (lower than 100 kW), in a zone like the site of Tarnos which can be considered as "offshore". Furthermore, this price list is fixed during ten years, then he can fall in ten years, according to the rate of production. We realized the simulations with an average price list estimated at 8 c€ (9,84 c$).

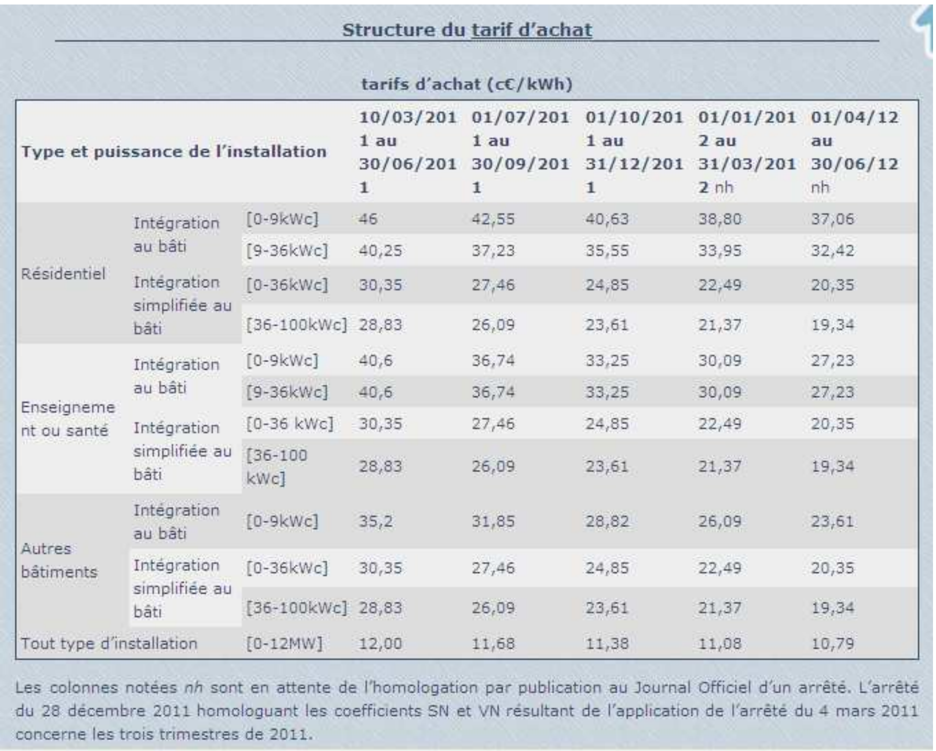

Structure du tarif d'achat

tarifs d'achat (c€/kWh)

Type et puissance de l'installation			**10/03/2011 au 30/06/2011**	**01/07/2011 au 30/09/2011**	**01/10/2011 au 31/12/2011**	**01/01/2012 au 31/03/2012** nh	**01/04/12 au 30/06/12** nh
Résidentiel	Intégration au bâti	[0-9kWc]	46	42,55	40,63	38,80	37,06
		[9-36kWc]	40,25	37,23	35,55	33,95	32,42
	Intégration simplifiée au bâti	[0-36kWc]	30,35	27,46	24,85	22,49	20,35
		[36-100kWc]	28,83	26,09	23,61	21,37	19,34
Enseignement ou santé	Intégration au bâti	[0-9kWc]	40,6	36,74	33,25	30,09	27,23
		[9-36kWc]	40,6	36,74	33,25	30,09	27,23
	Intégration simplifiée au bâti	[0-36 kWc]	30,35	27,46	24,85	22,49	20,35
		[36-100 kWc]	28,83	26,09	23,61	21,37	19,34
Autres bâtiments	Intégration au bâti	[0-9kWc]	35,2	31,85	28,82	26,09	23,61
	Intégration simplifiée au bâti	[0-36kWc]	30,35	27,46	24,85	22,49	20,35
		[36-100kWc]	28,83	26,09	23,61	21,37	19,34
Tout type d'installation		[0-12MW]	12,00	11,68	11,38	11,08	10,79

Les colonnes notées *nh* sont en attente de l'homologation par publication au Journal Officiel d'un arrêté. L'arrêté du 28 décembre 2011 homologuant les coefficients SN et VN résultant de l'application de l'arrêté du 4 mars 2011 concerne les trois trimestres de 2011.

Fig. 1.22. Price of purchases of electricity of origin PV in France

1.2.1.5 *Other configurations*

Another component used for the design is the converter DC / AC for PV panels. The data of configuration which are integrated in HOMER were supplied by CENER (see Fig. 1.23).

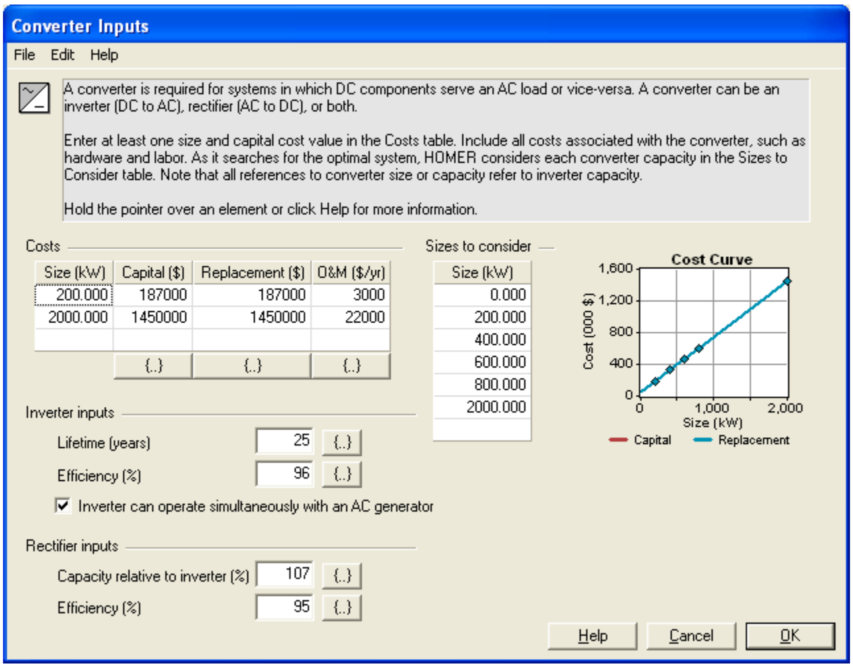

A converter is required for systems in which DC components serve an AC load or vice-versa. A converter can be an inverter (DC to AC), rectifier (AC to DC), or both.

Enter at least one size and capital cost value in the Costs table. Include all costs associated with the converter, such as hardware and labor. As it searches for the optimal system, HOMER considers each converter capacity in the Sizes to Consider table. Note that all references to converter size or capacity refer to inverter capacity.

Hold the pointer over an element or click Help for more information.

Costs

Size (kW)	Capital ($)	Replacement ($)	O&M ($/yr)
200.000	187000	187000	3000
2000.000	1450000	1450000	22000

Sizes to consider

Size (kW)
0.000
200.000
400.000
600.000
800.000
2000.000

Inverter inputs

Lifetime (years) 25

Efficiency (%) 96

☑ Inverter can operate simultaneously with an AC generator

Rectifier inputs

Capacity relative to inverter (%) 107

Efficiency (%) 95

Fig. 1.23. Configuration of converters associated to panels PV

We can see that the cost of converters depends of the size. For a converter of 200 kW, the cost estimated by the component is 187.000 $, and the costs for the functioning and maintenance are estimated at 3.000 $/ year. The estimated life cycle is 25 years and the efficiency is 96 %. For the HOMER simulation HOMER, there are 4 sizes of association of converters: 0, 200, 400, 600, 800 and 2.000 kW.

The Fig. 1.24 illustrates the configuration of the economic part of the project. We indicate that the project is designed for 25 years and that the annual interest rate of the signed loans is 6 %.

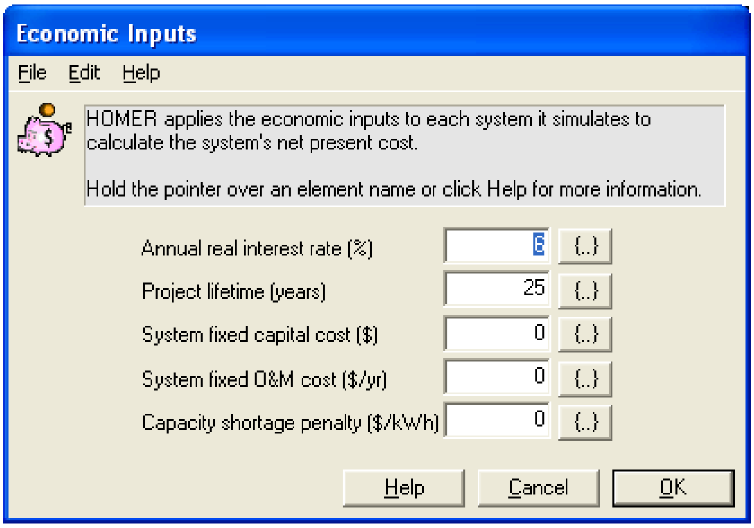

HOMER applies the economic inputs to each system it simulates to calculate the system's net present cost.

Hold the pointer over an element name or click Help for more information.

Annual real interest rate (%) 6

Project lifetime (years) 25

System fixed capital cost ($) 0

System fixed O&M cost ($/yr) 0

Capacity shortage penalty ($/kWh) 0

Fig. 1.24. Configuration of economy part of report

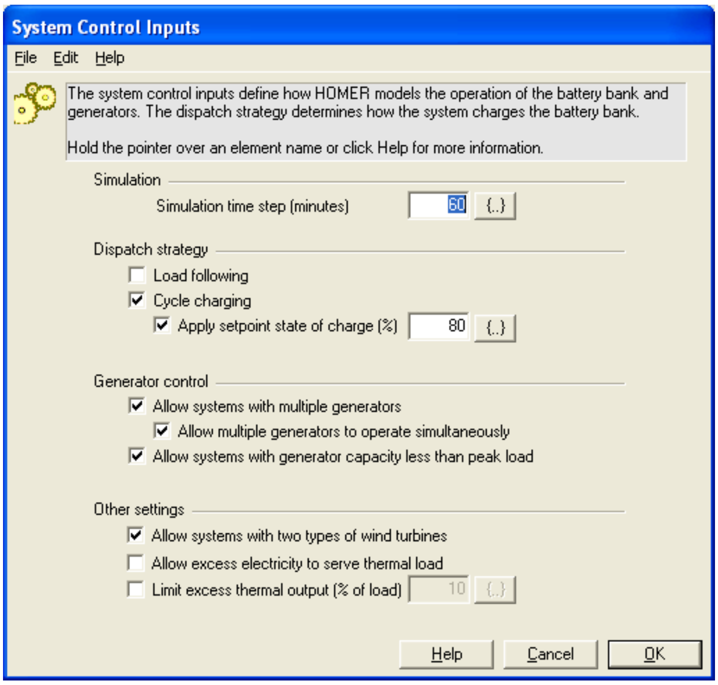

System Control Inputs

The system control inputs define how HOMER models the operation of the battery bank and generators. The dispatch strategy determines how the system charges the battery bank.

Hold the pointer over an element name or click Help for more information.

Simulation
Simulation time step (minutes) 60

Dispatch strategy
☐ Load following
☑ Cycle charging
☑ Apply setpoint state of charge (%) 80

Generator control
☑ Allow systems with multiple generators
☑ Allow multiple generators to operate simultaneously
☑ Allow systems with generator capacity less than peak load

Other settings
☑ Allow systems with two types of wind turbines
☐ Allow excess electricity to serve thermal load
☐ Limit excess thermal output (% of load) 10

Fig. 1.25. Configuration of electric system management in general

The Fig. 1.25 shows the configuration of the system of sources managment, systems of storage (when they are), the supervision / distribution (dispatching) of the energy …

We don’t consider batteries for this first scenario. Here the important information are:

- we authorize the simultaneous use of several generators;
- we authorize the use of generators which have a capacity lower than the peak of consumption and that the association of two types of wind generator is also authorized.

1.2.1.6 *Results of the calculations of optimization*

1.2.1.6.1 Configuration with only PV panels

Considering the complications quoted previously on the difficulty of consideration of the diverse price lists of repurchase of electricity by EDF with HOMER, a first simulation is realized by considering for the microgrid only PV panels. The optimization results are in the Fig. 1.26. We observe that the most interesting configuration of an economic point of view is the one where the design is the biggest: 2.000 kW. The cost of the electricity calculated over 25 years is 7,7 c$ / kWh, better that with the elctrical grid ($7,8 c / kWh).

As regards the average cost of the electricity bought from the main grid (to EDF), we can see that this cost indicated on EDF invoices is different: 10,9 c$ / kWh for the supply of cranes and 12,5 c$€ / kWh for the supply of workshops, cloakrooms and offices. This difference can have various explanations. In the first one, the pricing can be different for each of both types of contract with EDF, while that in HOMER is unique. Furthermore, the curve of load is different, on average, with the HOMER one (Fig. 1.17), where the main consumption occurs at night (which is surprising), when the price lists (rates) of the electricity EDF are the lowest. We can suppose that the real cost of the electricity EDF is bigger than 7,8 c$ / kWh (10 c$ / kWh).

We also observe that the economic profitability of the system increases with the size of the installation.

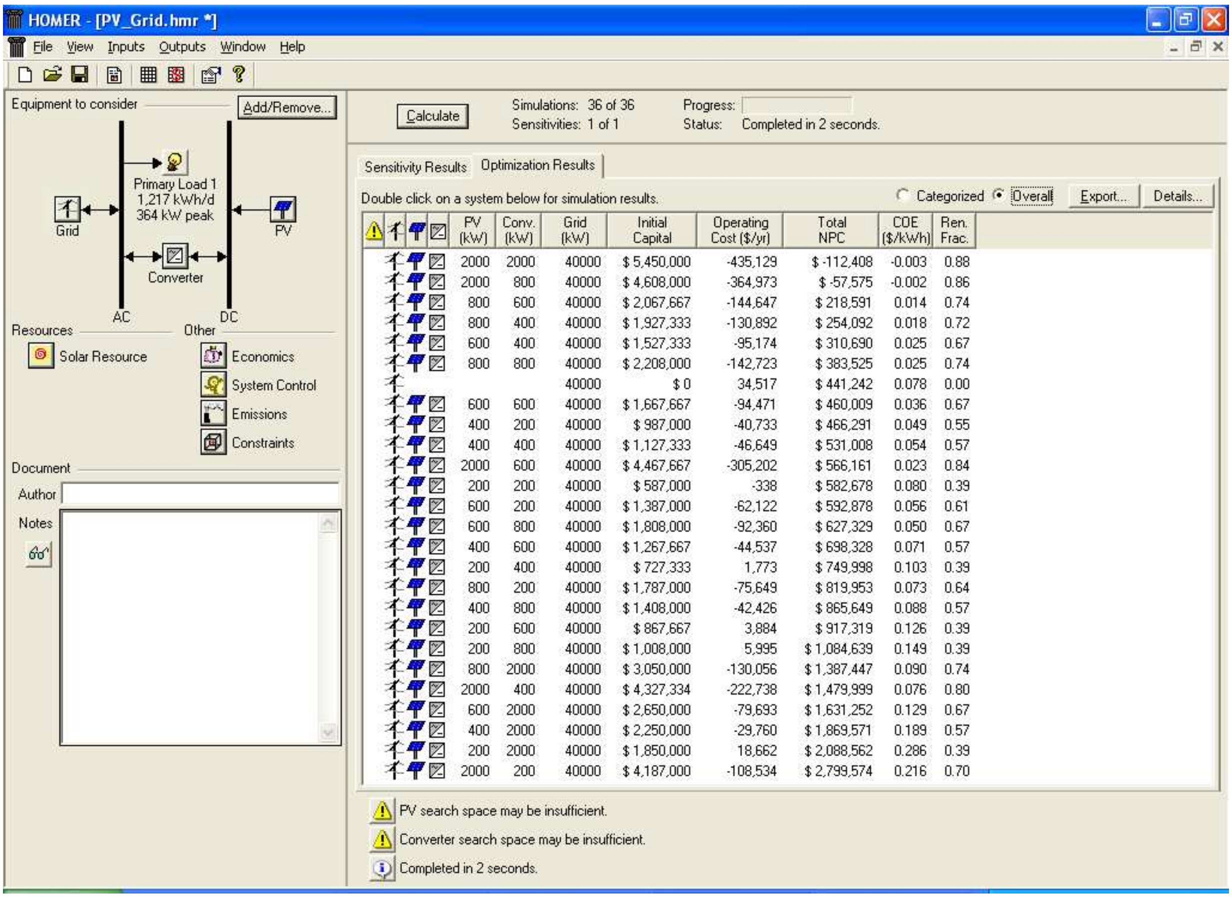

Simulations: 36 of 36
Sensitivities: 1 of 1
Progress:
Status: Completed in 2 seconds.

Double click on a system below for simulation results.

PV (kW)	Conv. (kW)	Grid (kW)	Initial Capital	Operating Cost ($/yr)	Total NPC	COE ($/kWh)	Ren. Frac.
2000	2000	40000	$ 5,450,000	-435,129	$ -112,408	-0.003	0.88
2000	800	40000	$ 4,608,000	-364,973	$ -57,575	-0.002	0.86
800	600	40000	$ 2,067,667	-144,647	$ 218,591	0.014	0.74
800	400	40000	$ 1,927,333	-130,892	$ 254,092	0.018	0.72
600	400	40000	$ 1,527,333	-95,174	$ 310,690	0.025	0.67
800	800	40000	$ 2,208,000	-142,723	$ 383,525	0.025	0.74
		40000	$ 0	34,517	$ 441,242	0.078	0.00
600	600	40000	$ 1,667,667	-94,471	$ 460,009	0.036	0.67
400	200	40000	$ 987,000	-40,733	$ 466,291	0.049	0.55
400	400	40000	$ 1,127,333	-46,649	$ 531,008	0.054	0.57
2000	600	40000	$ 4,467,667	-305,202	$ 566,161	0.023	0.84
200	200	40000	$ 587,000	-338	$ 582,678	0.080	0.39
600	200	40000	$ 1,387,000	-62,122	$ 592,878	0.056	0.61
600	800	40000	$ 1,808,000	-92,360	$ 627,329	0.050	0.67
400	600	40000	$ 1,267,667	-44,537	$ 698,328	0.071	0.57
200	400	40000	$ 727,333	1,773	$ 749,998	0.103	0.39
800	200	40000	$ 1,787,000	-75,649	$ 819,953	0.073	0.64
400	800	40000	$ 1,408,000	-42,426	$ 865,649	0.088	0.57
200	600	40000	$ 867,667	3,884	$ 917,319	0.126	0.39
200	800	40000	$ 1,008,000	5,995	$ 1,084,639	0.149	0.39
800	2000	40000	$ 3,050,000	-130,056	$ 1,387,447	0.090	0.74
2000	400	40000	$ 4,327,334	-222,738	$ 1,479,999	0.076	0.80
600	2000	40000	$ 2,650,000	-79,693	$ 1,631,252	0.129	0.67
400	2000	40000	$ 2,250,000	-29,760	$ 1,869,571	0.189	0.57
200	2000	40000	$ 1,850,000	18,662	$ 2,088,562	0.286	0.39
2000	200	40000	$ 4,187,000	-108,534	$ 2,799,574	0.216	0.70

PV search space may be insufficient.

Converter search space may be insufficient.

Completed in 2 seconds.

Fig. 1.26. Result of calculation with the electrical grid for the port containing only panels PV

The study for the exchanges of electrical energy for this configuration shows that we produce much more energy than what is consumed in the harbour (see Fig. 1.27). With 2.000 kW of panels PV, we produce 2.309.847 kWh in one year, while the annual consumption of electricity is 444.000 kWh / year.

One of the criteria of the Optimagrid project is to try toconsume the locally renewable power production. In this optics, an installation so big has no sense.

The Fig. 1.27 shows the results, with an installation of 400 kW, frome electrical energy point of view. PV panels produces 461.970 kWh / year. We produce also more that we consume. In this computation, 329.248 kWh / year is consumed from the main electrical grid. The rest of the consumption then result from PV panels. The electric energy cost in this configuration returns to 9,5 c$ / kWh.

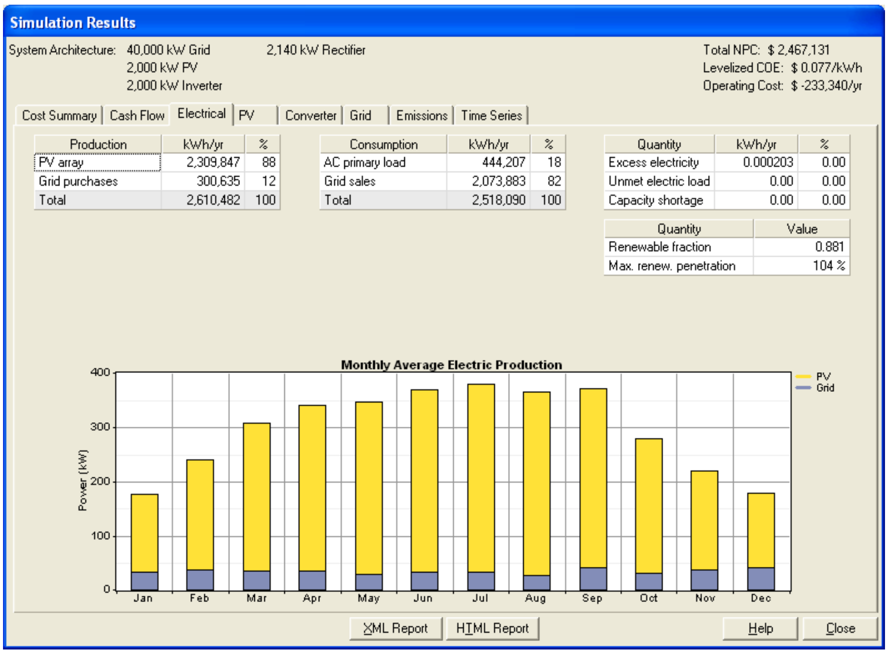

Simulation Results

System Architecture: 40,000 kW Grid, 2,000 kW PV, 2,000 kW Inverter, 2,140 kW Rectifier

Total NPC: $ 2,467,131
Levelized COE: $ 0.077/kWh
Operating Cost: $ -233,340/yr

Production	kWh/yr	%
PV array	2,309,847	88
Grid purchases	300,635	12
Total	2,610,482	100

Consumption	kWh/yr	%
AC primary load	444,207	18
Grid sales	2,073,883	82
Total	2,518,090	100

Quantity	kWh/yr	%
Excess electricity	0.000203	0.00
Unmet electric load	0.00	0.00
Capacity shortage	0.00	0.00

Quantity	Value
Renewable fraction	0.881
Max. renew. penetration	104 %

Fig. 1.27. Résultats *électriques* de la simulation avec le réseau contenant des panneaux PV de 2.000 kW

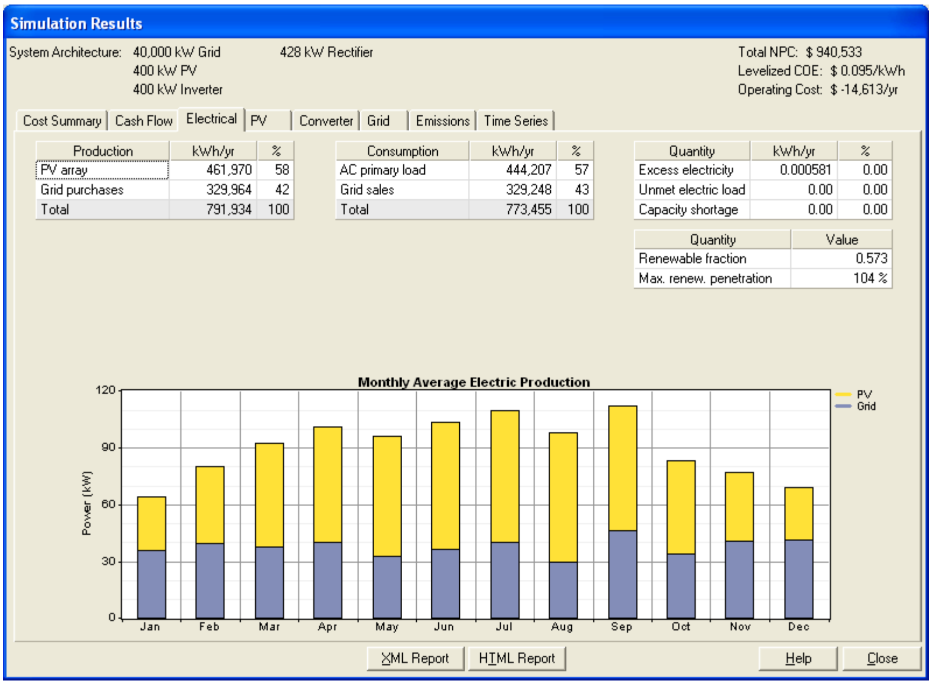

Simulation Results

System Architecture: 40,000 kW Grid, 400 kW PV, 400 kW Inverter, 428 kW Rectifier

Total NPC: $ 940,533
Levelized COE: $ 0.095/kWh
Operating Cost: $ -14,613/yr

Production	kWh/yr	%
PV array	461,970	58
Grid purchases	329,964	42
Total	791,934	100

Consumption	kWh/yr	%
AC primary load	444,207	57
Grid sales	329,248	43
Total	773,455	100

Quantity	kWh/yr	%
Excess electricity	0.000581	0.00
Unmet electric load	0.00	0.00
Capacity shortage	0.00	0.00

Quantity	Value
Renewable fraction	0.573
Max. renew. penetration	104 %

Fig. 1.28. Electric results of simulation with the electrical grid containing panels PV of 400 kW

1.2.1.6.2 Configuration with only wind turbines

The results of the simulation are in the Fig. 1.28. The best design corresponds to the installation of 10 wind turbine PGE 25. The return of investment is very good for this configuration. The calculation for 25 years gives a price of 5,2 c$ / kWh, better than the scenario with only the electrical grid EDF.

This result is to put in perspective. On one hand the study of the wind potential is not rather rigorous. On the other hand, the costs of functioning and maintenance of this wind turbine are low as they are a little bit suspects. Finally, the repurchase of electricity is guaranteed only over 20 years.

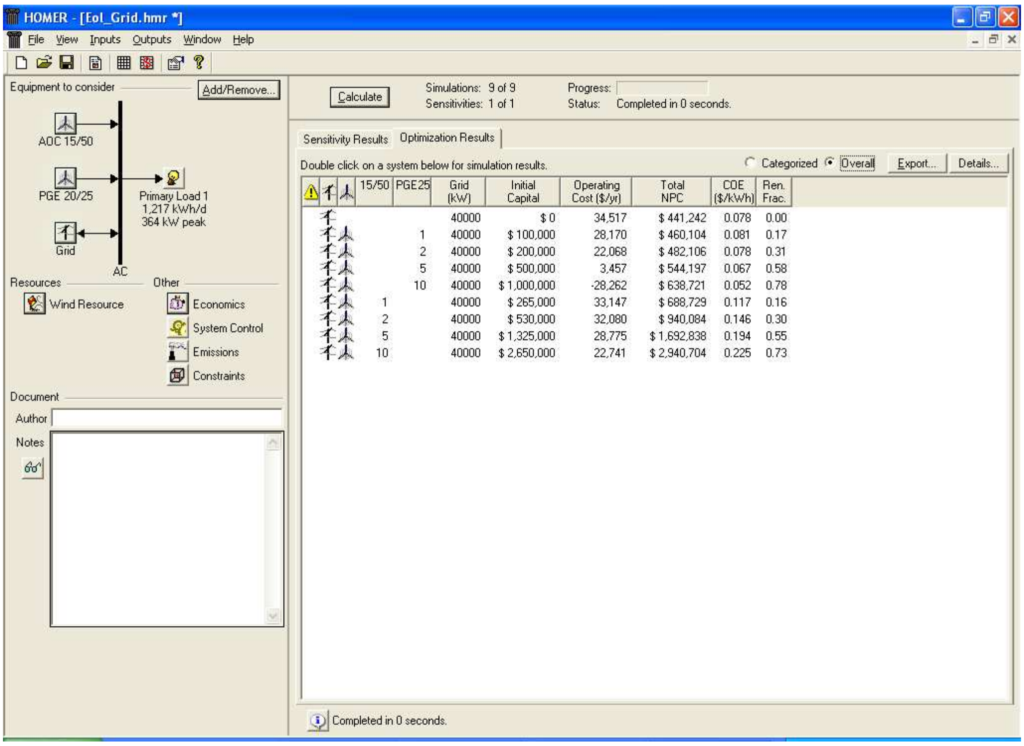

Simulations: 9 of 9
Sensitivities: 1 of 1
Progress:
Status: Completed in 0 seconds.

Double click on a system below for simulation results.

15/50	PGE25	Grid (kW)	Initial Capital	Operating Cost ($/yr)	Total NPC	COE ($/kWh)	Ren. Frac.
		40000	$ 0	34,517	$ 441,242	0.078	0.00
	1	40000	$ 100,000	28,170	$ 460,104	0.081	0.17
	2	40000	$ 200,000	22,068	$ 482,106	0.078	0.31
	5	40000	$ 500,000	3,457	$ 544,197	0.067	0.58
	10	40000	$ 1,000,000	-28,262	$ 638,721	0.052	0.78
1		40000	$ 265,000	33,147	$ 688,729	0.117	0.16
2		40000	$ 530,000	32,080	$ 940,084	0.146	0.30
5		40000	$ 1,325,000	28,775	$ 1,692,838	0.194	0.55
10		40000	$ 2,650,000	22,741	$ 2,940,704	0.225	0.73

Completed in 0 seconds.

Fig. 1.29. Results of calculation with the electrical grid of the port containing only wind turbines

The Fig. 1.29 illustrates the results on exchanges of electrical energy obtained with this optimal configuration. We can see that the wind production is 745.145 kWh/ year which is much bigger that the consumption (approximately 444.000 kWh / year). For the previous same reasons, we research a configuration where the production would be equivalent to the consumption.

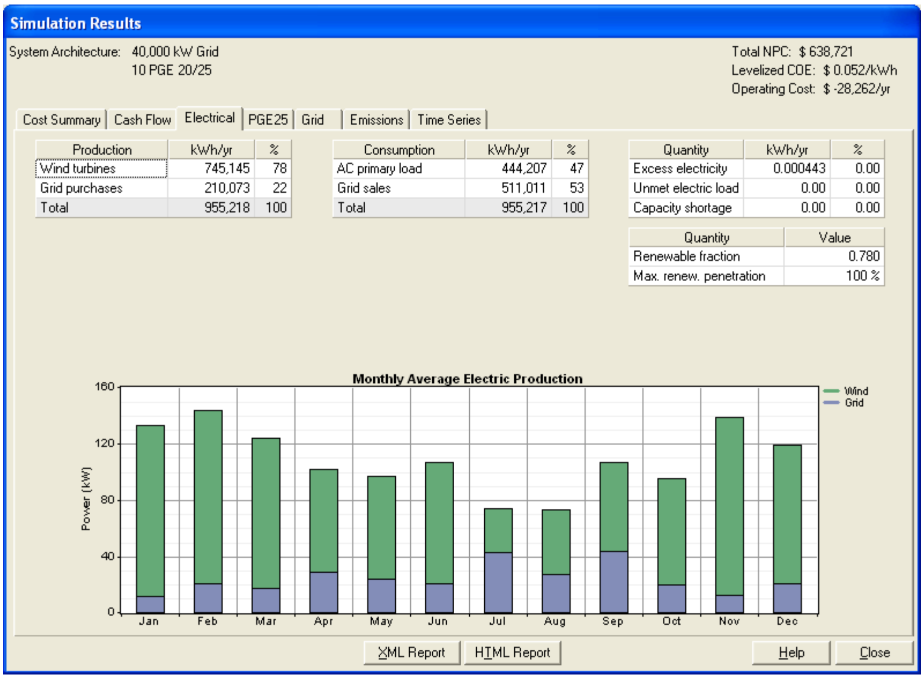

System Architecture: 40,000 kW Grid
10 PGE 20/25

Total NPC: $ 638,721
Levelized COE: $ 0.052/kWh
Operating Cost: $ -28,262/yr

Production	kWh/yr	%
Wind turbines	745,145	78
Grid purchases	210,073	22
Total	955,218	100

Consumption	kWh/yr	%
AC primary load	444,207	47
Grid sales	511,011	53
Total	955,217	100

Quantity	kWh/yr	%
Excess electricity	0.000443	0.00
Unmet electric load	0.00	0.00
Capacity shortage	0.00	0.00

Quantity	Value
Renewable fraction	0.780
Max. renew. penetration	100 %

Fig. 1.30. Electric Result for a configuration with 10 wind turbines PGE 25

We can see in the Fig. 1.30 that we aren’t far from this objective when we consider 5 wind turbines. In effect, the electric power production is 372.573 kWh/year.

1.2.1.6.3 Configuration wtih PV panels and wind turbines

A last study is realized by trying to associate wind turbine and PV panels which produce he same quantity of energy, approximately the half of energy consumed in the port for every technology. For this, we suppose that the price of purchase of electricity produced by the renewable source is an average of previous both price list ($9,4 c€ / kWh or 11,55 c$ / kWh).

The Fig. 1.31 illustrates the results for this simulation. With the previous results, the configuration with 3 wind turbine and 200 kW of panels PV is chosen. The cost of electricity is 9 c$ / kWh.

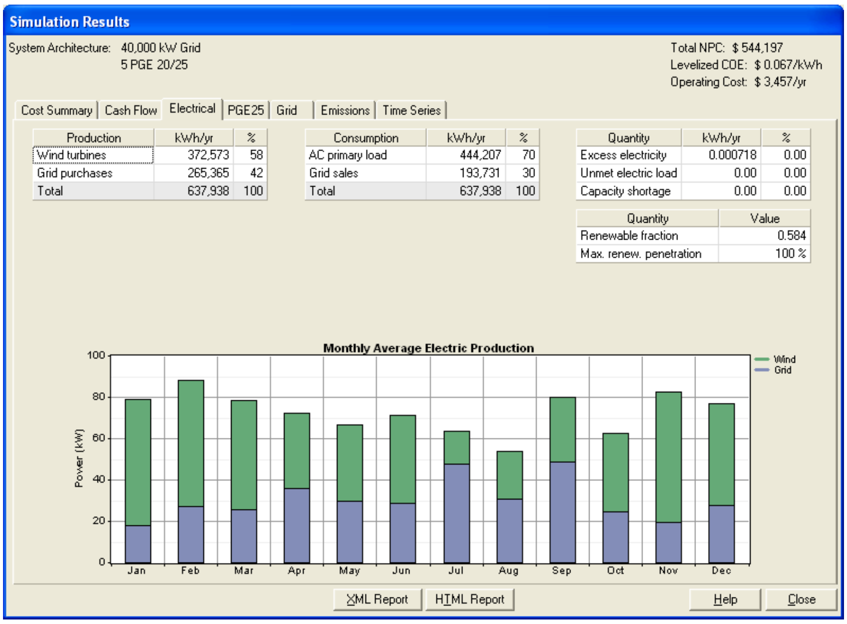

Simulation Results

System Architecture: 40,000 kW Grid
5 PGE 20/25

Total NPC: $ 544,197
Levelized COE: $ 0.067/kWh
Operating Cost: $ 3,457/yr

Production	kWh/yr	%
Wind turbines	372,573	58
Grid purchases	265,365	42
Total	637,938	100

Consumption	kWh/yr	%
AC primary load	444,207	70
Grid sales	193,731	30
Total	637,938	100

Quantity	kWh/yr	%
Excess electricity	0.000718	0.00
Unmet electric load	0.00	0.00
Capacity shortage	0.00	0.00

Quantity	Value
Renewable fraction	0.584
Max. renew. penetration	100 %

Fig. 1.31. Electric result for configuration with 5 wind turbines PGE 25

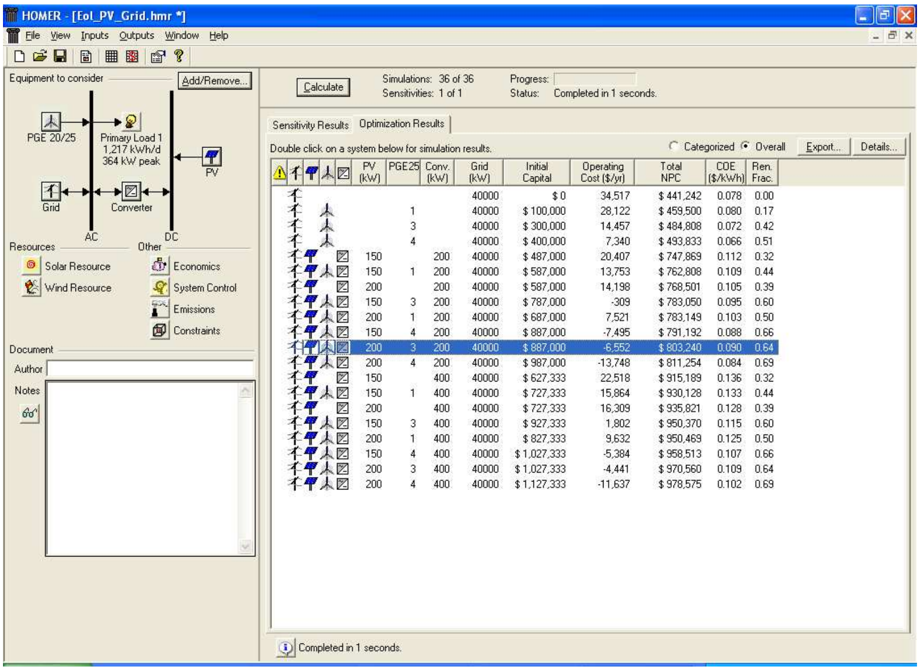

Simulations: 36 of 36
Sensitivities: 1 of 1
Progress:
Status: Completed in 1 seconds.

Double click on a system below for simulation results.

PV (kW)	PGE25	Conv. (kW)	Grid (kW)	Initial Capital	Operating Cost ($/yr)	Total NPC	COE ($/kWh)	Ren. Frac.
			40000	$ 0	34,517	$ 441,242	0.078	0.00
	1		40000	$ 100,000	28,122	$ 459,500	0.080	0.17
	3		40000	$ 300,000	14,457	$ 484,808	0.072	0.42
	4		40000	$ 400,000	7,340	$ 493,833	0.066	0.51
150		200	40000	$ 487,000	20,407	$ 747,869	0.112	0.32
150	1	200	40000	$ 587,000	13,753	$ 762,808	0.109	0.44
200		200	40000	$ 587,000	14,198	$ 768,501	0.105	0.39
150	3	200	40000	$ 787,000	-309	$ 783,050	0.095	0.60
200	1	200	40000	$ 687,000	7,521	$ 783,149	0.103	0.50
150	4	200	40000	$ 887,000	-7,495	$ 791,192	0.088	0.66
200	3	200	40000	$ 887,000	-6,552	$ 803,240	0.090	0.64
200	4	200	40000	$ 987,000	-13,748	$ 811,254	0.084	0.69
150		400	40000	$ 627,333	22,518	$ 915,189	0.136	0.32
150	1	400	40000	$ 727,333	15,864	$ 930,128	0.133	0.44
200		400	40000	$ 727,333	16,309	$ 935,821	0.128	0.39
150	3	400	40000	$ 927,333	1,802	$ 950,370	0.115	0.60
200	1	400	40000	$ 827,333	9,632	$ 950,469	0.125	0.50
150	4	400	40000	$ 1,027,333	-5,384	$ 958,513	0.107	0.66
200	3	400	40000	$ 1,027,333	-4,441	$ 970,560	0.109	0.64
200	4	400	40000	$ 1,127,333	-11,637	$ 978,575	0.102	0.69

Completed in 1 seconds.

Fig. 1.32. Results of calculation with the electrical grid in the port containing wind turbines and panels PV

The Fig. 1.33 shows the exchanges of electrical energy for this configuration. We observe that wind turbine produce 223.543 kWh / year, and that panel PV produces 230.985 kWh / year (sum of two 454.000 kWh / year). We produce more PV energy, the average price of repurchase of electricity previously done should be higher, what lowers the cost of electricity obtained with this configuration.

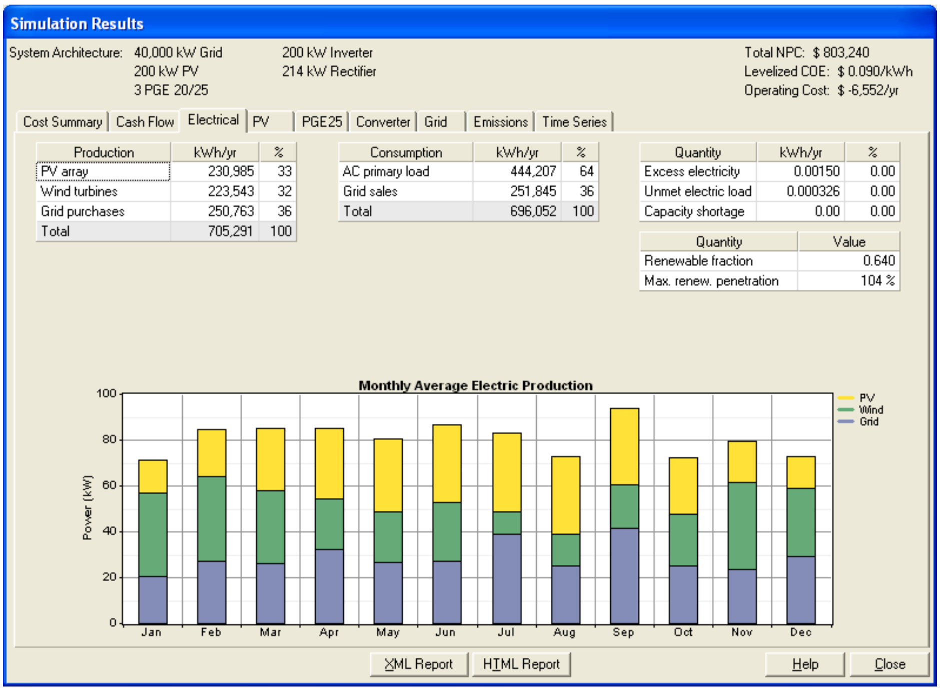

Simulation Results

System Architecture: 40,000 kW Grid; 200 kW PV; 3 PGE 20/25; 200 kW Inverter; 214 kW Rectifier

Total NPC: $ 803,240
Levelized COE: $ 0.090/kWh
Operating Cost: $ -6,552/yr

Production	kWh/yr	%
PV array	230,985	33
Wind turbines	223,543	32
Grid purchases	250,763	36
Total	705,291	100

Consumption	kWh/yr	%
AC primary load	444,207	64
Grid sales	251,845	36
Total	696,052	100

Quantity	kWh/yr	%
Excess electricity	0.00150	0.00
Unmet electric load	0.000326	0.00
Capacity shortage	0.00	0.00

Quantity	Value
Renewable fraction	0.640
Max. renew. penetration	104 %

Fig. 1.33. Electric result of configuration with 3 wind turbine PGE 25 and 200 kW of panel PV

The Fig. 1.34 summarizes the costs for the configuration with 3 wind turbine PGE 25 and 200 kW of panels PV. We can see that the main costs are related to PV panels and to associated converters. Furthermore, the sale of renewable electricity allows to recover approximately 150.000 $ in 25 years.

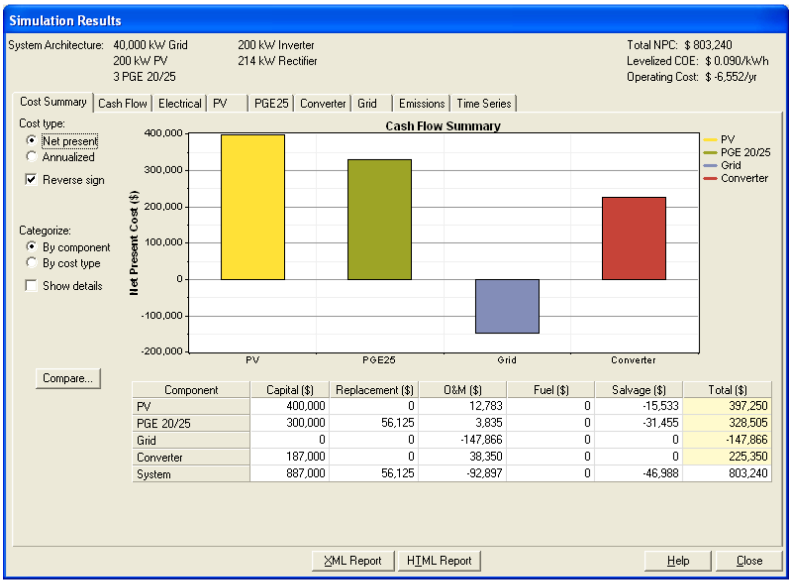

Simulation Results

System Architecture: 40,000 kW Grid; 200 kW PV; 3 PGE 20/25; 200 kW Inverter; 214 kW Rectifier

Total NPC: $ 803,240
Levelized COE: $ 0.090/kWh
Operating Cost: $ -6,552/yr

Cost type: ● Net present ○ Annualized
☑ Reverse sign
Categorize: ● By component ○ By cost type
☐ Show details

Component	Capital ($)	Replacement ($)	O&M ($)	Fuel ($)	Salvage ($)	Total ($)
PV	400,000	0	12,783	0	-15,533	397,250
PGE 20/25	300,000	56,125	3,835	0	-31,455	328,505
Grid	0	0	-147,866	0	0	-147,866
Converter	187,000	0	38,350	0	0	225,350
System	887,000	56,125	-92,897	0	-46,988	803,240

Fig. 1.34. Summary of the costs associated with the configuration with 3 wind turbines PGE 25 and 200 kW of panels PV

1.2.2 Design with renewable technology and the storage systems

In this section, the inclusion of a storage system is taken into account. Except the configuration of islanding which is not studied in Optimagrid, from a technico-economic point of view, the system of storage can have an interest to store energy when the price of purchase of electricity of EDF are low, and to feed the electrical grid of the port when these price are high (in P1 and P2). The HOMER software doesn't allow to configure this type of functioning.

Considering the high cost of storage system, is use is difficult to prove with HOMER. It's the reason why the storage system design is realized "with the hand ", without HOMER.

1.2.2.1 *Calculation of the necessary storage capacity*

Price list P2 applies only over 5 months, and the price P1 over 3 months. This returns the sizing task more difficult.

To simplify, we calculate the necessary storage capacity to supply port electricity needs during slot P1, that is twice two hours during three months. Over two other months, this system can be used to supply electricity in the slot corresponding to P2. The rest of the time, even if the interest is rather low, the system of storage could be used to store in P4 (the weekend) and supply with P5.

Consequently, the storage capacity is calculated on the consumption occurring in winter between 11 am and 1 pm. On EDF contract for cranes, we consume from December till February respectively 40.776, 30.429 and 25.501 kWh. On the second invoice corresponding to the consumption in workshops, cloakrooms and offices, we can read that we consume, in December till February, 15.928, 19.007 and 9.556 kWh.

The total energy consumed for this period is 141.197 kWh (approximately 1.535 kWh / day). To simplify, if we suppose that the consumption between 11am and 13pm is equal to the average over 24 hours, we estimate is value at 127 kWh.

1.2.2.2 *Calculation of necessary power*

With the profile of charge of the Fig. 1.17 of the report on the first part of the study, and by taking into account that this profile doesn't consider the consumption in workshops, offices and changing rooms (1/4 of the consumption), the power of the storage system can be designed to 100 kW. If the additional cost is important, we could also design the nominal power of the storage system at 80 kW.

In these conditions, the storage system cannot supply the whole power to the loads. When this will become the power will be obtained from the main grid (EDF).

1.2.2.3 *Calculation of economies which can be realized*

During three months, in the first bracket P1, we could have electricity at 8,3 c$/kWh instead of $35,9 c$/kWh. The corresponding economies would be 35 $/day, that is for 25 years 80.620 $.

During three months, in the second bracket P1, we could have electricity at 15,5 c$/kWh instead of 35,9 c$/kWh. The corresponding economies would be 26 $/day, that is for 25 years 59.590 $.

During two months, at the beginning of bracket P2, we could have some electricity in 8,3 $/kWh instead of 15,5 c$/kWh. The corresponding economies would be 9$a day, that is for 25 years 13.940 $.

Economies over 25 years corresponding to these 5 months would be 154.150 $. In reality, we couldn't keep a money in the week ends. Then this sum is reduced to 110.110 $.

For the other 7 months, on Monday morning, we could have electricity at 4,1 c$/kWh instead of 6,8 c$/kWh. The corresponding economies would be over 25 years of 2.600 $.

Consequently, economies which correspond to a storage system with a capacity of 127 kWh would be, over 25 years, 112.710 $. In reality, they would be smaller because of the real efficiency on the storage system and the incapacity to supply the totally of power during the peaks of power. Furthermore, the capacity of converters should be increased and reduce these economies.

1.2.2.4 *Choice of storage's system*

The type of storage system chosen by ESTIA was a Redox battery. ESTIA is interested by the characteristics of this type of storage. The Fig. 1.35 shows the costs for this type of technology. These data were supplied by CENER.

We can see that this technology is too expensive considering it as storage system, to have a profitable system.

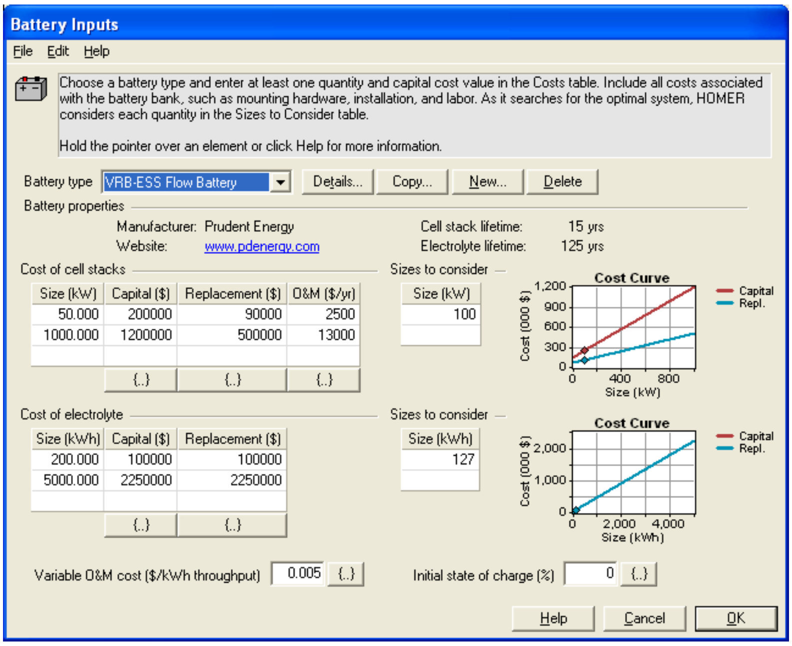

Battery Inputs

Choose a battery type and enter at least one quantity and capital cost value in the Costs table. Include all costs associated with the battery bank, such as mounting hardware, installation, and labor. As it searches for the optimal system, HOMER considers each quantity in the Sizes to Consider table.

Hold the pointer over an element or click Help for more information.

Battery type: VRB-ESS Flow Battery

Battery properties

Manufacturer: Prudent Energy
Website: www.pdenergy.com
Cell stack lifetime: 15 yrs
Electrolyte lifetime: 125 yrs

Cost of cell stacks

Size (kW)	Capital ($)	Replacement ($)	O&M ($/yr)
50.000	200000	90000	2500
1000.000	1200000	500000	13000

Sizes to consider

Size (kW)
100

Cost of electrolyte

Size (kWh)	Capital ($)	Replacement ($)
200.000	100000	100000
5000.000	2250000	2250000

Sizes to consider

Size (kWh)
127

Variable O&M cost ($/kWh throughput): 0.005

Initial state of charge (%): 0

Fig. 1.35. Costs of system of type Redox's storage

Other less expensive technologies exist, but the inclusion of a storage system in the port of Bayonne is difficult to justify from a point of view economic level with the current technologies of storage.

1.2.3 Conclusions

The study presented in this chapter allowed to design the renewable sources and the storage system. As said above, this design depends on various parameters with values that we don't know exactly.

The renewable sources were designed for that the production corresponds to the annual consumption on the site of Tarnos. We have chosen 3 wind turbines PGE 25 of 25 kW and 200 kW of panels PV.

The design of the storage system was realized "with the hand", because of the difficulty taking into account constraints with HOMER. The capacity of the storage system shall be 127 kWh and the power of 100 kW.

1.3 Modelling

1.3.1 Eurostag modelling

The simulations realized on Eurostag are based on models supplied by the library (bookcase) of this software. As novelty with regard to the simulations realized in the first phase of this study, we represent in this second phase two types of renewable sources: wind turbines and panels PV. Their modelling on Eurostag is described in the following sections.

1.3.1.1 Wind Turbine modeling

This model represents a fixed speed wind turbine. The turbine is connected to a squirrel-cage asynchronous machine.

1.3.1.1.1 General description

This kind of wind turbine consists of fixed speed turbine (neglecting the 1 to 2% fluctuation due to the slip of asynchronous generator) connected via a gearbox to an induction generator. The macroblock describes hereafter represents the energy conversion from the wind speed to the mechanical torque. It has to be coupled with a induction machine. It includes the aerodynamic equation (wind speed --> aerodynamic torque CM). The Fig. 1.36 represents the evolution of the mechanical torque in terms of the wind speed.

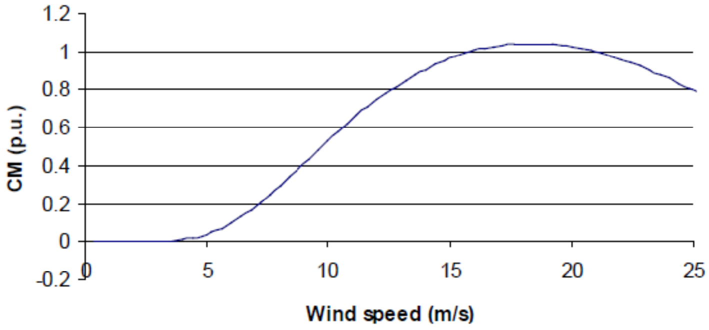

Fig. 1.36. Mechanical torque vs wind speed.

It is recommended to connect to this wind turbine a speed protection in order to trip the asynchronous generator in stalling conditions.

1.3.1.1.2 Eurostag model

Name : IMSTALL

Table 1.1. Wind Turbine model parameters

Parameters		**Values**
		Set 1
C1	Parameters of the equation given mechanical torque (p.u.) versus the wind speed (m/s)	175
C2		-0.155
C3		34
VCUTIN	Cut in wind speed (m/s)	4
VCUTOUT	Cut out wind speed (m/s)	25.0
%FVCM	Wind speed (m/s) versus mechanical torque (p.u.) (for initialization)	

Input variable: OMEGA, rotor speed

Output variable: CM, mechanical torque

Setpoint: @VENT, user defined wind speed (setpoint block 1 for step variation, setpoint block 7 for wind speed variation)

1.3.1.2 PV panels modeling

1.3.1.2.1 General description

The proposed model includes a solar array feeding, a dc capacitor and a power conditioner formed by a chopper, a dc capacitor and an inverter that converts dc power to ac power output (see Fig. 1.37). It includes current, voltage and frequency control.

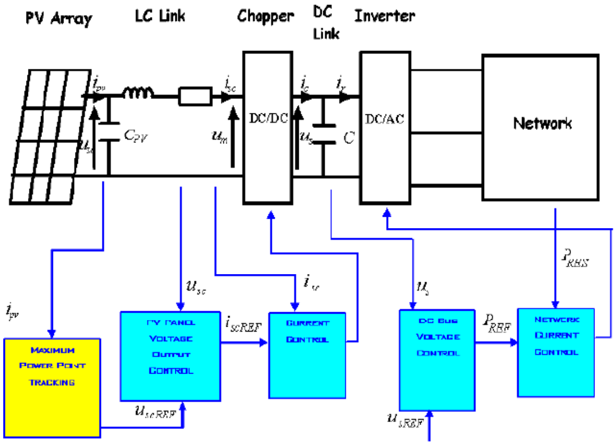

Fig. 1.37. General description of the photovoltaic model.

The output current and voltage of the photovoltaic (PV) panel are set to match the maximum power point that depends on insolation (incoming solar radiation) and temperature. The method used is maximum power point tracking (MPPT) control which continuously tracks and matches the output characteristics of the solar array to the input characteristics of the converter. The model simulates the MPPT by using a piecewise function to generate the solar array output voltage from a function of the photovoltaic panel current, the insolation and the temperature.

During the initialization phase, the number of photovoltaic panels needed to reach the injector rated power is calculated from the rated power PR of one panel. The values presented hereunder are those of a unitary 150 W photovoltaic array.

One input of the model is @G, the photovoltaic panel irradiance level in W/m^2. The ratio of the rated power generated by the injector depends directly on this parameter but also on the ambient temperature.

The model takes into account the following features:

- The purpose of the interface with the network is to maintain the DC bus voltage at a reference value and to inject into the grid a current in phase with the voltage on the network;
- The proposed model corresponds to a current injector. The electrical output is modelled by a negative consumption.

1.3.1.2.2 Model limitation

In performing the load-following function, the frequency deviation is not taken into account.

The model does not include the start-up transients.

The commutation losses in the converter and the losses in the inductive filter are neglected. The power produced by the primary source is equal to the power at the connection node at the network.

1.3.1.2.3 Eurostag model

Name : INTERPV

Table 1.2. Photovoltaic model parameters

Parameters		Values
		Set 1
ALPHAT	Temperature coefficient of current (A/°C)	$2.06*10^{-3}$
BETAOCT	Temperature coefficient of voltage (V/°C)	$-77*10^{-3}$
CPV	Value of the DC bus capacitor at the PV panel output (F)	0.01
CS	Value of the DC bus capacitor at the chopper output (F)	0.05
GSTC	Irradiance level (standard conditions) (W/m^2)	1000
IMAX	Maximum value of the current through the inverter (A)	200
IMPP	Current at maximal power (A)	4.4
ISC	Short circuit current (A)	4.8
K1	Conversion constant	$1.175*10^{-2}$
NOCT	Normal operating cell temperature (°C)	45
PI	Constant π	3.14159
PR	Rated power of one PV panel (W)	0.00015
QSIUS	Parameter of the regulators of the DC capacitors voltage	1
RCOND	Internal resistance of the PV panel output DC capacitor (Ω)	10^5
RCPV	Internal resistance of the chopper output DC capacitor (Ω)	10^5
RS	Shunt resistance of the equivalent model (Ω)	0.91
TA	Ambient temperature (°C)	25
TAREF	Ambient temperature (standard conditions) (°C)	20
TAUIPV	Response time for the chopper (s)	10^{-3}
TRI	Response time for the inverter (s)	10^{-2}
TRUS	Parameter of the regulators of the DC capacitors voltage	0.1
TSTC	PV module temperature (standard conditions) (°C)	25.
URES	Grid nominal voltage (V)	400.
USREF	Reference value of the chopper output voltage (V)	700.
VCONDREF	Reference value of the DC capacitor voltage (V)	700.
VMPP	Voltage at maximal power (V)	34
VOC	Open circuit voltage (standard conditions) (V)	43.4

Input variables: V, module terminal voltage (p.u.)

P: active power output expressed in the base of the apparent rated power of the generator with a load convention (p.u.)

Output variables: I, current module (p.u.)

PHI: phase difference between current and terminal voltage (rad)

Remark: the injected current is in phase with the connection node voltage and the electrical output is modelled by a negative consumption. As a consequence, PHI is constant and equal to – π.

IEFFRES: current module (A)

Setpoint: @G, irradiance level (W/m^2)

Table 1.3. Other photovoltaic model parameters.

		x	y
%FINIT	Initial insolation (W/m^2) versus the initial PV panel output voltage (V)	0	4.35
		24.	50.57
		27	106.1
		30.	202.
		31.	302.
		34.	405.57
		34.00001	502.
		35.	705.47
		36.	806.8
		36.00001	906.
		37.	1010.
%FMPPT	PV panel output voltage (V) versus a function of the PV panel current, the insolation and the temperature (A)	x	y
		0	0.
		0.17535	24.
		0.40732	27.
		0.80508	30.
		1.261600	31.
		1.597900	34.
		2.097400	34.
		3.0244	35.
		3.437100	36.
		3.948300	36.
		4.3492	37.
%FMTINV	Initial PV panel output voltage (V) versus the power delivered by the PV array (W)	x	y
		0.	0.
		4.20816	24.
		10.99737	27.
		24.15210	30.
		39.10929	31.
		54.32826	34.
		71.31126	34.
		105.8537	35.
		123.7352	36.
		142.1384	36.
		160.9200	37.

1.4 Emulation of a wind turbine for the ENERGEA microgrid

Once the simulation results obtained, the ESTIA would work in a later phase to validate the results of the microarray experimental EneR-GEA. These experimental require advance preparation of this microarray. This includes developing both emulators contained in the experimental platform: a multi-source emulator and emulator wind (see the yellow part on the sources of electricity in Fig. 1.38).

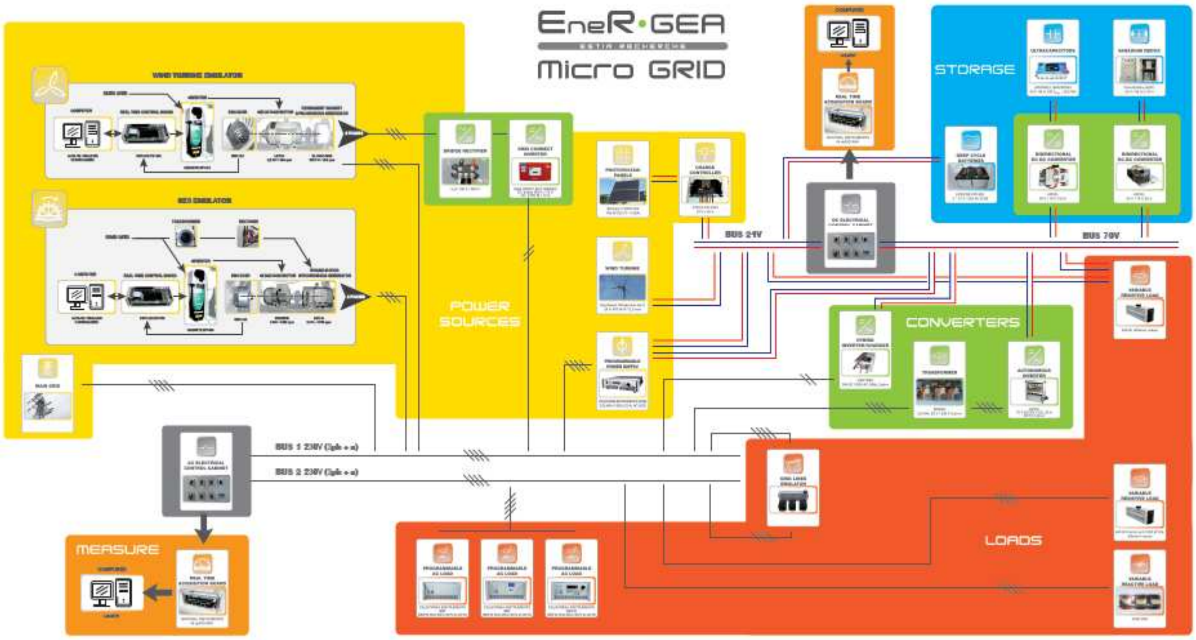

Fig. 1.38. EneR-GEA microgrid illustration

These emulators are designed exactly the same way as diesel emulator described in the report on the first part of this study. The only differance is the simulation model implemented in the emulator. For example, to emulate the wind, just implement the simulation model of wind described in Chapter 4 of this document.

1.5 Simulations

The study is done as a top-down process. Indeed, the section 3 of the report has permitted to size micro-grid components and define the models used for the simulation. In order to use the EUROSTAG tool it's necessary to know the maximum informations about the electrical infrasctructure.

1.5.1 Electrical infrastructure description

1.5.1.1 Electrical grid

Some elements of the electrical grid have benn presented in the GT2_Deliverable7 document. Hereafter will be presented in particular the electrical grid components defined for the EUROSTAG simulation.

1.5.1.1.1 Electrical grid characterisitics

In this modelisation we don't use electrical protection (circuit breaker, fuse). On the harbor grid 7 transformers are used. The voltage goes from 20 kV (EDF grid) to 5.5 kV and finally the cranes use 0.4 kV voltage. All electricity is triphased.

1.5.1.1.2 Electrical grid lines

This section details the characteristics of power lines:

- Crane GR11, Crane GR12, Crane GR13: 250m of cable 3x50mm² twisted AL 12/20kV + 200 m CU special cable 3x25mm² + 3x25mm²;
- Crane GR14: 250 m of cable 3x50mm² twisted AL 12/20kV + 200 m CU special cable 3x35mm² + 3x25mm²

The cables respect the standard reference NFC 33226 HT. More details can be found on harbor internal document (see ANNEX 2). The cranes characteristics can be found at the beginning of this report and also in the GT2_Deliverable7 document.

The Fig. 1.39 (see ANNEX 3) shows in detail the electrical grid modelised into Eurostag in order to do the simulations.

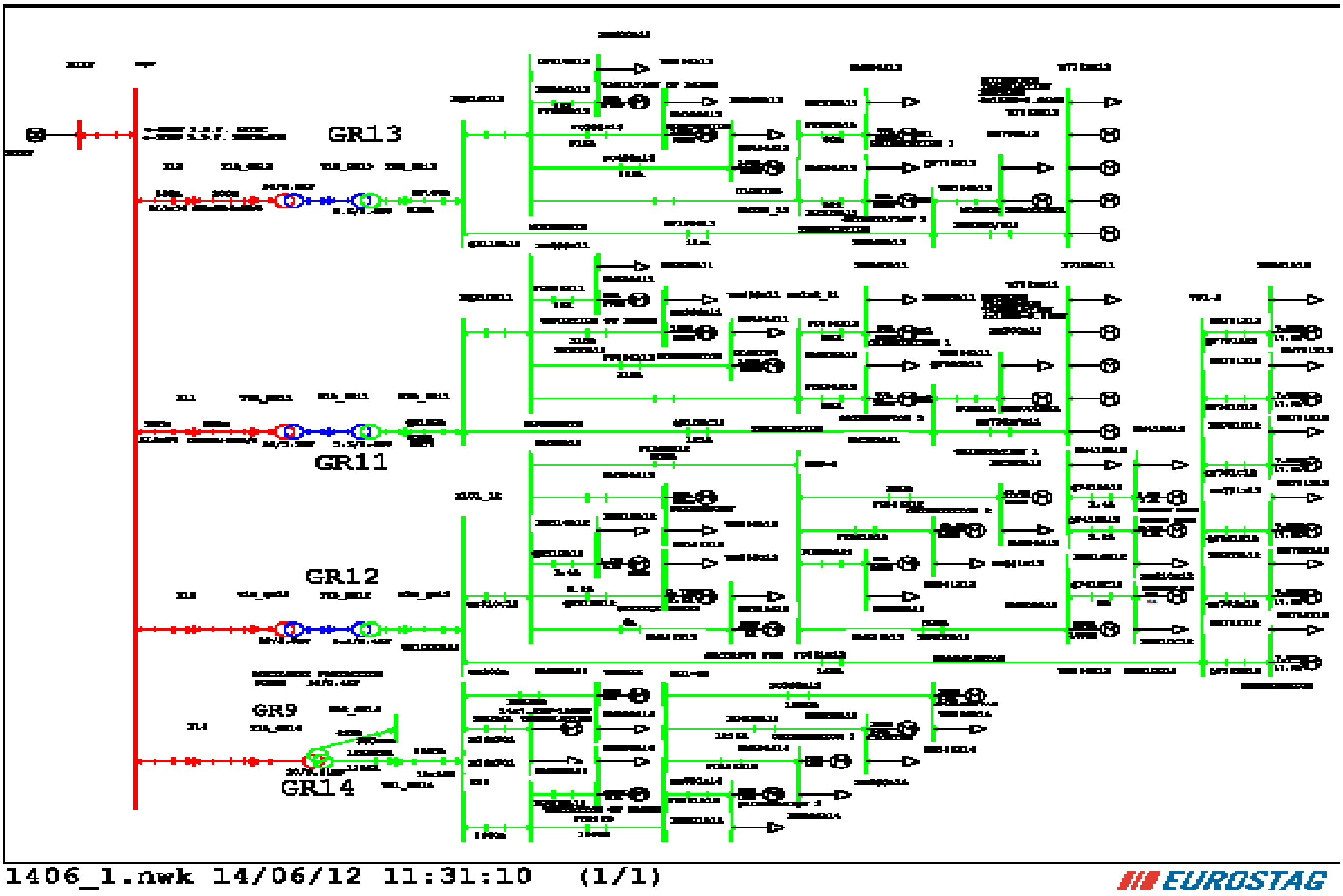

Fig. 1.39: Harbor grid model in EUROSTAG

In this part will be presented simulations without storage. This choice has been done, in order ton apply simply the sizing done with the HOMER simulation in the part §3.1.

1.5.2 Simulation with renewable resources

On HOMER, the configuration of the micro-grid is illustrated in Fig. 1.40.

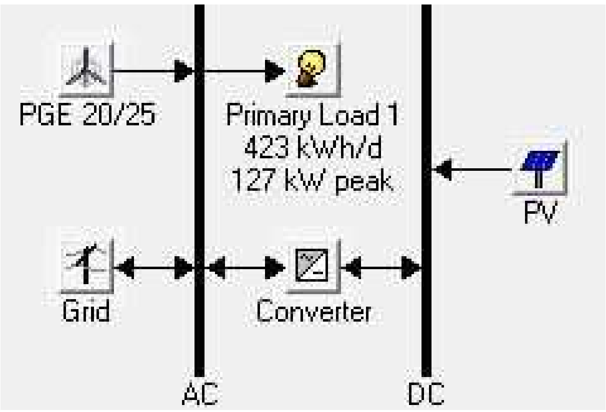

Fig. 1.40: HOMER micro-grid configuration

The configuration of the micro-grid illustrated in Fig. 1.40 was implemented using EUROSTAG®, the software for dynamic operation investigation and the main electrical scheme of the Tarnos harbor area. The parameters defined in the §5.1 have been used to define the micro-grid illustrated by the Fig. 1.41(see ANNEX 6). We have simplified the harbor micro-grid by not incorporating electrical protections.

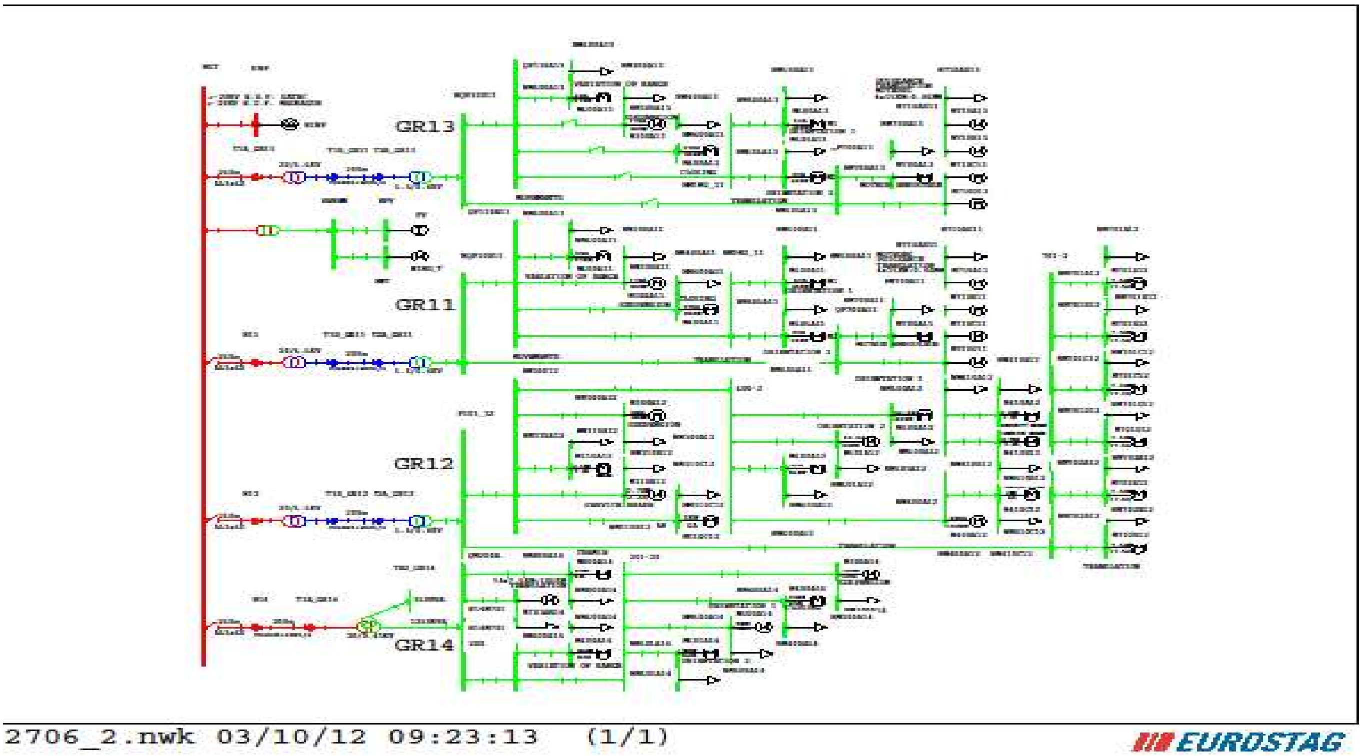

Fig. 1.41: Harbour micro-grid with wind turbine and PV panels

The Fig. 1.42 shows the real load profile of the crane 12 (see GT2_deliverable7 document).

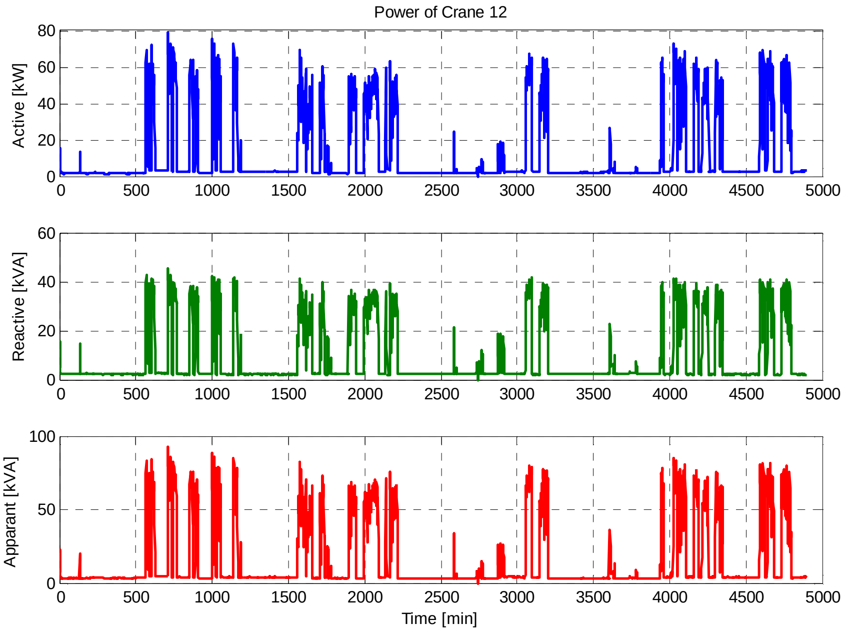

Fig. 1.42: Active, reactive and apparent power of crane 12

As can be seen in Fig. 1.43, using the EUROSTAG® microgrid dynamic model, it is possible to approximate in simulation the real load profile of the crane 12.

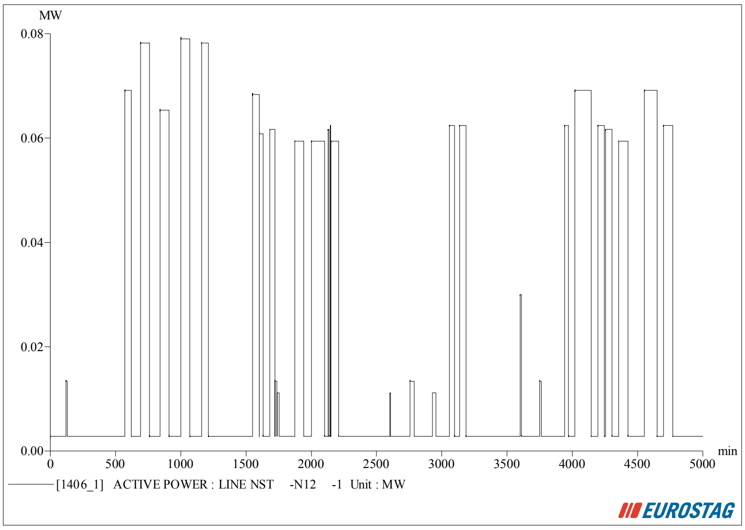

Fig. 1.43: EUROSTAG® simulation load profile of the crane 12

Many simulations have been conducted in order to validate the dynamic model of the micro-grid.

1.5.2.1 Only solar irradiation

In this part, the used renewable source is only the solar one. Fig. 1.44 shows the operation of the micro-grid according with the solar irradiation variation and load demand. At t=60s, when the solar irradiation level increases from 0 to 500 W/m^2, the power of the PV system rises from 0 to 0.16 MW.

At t=120s, another solar irradiation step (from 500 to 1000 W/m^2) is applied to the PV system input and the output power increases to the rated value (0.32 MW). As it can be seen, as soon as the solar irradiation increases, almost half of the total active power requested by cranes 12 and 13 (around 0.65 MW) will be supplied locally by the PV system. Consequently, the power requested from the main grid will decrease proportionally.

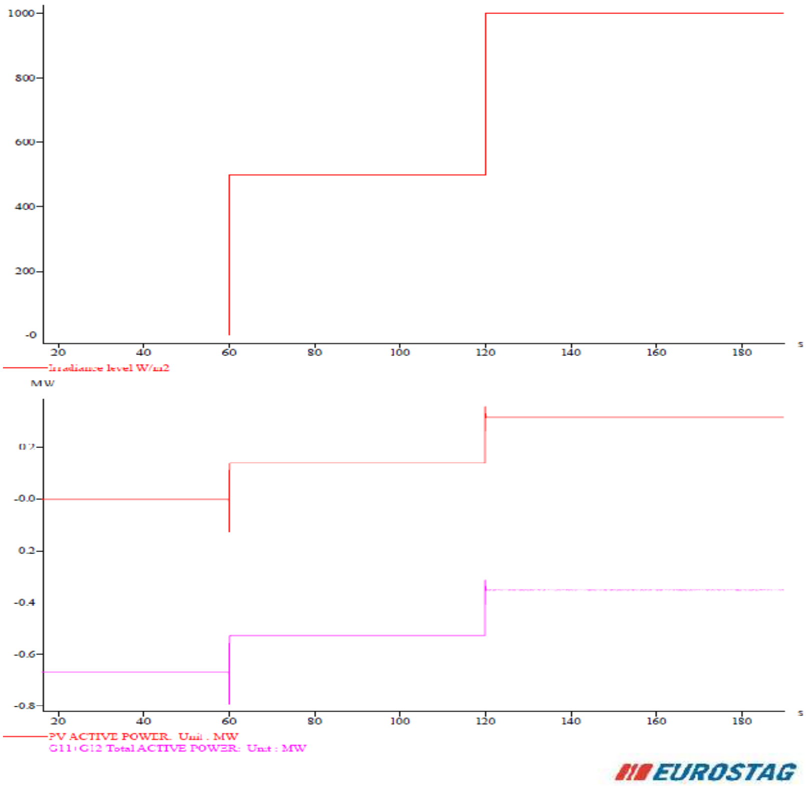

Fig. 1.44: Solar Irradiation, PV active power and total active power

1.5.2.2 Only wind resource

The same tests have been run varying the wind speed in the input of the wind turbine and the results are illustrated in Fig. 1.45.

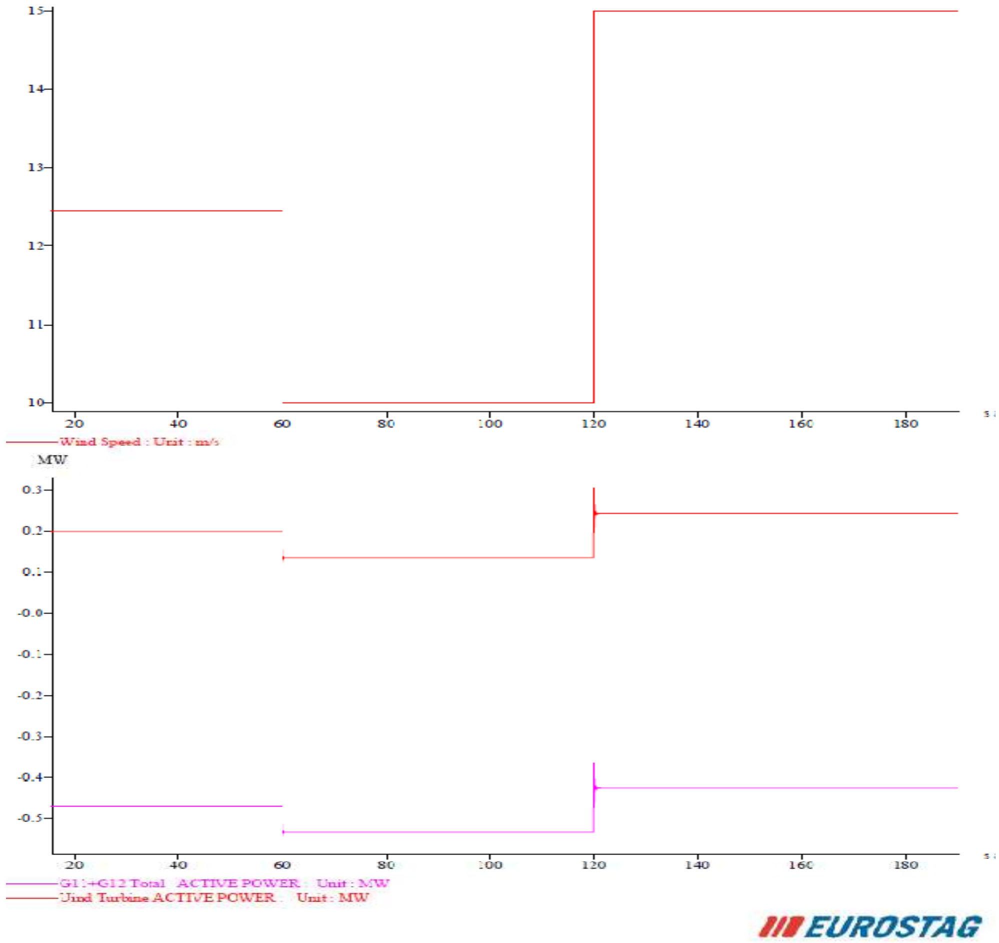

Fig. 1.45: Wind speed, Wind Turbine active power and total active

The step wind speed applied varies between 12.5 and 15 m/s, with an intermediary value of 10 m/s. As for the PV system, the power absorbed from the main grid in order to supply the power requested by cranes 12 and 13 will decrease according with the power produced by the wind turbine.

1.5.3 Conclusion

In this part, the first stage of a study made to design and investigate the dynamic operation of a micro-grid for an industrial harbor area has been presented. The operation of the obtained architecture was dynamically investigated using EUROSTAG® software. The first simulation results showed the accuracy and validate the micro-grid dynamic model. In future works, different simulation case studies will be investigated using the dynamic model in order to analyze the micro-grid stability.

1.6 Results of the study

This study of Bayonne port is composed of different parts. The chapter 1 has analysed the renewable resources.

The main conclusions for the wind resources are:

- The annual average speed of wind with a height of 50 m compared with the sea level on the site of Tarnos is 5,35 m/s;
- The wind is more powerful in winter than in summer;
- This resource is complementary with the curve of annual consumption of the site of Tarnos.

For the solar resources, the mean conclusions are:

- The annual average solar illumination is 0,15 kW / m^2;
- The solar potential is more important in summer than in winter. The annual evolution is very regular. This resource is complementary compared with the wind potential;

The daily variation of illumination is important. It’s problematic from the point of view of the smartgrid control, and can lead to use storage systems, according to the quantity of solar energy in the smartgrid.

The chapter 2, using HOMER software presented the design of a microgrid taking into account renewable sources, harbor consuption, storage system. The microgrid without storage seems to be economically more interesting. It’s composed by 3 wind turbines PGE 25 of 25 kW and 200 kW of panels PV.

But, taking into account the aim of the project to product locally what is consumed, the design of the storage system was realized “with the hand”, because of the difficulty taking into account constraints with HOMER. The capacity of the storage system shall be 127 kWh and the power of 100 kW.

The chapter 4 presents more precisely the mathematical models developed in order to study dynamically with the ENERGEA microgrid the Tarnos harbor. This modelisation using emulators is explained in the Chapter 5.

However for the moment, this study have been replaced by a study done on Eurostag.

The Chapter 5 show results of the simulation done without taking into account the storage system. The designed grid with WT and PV panels, is able to replace the main grid electricity with a good quality of energy when the renewable resources are available.

In conclusion, this work shows that with the present purchase prices is complicated to install a micro-grid in the harbor of Tarnos. Now, in a technical point of view, the harbor seems to be a place where it would be appropriate to develop a micro-grid because renewable energy resources are important and available spaces for installing production means are big.

2 WALQA TECHNOLOGY PARK

2.1 Installation description

ITHER Project is the development of infrastructure for hydrogen generation from renewable energies, belonging to Foundation for the development of new hydrogen technologies in Aragón. The ultimate aim of the project is to create a solid infrastructure for various renewable power generation technologies, allowing a laboratory feeding hydrogen production by electrolysis located in Hydrogen Foundation building.

The following section shows the different generation systems and management:

- Wind generation.
- Solar generation.
- Electrical switchgear and distribution connection.

Walqa Technological Park has 100 kW more of photovoltaic power in OX – CTA building.

2.1.1 Wind generation installation

The small wind farm owned by The Hydrogen Foundation is composed by three wind turbines with a combined output power of 635 kW. These machines are from “repowering” because it is difficult to find this low level of power in new machines and they are cheaper in terms of device acquisition. Specifically wind generators installed are:

Table 2.1. Wind turbine characteristics in Walqa Technological Park.

DENOMINATION	**POWER (kW)**
Vestas Turbine V29	225 kW
Enercon Turbine – 33	330 kW
Lagerway Turbine two bladed	80 kW

Fig. 2.1. Wind turbines.

Table 2.2. Wind turbines characteristics.

VESTAS	ENERCON	LAGERWAY
Power: 225 kW	**Power: 330 kW**	**Power: 80 kW**
Height: 30 m.	**Height: 40 m.**	**Height: 40 m.**
Technology: Doubly fed asynchronous.	**Technology: Full converter synchronous.**	**Technology: Squirrel-cage asynchronous.**
Diameter: 27 m.	**Diameter: 33 m.**	**Diameter: 18 m.**

Three very different turbines were chosen in order to enhance research orientation of facility, because it's possible to test different technologies allowing greater flexibility. The distribution of these turbines along Walqa Technological Park can be seen in the image below.

Fig. 2.2. Wind turbine locations in Walqa Technological Park.

2.1.2 Photovoltaic installation

The microgrid also includes photovoltaic generation with an installed peak power of 100 kW, divided as follows:

Table 2.3. Characteristics of Photovoltaic installation.

DENOMINATION	POWER (kW)
Fixed installation in parking canopies	60 kW
ADES solar tracker	20 kW
DEGUER solar tracker	5 kW
MECASOLAR solar tracker	10 kW

Fig. 2.3. Fixed installation in parking canopies of Walqa Technological Park.

Just as the wind farm, there are various tracking technologies as both of their own solar panel. This only reinforces the research orientation of ITHER project. There are three photovoltaic generation technologies and two tracking technologies:

Table 2.4. Technologies of photovoltaic electric power generation.

TECHNOLOGY	EFFICIENCY
Polycrystalline	12%
Monocrystalline	14%
Heterogeneous Union	17%

Fig. 2.4. DEGUER solar trackers and behind MECASOLAR solar tracker.

Fig. 2.5. ADES solar tracker.

Table 2.5. Solar tracking technologies.

SOLAR TRACKING TECHNOLOGIES
Tracking by calendar or astronomical calendar
Tracking by maximum brightness point

2.1.3 Interconnection center

Finally, the Project has a central interconnection with medium voltage cells motorized automated, which by means of a PLC and SCADA, you can choose at any time whether to sell generated electricity as a generator attached to the special regime or the energy is sent to the Hydrogen Foundation laboratory to generate hydrogen by electrolysis. Below are some general diagrams of the facility, its location and interconnection of the different generators:

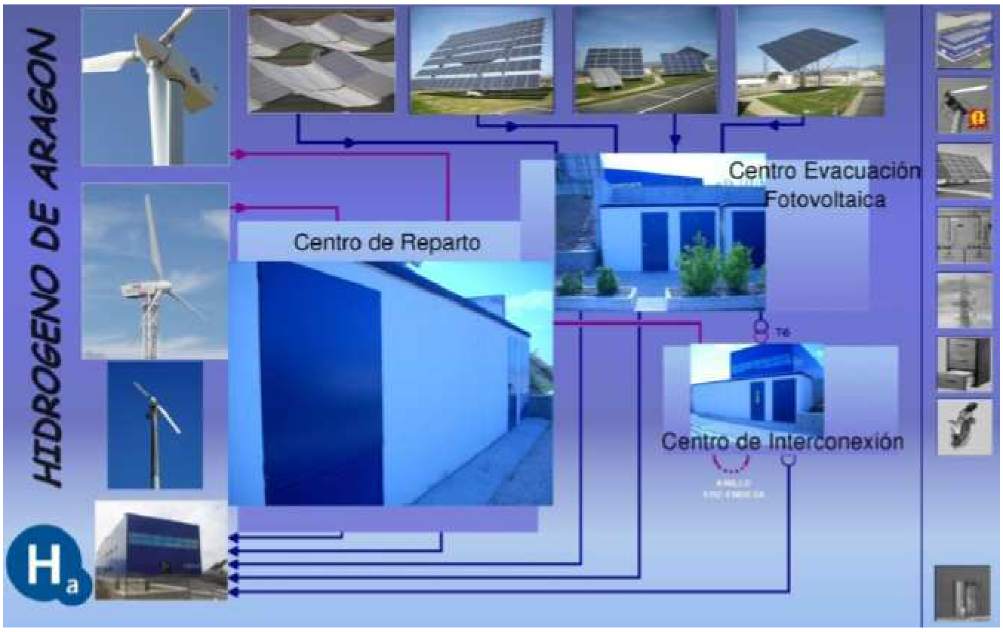

Fig. 2.6. Diagram of the Project ITHER.

Fig. 2.7. Locations of distribution centers and evacuation.

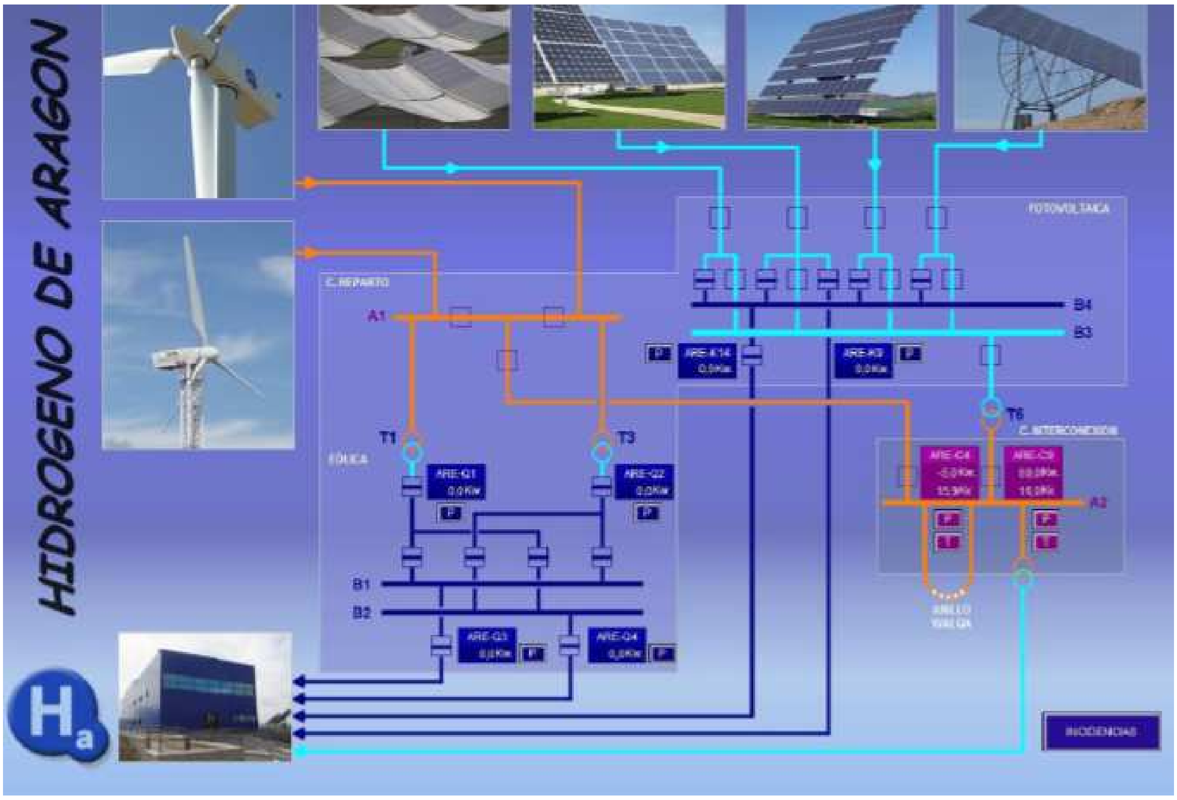

Fig. 2.8. Line diagram of the installation.

2.2 Introduction of the system in HOMER program

2.2.1 Introduction to HOMER

HOMER program is an optimization model for electric generation power systems, both isolated and connected to the grid. It simplifies equipment sizing.

To download the program free for 15 days can be done through the following website:

www.nrel.gov/homer

2.2.2 Mode of use of HOMER

The HOMER program uses input data describing the costs of each component and the availability of resources. HOMER simulates the operation of a system making energy balance calculations for each of the 8760 hours a year.

2.2.3 Case study introduction with energy storage

This section will introduce the electrical microgrid for analysis in HOMER program. It starts by entering the location coordinates and solar radiation data.

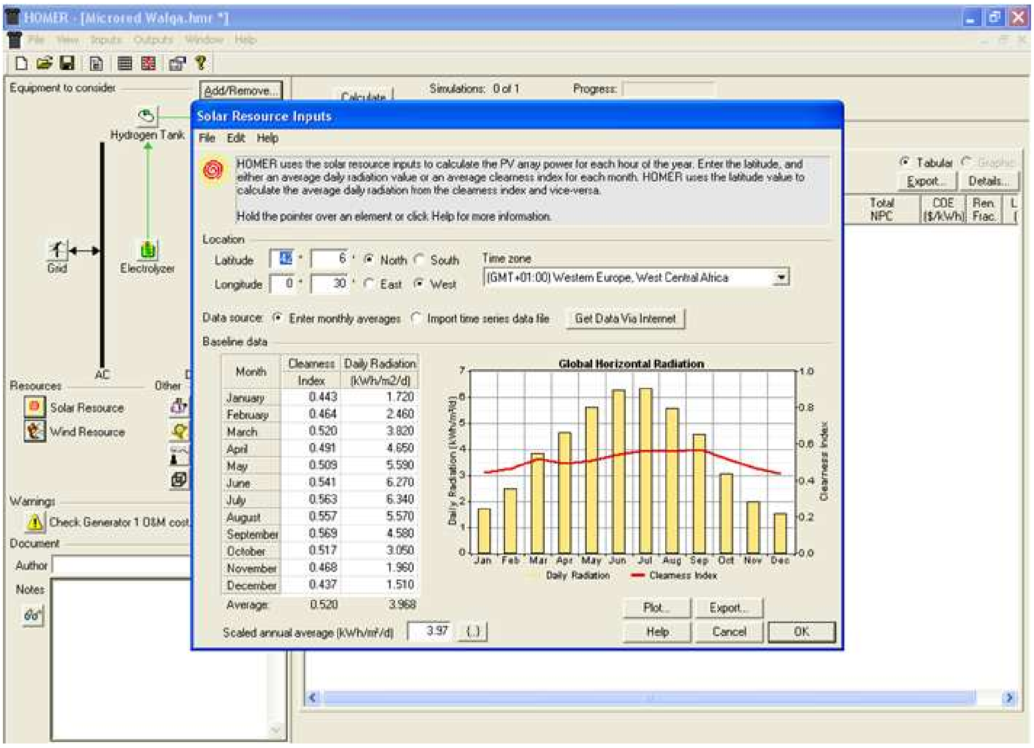

Simulations: 0 of 1

HOMER uses the solar resource inputs to calculate the PV array power for each hour of the year. Enter the latitude, and either an average daily radiation value or an average clearness index for each month. HOMER uses the latitude value to calculate the average daily radiation from the clearness index and vice-versa.

Hold the pointer over an element or click Help for more information.

Latitude 42 ° 6 ' ● North ○ South
Longitude 0 ° 30 ' ○ East ● West
Time zone (GMT+01:00) Western Europe, West Central Africa

Data source: ● Enter monthly averages ○ Import time series data file

Month	Clearness Index	Daily Radiation (KWh/m2/d)
January	0.443	1.720
February	0.464	2.460
March	0.520	3.820
April	0.491	4.650
May	0.509	5.590
June	0.541	6.270
July	0.563	6.340
August	0.557	5.570
September	0.569	4.580
October	0.517	3.050
November	0.468	1.960
December	0.437	1.510
Average	0.520	3.968

Scaled annual average (kWh/m²/d) 3.97

Fig. 2.9. Introduction of solar radiation data.

Then, PV system data will be inserted.

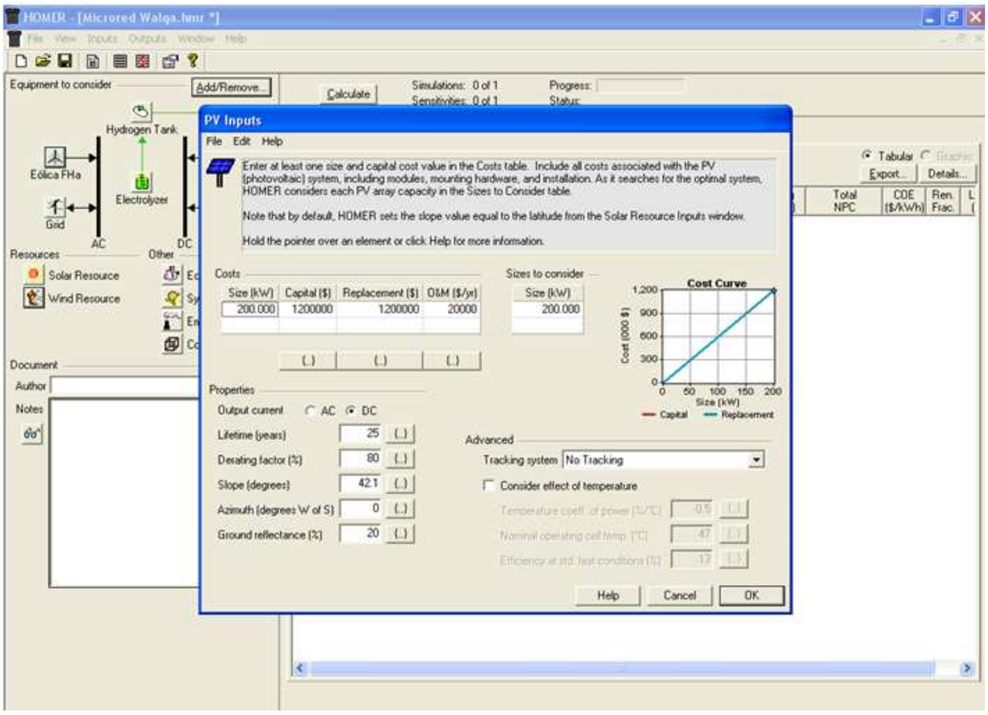

Simulations: 0 of 1
Sensitivities: 0 of 1
Progress:
Status:

Enter at least one size and capital cost value in the Costs table. Include all costs associated with the PV (photovoltaic) system, including modules, mounting hardware, and installation. As it searches for the optimal system, HOMER considers each PV array capacity in the Sizes to Consider table.

Note that by default, HOMER sets the slope value equal to the latitude from the Solar Resource Inputs window.

Hold the pointer over an element or click Help for more information.

Costs

Size (kW)	Capital ($)	Replacement ($)	O&M ($/yr)
200.000	1200000	1200000	20000

Sizes to consider

Size (kW)
200.000

Properties

Output current ○ AC ● DC
Lifetime (years) 25
Derating factor (%) 80
Slope (degrees) 42.1
Azimuth (degrees W of S) 0
Ground reflectance (%) 20

Advanced

Tracking system No Tracking
☐ Consider effect of temperature
Temperature coeff. of power (%/°C) -0.5
Nominal operating cell temp. (°C) 47
Efficiency at std. test conditions (%) 13

Fig. 2.10. PV system data.

After defining PV system, we continue defining wind data.

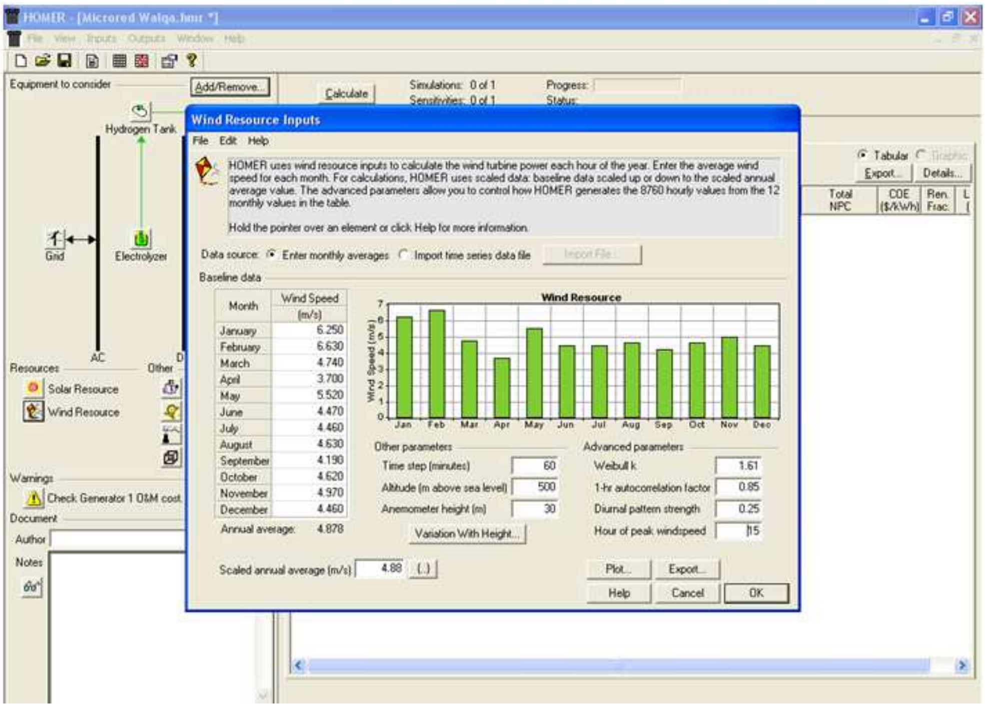

Simulations: 0 of 1
Sensitivities: 0 of 1
Progress:
Status:

HOMER uses wind resource inputs to calculate the wind turbine power each hour of the year. Enter the average wind speed for each month. For calculations, HOMER uses scaled data: baseline data scaled up or down to the scaled annual average value. The advanced parameters allow you to control how HOMER generates the 8760 hourly values from the 12 monthly values in the table.

Hold the pointer over an element or click Help for more information.

Data source: ● Enter monthly averages ○ Import time series data file

Baseline data

Month	Wind Speed (m/s)
January	6.250
February	6.630
March	4.740
April	3.700
May	5.520
June	4.470
July	4.460
August	4.630
September	4.190
October	4.620
November	4.970
December	4.460

Annual average: 4.878

Other parameters

Time step (minutes) 60
Altitude (m above sea level) 500
Anemometer height (m) 30

Advanced parameters

Weibull k 1.61
1-hr autocorrelation factor 0.85
Diurnal pattern strength 0.25
Hour of peak windspeed 15

Scaled annual average (m/s) 4.88

Fig. 2.11. Wind data in Walqa Technological Park.

We enter wind installation data.

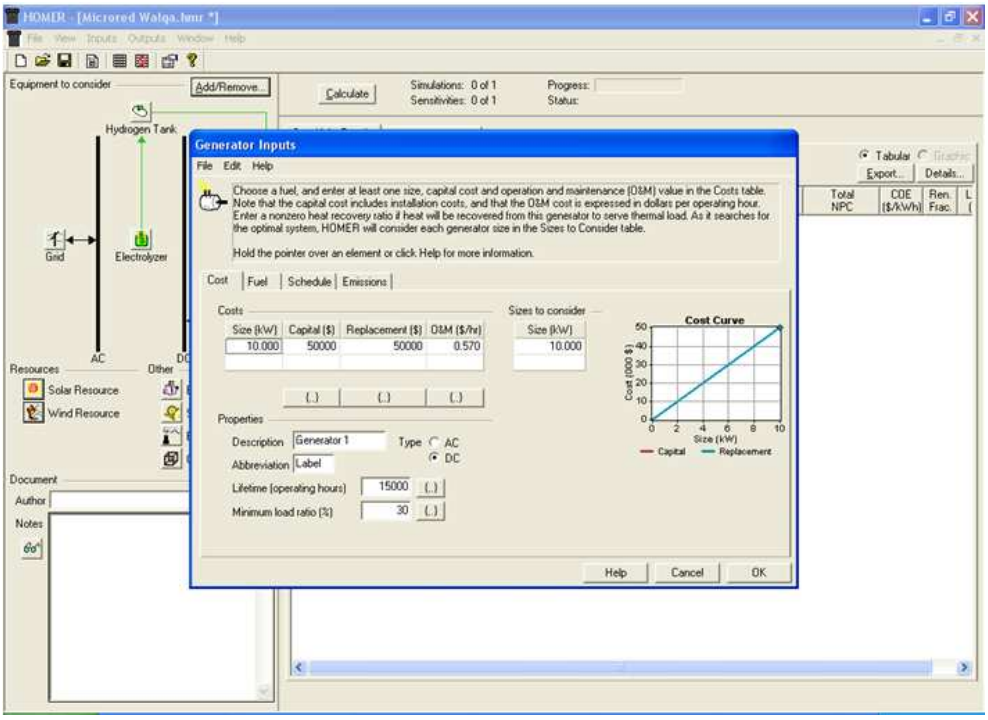

Simulations: 0 of 1
Sensitivities: 0 of 1
Progress:
Status:

Choose a fuel, and enter at least one size, capital cost and operation and maintenance (O&M) value in the Costs table. Note that the capital cost includes installation costs, and that the O&M cost is expressed in dollars per operating hour. Enter a nonzero heat recovery ratio if heat will be recovered from this generator to serve thermal load. As it searches for the optimal system, HOMER will consider each generator size in the Sizes to Consider table.

Hold the pointer over an element or click Help for more information.

Costs

Size (kW)	Capital ($)	Replacement ($)	O&M ($/hr)
10.000	50000	50000	0.570

Sizes to consider

Size (kW)
10.000

Properties

Description: Generator 1
Abbreviation: Label
Type: ○ AC ● DC
Lifetime (operating hours): 15000
Minimum load ratio (%): 30

Fig. 2.12. Wind installation in Walqa Technological Park.

HOMER has the limitation that only it's possible to enter a turbine technology in the simulation thus simulates a wind generator whose output is the sum of the wind farm that is available in Walqa Technological Park.

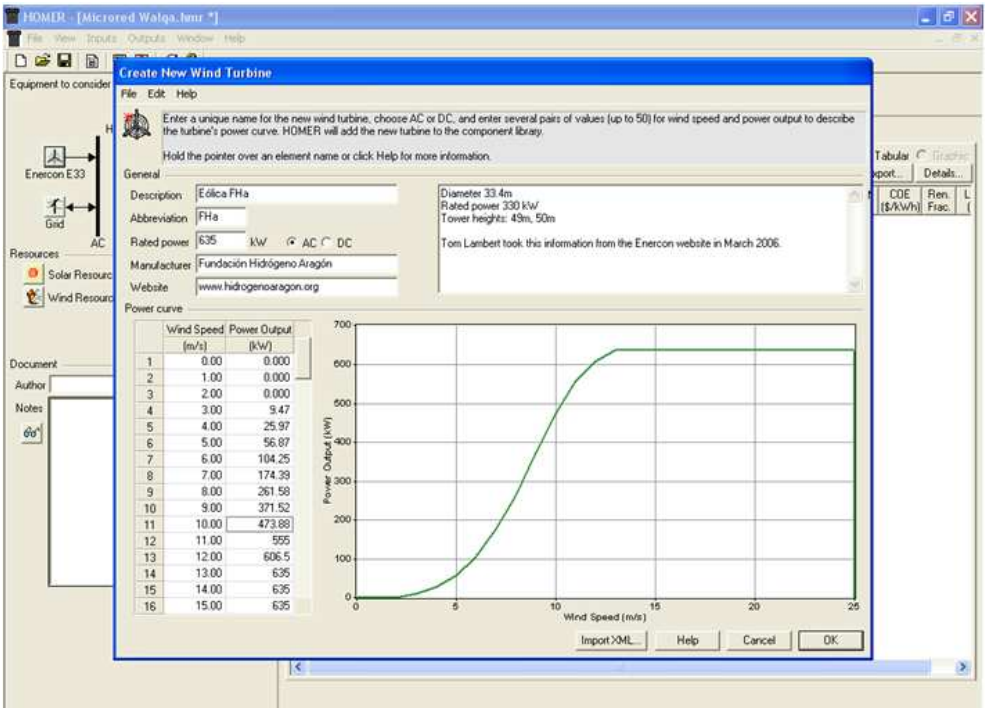

Enter a unique name for the new wind turbine, choose AC or DC, and enter several pairs of values (up to 50) for wind speed and power output to describe the turbine's power curve. HOMER will add the new turbine to the component library.

Hold the pointer over an element name or click Help for more information.

General

Description: Eólica FHa
Abbreviation: FHa
Rated power: 635 kW ● AC ○ DC
Manufacturer: Fundación Hidrógeno Aragón
Website: www.hidrogenoaragon.org

Diameter 33.4m
Rated power 330 kW
Tower heights: 49m, 50m

Tom Lambert took this information from the Enercon website in March 2006.

Power curve

	Wind Speed (m/s)	Power Output (kW)
1	0.00	0.000
2	1.00	0.000
3	2.00	0.000
4	3.00	9.47
5	4.00	25.97
6	5.00	56.87
7	6.00	104.25
8	7.00	174.39
9	8.00	261.58
10	9.00	371.52
11	10.00	473.88
12	11.00	555
13	12.00	606.5
14	13.00	635
15	14.00	635
16	15.00	635

Fig. 2.13. Wind farm data.

Data for photovoltaic converters is entered.

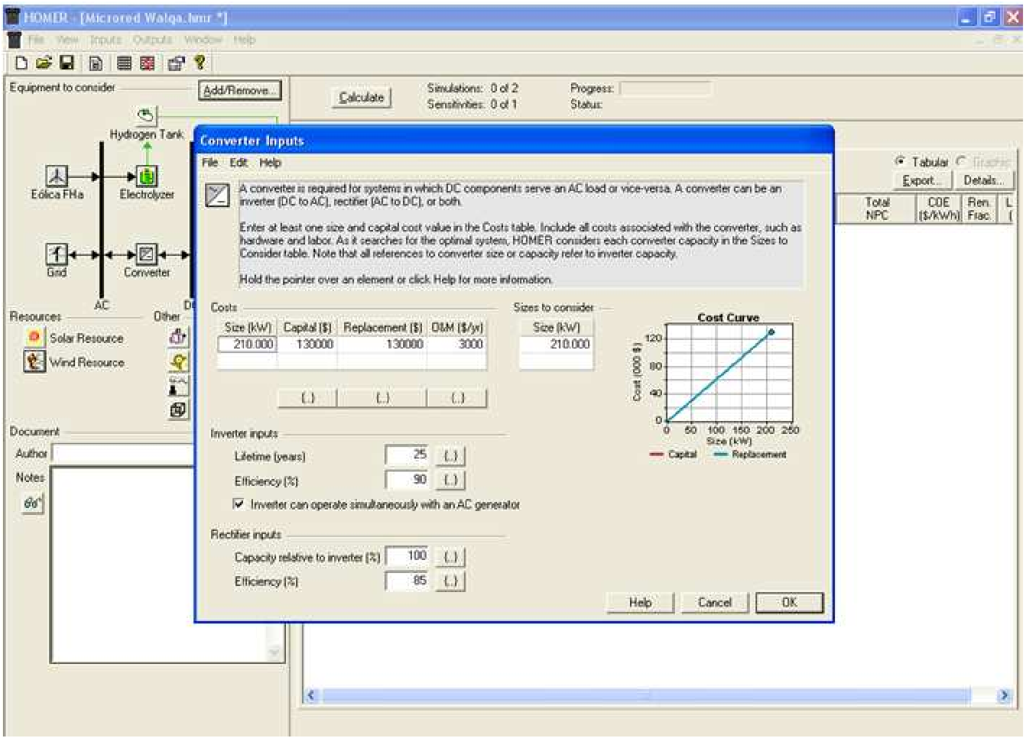

Simulations: 0 of 2
Sensitivities: 0 of 1
Progress:
Status:

A converter is required for systems in which DC components serve an AC load or vice-versa. A converter can be an inverter (DC to AC), rectifier (AC to DC), or both.

Enter at least one size and capital cost value in the Costs table. Include all costs associated with the converter, such as hardware and labor. As it searches for the optimal system, HOMER considers each converter capacity in the Sizes to Consider table. Note that all references to converter size or capacity refer to inverter capacity.

Hold the pointer over an element or click Help for more information.

Costs

Size (kW)	Capital ($)	Replacement ($)	O&M ($/yr)
210.000	130000	130000	3000

Sizes to consider

Size (kW)
210.000

Inverter inputs
Lifetime (years) 25
Efficiency (%) 90
☑ Inverter can operate simultaneously with an AC generator

Rectifier inputs
Capacity relative to inverter (%) 100
Efficiency (%) 85

Fig. 2.14. Photovoltaic converters data.

Electrolizer data is entered. The electrolizer is installed in Hydrogen Foundation facilities.

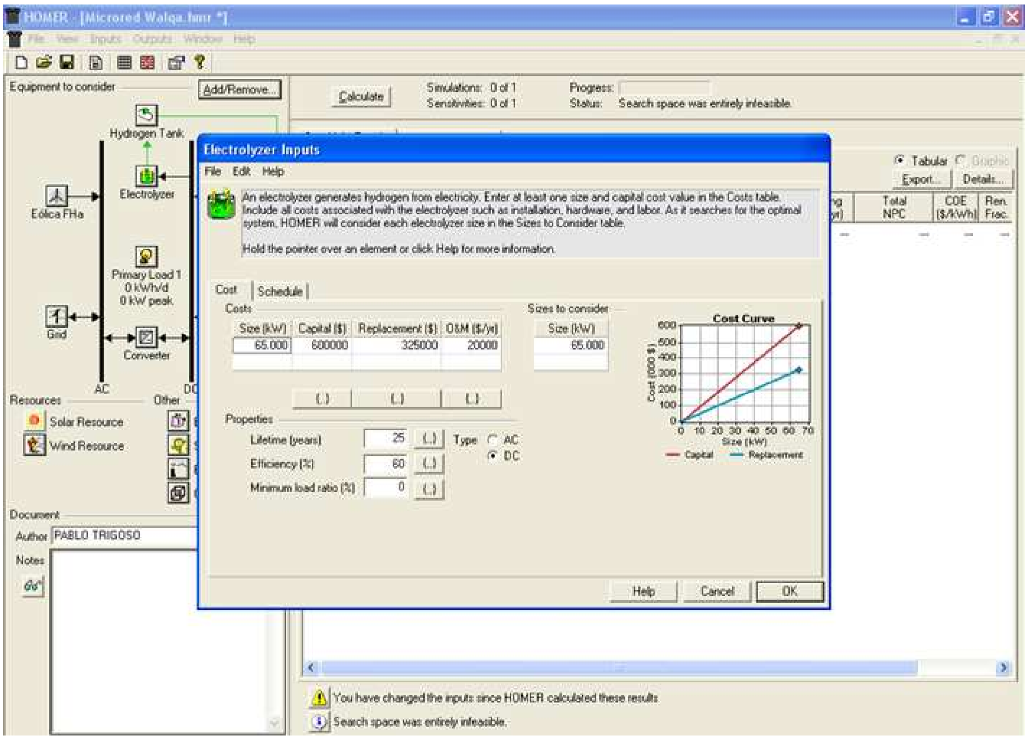

Author PABLO TRIGOSO

Simulations: 0 of 1
Sensitivities: 0 of 1
Progress:
Status: Search space was entirely infeasible.

An electrolyzer generates hydrogen from electricity. Enter at least one size and capital cost value in the Costs table. Include all costs associated with the electrolyzer such as installation, hardware, and labor. As it searches for the optimal system, HOMER will consider each electrolyzer size in the Sizes to Consider table.

Hold the pointer over an element or click Help for more information.

Costs

Size (kW)	Capital ($)	Replacement ($)	O&M ($/yr)
65.000	600000	325000	20000

Sizes to consider

Size (kW)
65.000

Properties
Lifetime (years) 25
Efficiency (%) 60
Minimum load ratio (%) 0
Type ○ AC ● DC

You have changed the inputs since HOMER calculated these results
Search space was entirely infeasible.

Fig. 2.15. Defining the electrolizer.

Defining hydrogen storage system.

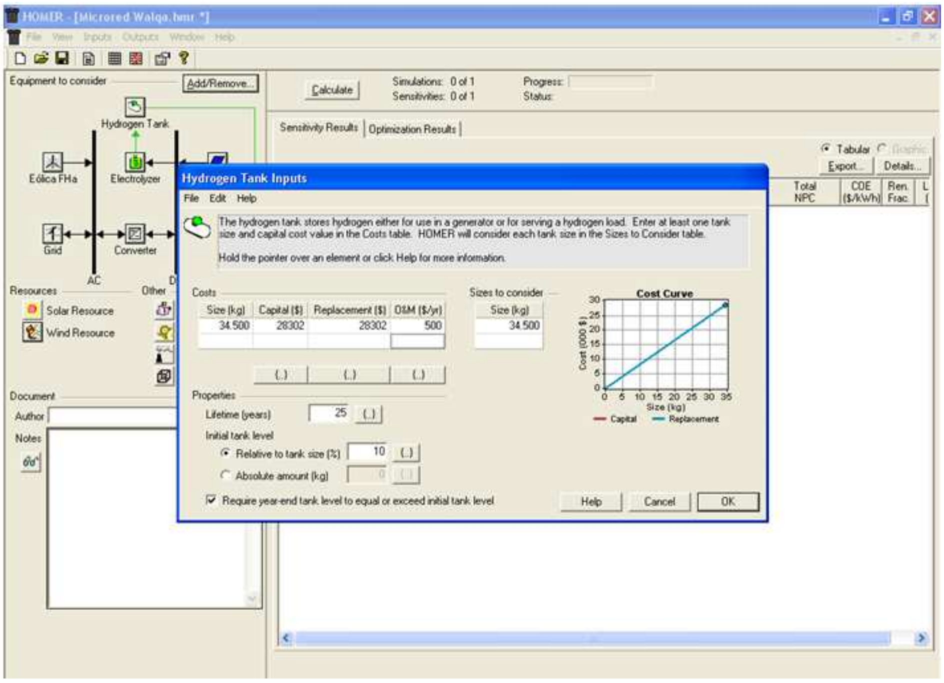

Simulations: 0 of 1
Sensitivities: 0 of 1

The hydrogen tank stores hydrogen either for use in a generator or for serving a hydrogen load. Enter at least one tank size and capital cost value in the Costs table. HOMER will consider each tank size in the Sizes to Consider table.

Hold the pointer over an element or click Help for more information.

Costs

Size (kg)	Capital ($)	Replacement ($)	O&M ($/yr)
34.500	28302	28302	500

Sizes to consider

Size (kg)
34.500

Properties

Lifetime (years) 25

Initial tank level

● Relative to tank size (%) 10

○ Absolute amount (kg) 0

☑ Require year-end tank level to equal or exceed initial tank level

Fig. 2.16. Hydrogen storage system.

Walqa Technological Park electric consumption is defined in HOMER program. Some assumptions have been taken into account:

- Monthly consumption (It has been taken the average of the twelve months of the year): 451339,33 kWh/month.
- Power consumption in working hours (7h – 19h): X
- Power consumption outside working hours: X/10

Results:

- Working hours power: 1339,28 kW.
- Non – work hours power: 133,93 kW.

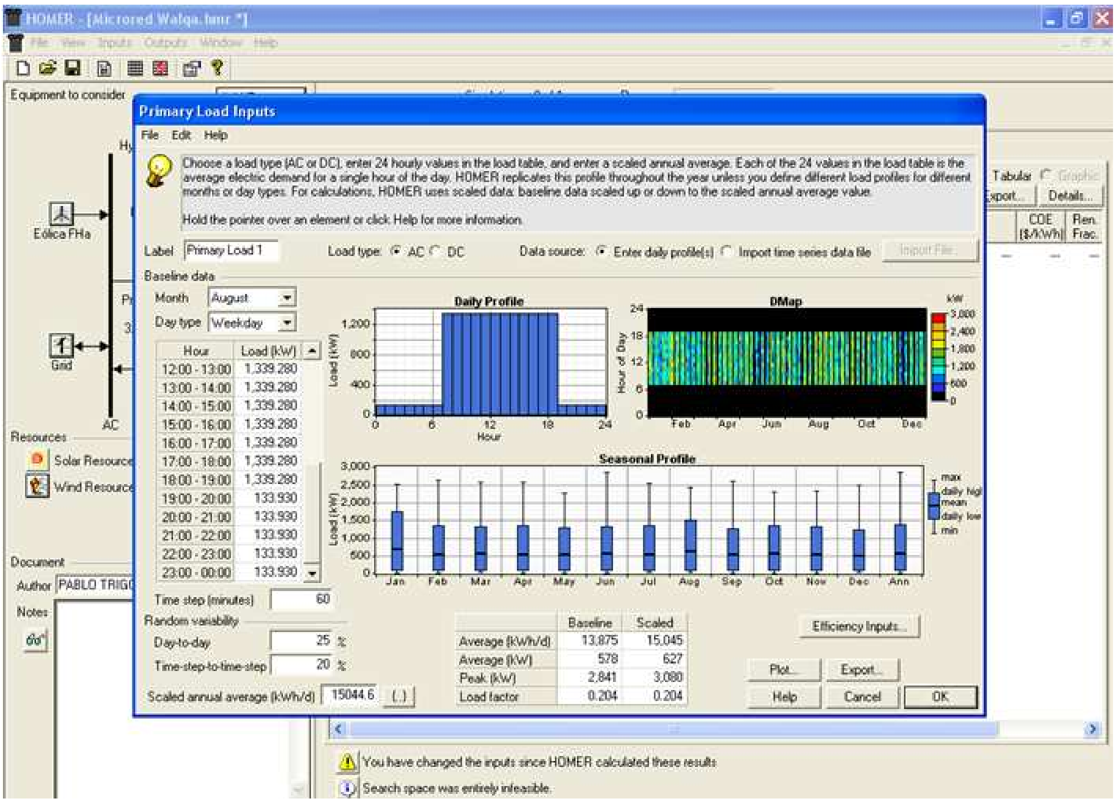

Choose a load type (AC or DC), enter 24 hourly values in the load table, and enter a scaled annual average. Each of the 24 values in the load table is the average electric demand for a single hour of the day. HOMER replicates this profile throughout the year unless you define different load profiles for different months or day types. For calculations, HOMER uses scaled data: baseline data scaled up or down to the scaled annual average value.

Hold the pointer over an element or click Help for more information.

Label: Primary Load 1
Load type: ● AC ○ DC
Data source: ● Enter daily profile(s) ○ Import time series data file

Baseline data
Month: August
Day type: Weekday

Hour	Load (kW)
12:00 - 13:00	1,339.280
13:00 - 14:00	1,339.280
14:00 - 15:00	1,339.280
15:00 - 16:00	1,339.280
16:00 - 17:00	1,339.280
17:00 - 18:00	1,339.280
18:00 - 19:00	1,339.280
19:00 - 20:00	133.930
20:00 - 21:00	133.930
21:00 - 22:00	133.930
22:00 - 23:00	133.930
23:00 - 00:00	133.930

Time step (minutes): 60
Random variability
Day-to-day: 25 %
Time-step-to-time-step: 20 %
Scaled annual average (kWh/d): 15044.6

	Baseline	Scaled
Average (kWh/d)	13,875	15,045
Average (kW)	578	627
Peak (kW)	2,841	3,080
Load factor	0.204	0.204

You have changed the inputs since HOMER calculated these results.
Search space was entirely infeasible.

Fig. 2.17. Electric consumption in Walqa Technological Park.

It removes the limitation of power capacity exchange with the grid. It is entered the costs of energy exchange in both sale and purchase.

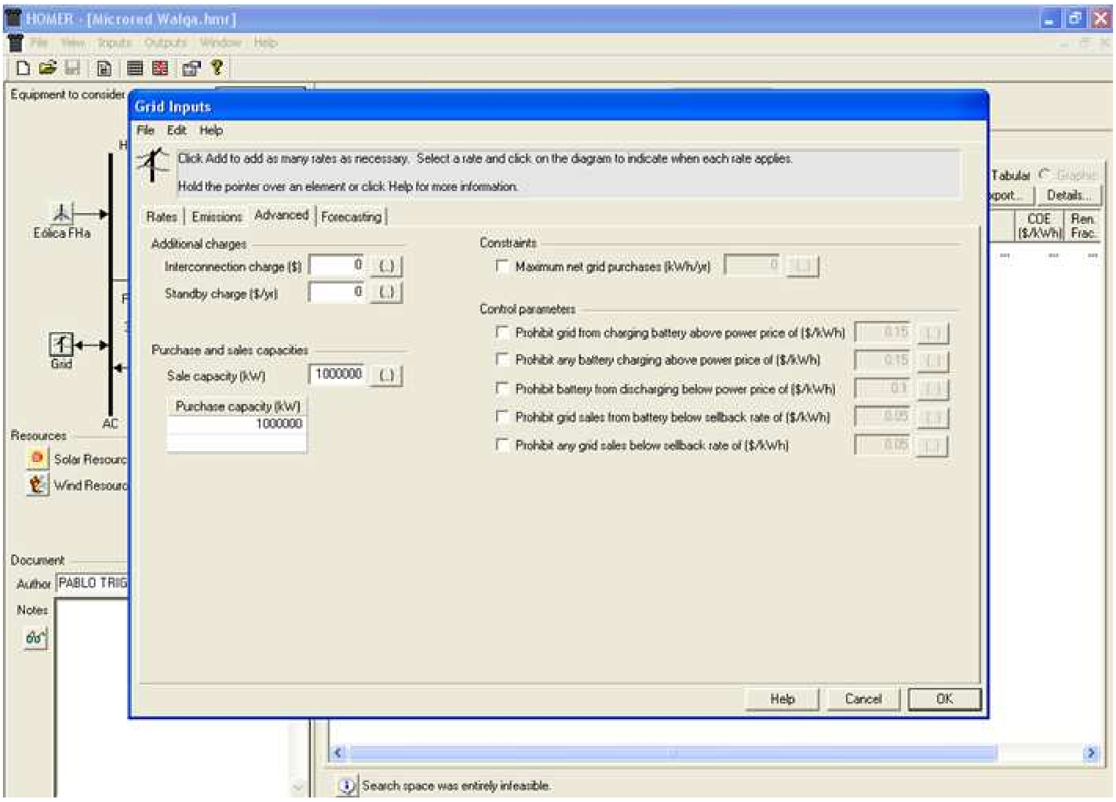

Click Add to add as many rates as necessary. Select a rate and click on the diagram to indicate when each rate applies.

Hold the pointer over an element or click Help for more information.

Additional charges
Interconnection charge ($): 0
Standby charge ($/yr): 0

Purchase and sales capacities
Sale capacity (kW): 1000000

Purchase capacity (kW)
1000000

Constraints
☐ Maximum net grid purchases (kWh/yr): 0

Control parameters
☐ Prohibit grid from charging battery above power price of ($/kWh): 0.15
☐ Prohibit any battery charging above power price of ($/kWh): 0.15
☐ Prohibit battery from discharging below power price of ($/kWh): 0.1
☐ Prohibit grid sales from battery below sellback rate of ($/kWh): 0.05
☐ Prohibit any grid sales below sellback rate of ($/kWh): 0.05

Search space was entirely infeasible.

Fig. 2.18. Defining power capacity Exchange with the grid.

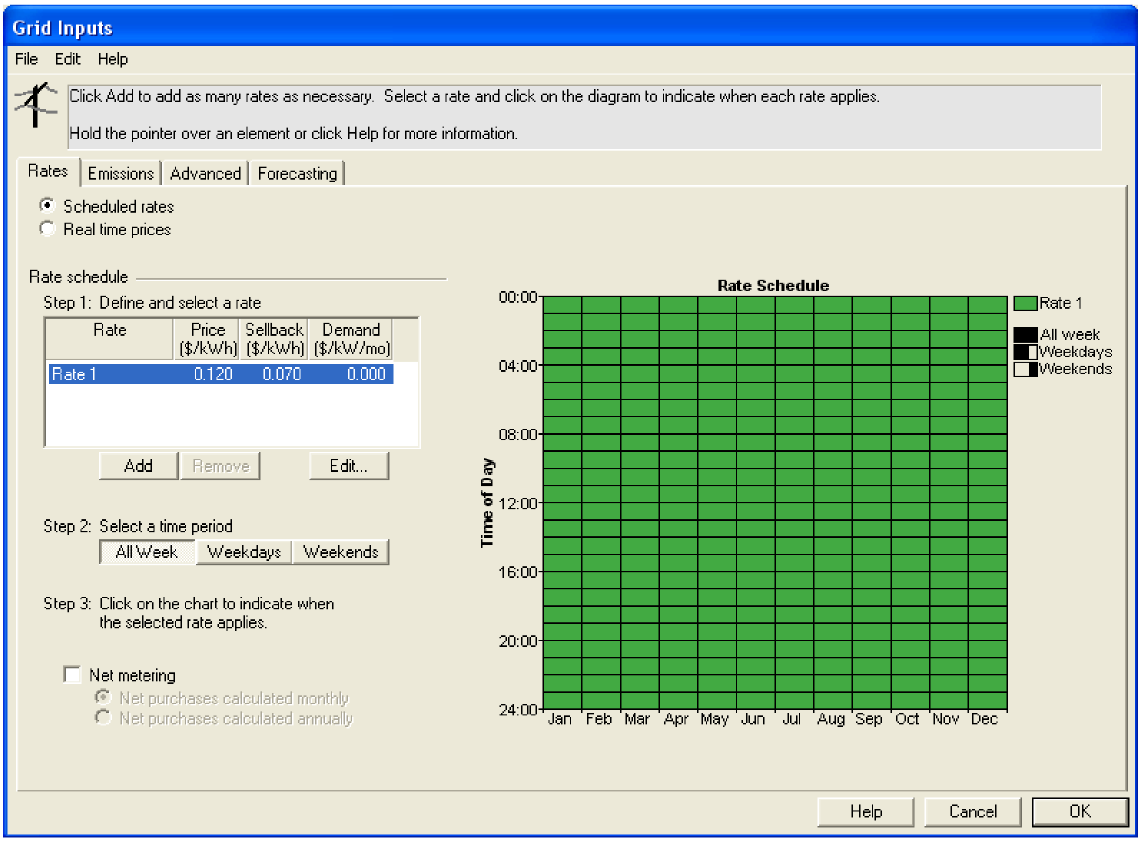

Click Add to add as many rates as necessary. Select a rate and click on the diagram to indicate when each rate applies.

Hold the pointer over an element or click Help for more information.

● Scheduled rates
○ Real time prices

Rate schedule

Step 1: Define and select a rate

Rate	Price ($/kWh)	Sellback ($/kWh)	Demand ($/kW/mo)
Rate 1	0.120	0.070	0.000

Step 2: Select a time period

Step 3: Click on the chart to indicate when the selected rate applies.

☐ Net metering
● Net purchases calculated monthly
○ Net purchases calculated annually

Fig. 2.19. Cost of purchase and sale of electric energy.

2.2.4 Case study introduction without energy storage

This section will introduce the electrical microgrid without energy storage for analysis in HOMER program. It will be described only the differences in comparison with the case study introduction with energy storage.

In this model we will not have an electrolyzer, a hydrogen storage system and a fuel cell system.

2.3 Results and analysis with energy storage

The total cost of the microgrid introduced is almost 10 million euros[1].

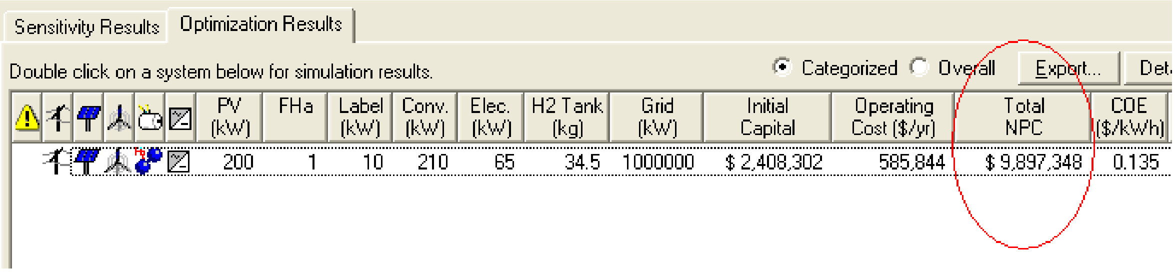

Double click on a system below for simulation results.

● Categorized ○ Overall

PV (kW)	FHa	Label (kW)	Conv. (kW)	Elec. (kW)	H2 Tank (kg)	Grid (kW)	Initial Capital	Operating Cost ($/yr)	Total NPC	COE ($/kWh)
200	1	10	210	65	34.5	1000000	$ 2,408,302	585,844	$ 9,897,348	0.135

Fig. 2.20. Walqa Technological Park microgrid.

In the electrical simulation results shown below is possible to check that interacting with the network represents 78% of electricity production, wind generation represented 17% and 5% represented photovoltaic generation of energy produced during the year.

---

[1] All the amounts have been entered in euros so that although the image appears in dollars, actually for our exercise will be euros.

As for consumption 96% is comparable to the consumption of the Technology Park and 4% of sales to the grid. Both in production and consumption, the use of hydrogen from a standpoint of optimizing the system is negligible.

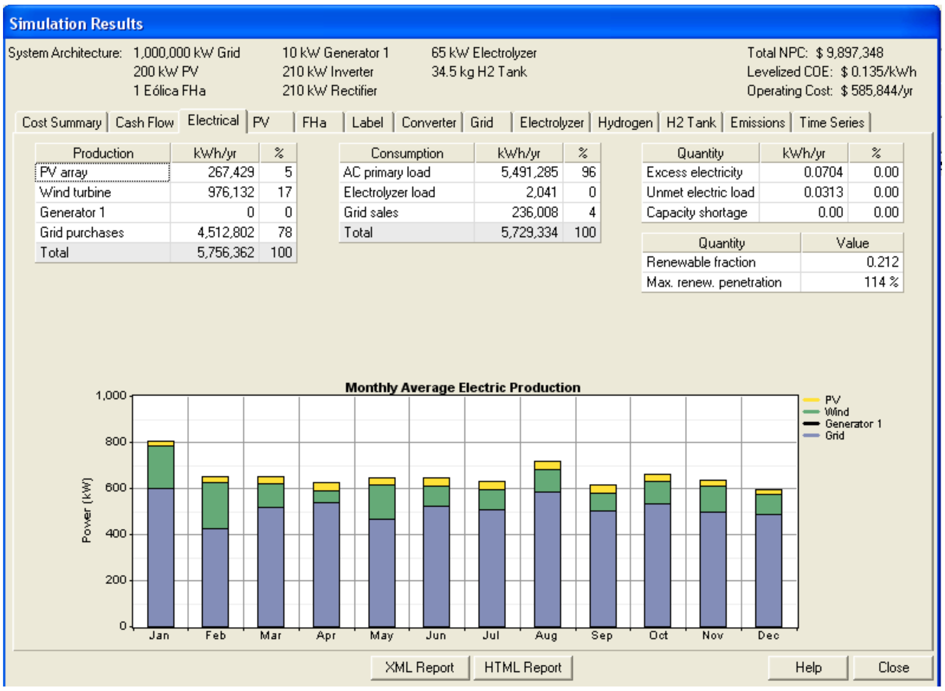

Simulation Results

System Architecture: 1,000,000 kW Grid
200 kW PV
1 Eólica FHa
10 kW Generator 1
210 kW Inverter
210 kW Rectifier
65 kW Electrolyzer
34.5 kg H2 Tank

Total NPC: $ 9,897,348
Levelized COE: $ 0.135/kWh
Operating Cost: $ 585,844/yr

Production	kWh/yr	%
PV array	267,429	5
Wind turbine	976,132	17
Generator 1	0	0
Grid purchases	4,512,802	78
Total	5,756,362	100

Consumption	kWh/yr	%
AC primary load	5,491,285	96
Electrolyzer load	2,041	0
Grid sales	236,008	4
Total	5,729,334	100

Quantity	kWh/yr	%
Excess electricity	0.0704	0.00
Unmet electric load	0.0313	0.00
Capacity shortage	0.00	0.00

Quantity	Value
Renewable fraction	0.212
Max. renew. penetration	114 %

Fig. 2.21. Electric simulation results.

2.4 Results and analysis without energy storage

The total cost of the microgrid introduced is almost 9 million euros, 1 million less than in the other case of study.

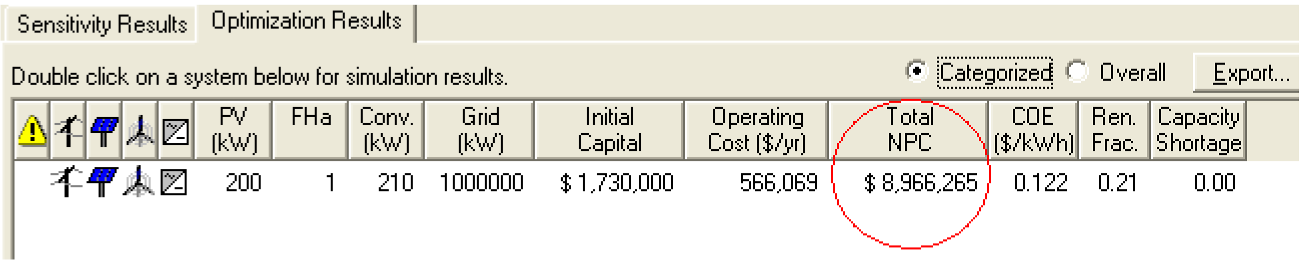

Double click on a system below for simulation results.

					PV (kW)	FHa	Conv. (kW)	Grid (kW)	Initial Capital	Operating Cost ($/yr)	Total NPC	COE ($/kWh)	Ren. Frac.	Capacity Shortage
					200	1	210	1000000	$ 1,730,000	566,069	$ 8,966,265	0.122	0.21	0.00

Fig. 2.22. Walqa Technological Park microgrid without energy storage.

As can be seen in the results, seen only a slight difference in grid sales term that rises in 2326 kWh / year, an utterly despicable amount.

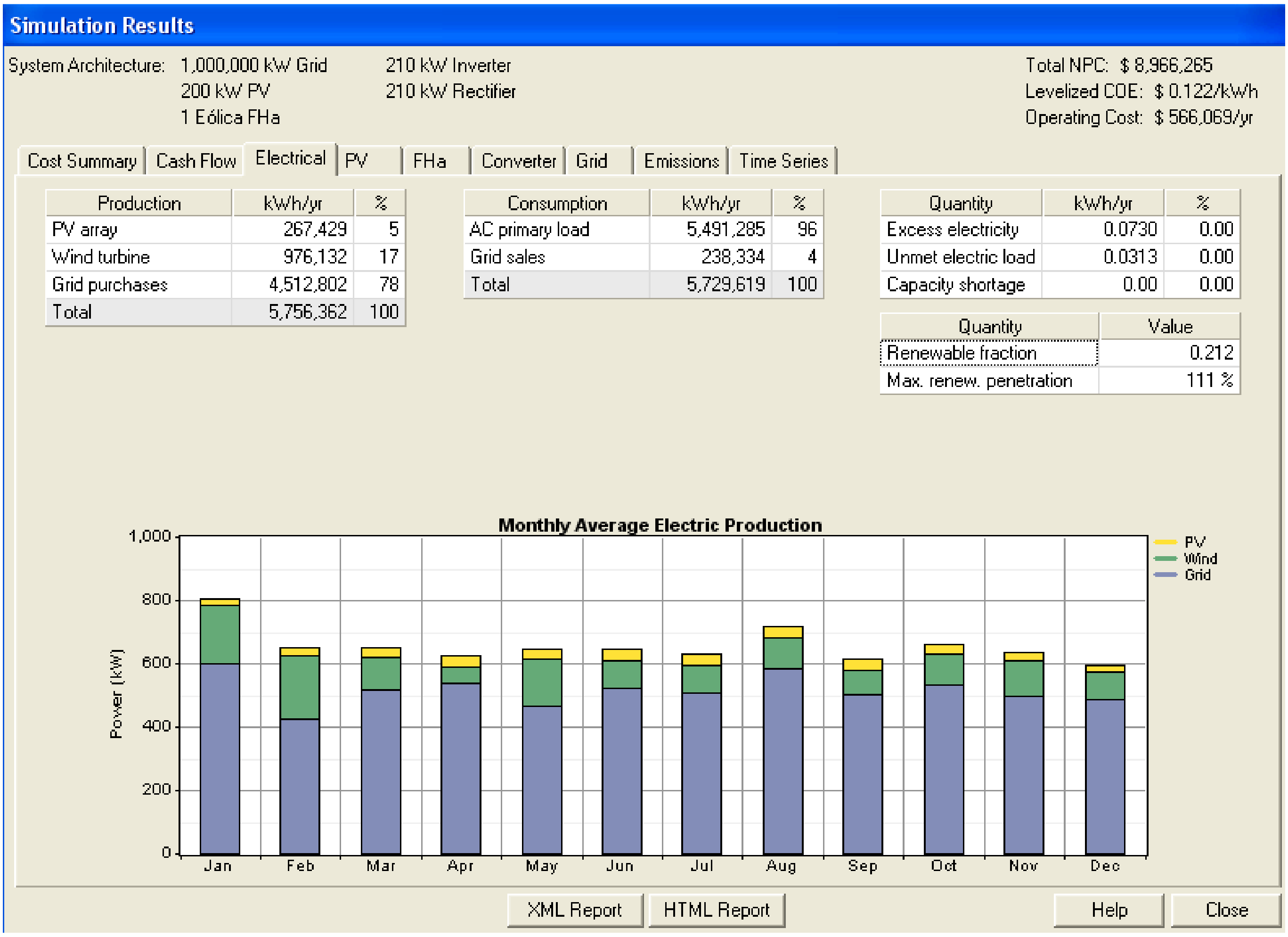

System Architecture: 1,000,000 kW Grid
200 kW PV
1 Eólica FHa
210 kW Inverter
210 kW Rectifier

Total NPC: $ 8,966,265
Levelized COE: $ 0.122/kWh
Operating Cost: $ 566,069/yr

Production	kWh/yr	%
PV array	267,429	5
Wind turbine	976,132	17
Grid purchases	4,512,802	78
Total	5,756,362	100

Consumption	kWh/yr	%
AC primary load	5,491,285	96
Grid sales	238,334	4
Total	5,729,619	100

Quantity	kWh/yr	%
Excess electricity	0.0730	0.00
Unmet electric load	0.0313	0.00
Capacity shortage	0.00	0.00

Quantity	Value
Renewable fraction	0.212
Max. renew. penetration	111 %

Fig. 2.23. Electric simulation results.

The conclusion is that the energy storage of hydrogen is hardly used in the simulation, whereby the solution with and without storage are obtained practically the same results. This implies that in the microgrid hydrogen would not be a good transmission system because it is underutilized.

2.5 Sensitivity analysis

In this section it will be studied the optimization of generation sources trying to introduce more renewable energy power in the microgrid.

2.5.1 Data introduction

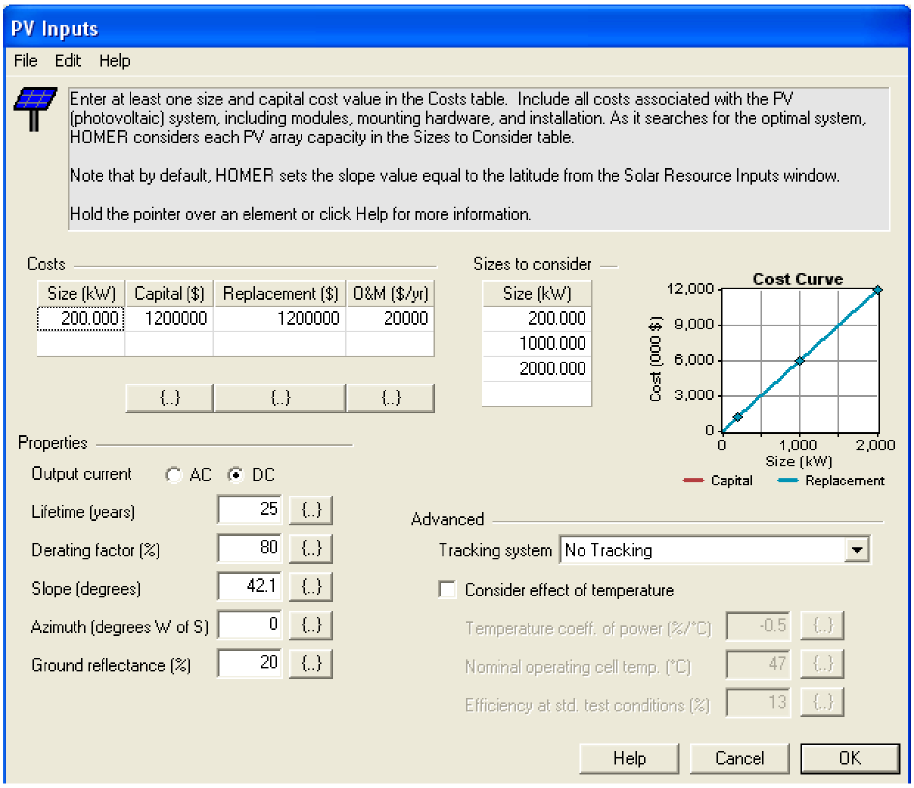

Enter at least one size and capital cost value in the Costs table. Include all costs associated with the PV (photovoltaic) system, including modules, mounting hardware, and installation. As it searches for the optimal system, HOMER considers each PV array capacity in the Sizes to Consider table.

Note that by default, HOMER sets the slope value equal to the latitude from the Solar Resource Inputs window.

Hold the pointer over an element or click Help for more information.

Costs

Size (kW)	Capital ($)	Replacement ($)	O&M ($/yr)
200.000	1200000	1200000	20000

Sizes to consider

Size (kW)
200.000
1000.000
2000.000

Properties

Output current ○ AC ● DC

Lifetime (years) 25

Derating factor (%) 80

Slope (degrees) 42.1

Azimuth (degrees W of S) 0

Ground reflectance (%) 20

Advanced

Tracking system No Tracking

☐ Consider effect of temperature

Temperature coeff. of power (%/°C) -0.5

Nominal operating cell temp. (°C) 47

Efficiency at std. test conditions (%) 13

Fig. 2.24. Different powers of PV for the optimization exercise.

In wind power generation will be evaluated by multiplying the current installation to a factor of five and ten.

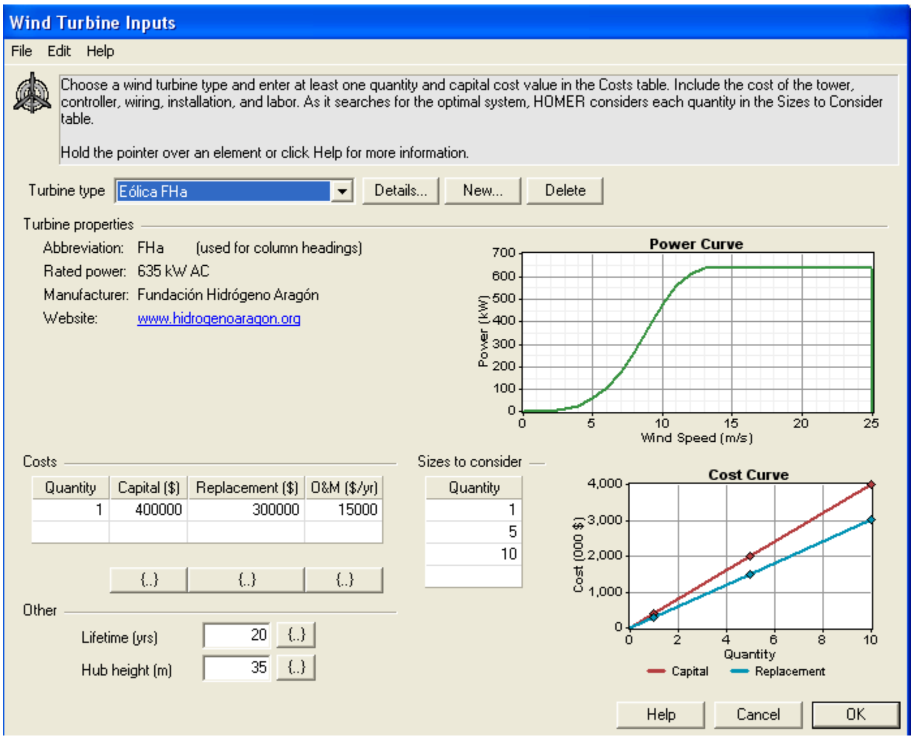

Choose a wind turbine type and enter at least one quantity and capital cost value in the Costs table. Include the cost of the tower, controller, wiring, installation, and labor. As it searches for the optimal system, HOMER considers each quantity in the Sizes to Consider table.

Hold the pointer over an element or click Help for more information.

Turbine type Eólica FHa

Turbine properties

Abbreviation: FHa (used for column headings)
Rated power: 635 kW AC
Manufacturer: Fundación Hidrógeno Aragón
Website: www.hidrogenoaragon.org

Costs

Quantity	Capital ($)	Replacement ($)	O&M ($/yr)
1	400000	300000	15000

Sizes to consider

Quantity
1
5
10

Other

Lifetime (yrs) 20

Hub height (m) 35

Fig. 2.25. Wind farm sizes to be considered in the optimization.

Fuel cell up to 100 kW.

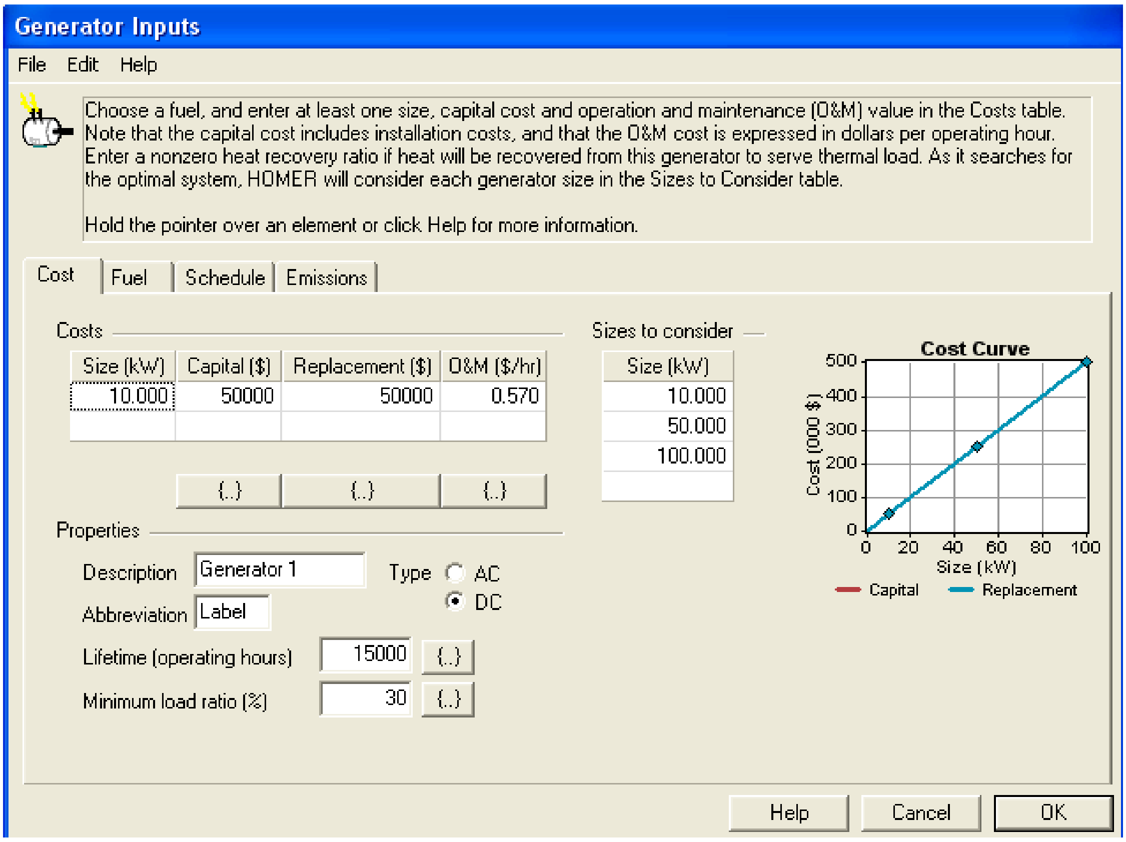

Choose a fuel, and enter at least one size, capital cost and operation and maintenance (O&M) value in the Costs table. Note that the capital cost includes installation costs, and that the O&M cost is expressed in dollars per operating hour. Enter a nonzero heat recovery ratio if heat will be recovered from this generator to serve thermal load. As it searches for the optimal system, HOMER will consider each generator size in the Sizes to Consider table.

Hold the pointer over an element or click Help for more information.

Costs

Size (kW)	Capital ($)	Replacement ($)	O&M ($/hr)
10.000	50000	50000	0.570

Sizes to consider

Size (kW)
10.000
50.000
100.000

Properties

Description: Generator 1

Abbreviation: Label

Type: ○ AC ● DC

Lifetime (operating hours): 15000

Minimum load ratio (%): 30

Fig. 2.26. Fuel cell powers to evaluate.

Electrolyzer up to 650 kW

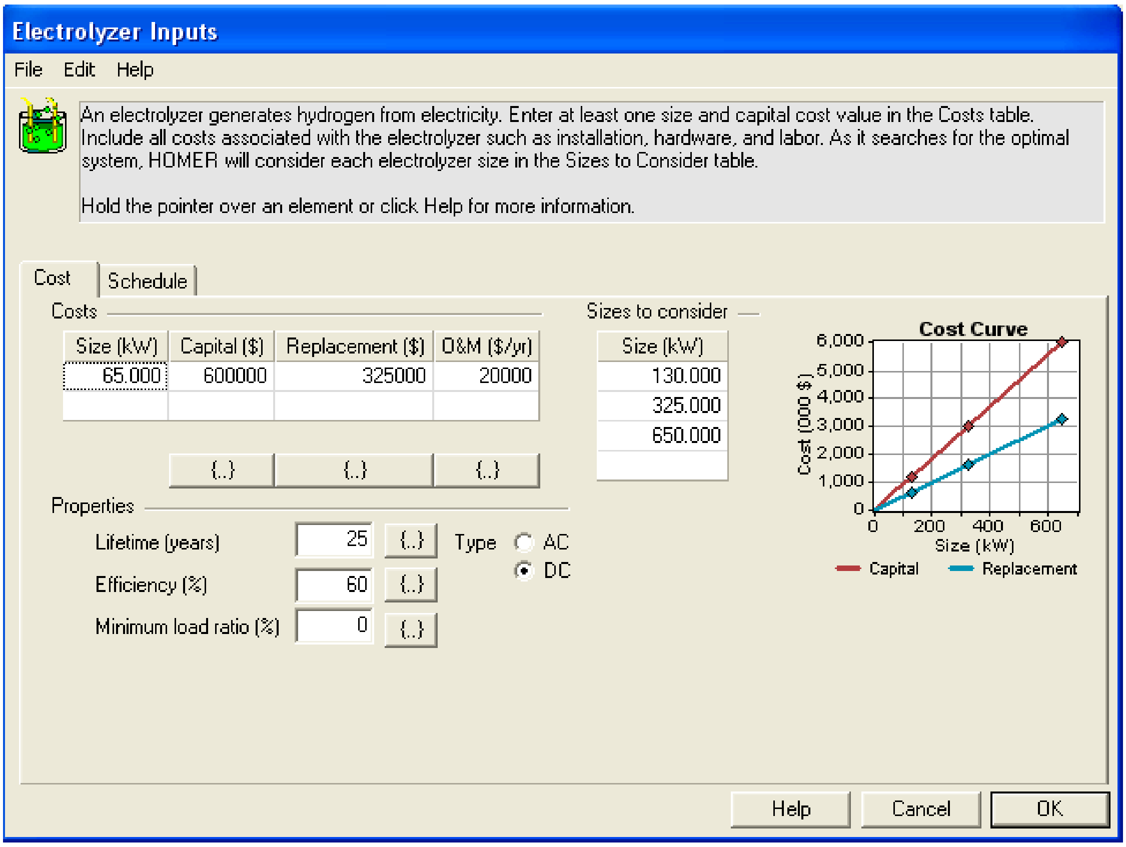

An electrolyzer generates hydrogen from electricity. Enter at least one size and capital cost value in the Costs table. Include all costs associated with the electrolyzer such as installation, hardware, and labor. As it searches for the optimal system, HOMER will consider each electrolyzer size in the Sizes to Consider table.

Hold the pointer over an element or click Help for more information.

Costs

Size (kW)	Capital ($)	Replacement ($)	O&M ($/yr)
65.000	600000	325000	20000

Sizes to consider

Size (kW)
130.000
325.000
650.000

Properties

Lifetime (years): 25

Efficiency (%): 60

Minimum load ratio (%): 0

Type: ○ AC ● DC

Fig. 2.27. Electrolizers power for the optimization study.

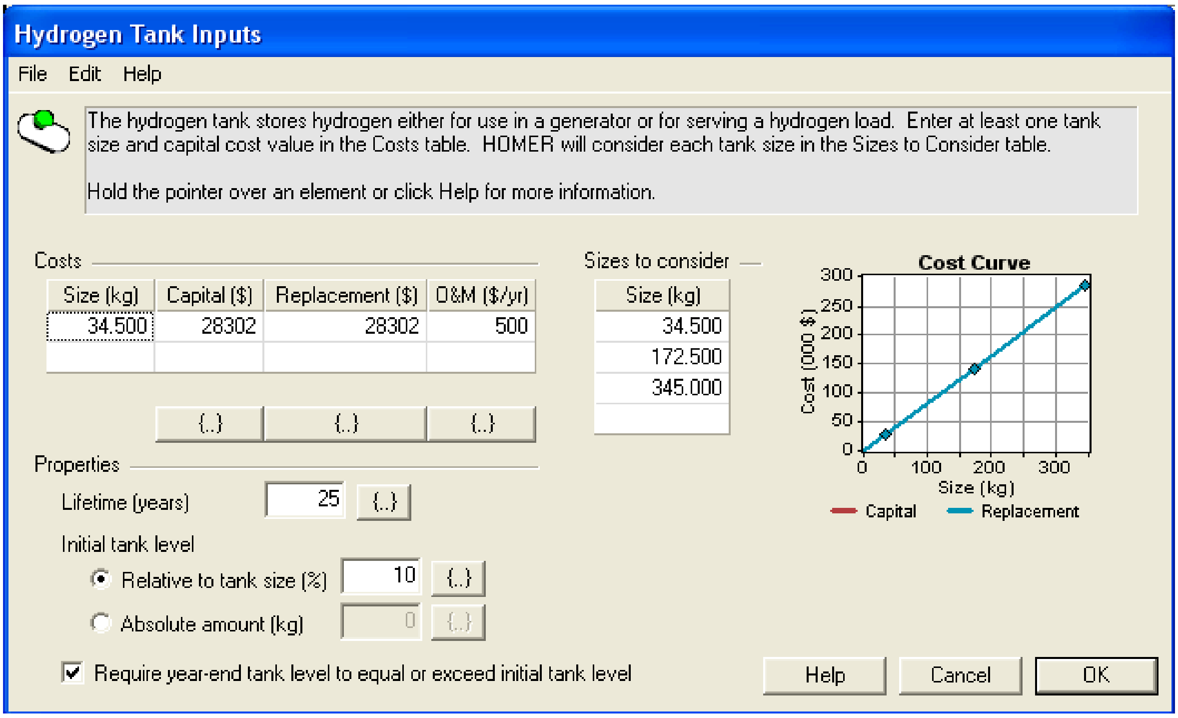

The hydrogen tank stores hydrogen either for use in a generator or for serving a hydrogen load. Enter at least one tank size and capital cost value in the Costs table. HOMER will consider each tank size in the Sizes to Consider table.

Hold the pointer over an element or click Help for more information.

Costs

Size (kg)	Capital ($)	Replacement ($)	O&M ($/yr)
34.500	28302	28302	500

Sizes to consider

Size (kg)
34.500
172.500
345.000

Properties

Lifetime (years) 25

Initial tank level

● Relative to tank size (%) 10

○ Absolute amount (kg) 0

☑ Require year-end tank level to equal or exceed initial tank level

Fig. 2.28. Hydrogen storage system sizes for the optimization study.

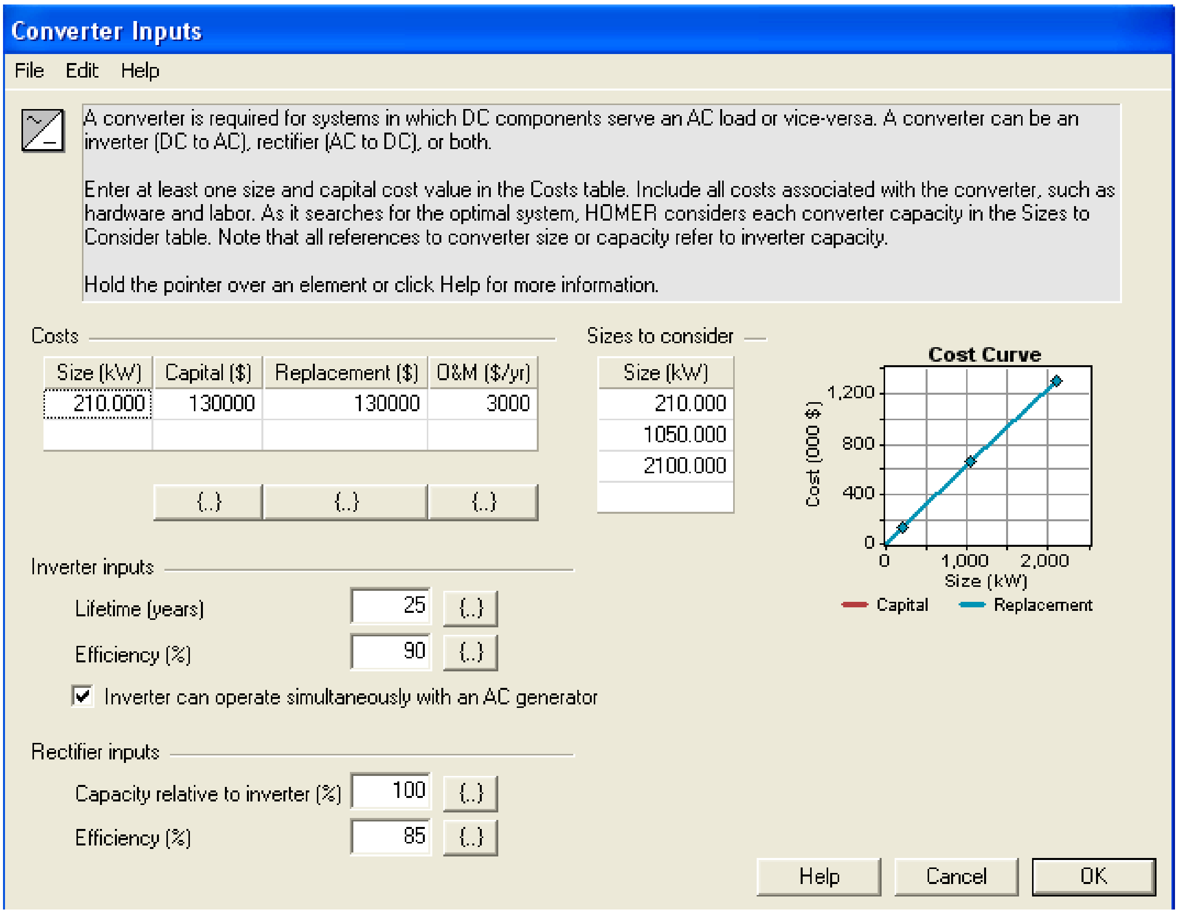

A converter is required for systems in which DC components serve an AC load or vice-versa. A converter can be an inverter (DC to AC), rectifier (AC to DC), or both.

Enter at least one size and capital cost value in the Costs table. Include all costs associated with the converter, such as hardware and labor. As it searches for the optimal system, HOMER considers each converter capacity in the Sizes to Consider table. Note that all references to converter size or capacity refer to inverter capacity.

Hold the pointer over an element or click Help for more information.

Costs

Size (kW)	Capital ($)	Replacement ($)	O&M ($/yr)
210.000	130000	130000	3000

Sizes to consider

Size (kW)
210.000
1050.000
2100.000

Inverter inputs

Lifetime (years) 25

Efficiency (%) 90

☑ Inverter can operate simultaneously with an AC generator

Rectifier inputs

Capacity relative to inverter (%) 100

Efficiency (%) 85

Fig. 2.29. Converters for the optimization study.

2.5.2 Results

Below it is the optimization of the system. As seen HOMER has taken the largest wind farm and the medium size electrolyzer. The percentage of wind power has risen to 78% having decreased both the input of the grid such as the photovoltaic power. These results are due to low acquisition cost of wind generators because they are repowering machines.

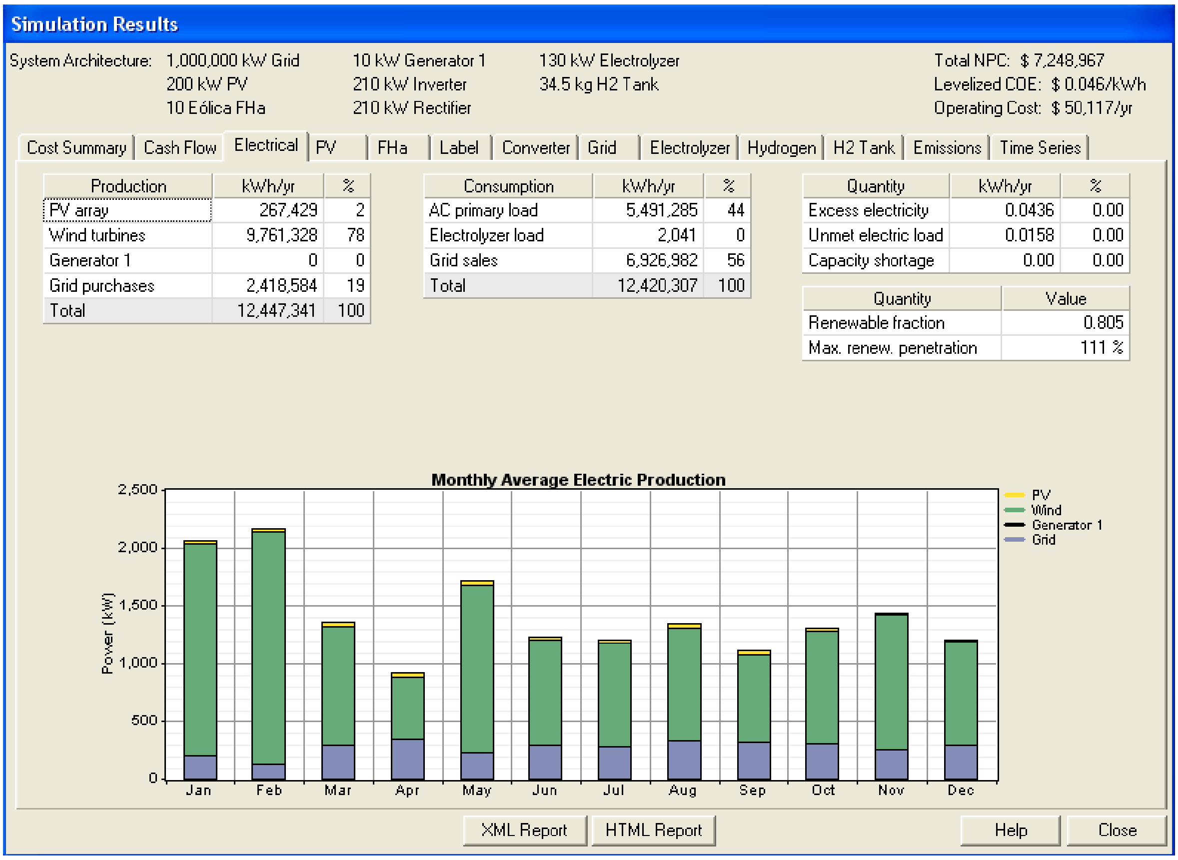

Simulation Results

System Architecture: 1,000,000 kW Grid; 200 kW PV; 10 Eólica FHa; 10 kW Generator 1; 210 kW Inverter; 210 kW Rectifier; 130 kW Electrolyzer; 34.5 kg H2 Tank

Total NPC: $ 7,248,967
Levelized COE: $ 0.046/kWh
Operating Cost: $ 50,117/yr

Production	kWh/yr	%
PV array	267,429	2
Wind turbines	9,761,328	78
Generator 1	0	0
Grid purchases	2,418,584	19
Total	12,447,341	100

Consumption	kWh/yr	%
AC primary load	5,491,285	44
Electrolyzer load	2,041	0
Grid sales	6,926,982	56
Total	12,420,307	100

Quantity	kWh/yr	%
Excess electricity	0.0436	0.00
Unmet electric load	0.0158	0.00
Capacity shortage	0.00	0.00

Quantity	Value
Renewable fraction	0.805
Max. renew. penetration	111 %

Fig. 2.30. Electric simulation results of optimization system.

2.6 Sensitivity analysis without energy storage system

In this section it will be studied the optimization of generation sources trying to introduce more renewable energy power in the microgrid without an energy storage system.

2.6.1 Data introduction

It has been entered the same data as in the case with energy storage system.

2.6.2 Results

Below is the optimization of the system. As seen HOMER has taken the largest wind farm and the smallest PV system. The percentage of wind power has risen to 78% having decreased both the input of the grid such as photovoltaic power. These results are due to low acquisition cost of wind generators because they are repowering machines.

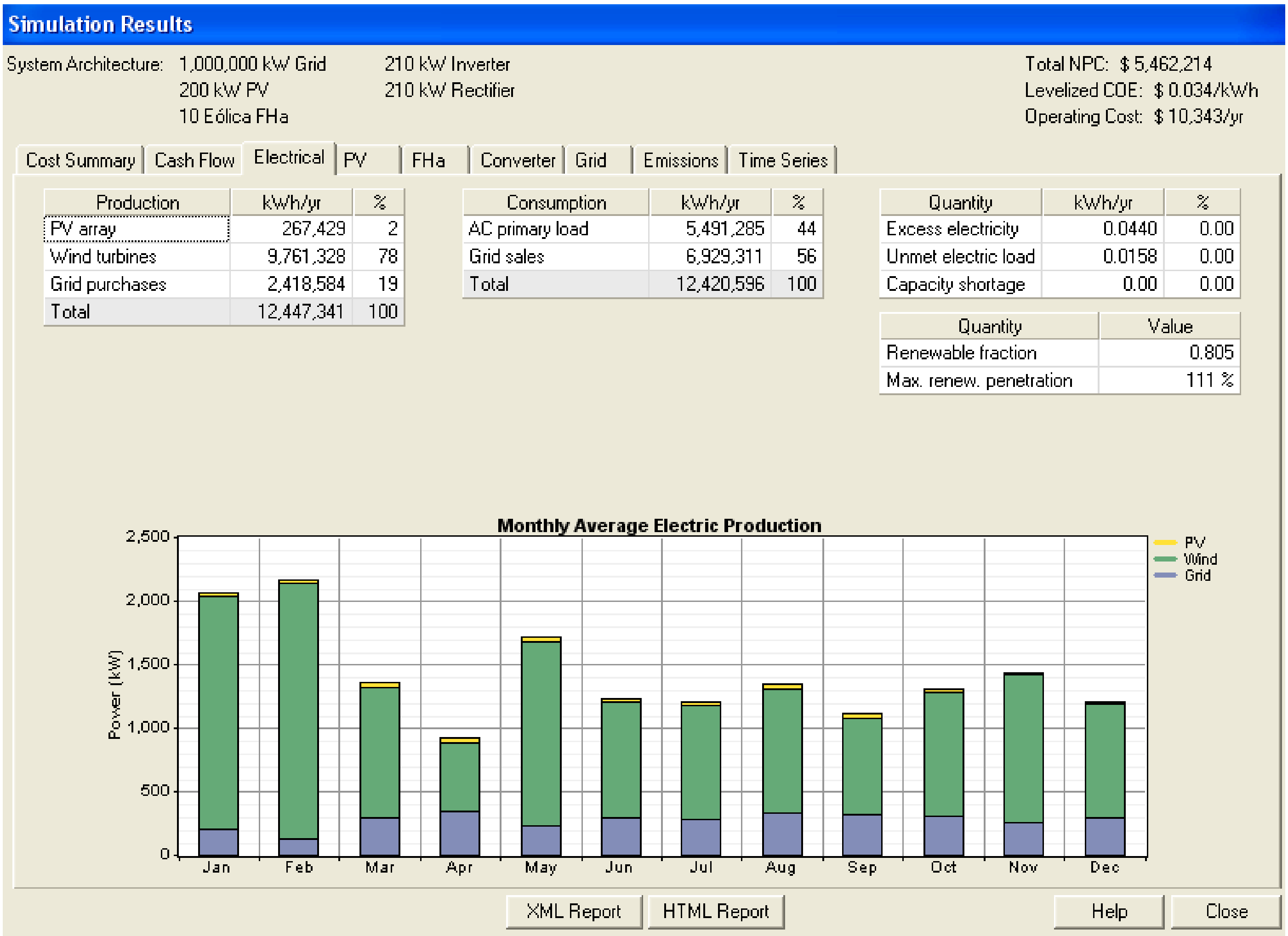

Simulation Results

System Architecture: 1,000,000 kW Grid, 200 kW PV, 10 Eólica FHa, 210 kW Inverter, 210 kW Rectifier

Total NPC: $ 5,462,214
Levelized COE: $ 0.034/kWh
Operating Cost: $ 10,343/yr

Production	kWh/yr	%
PV array	267,429	2
Wind turbines	9,761,328	78
Grid purchases	2,418,584	19
Total	12,447,341	100

Consumption	kWh/yr	%
AC primary load	5,491,285	44
Grid sales	6,929,311	56
Total	12,420,596	100

Quantity	kWh/yr	%
Excess electricity	0.0440	0.00
Unmet electric load	0.0158	0.00
Capacity shortage	0.00	0.00

Quantity	Value
Renewable fraction	0.805
Max. renew. penetration	111 %

Fig. 2.31. Electric simulation results of optimization system.

3 LANDABEN INDUSTRIAL AREA

3.1 Introduction

Landaben (1964) and Arazuri-Orcoyen (1999) are two industrial areas located at the west of Pamplona, in an industrial environment of 5 million m2 with all kind of suppliers. Volkswagen Navarra, with more than 5,000 employees, is the heart of the industrial area and the biggest industry in the region of Pamplona. Arazuri-Orcoyen was finished in 1999 with the aim of accommodating many of the companies that work as suppliers for Volkswagen.

Fig. 3.1. View of Landaben industrial area

3.2 Power demand profile

Using the data of electricity demand of the automotive industrial area compiled for GT2, a synthetically generated hourly demand profile has been generated for a typical year. The resulting demand profile is shown in Fig. 3.2.

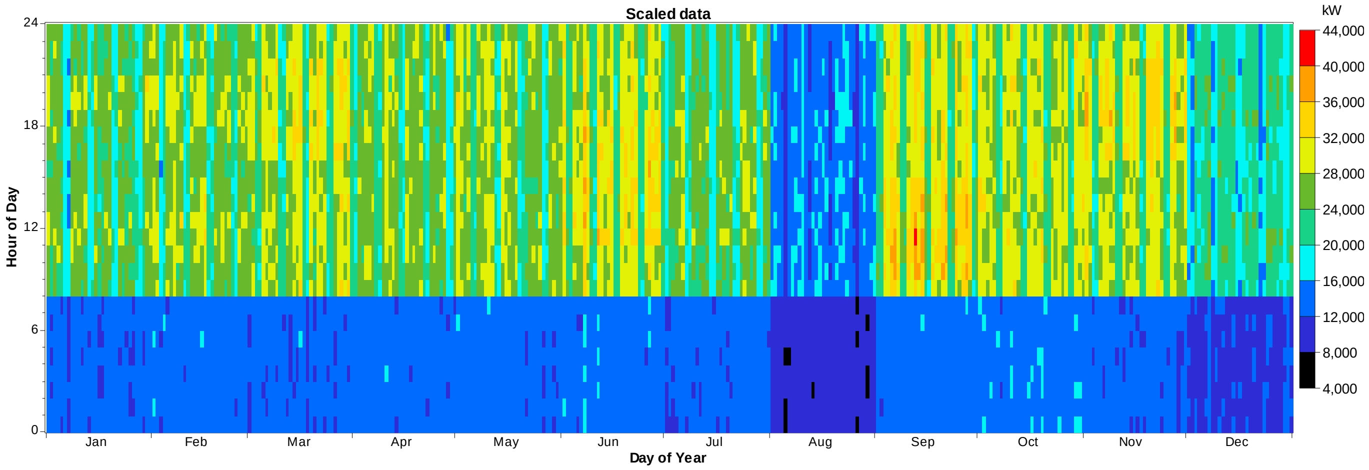

Fig. 3.2. Result of the synthetically generated annual electrical demand profile

The electricity tariffs used for the simulations are detailed in Table 3.1. On the other hand, Fig. 3.3 outlines the share of hours along the year included in each of the existing tariffs.

Table 3.1. Electricity price for the simulations

Tariff period	Energy price (c€/kWh)	Capacity price (c€/kW/month)
P1	11.3	90.7
P2	9.5	45.4
P3	8.0	33.3
P4	8.0	33.3
P5	7.2	33.3
P6	5.6	15.1

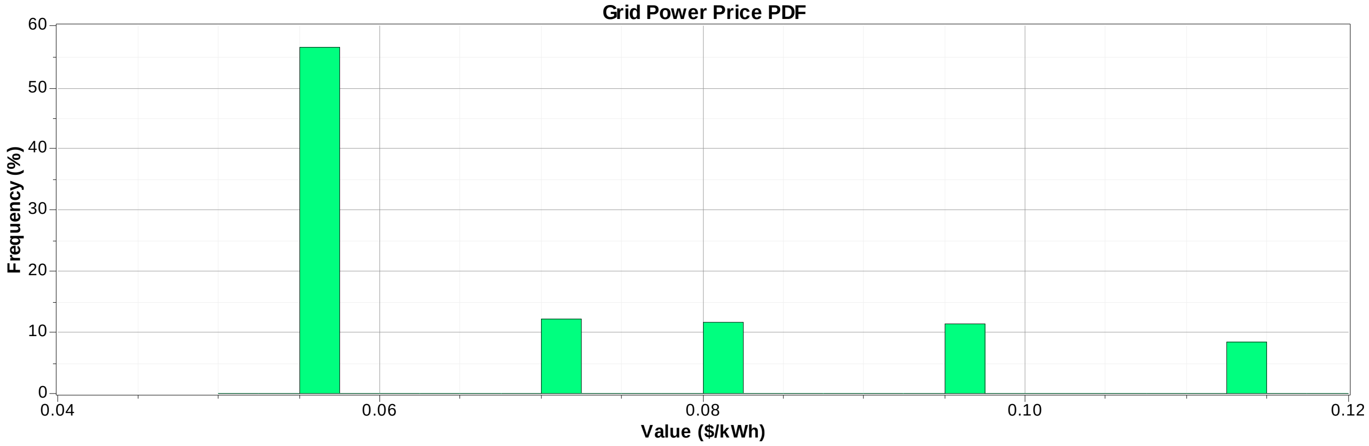

Fig. 3.3. Share of hours corresponding to the different tariffs

In order to estimate the emissions avoided through the renewable systems for the different scenarios simulated, the data depicted in Table 3.2 are used in the model.

Table 3.2. Equivalent emissions for the Spanish electricity grid

	CO2 (kg/kWh)	SO2 (g/kWh)	NOx (g/kWh)
2008	0.279	0.481	0.345
2009	0.232	0.381	0.312
2010	0.166	0.254	0.217
2011	0.210	0.364	0.278
Average	**0.222**	**0.370**	**0.288**

3.3 Simulations without energy storage

3.3.1 Model construction

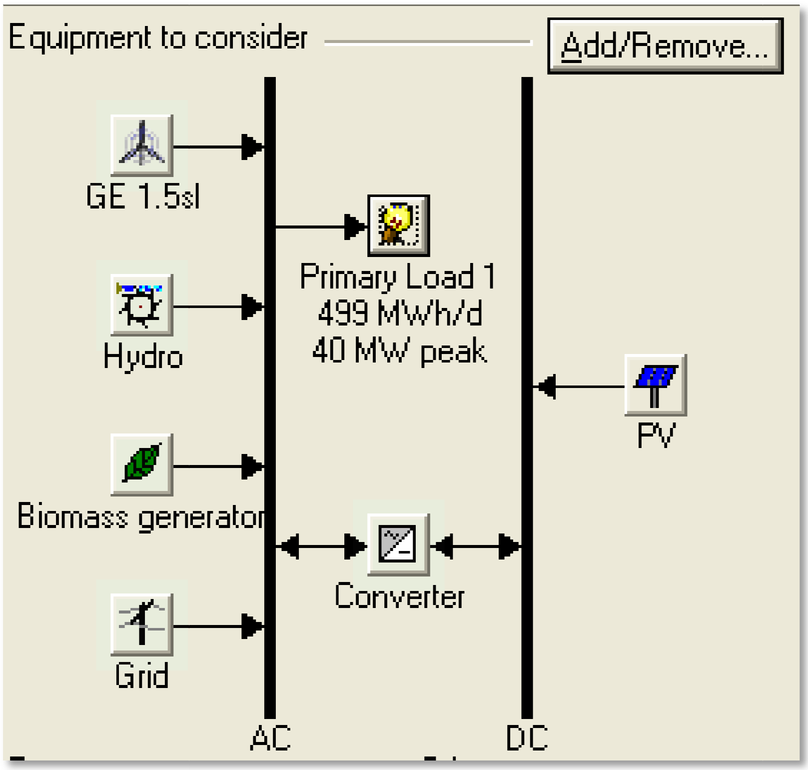

Fig. 3.4. General diagram of the model

As outlined in Fig. 3.4, for the study of the optimum configuration of the system, different options are presented for the simulation software. Four possible renewable installations are defined, which can be installed or not depending on the technical and economical calculations. Taking into account that the 40 MW connection to the grid limits the possible renewable power installed, the four possible installations are the following.

• Photovoltaic system	15 MW
• Wind farm	15 MW
• Hydropower	10 MW
• Biomass plant	10 MW

Among these, the biomass plant is the only generating system whose operation does not depend on meteorology/hydrology, if we accept the assumption that the needed biomass is always available.

3.3.2 Results of the simulations

In Table 3.3, the results of the simulations are presented. According to the model, the best option from the economical point of view is the system Wind+Hydro with an average cost of the energy of 7.1 c€/kWh through the life of the project, which is fixed at 25 years. On the contrary, the system with the highest NPC (Net Present Cost) is the PV+Biomass option with a COE of 8.9 c€/kWh, being 25% more expensive than the first option.

As shown in the table, the renewable fraction can reach up to 46% when the four options of renewable systems are introduced in the simulations. That means that, for the proposed system, the maximum share of the electricity demand that can be supplied by renewable energies without making use of energy storage means is about 50%, and few cases go further than 33%.

Table 3.3. Results of the simulations for the different options presented

PV	Wind	Hydro	Biomass	Initial capital (M€)	Operating cost (M€/yr)	Total NPC (M€)	COE (c€/kWh)	Renewable fraction
	🟩	🟩		35.0	10.2	165.3	7.1	32%
		🟩		20.0	11.7	169.3	7.3	17%
	🟩			15.0	12.3	172.4	7.4	15%
	🟩	🟩	🟩	55.0	9.4	175.6	7.5	36%
				0.0	**13.9**	**177.5**	**7.6**	**0%**
		🟩	🟩	40.0	10.9	179.5	7.7	22%
	🟩		🟩	**35.0**	**11.5**	**182.4**	**7.8**	**20%**
🟩	🟩	🟩		72.5	8.9	185.9	8.0	41%
			🟩	20.0	13.1	187.7	8.1	5%
🟩		🟩		**57.5**	**10.3**	**189.2**	**8.1**	**27%**
🟩	🟩			52.5	10.9	192.4	8.3	25%
🟩	🟩	🟩	🟩	**92.5**	**8.1**	**196.4**	**8.4**	**46%**
🟩				37.5	12.5	197.4	8.5	10%
🟩		🟩	🟩	77.5	9.5	199.4	8.6	32%
🟩	🟩		🟩	72.5	10.2	202.6	8.7	30%
🟩			🟩	57.5	11.7	207.5	8.9	15%

In Fig. 3.5, the hourly generation for the whole year is detailed for the four possible renewable systems in the model. Each of them follows a predetermined profile according to the characteristics of the technology.

The PV array generates power mainly during the central hours of the day, and especially during the summer. The wind turbines also follow a seasonal profile but they can produce high power during a week and fall dramatically during the next one. The hydro turbine production is much more seasonal dependent, and less stochastic and unpredictable than wind power, although it can be almost stopped during a big part of the year.

On the contrary, the biomass generator is fully controllable and can be used to generate during peak hours where the electricity price is higher, as it happens in these simulations.

In order to explain some results in detail in the next section, some concrete cases have been chosen which are in boldface in Table 3.3, Wind+Biomass and PV+Hydro. Finally, the all-renewable case (4 renewables installed) is also studied and compared to the Base Case (no renewables installed).

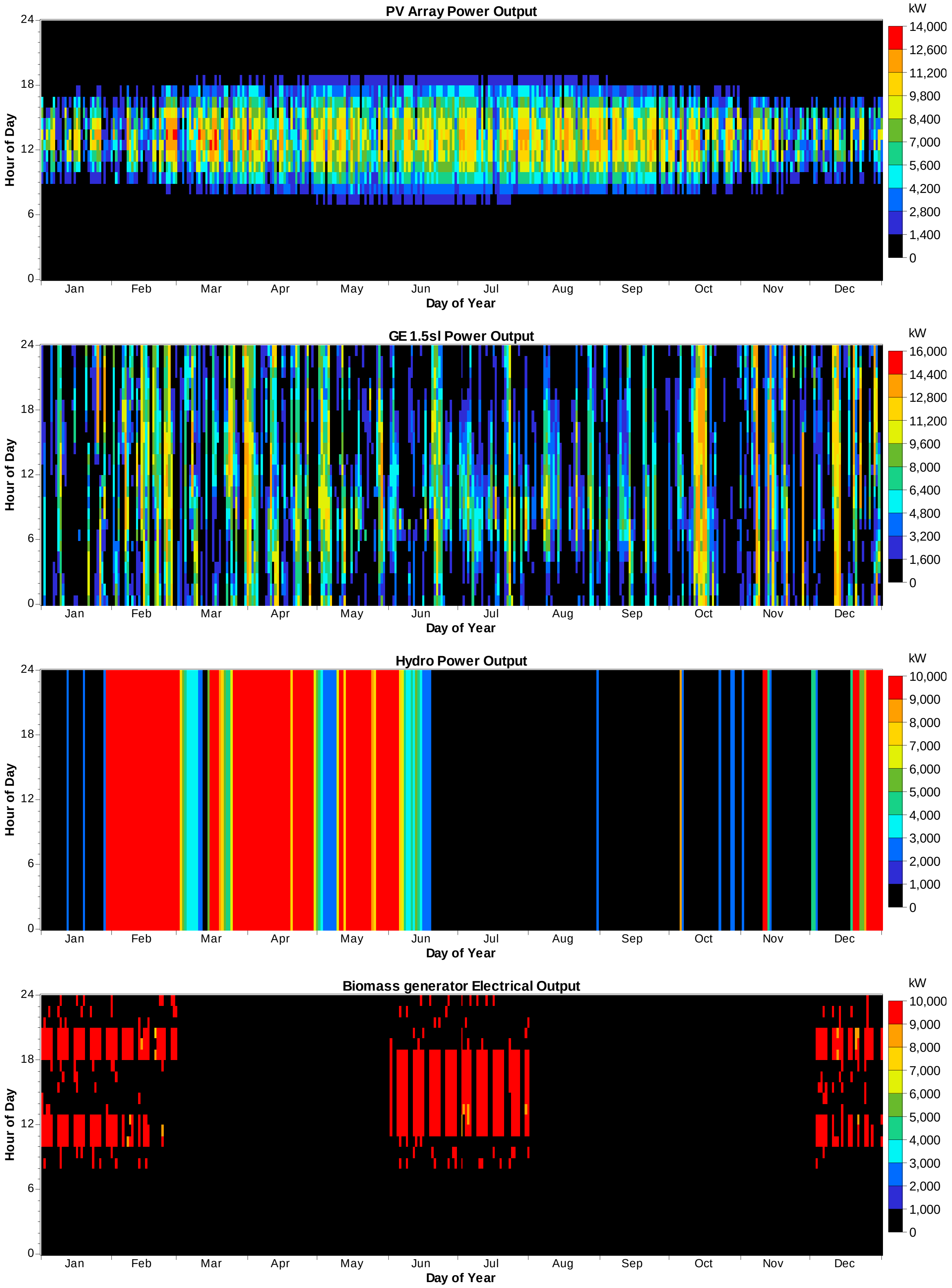

Fig. 3.5. Graphic of the annual generation of the renewable technologies

3.3.3 Wind + Biomass combined system

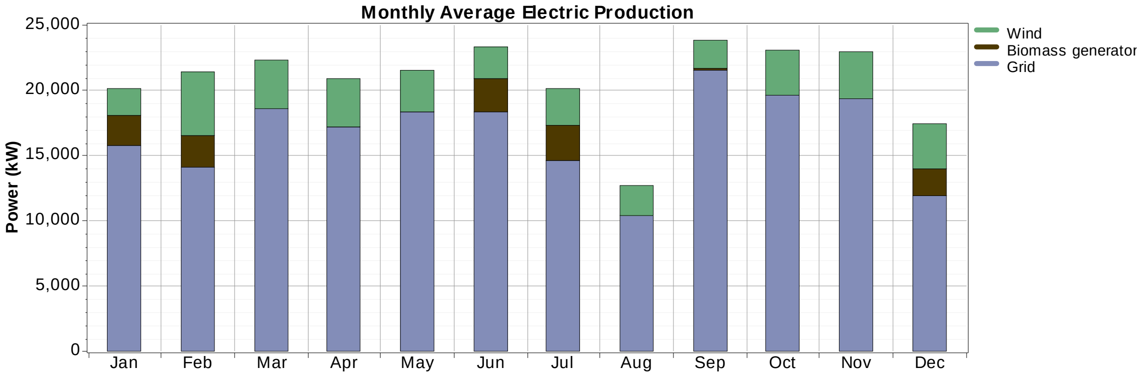

Fig. 3.6. Electricity production in the Wind+Biomass case

In Fig. 3.6 we can see that the biomass generator is only running during some months, depending on the grid electricity prices. This means that according to the cost assumptions made, the biomass generator is only profitable when compared to the P1 tariff, that is, the most expensive one. In total, the wind turbines produce three times the electricity produced by the biomass system, as seen in Table 3.4.

Taking into account all the renewable production, the grid purchases are reduced by a 20%.

Table 3.4. Electricity production in the Wind+Biomass case

Production	MWh/yr	%
Wind turbines	27,872	15
Biomass generator	8,779	5
Grid purchases	145,560	80
Total	**182,210**	**100**

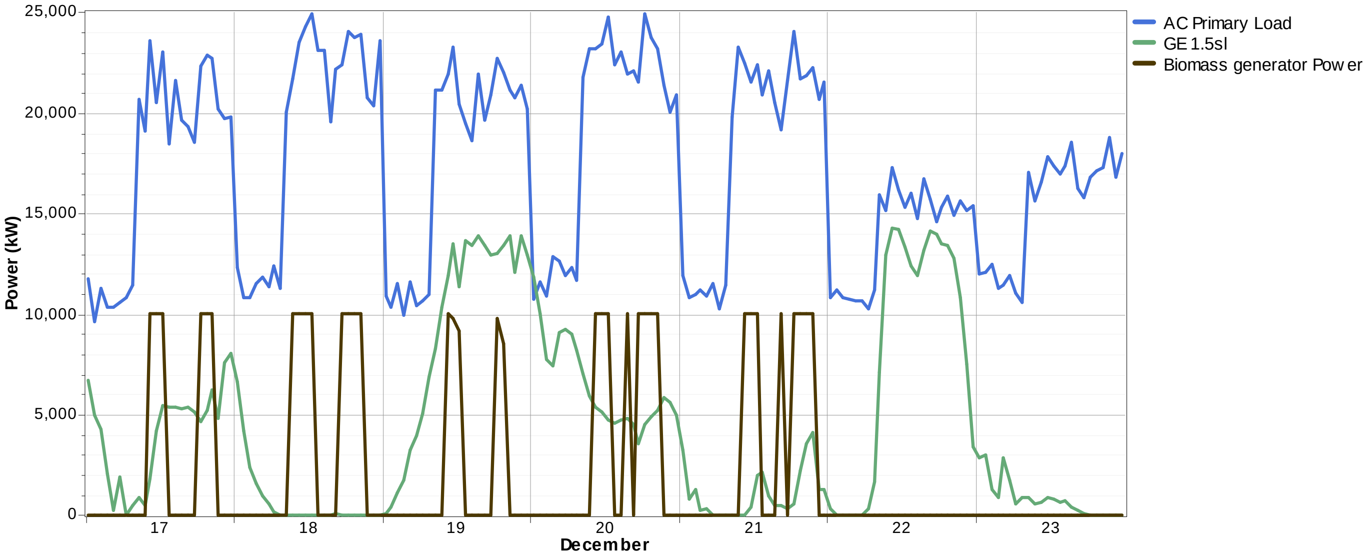

Fig. 3.7. Detail of a week in the Wind+Biomass case

In Fig. 3.7, the result of the simulation for a week is shown. Here, we can see that the biomass generator is running in determined hours of the day, corresponding to the P1 tariff. That means that the biomass generator is avoiding some of the purchase of this expensive electricity thanks to its controllability.

At the same time, the wind turbines generate electricity according to the resource in every moment. This way, we can see that there are moments where the renewable production can equal or even surpass the load demand, as in day 19 or 22 in the figure.

In the simulated model, the biomass generator works only during the 10% of the hours every year, which makes very difficult the return of the investment. Of course, the evolution of the costs can make the biomass option more interesting if the biomass resource remains constant and the electricity cost continues rising. The controllability of the generation is a very interesting feature to fight against peak prices.

3.3.4 Photovoltaic + Hydro combined system

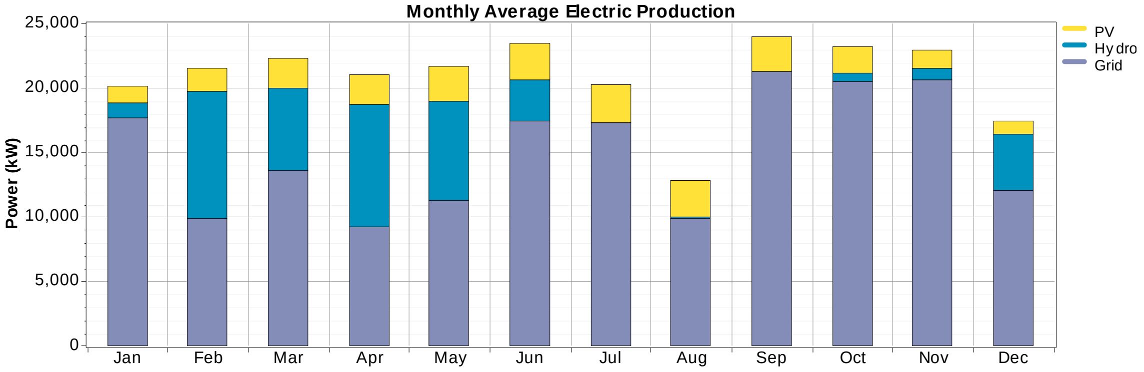

Fig. 3.8. Electricity production in the PV+Hydro case

In this case, the combination of a PV system with a hydraulic power station is studied. In the figure, we can see that the PV array does not vary a big deal from month to month, while the hydro power production is concentrated in some months every year. Moreover, the resource can vary deeply from one year to another.

Among the studied options, the hydro turbine is the most profitable one, generating a 17% of the total demand at a reasonable cost. On the contrary, the PV array is the least profitable option according to the economical assumptions and to the solar resource of the location considered. In this case, the PV array accounts for the 11% of the total demand.

Table 3.5. Electricity production in the PV+Hydro case

Production	**MWh/yr**	**%**
PV array	19,281	11
Hydro turbine	31,574	17
Grid purchases	132,096	72
Total	**182,951**	**100**

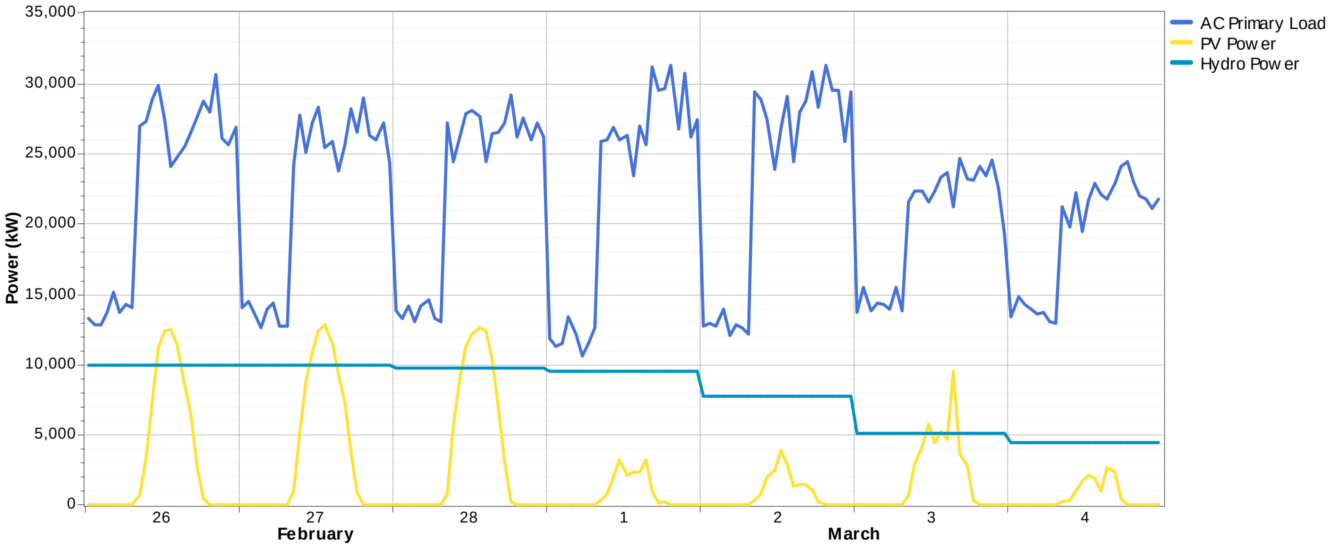

Fig. 3.9. Detail of a week in the PV+Hydro case

In Fig. 3.9, the result of the simulation for a week is shown. Here, we can see that the hydro turbine is generating at full power and gradually falls as the flow of the river decreases. At the same time we can see the typical daily profile of the PV generation, with some cloudy days where the production is dramatically reduced.

In this case, neither one nor another can be controlled so the renewable system fully depends on meteorological/hydrological conditions. Again, there are moments where the renewable generation can equal the load demand or even surpass it. During these moments, a part of the generated power is either fed into the grid or lost as an excess.

3.3.5 PV + Wind + Hydro + Biomass combined system

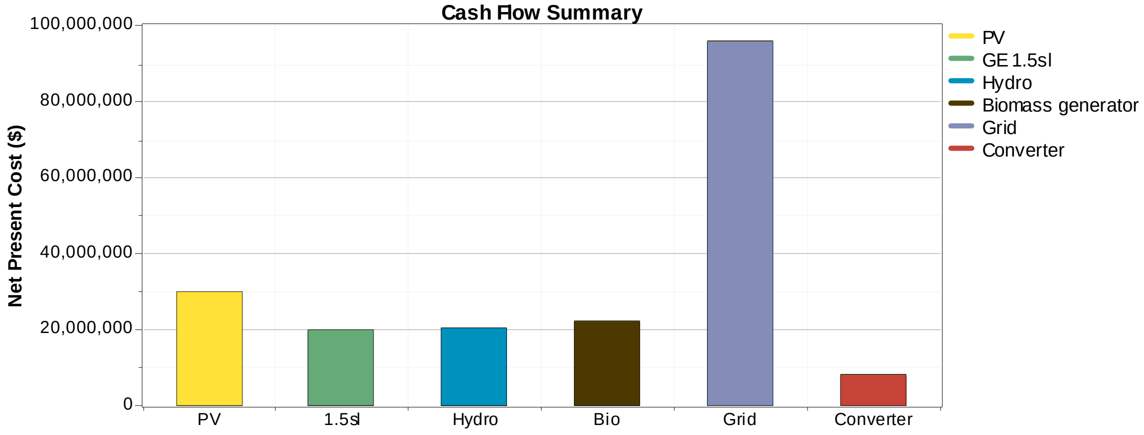

Fig. 3.10. Net Present Cost of each part of the system in the 4-renewables case

In this section, it is considered that the 4 different renewable options for generation systems are installed in order to evaluate the case where the maximum renewable coverage exists.

First, in Fig. 3.10 the breakdown of the net present cost of the project is shown, where we can see the contribution of every component. These costs include all the costs (O&M, fuel, etc.) related to each component through the entire life of the project.

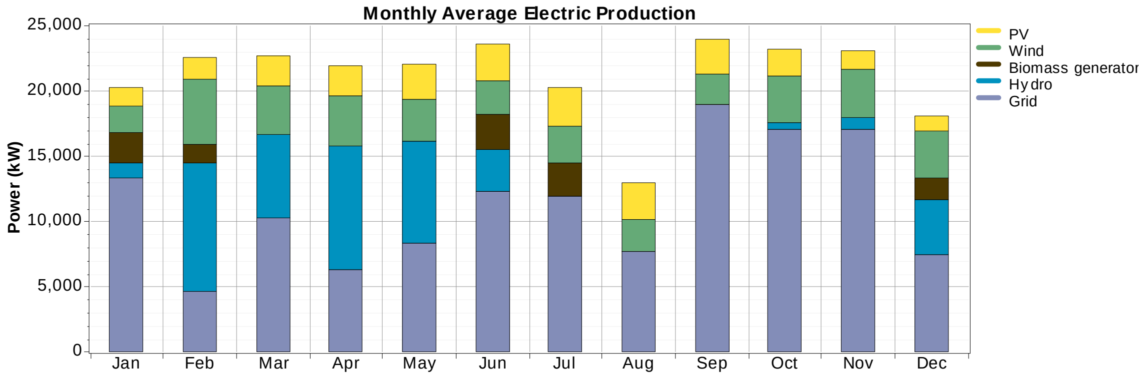

Fig. 3.11. Electricity production in the 4-renewables case

The contribution of each renewable energy is depicted in Fig. 3.11. We can see how, depending on the different renewable resources, there are some months (i.e. February) where the renewable sources cover most of the demand and others (i.e. September) where the renewable contribution is really low.

In Fig. 3.12 the duration curve of the electricity purchased from the grid in this case is shown, together with the case without renewable energies or base case. We can see that there are some hours where there is not electricity purchase, because the renewable energies fully cover the demand.

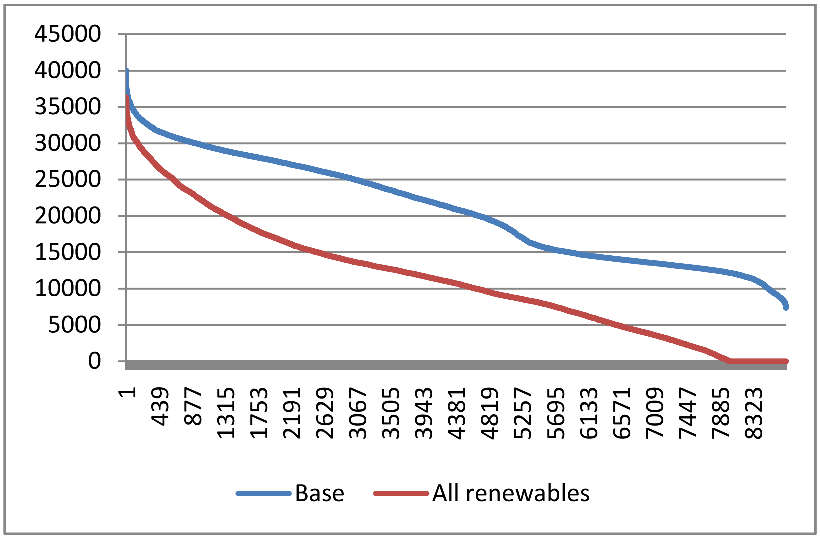

Fig. 3.12. Duration curve of electricity purchased from the grid in the 4-renewables case

Taking into account all the renewable production, the grid purchases are reduced by a 47% as shown in Table 3.6. Nevertheless, in this case the system faces a new problem, given that 1.4% of the production along the year exceeds the instant demand. Depending on the market conditions, this amount of renewable energy will have to be sold or lost because of the lack of energy storage.

Table 3.6. Electricity production in the 4-renewables case

Production	**MWh/yr**	**%**
PV array	19,281	10
Wind turbines	27,872	15
Hydro turbine	31,574	17
Biomass generator	7,823	4
Grid purchases	98,954	53
Total	**185,504**	**100**
Excess	2,634	1.4

In the first part of Fig. 3.13 we can see the monthly averages of the excess electrical production. In the second part the daily profile of the excess in February is shown, where we can identify that most of the excesses occur during night-time because of a lower demand or during the central hours of the day in line with the PV production.

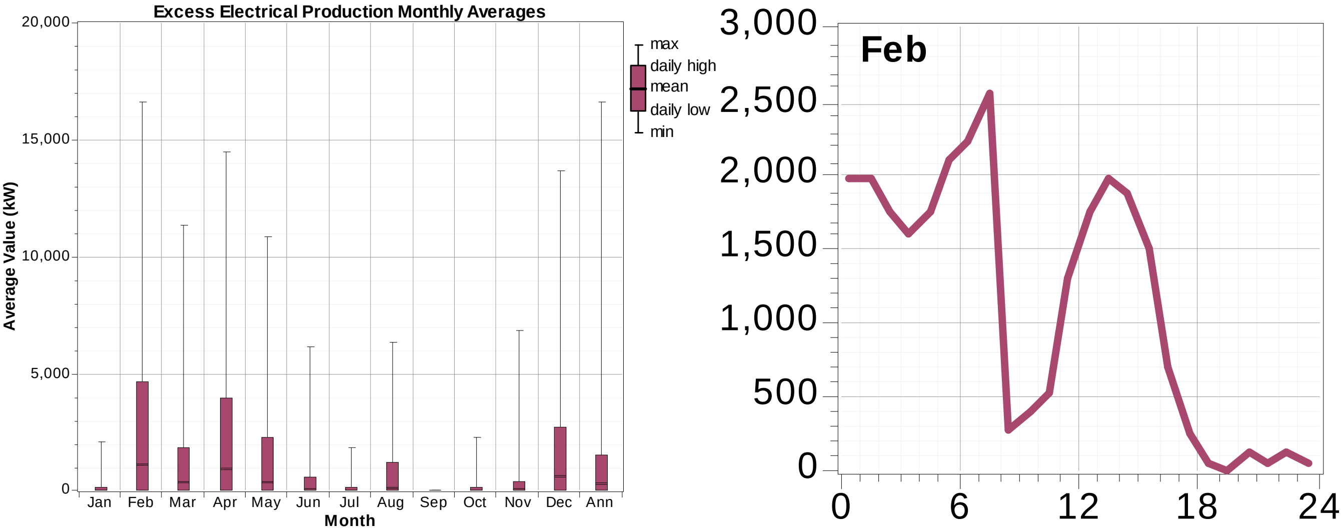

Fig. 3.13. Excess electricity generated in the 4-renewables case

Needless to mention, the biomass plant could raise the overall 47% coverage of the supply if it becomes cost competitive against grid tariffs in the future. In the model evaluated, this plant only runs during peak hours to avoid expensive purchases of electricity. In the next section a new approach will be studied, where the biomass plant works as a base generation plant, like in an isolated system.

3.4 Simulations with energy storage

3.4.1 Model construction

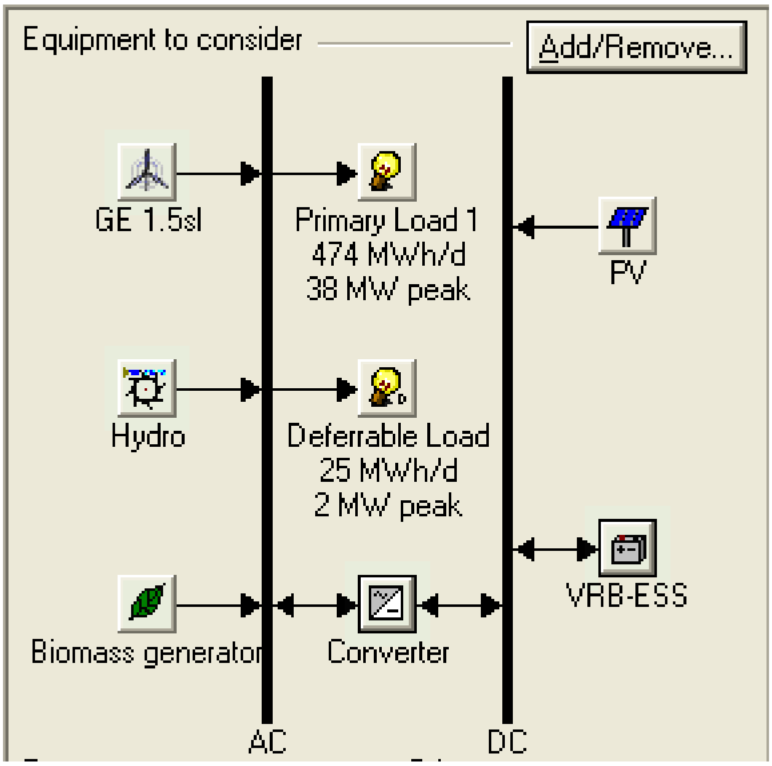

Fig. 3.14. General diagram of the model

In Fig. 3.14, the proposed configuration of the system is shown. There are four different renewable generation sources, and two ways of storing energy. On the one hand, a vanadium redox flow battery is available to store excess energy that can be used later. On the other hand, a virtual energy storage means is contemplated assuming that a deferrable load exists. This load can be related either to a heating or cooling system, or an electric vehicle battery charging system, for instance.

Regarding the renewable generation and taking into account that the connection to the grid, with a capacity of 40 MW, limits the possible renewable power installed, the proposed dimensioning is the following.

Photovoltaic system	15 MW
Wind farm	15 MW
Hydropower	10 MW
Biomass plant	10 MW

Among these, the biomass plant is the only generating system whose operation does not depend on meteorology/hydrology, if we accept the assumption that the needed biomass is always available.

In the same way, the features of the mentioned energy storage means are described below.

- Vanadium Redox Flow Battery (VRB), 6 MW, 24 MWh
- Deferrable load, 4 MW, 24 MWh

3.4.2 Results of the simulations

Once determined the type and the size of the components to be included in the system, the simulations have been performed. It is worth mentioning that the same model has been simulated with and without energy storage in order to evaluate the benefits that energy storage presents for the kind of system under study. In the table, the without storage case excludes both the deferrable load and the VRB. Also, the model has been simulated in both grid-connected and isolated mode, to assess the different performance of the energy storage.

3.4.2.1 Without storage vs with storage mode

Table 3.7. Balance of electricity with and without energy storage

	w/o storage	w storage
Microgrid generated electricity (MWh/yr)	149,325	151,276
Excess electricity (MWh/yr)	5,466	1,751
Grid purchases (MWh/yr)	38,603	34,288
Microgrid supply	78.8 %	81.1 %

In Table 3.7, we can see the comparison of the electricity generation results between the cases with and without energy storage. First, we can see that the electricity generated in the microgrid is lower in the case without storage. When an energy storage means is available, a dispatchable generator, like the biomass power plant in our case, can generate during low demand hours in order to store this energy to be used when needed. That is, the absence of energy storage limits the operation of the biomass power plant, causing at the same time an increase in the purchasing of electricity from the grid.

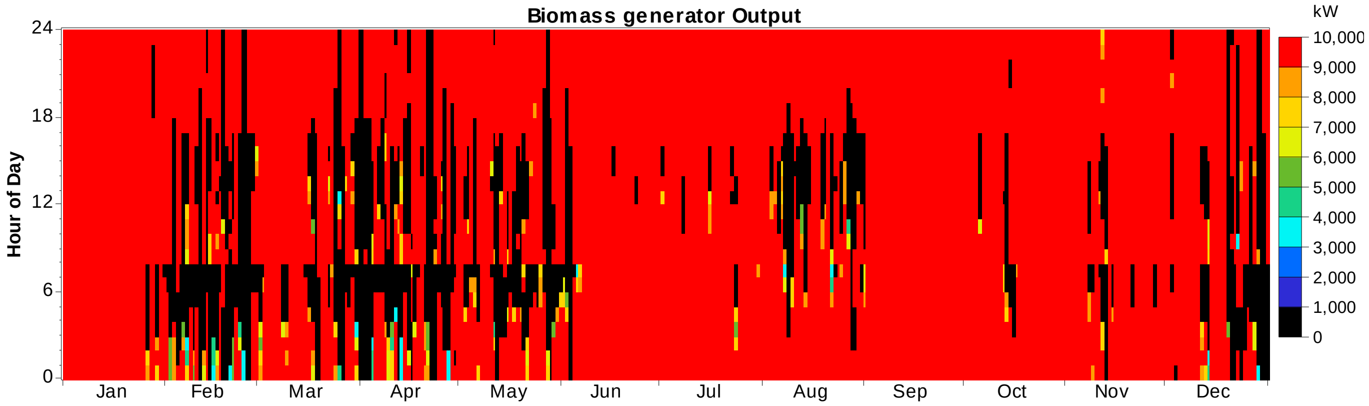

Fig. 3.15. Operation of the biomass power plant in isolated mode

The performance of the biomass power plant in the case with storage is shown in Fig. 3.15. This simulation was carried out in isolated mode, to check how far the micro-grid can reach meeting the load demand, giving as a result a capacity factor of 82.8% for the biomass power plant. That means that the biomass power plant runs as a base generation plant, generating electricity during most of the time along the year.

It is worth noting that according to the modelled system, it is only needed a 16 MW grid connection to meet 99.9% of the demand, compared to the 40 MW connection in the original situation.

Nevertheless, depending on both electricity and biomass resource prices the operation of this power plant in the grid connected mode can be very different, running only in tariff periods with high electricity prices. Namely, according to the price assumptions used in the model the capacity factor of the biomass power plant would be 8.8% in the grid connected mode. Thus, it would be difficult to justify the investment with such a low amount of working hours. In the previous section, a maximum renewable generation of 47% was reached, given that when working in connected mode the biomass plant runs only during peak hours.

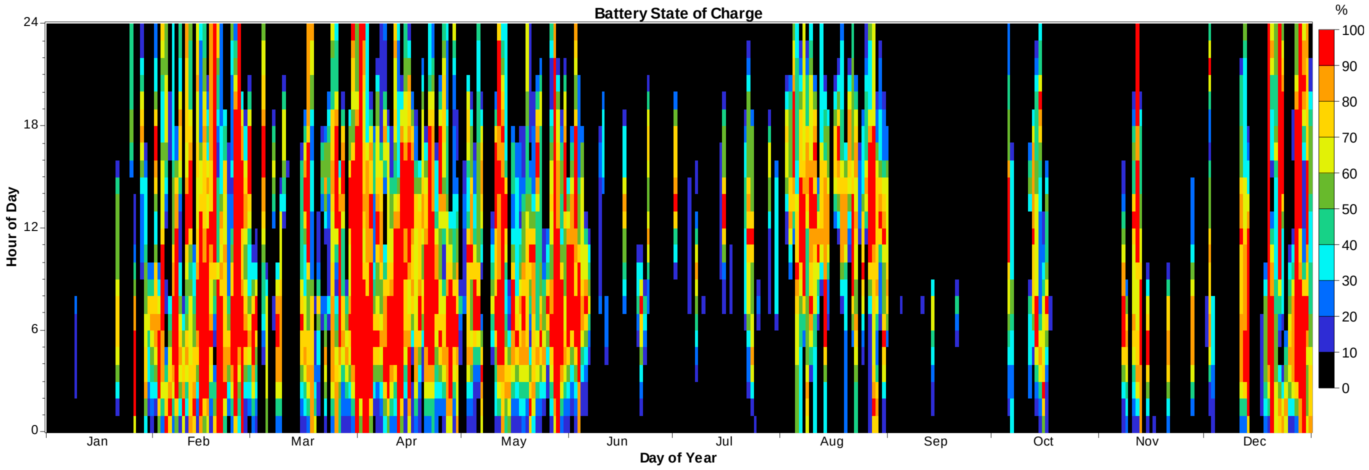

Fig. 3.16. State of charge of VRB in isolated mode

In the same way, when working in grid connected mode the profitability of the VRB will depend on factors like grid fees, selling prices, net metering and so on.

In the grid connected mode, according to the simulations neither the biomass power plant nor the VRB are cost effective with the current prices of the resources (biomass, electricity) and the components (biomass power plant, batteries). However, energy storage presents different features that are difficult to quantify from the economical point of view, i.e. to prevent system faults, or to feed critical loads acting as backup equipment.

3.4.2.2 Managing excess energy

In any case, in the kind of system under study with a high renewable penetration there is an inherent excess energy that needs to be handled, either storing it or selling it. In Fig. 3.17, the energy generation that exceeds the demand is shown. Depending on the situation, this energy will be fed into the grid, used for the deferrable load or stored in the VRB. Needless to say, in a system without storage this energy would be always fed in to the grid whatever the price would be. An energy storage system allows keeping this energy to sell it at peak price hours, or to use it later avoiding further purchases from the grid.

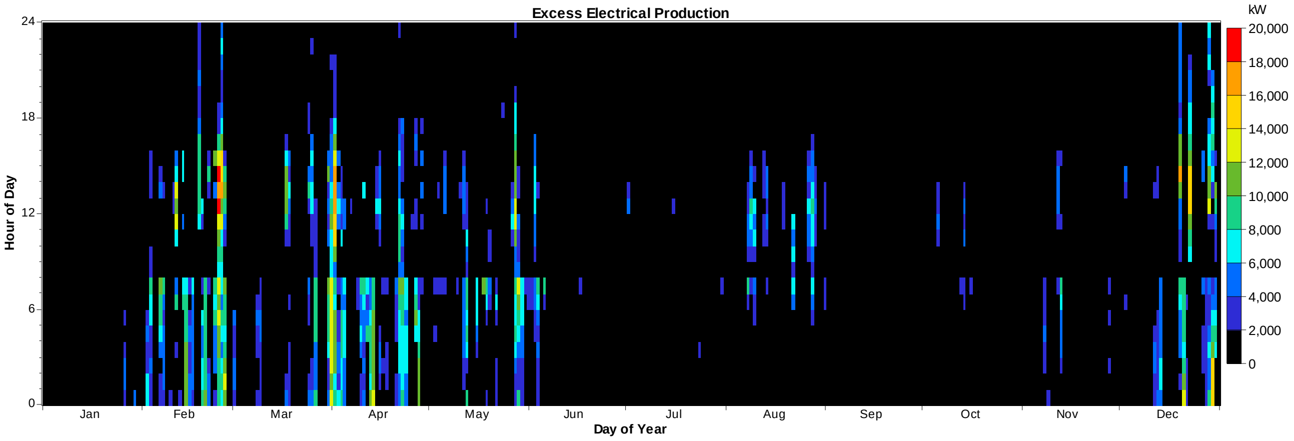

Fig. 3.17. Diagram of the excess electricity generated

From the control perspective, it is worth mentioning that in the proposed system there are three manageable components available. These are the biomass power plant (dispatchable generation), the deferrable load (virtual energy storage) and the VRB (real energy storage).

In Fig. 3.18, an example of energy being stored in the deferrable load and in the VRB is shown. On the left axis, the energy stored in both means is shown in kWh. On the right axis, the excess power that cannot be stored is shown in kW. The amount of energy stored in the deferrable load is shown in light blue and the energy stored in the VRB is shown in dark blue in the figure.

According to the strategy, the generated energy that exceeds the primary load goes first to meet the deferrable load. In some cases, the excess is higher than the available power for the deferrable load, so that at the same time some energy can be stored in the VRB. In moments where both the deferrable load and the VRB have reached their limit of storage, the energy cannot be further stored and this excess energy will have to be either fed into the grid or lost. This excess is shown in red colour in the figure.

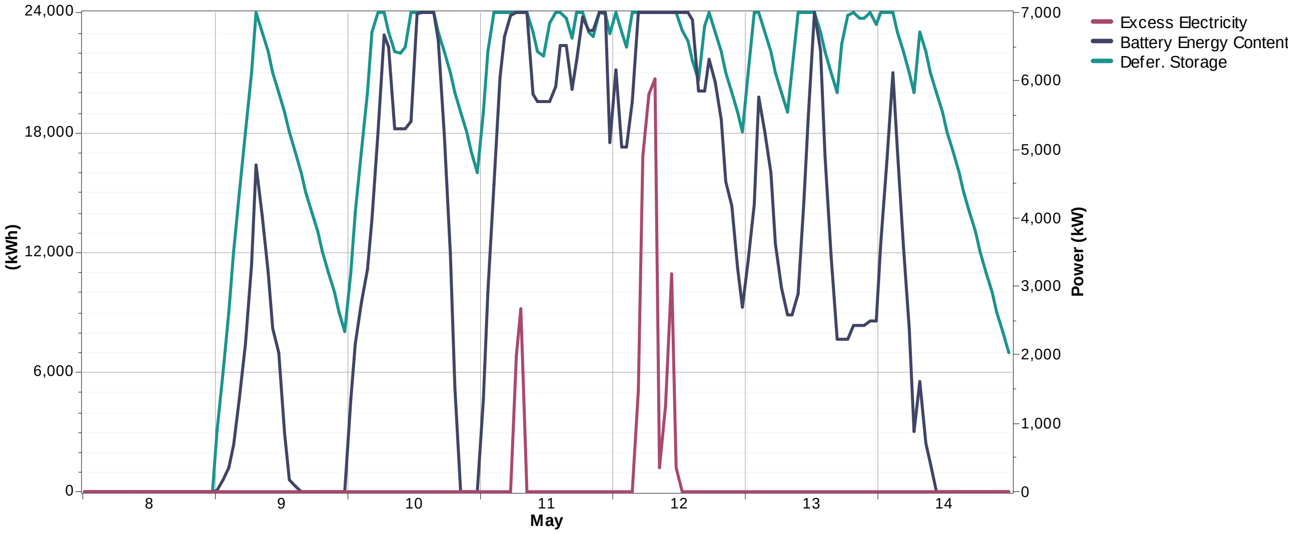

Fig. 3.18. Detail of energy management through storage

On the other hand, in Fig. 3.19 the purchased electricity from the grid is shown. Each little graph details the average electricity demanded from the grid in every month.

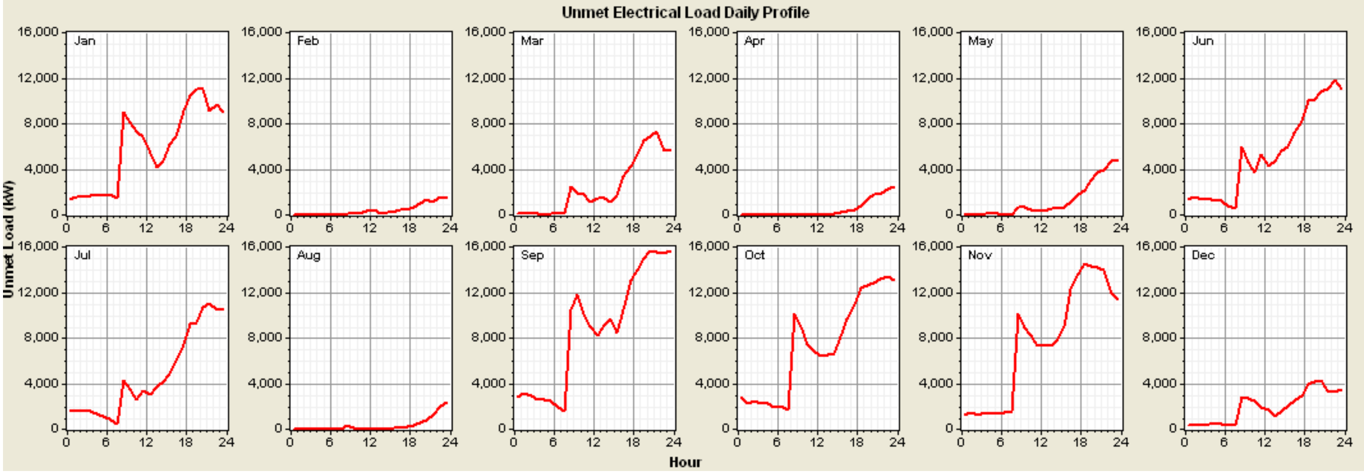

Fig. 3.19. Electricity purchased from the grid in each month

3.5 Conclusion

An analysis has been carried out for a micro-grid system implemented in an automotive industrial area. Both cases with and without energy storage have been studied in order to evaluate the benefits of energy storage regarding the share of renewable energy in the overall electricity supply.

In most options of the case without storage, the renewable generation accounted for about one third of the electricity demand. One of the reasons is the low capacity factor of the biomass plant, only running during peak hours. In the case with the maximum renewable generation capacity installed, the coverage of the electricity demand was that of 47%.

Regarding the simulations with energy storage available, the system could meet up to 81% of the load demand, operating the biomass plant as a base generation plant. In this case, it is worth noting that only a 16 MW grid connection is needed to meet 99.9% of the demand, compared to the 40 MW connection in the original situation. This reduction in the power capacity of the grid connection could mean a huge saving in certain systems. Moreover, some equipments such as the biomass plant and the energy storage can be used as a backup, providing energy security for systems connected to a weak grid.

In any case, it is clear that the management strategy of the energy generated and stored in the system is a key factor for the cost-competitiveness of the whole installation. Meanwhile, energy storage may not be cost-competitive at current prices, but still presents several features for the stability of a micro-grid that have to be taken into account.

4 VALDABRA PUMPING STATION

4.1 Description of the modelled areas

Within WG2, in deliverable D2/D3 ("Description of test cases and consumption patterns"), a detailed description of the test cases from CIRCE is given and D7 ("Microgrid computer models") contains a brief summary which is repeated below, in order to put in a right context the simulation results.

4.1.1 Real Case: Rural microgrid for irrigation pumping

The microgrid to be simulated in detail is an irrigation pumping station with wind power support and storage, located in the Valdabra reservoir (Huesca). In this microgrid there are integrated wind power generation, a reversible hydraulic pump, hydrogen storage and ultracapacitors. The objective of this installation is to support water pumping but in addition to increase the transport capacity of the rural network, avoiding grid extensions in the case of the connection of new consumption. The pumping station at Valdabra, consists of the following elements:

- AC/DC converter for grid connection (250 kW)
- Chopper with resistors (rated at 250 kW)
- ADES Wind Turbine 250 kW
- Three simple (110.4 kW) and one reversible hydraulic pump (160 kW)
- Energy storage with 260 Maxwell 3 kF ultracaps (700V, 11.5 F)
- Portable energy storage system
- Control and communication system (Measurement, PLC and SCADA)

4.1.2 Generic case: Industrial area with small workshops and industrial stores

The generic case describes typical industrial areas where the activity is dominated by small workshops, small factories and industrial stores. This type of industrial areas is very common in the entire zone of SUDOE (Portugal, Spain and south-west France).

In this case, no renewable energy generation is present and the aim of the model is twofold. First, a possible development of distributed generation is simulated as an optimised planning problem with a planning horizon of 20 years. In a second step, the operation of a developed microgrid after 20 years is simulated. It is assumed that solar pv and wind power resources are available The topology of such a microgrid is basically linear, as these industrial areas are distributed along a road. In Fig. 4.1, the assumed grid structure is depicted. In this example, the wind generator is connected to node 1 while solar pv is assumed to be possible at all nodes.

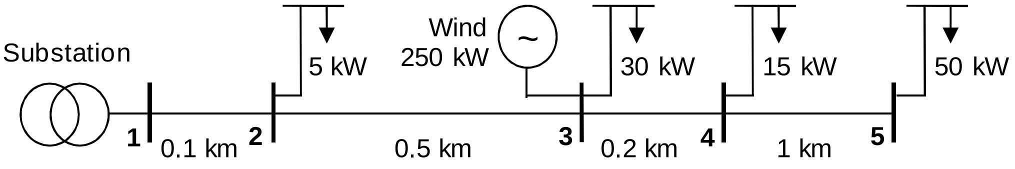

Fig. 4.1. Microgrid structure of assumed industrial area of 100 kW total mean power.

4.1.3 Consumption profiles

Consumption profiles are introduced from text files with 8760 hourly values. In Fig. 4.2 hourly values of the load for the two cases are represented. In case 1 there is AC and DC demand, as one of the pumps is connected to the DC bus. In case 2 there is only DC load.

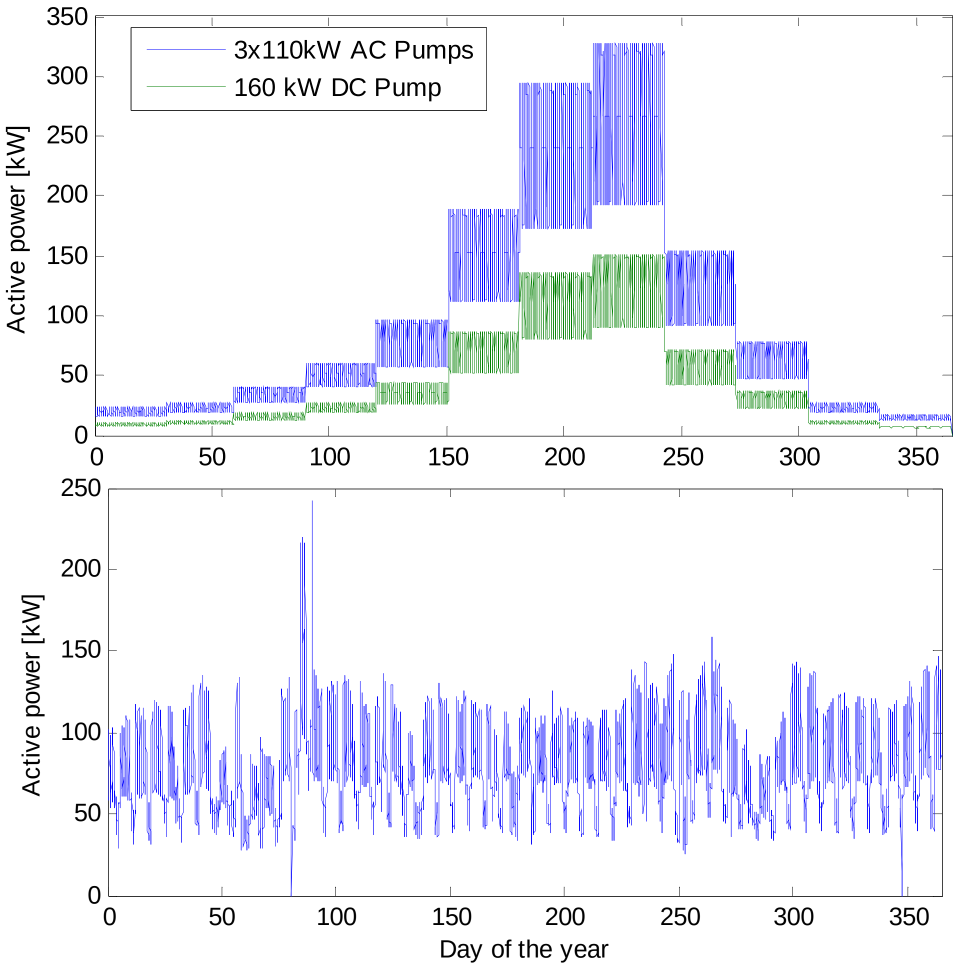

Fig. 4.2. Demand profile of AC and DC pumps of case 1 (up) and AC load of industrial area of case 2 (below).

In Fig. 4.3 a box plot of the same demand is shown. Values are given per unit (p.u.) as they are the same for AC and DC load in case 1. Actual loads are obtained with different scaling factors.

In both representations it can be clearly seen that in case 1 there is a large seasonality of the load, while in case 2 the variability is similar all over the year. In case 2 there are only three special events. After 50 and after 280 days, there are some weeks with low demand. These weeks are Christmas and summer holidays. Finally there is a demand peak during one week after approximately 90 days.

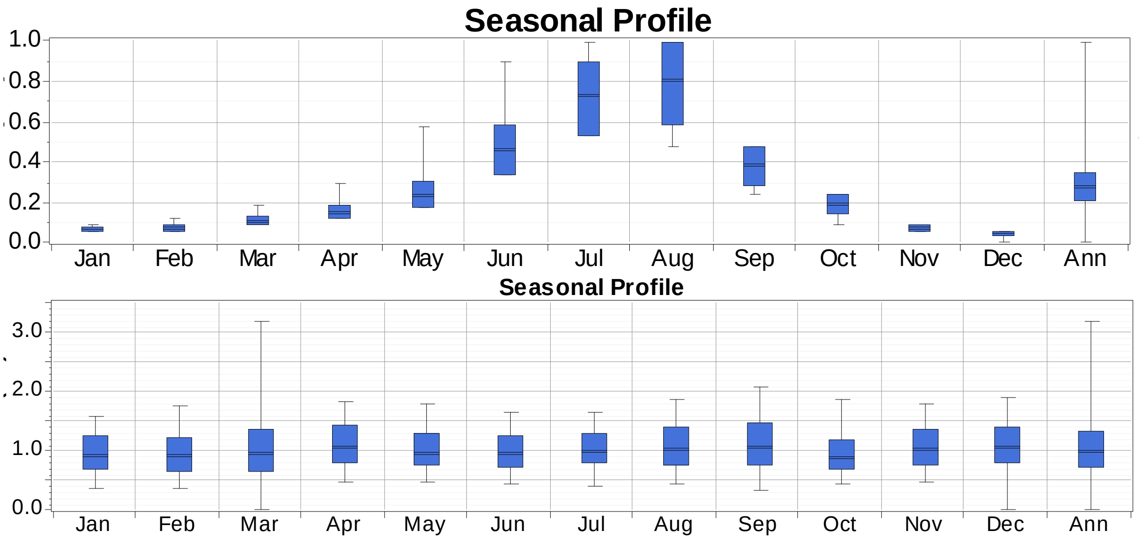

Fig. 4.3. Box plot of Seasonal load profile of the pumping station, given per unit.

Another type of representation which offers HOMER is the so called DMap (see Fig. 4.4). In such a map, all hourly data can be seen at a glance. Every column is a day of the year and every line is an hour of the day. It can be seen at once, that in case 1, there are only monthly estimations, while in case 2 every hour of the year is different.

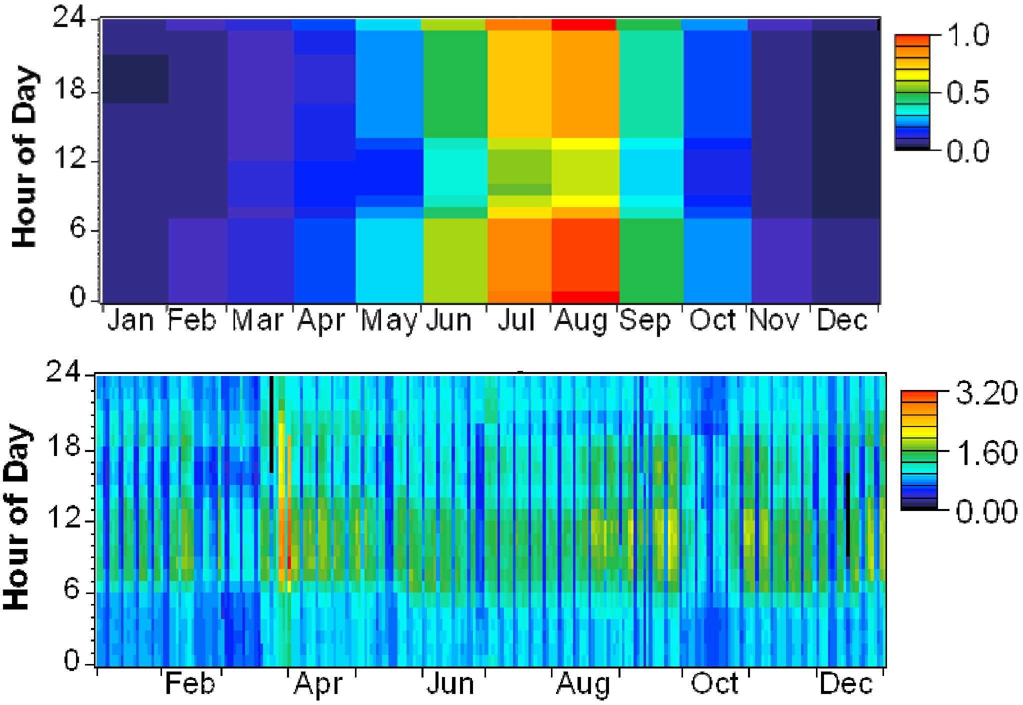

Fig. 4.4. DMap of hourly load given per unit of the pumping station (up) and industrial area (below),

4.2 Simulation models

The simulation models and applied Software were described in detail in GT2 deliverable D7 ("Microgrid computer models"). Therefore, here only a short introduction is presented. At first, the mirco-grid is simulated with the hybrid system software HOMER and HOGA. The objective is to obtain a first guess of what would be a good configuration of the micro grid. The sizing is done with two different tools, in order to compare results. These two tools are similar but they have features which complement each other.

HOMER, due to the intuitive user interface, permits to obtain results quickly. The drawback of this program is that no actual optimization algorithm is implemented. The user must provide ALL possible options and HOMER just tries out all combinations and gives as result all feasible solution, sorted by the cost of energy (COE) in $/kWh. As a result, of the search space is too large simulations can quickly take very long time.

The main difference between HOMER and HOGA is that HOGA actually uses optimization algorithms which make it much more effective searching for an optimum solution. HOGA tends to propose larger system elements. Thus, a sensitivity study with HOMER might be useful to obtain a solution with lower system costs.

As a result of the simulation with HOGA and HOMER will stand a proposal for an optimized configuration in order to introduce distributed generation into the industrial areas under study.

4.2.1 Comparison of HOGA and HOMER

It can be stated that these two software tools are complementary. In order to obtain best results, the following strategy may be used:

- Simulation of consumption profiles with HOGA in order to optimize the sizing of System elements and control strategies
- Sensitivity analysis with HOMER, using as base case the configuration found with HOGA. Possible variables for this analysis: annual mean values of wind speed and solar radiation, height of the wind turbine, interest rates, prices of the elements

4.2.2 Operational simulation with Matlab/Simulink®

In this simulation, a certain micro-grid configuration is simulated more in detail in order to evaluate operation strategies. Although in D7 it was announced that PSAT would be used as simulation platform, finally, Matlab Simulink has been preferred. Based on a given configuration of the system, with and without energy storage, possible operational strategies are presented and discussed.

4.2.2.1 Description of the Model

In Fig. 4.5 a schema of the proposed model is presented. The simulation includes control of active and reactive power using converters and a battery storage system (BSS). As input, several time series are possible. In the first place, the demand with active and reactive power ($\mathrm{P_{load}}$ and $\mathrm{Q_{load}}$) with a time step of 30 min. In addition, time series of renewable sources such as wind ($\mathrm{P_{genw}}$) and solar pv ($\mathrm{P_{genpv}}$) are considered. In this case, time series are adopted from HOMER simulations (but with 30-min time step).

The output of the model is the power flow at the point of common coupling (PCC), which are active and reactive power $\mathrm{P_{red}}$ and $\mathrm{Q_{red}}$. Secondary results are the state of charge of the battery (SOC) and the power factor (PF) of the mini-grid.

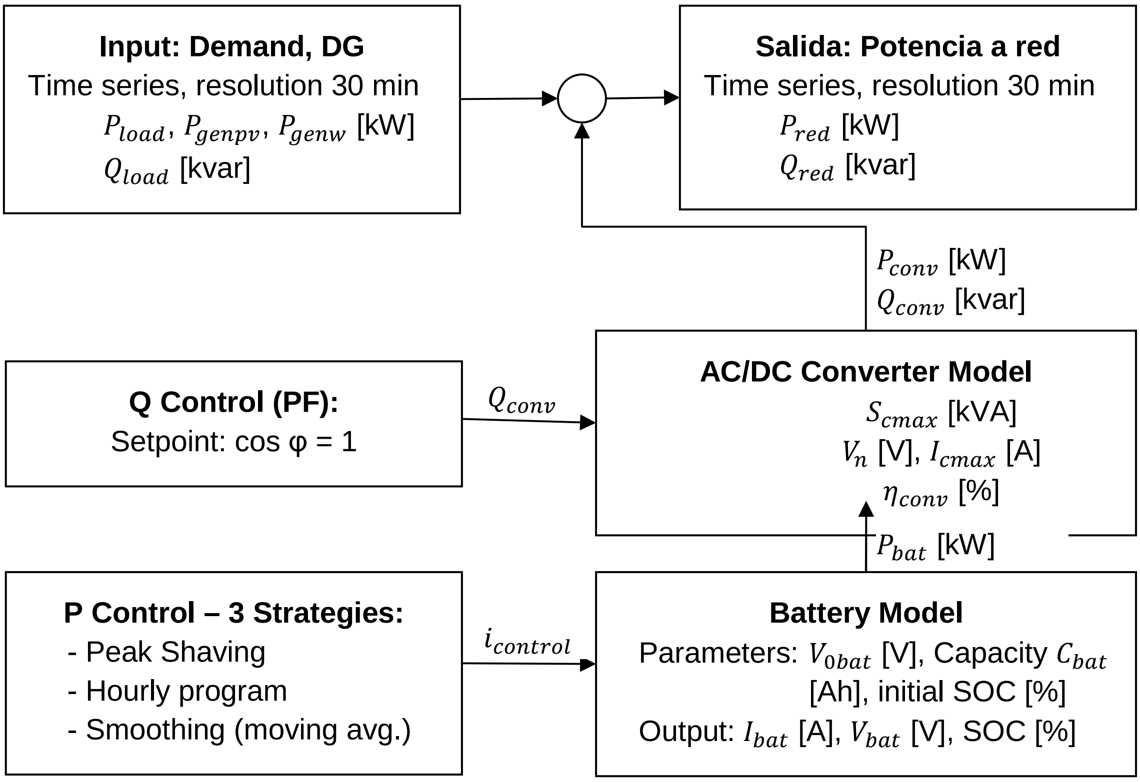

Fig. 4.5. Schema of the simulation model with active (P) and reactive (Q) power control of a grid-connected System with battery energy storage..

For the active power control (P Control) 3 strategies have been chosen to give some examples: Peak shaving, hourly program and demand curve smoothing (with moving average). These strategies are described more in detail in the following paragraphs.

The reactive power control (Q Control) only considers as setpoint a minimum power factor (PF or cos φ). If the PF falls below the established minimum, the converter injects reactive power, if possible. Find more details on this control below.

The converter model simply consists in a number of operational constraints such as its maximum apparent power $\mathrm{S_{cmax}}$ and current$\mathrm{I_{cmax}}$. In addition, the converter efficiency η_{conv} is taken into account, as it is crucial for the calculation of effectively stored and released energy from the battery storage system.

For the Battery Model the standard model in Simulink was used. More details on that model are given in this report in the following pages.

4.2.2.2 Data input and output

The inputs of the model are 30-min time step series of the demand (P and Q) and the renewable generation (solar and wind). Thus, for every variable, 17,520 values are available, covering one year.

The file format for Simulink requires data in lines. The first line always contains the time axis in seconds. Demand and generation data are introduces with separate files. Results are saved in an output file with the following nomenclature:

"Optimagrid1_180kW1MWh_120710.mat"

The number after "Optimagrid" represents the P-control strategy, after that power and energy parameters of the battery are given and finally the creation date of the file is included in the format YYMMDD.

Values are organized in lines such as input files and are saved with 30-min time step such as input data. The output file contains 13 lines with variables listed in the table below.

Table 4.1. Structure of output file of the Simulink model.

Line	Variable	Description
1	t	Simulation time
2	$P_{gen,DG}$	DG (solar+wind) active power [kW]
3	P_{load}	Demand active power [kW]
4	P_{sum}	Sum of micro-grid active power [kW]
5	P_{conv}	Battery converter active power [kW]
6	P_{red}	PCC active power [kW]
7	Q_{load}	Demand reactive power [kvar]
8	Q_{conv}	Converter reactive power [kvar]
9	Q_{red}	PCC reactive power [kvar]
10	$i_{control}$	Current control set point (P control) [A]
11	I_{bat}	Battery current [A]
12	V_{bat}	Battery voltage [V]
13	SOC	State of charge of the battery [%]

4.2.2.3 Strategies of P Control (active power)

The output of the block "P Control" is the variable $\mathrm{i_{control}}$ which represents directly the charging current of the battery.

Strategy 1: Peak shaving

Within this scenario, the aim is to reduce demand peaks which surpass certain power limits. The battery is recharged during low demand hours. Thus, two parameters are established: $\mathrm{P_{max}}$ and $\mathrm{P_{min}}$. Hence, if the joint power $\mathrm{P_{sum}}$ of demand and distributed generation (DG), i.e. solar and wind generation, is below $\mathrm{P_{min}}$, the battery is recharged and if it is above $\mathrm{P_{max}}$, the battery is discharged in order to reduce the peak. The following equations represent the logic of this control.

$$P_{sum} = P_{load} - \left(P_{genpv} + P_{genw}\right) \tag{1}$$

$$\Delta P = \begin{cases} P_{min} - P_{sum}; & P_{\mathrm{sum}} < P_{min} \\ P_{max} - P_{sum}; & P_{sum} > P_{max} \\ 0; & P_{min} \le P_{\mathrm{sum}} \le P_{max} \end{cases} \tag{2}$$

$$i_{control} = \frac{\Delta P}{V_{bat}} \tag{3}$$

In order to facilitate the introduction of the parameters to the model, a mask has been created containing the parameters listed below in Table 4.2.

Table 4.2. Parameters of control strategy 1 (peak shaving), accessible through a dedicated Simulink mask.

Parameter	Description
P_{max}	Maximum demand desired [kW]
P_{min}	Low demand; enable recharge of the battery [kW]

If DG is present, “low demand” may mean negative demand or energy injection to the grid. Therefore, a negative value of $\mathrm{P_{min}}$ can be interesting. In this case, the peak shaving has a double function. In high demand hours, consumption power peaks are reduced. In low demand hours combined with high renewable generation, generation power peaks are reduced. In such a situation, an additional control algorithm is needed which defines an objective of SOC of the battery. This algorithm is activated if $\mathrm{P_{sum}}$ is within desired limits but SOC is outside a defined region of SOC. In the present model, this region is defined as +/- 5% around the initial state of charge of the battery $\mathrm{SOC_{init}}$.

Strategy 2: Hourly Program

In this scenario it is assumed that there is some daily program of charge and discharge of the battery. The idea of this strategy consists in the assumption that electricity prices may vary during the day and the battery is charged and discharged accordingly. In this simulation, no actual price information is included, but the tool for a charge/discharge program is implemented. Basically, a control variable a is introduced which can adopt the values -1, 0 and 1 (discharge, pause, charge). In Fig. 4.6 an example for a possible program is shown, where the intervals of charge and discharge last 8 h each. In this example, the charge is started at 00:30h ($\mathrm{t_{ch}} = 0{,}5$) and de discharge at 11:00 h ($\mathrm{t_{dch}} = 11$).

In the proposed model, as a simplification, only one charge and one discharge cycle per day is considered. In order to facilitate the introduction of the parameters to the model, a mask has been created containing the parameters listed below in

Table 4.3.

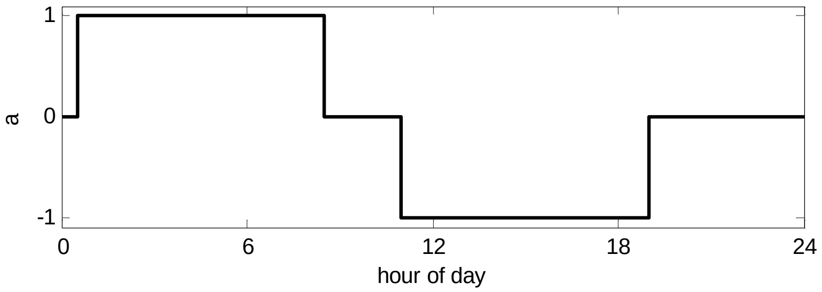

Fig. 4.6. Example of a daily program of charge and discharge of the battery storage system.

Table 4.3. Parameters of control scenario 2 (daily program), accessible through a dedicated Simulink mask.

Parameter	Description
t_{ch}	Start charging battery
t_{dch}	Start discharging battery
Δt_{ch}	Charging duration
Δt_{dch}	Discharging duration

The related control current $\mathrm{i_{control}}$ is calculated as a function of battery capacity $\mathrm{C_{bat}}$ and the charging and discharging duration ($\Delta\mathrm{t_{ch}}$ and $\Delta\mathrm{t_{dch}}$). The related equations are shown in the following table.

$$i_{control} = \begin{cases} \frac{a\ C_{bat}}{\Delta t_{ch}}; & a > 0 \\ \frac{a\ C_{bat}}{\Delta t_{dch}}; & a < 0 \\ 0; & a = 0 \end{cases} \tag{4}$$

As a result of such a strategy, undesirable power peaks can occur, as the control does not take into account actual consumption or generation levels at PCC. In order to avoid power peaks, an additional constraint is added to the control. Active power at PCC is limited according to power limits established in Strategy 1. These limits are more relaxed, but strictly based on the limits in Strategy 1. Actual values used in the showcase are presented in section 0. If active power at PCC surpasses established limits, the programmed charge or discharge of the battery is reduced. As peak shaving is not the objective of this strategy, no charging is permitted in the case of programmed discharge and vice-versa.

Strategy 3: Demand smoothing (with moving average)

The aim of this strategy is to smooth out rapid changes and peaks of the demand. The active power set point is calculated as the moving average of the last w known values. In this case of 30-min time steps, a value of $\mathrm{w} = 4$ results in an averaging window width of 2 hours. In the Simulink model this calculus is implemented with a FIR filter, introducing into the field “Numerator coefficient” the value “ones(1,w)/w”.

In order to facilitate the introduction of the parameters to the model, a mask has been created where only the parameter w must be introduced. The output of this control block is the power set point $\mathrm{P_{ref}}$ which is used to calculate the control set point $\mathrm{i_{control}}$, as shown in the following equation.

$$i_{control} = \frac{P_{ref} - P_{sum}}{V_{bat}} \tag{5}$$

In any case, $\mathrm{i_{control}}$ is subject to constraints which depend on the converter and the battery. These constraints are specified in the paragraphs where the related models are described.

4.2.2.4 Reactive power control (Q Control)

Besides the active power control, a reactive power control (Q Control) has been implemented, based on a set point for the power factor PF (or $\cos\varphi$). Always when the PF is below the established set point, the converter tries to inject reactive power ($\mathrm{Q_{conv}}$). The injection of reactive power is subject to the nominal apparent power of the converter ($\mathrm{S_{cmax}}$) and the current injected active power of the converter ($\mathrm{P_{conv}}$) due to the active power control. Thus, in this model, the reactive power control is subordinated to the active power control. If reactive power control is considered more important, the priorities can be changed easily. But that case has not been considered here.

$$Q_{conv} = \begin{cases} P_{red}\left(\tan\varphi - \tan\varphi_{ref}\right); & \cos\varphi < \cos\varphi_{ref} \\ 0; & \cos\varphi \geq \cos\varphi_{ref} \end{cases} \tag{6}$$

$$\tan\varphi = \frac{Q_{load}}{P_{sum} + P_{conv}} \tag{7}$$

As a result of the subordination of the reactive power control to the availability of free apparent power of the converter $\mathrm{S_{cmax}}$ (see section 4.2.2.5 Converter Model), the set point of $\mathrm{Q_{conv}}$ is subject to the following constraint:

$$Q_{conv} \leq Q_{max} \tag{8a}$$

$$Q_{max} = \sqrt{S_{cmax}^2 - P_{cmax}^2} \tag{8b}$$

4.2.2.5 Converter Model

The converter is modeled taking into account its maximum values of current $\mathrm{I_{cmax}}$ and apparent power $\mathrm{S_{cmax}}$. This limitation results in additional constraints of the active and reactive control. Maximum apparent converter power $\mathrm{S_{cmax}}$ is calculated from maximum renewable generation $\mathrm{P_{ren,max}}$ and a margin for reactive power control $\mathrm{S_{c,margin}}$. Renewable generation is assumed to be always active power, so apparent renewable generation is defined as $\mathrm{S_{ren,max} = P_{ren,max}}$.

$$S_{cmax} = S_{ren,max} + S_{c,margin} \tag{9}$$

In the base case of no renewable generation, $\mathrm{S_{ren,max}}$ is zero and $\mathrm{S_{c,margin}}$ is equal to total converter power and set equal to nominal battery power. No extra margin for Q control is assumed here, as reasonable results are obtained for power factor compensation.

In addition, converter efficiency η_{conv} is included, as it changes the energy which is actually exchanged with the battery. The related mathematical models are presented in paragraph “Constraints for P Control”.

In order to facilitate the introduction of the parameters to the model, a mask has been created containing the parameters listed below in Table 4.4.

Table 4.4. Model parameters of the converter (accessible through a dedicated Simulink mask).

Parameter	Description
$S_{c,margin}$	Converter power margin for reactive power control [kVA]
$I_{c,max}$	Maximum converter current [A] (currently no used)
η_{conv}	Converter efficiency [%]
S_{cmax}	$S_{ren,max} + S_{c,margin}$ (calculated, no direct input via mask)

Constraints for P Control

The control variable for P Control is the charge and discharge current of the battery $\mathrm{i_{control}}$. This current is actually the current to be supported by the DC/DC converter which controls de battery charging. Maximum allowable current of this converter is calculated from the nominal power and voltage of the battery $\mathrm{P_{0bat}}$ and $\mathrm{V_{0bat}}$ (see Battery Model below).

$$|i_{control}| \leq \frac{P_{0bat}}{V_{0bat}} \tag{10}$$

Assuming symmetric converter efficiency η_{conv} for positive and negative currents, the impact of that efficiency can be modeled as written in the following equation.

$$i_{control} = i_{control}[1 - (1 - \eta_{conv})\,\mathrm{sign}(i_{control})] \tag{11}$$

As a result, if $\mathrm{i_{control}} < 0$ (discharge of the battery), a higher discharge current is necessary, in order to satisfy the active power set point to be injected to the grid. In the opposite case, if $\mathrm{i_{control}} > 0$ (charge of the battery), a lower current reaches the battery because part of the power is consumed in the converter.

Limits for Q Control

The set point for the Q control is the PF (or $\cos\varphi$) and the output is directly the reactive power $\mathrm{Q_{conv}}$ injected to the grid by the converter. The equations which describe the constraints of $\mathrm{Q_{conv}}$ have been presented before in section 4.2.2.4.

4.2.2.6 Battery Model

Here, the detailed battery model of Simulink is not explained, as it can be consulted in the Matlab documentation. The battery is charged and discharged using a controlled current source with the input $\mathrm{i_{control}}$. Positive values of $\mathrm{i_{control}}$ charge the battery and negative values discharge it. As a result, the model output $\mathrm{I_{bat}}$ is just the inverse of $\mathrm{i_{control}}$, as from the battery point of view, positive current means discharging the battery.

$$I_{bat} = -i_{control} \tag{12}$$

The battery model also imposes some constraints to the control variable $\mathrm{i_{control}}$. It is assumed that the maximum converter current is always below the maximum allowable battery current, but a reduced charge/discharge regime has been introduced when the values of SOC (state of charge) are approaching its limits. Therefore, a factor f is introduced, which is unity while SOC is situated within intermediate limits and is reduced linearly until zero when SOC reaches the established limits of charge and discharge respectively. In the P Control, this constraint can be written as follows:

$$i_{control} = f\, i_{control} \tag{13}$$

$$f = \begin{cases} 1; & SOC_{min2} \le SOC \le SOC_{max2} \\ f_{ch}; & i_{control} > 0, \quad SOC > SOC_{max2} \\ f_{dch}; & i_{control} < 0, \quad SOC < SOC_{min2} \\ 0; & SOC_{min} > SOC > SOC_{max} \end{cases} \tag{14}$$

$$f_{ch} = \frac{SOC - SOC_{max}}{SOC_{max2} - SOC_{max}} \tag{15}$$

$$f_{dch} = \frac{SOC - SOC_{min}}{SOC_{min2} - SOC_{min}} \tag{16}$$

In Fig. 4.7 it can be observed how in the case of battery charging, f is unity until SOC reaches 80%. After that, it is reduced linearly until zero, when SOC reaches 100%. In the opposite case, when the battery is discharged, f is unity unitil SOC reaches 20% and reached zero at the established minimum allowable SOC of 5%.

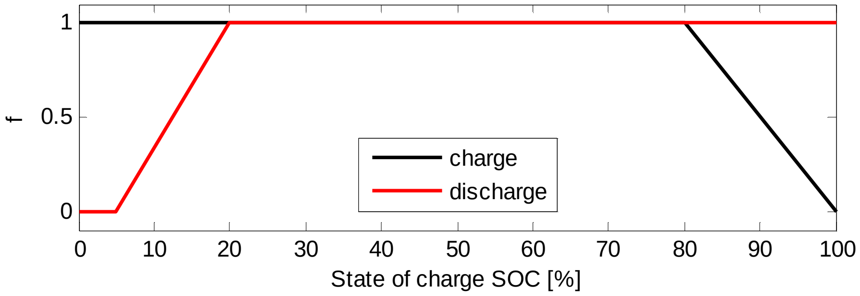

Fig. 4.7. Example of reduced charge/discharge applying the limits of the present case.

In order to facilitate the introduction of the parameters to the model, a mask has been created containing the parameters listed below in Table 4.5.

Table 4.5**.** Parameters of the battery model (accessible through a dedicated Simulink mask).

Parameter	Description
P_{0bat}	Nominal battery power [kW]
V_{0bat}	Nominal battery voltage [V]
C_{bat}	Nominal battery capacity [Ah]
SOC_{init}	Initial state of charge [%]
SOC_{min}	Minimum allowable SOC
SOC_{min2}	Minimum SOC to start reduced discharge
SOC_{max}	Maximum allowable SOC
SOC_{max2}	Maximum SOC to start reduced charge

4.2.3 Planning simulation with GAMS

In a second step, a longer term planning is proposed, using GAMS as software platform. This is motivated by the fact that in a beginning, no energy storage may be installed, because it is still very costly, but at a certain moment in the future, it will become interesting to install such systems, because they make excess energy generation useful and thus directly lower the overall cost of energy. Results of such a model developed in GAMS are presented.

The optimization algorithm is applied to Case 2 (Industrial area with small workshops and industrial stores). The micro-grid in Fig. 4.1 is implemented in detail, in order to consider losses in distribution lines and thermal limits of the existing installation. It is assumed that any installation of renewable energy is limited to the energy evacuation capacity of the existing distribution lines.

4.2.3.1 Reduction of input data using clustering

The model to be optimized considers 5 grid nodes, 20 years planning horizon (1-year time steps) and 4 input variables: demand, electricity price, solar resource, wind resource. The initial idea was to simulate this configuration with the same input at 1-h time steps, which means 8760 values per input variable. As a result, the input to the optimization problem grows up to 3.5 million values. The model contains 34 equations (objective function, load flow, cost calculations, restrictions). In many of these equations the entire 3.5 million values are present. As a result, the solver runs out of memory when trying to resolve the problem.

One simple way for reduction is increasing the time step. In this case, higher frequency effects cannot be accounted for. Therefore only a doubling to 2 h is considered here, leading to 4335 time steps. Simulation tests show that a model with 840 time steps is possible to solve with 3 GB RAM available.

Thus, in order to further reduce the size of the model, clustering is done with the help or Matlab function "kmeans". The clustering results are shown in the following paragraphs. The clustering is applied to the 365 daily time series (with 2-h time step) of the four input variables: demand (dem_t), wind (perf_w), solar pv (perf_pv) and electricity price (PE). If the four input variables are grouped into 2, 6, 5 and 3 clusters respectively, 100 combinations can represent the whole year. This means that not all possible combinations actually exist, as theoretically, 180 cluster combinations (2x6x5x3) are possible. Of these 100 combinations, 30 represent only one single day. It can be shown that a good approximation is obtained if all combinations which only represent 1 day are not considered. This leads to the 70 combinations considered for this model, which represent 92% of the days of the year. In the following table, the impact of reducing data by elimination of combinations which represent a low number days is shown.

Table 4.6. Overview of the effect of limiting the number of days per combinations.

Minimum number of days per combination	Number of cluster combinations	Days represented by remaining combinations
1	100	365
2	**70**	**335**
3	43	281
4	30	242
5	22	210

4.2.3.2 Demand profiles (dem_t)

For demand several daily patterns could be identified over the year and 3 clusters were created. In the following figure, the DMap of all demand data (left) and mean profiles of the three clusters (right) are shown. In the legend, beneath the cluster number, the cluster weight is provided in parentheses.

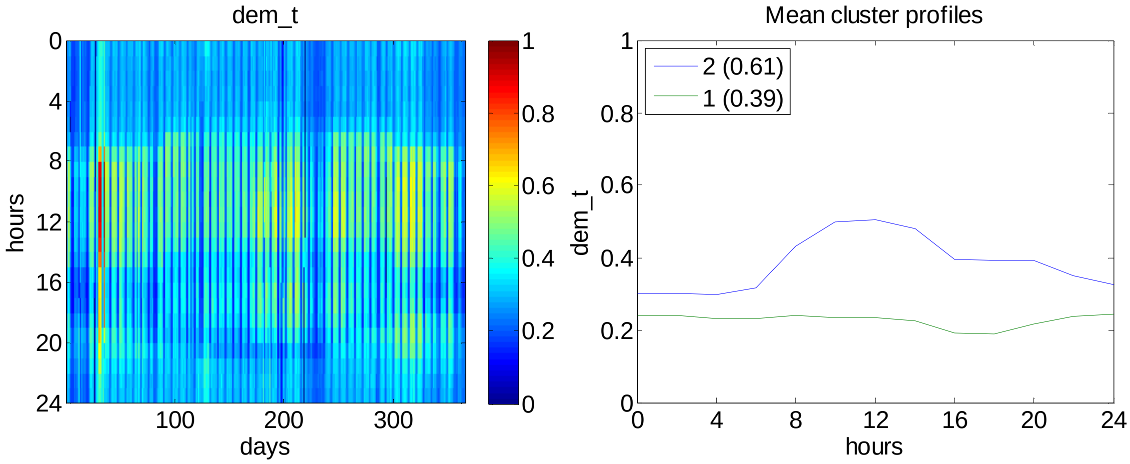

Fig. 4.8. DMap of demand (left) and mean profiles of 2 clusters (right).

Due to the similarity of many daily profiles, it was chosen to reduce the total number of clusters to only two. In order to give an impression of the variability within the clusters, the next figure shows all individual curves present in each of the two clusters.

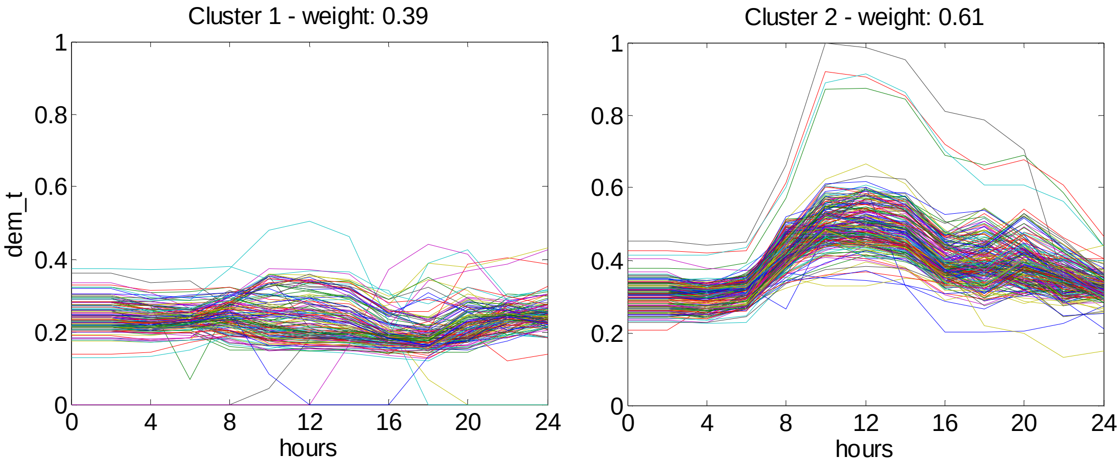

Fig. 4.9. Demand cluster 1 with low demand (left) and cluster 2 with high demand (right).

It can be seen that there is variability around the mean and some outliers. In the case of cluster 1 (left plot), there are several curves going to zero, which means outages. In the case of cluster 2 there are 4 curves with very high peak demand, which refers to 4 consecutive days in winter.

4.2.3.3 Wind and Solar resource (perf_w, perf_pv)

Due to the higher complexity of daily patterns, in this case 6 clusters were generated. DMap and the six mean curves are shown below.

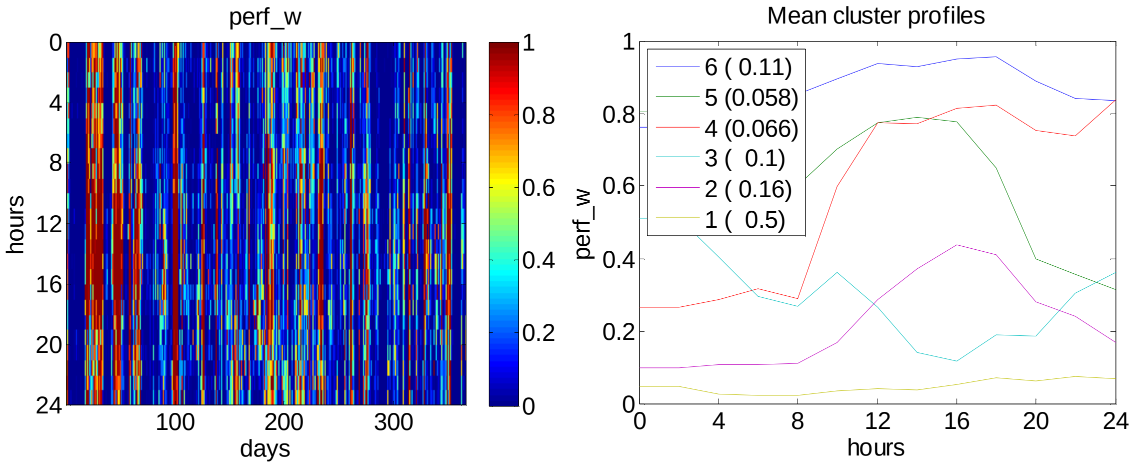

Fig. 4.10. DMap of wind generation (left) and mean profiles of 6 clusters (right).

As the variability of solar generation is slightly lower that wind, in this case 5 clusters were generated. DMap and the five mean curves are shown below.

In the case of renewable generation, it may be better to select a representative profile from each cluster, rather than using the average. This is because averaging leads to a too optimistic estimation of the available renewable power. But here, only mean curves are considered.

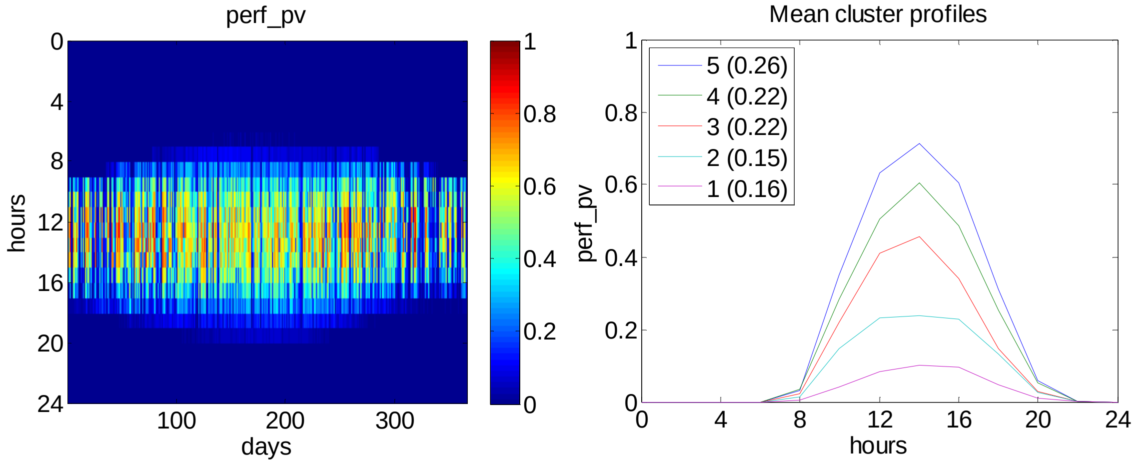

Fig. 4.11. DMap of solar generation (left) and mean profiles of 5 clusters (right).

4.2.3.4 Electricity price (PE)

There are only 5 different daily price profiles defined. As there are similarities between the different profiles, 3 clusters can be defined. DMap and the three price curves are shown below.

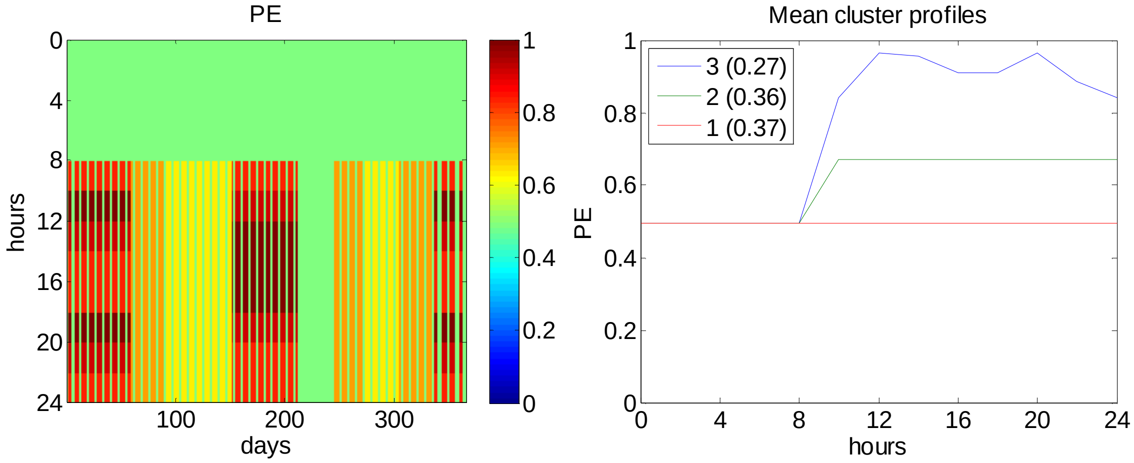

Fig. 4.12. DMap of electricity Prices (left) and 3 different daily profiles (right).

4.2.3.5 Creation of GAMS input from clustering results

From clustering, 70 representative days are obtained. In a first approximation, these days are calculated from the mean of all the days which fall into the corresponding cluster.

The clustering assigns a cluster number to each of the 365 days of the year. In the next figure, time series are shown which have been generated from the 70 combinations of 12-h days. The result is 840 time steps for the simulation in GAMS.

It can be seen very well the two demand clusters, sorted by mean demand. Below, corresponding renewable generation is shown. For every demand level, all existing combinations of renewable generation clusters can be seen, again sorted from highest to lowest means. Finally, corresponding electricity price curves are shown. There it can be seen clearly, hay low demand and low prices come together many times.

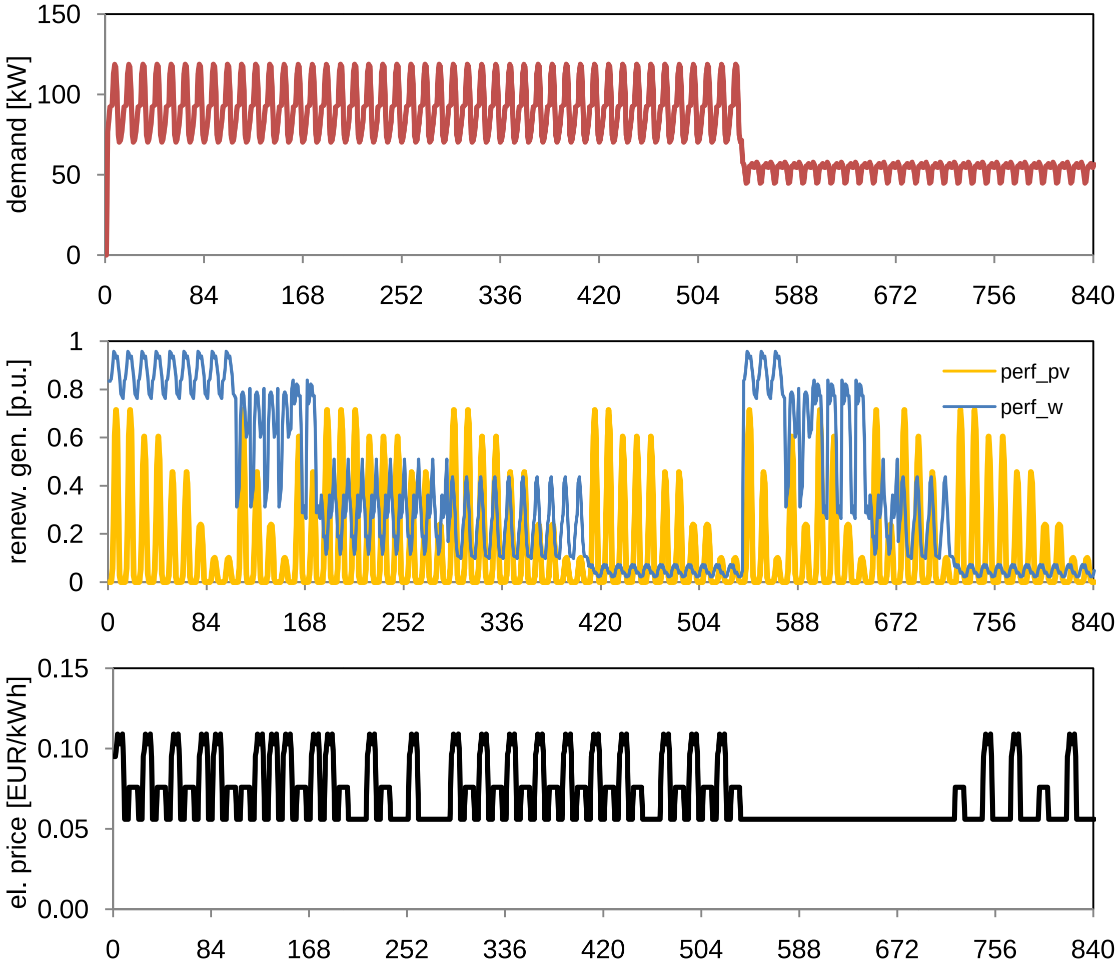

Fig. 4.13. Time series created from 70 cluster combinations for demand (above), renewable generation (middle) and electricity price (below).

4.3 Simulation results with HOMER and HOGA

4.3.1 Model Configuration

Below, the graphical appearance of the system configurations is shown. In case 1, it can be seen that two different load profiles are defined, in order to distinguish AC and DC pumps. In HOGA, all consumption profiles are loaded within one file. The presence of AC and DC loads is shown by the electrical outlet (AC) and the low consumption light bulb (AC). In HOGA, the DC-bus is highlighted with green color.

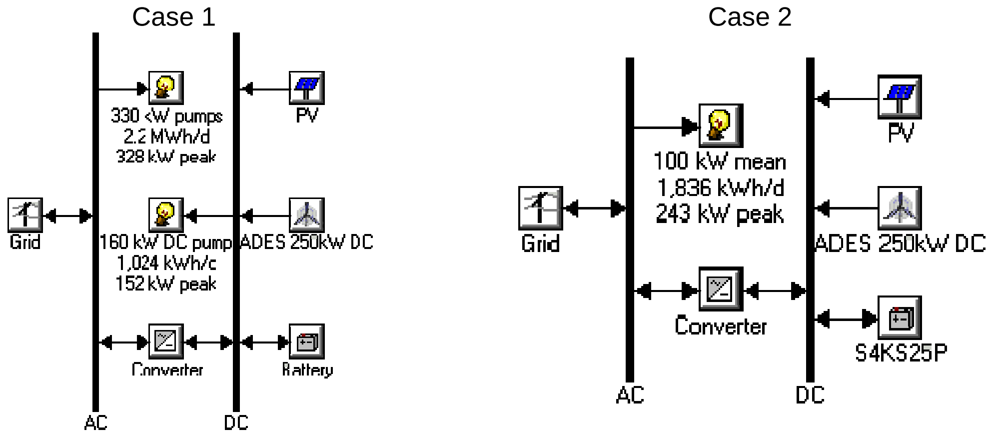
Case 1

Case 2

Fig. 4.14. System configuration in HOMER; Case 1: Valdabra irrigation pumping station (left) and Case 2: Industrial area (right).

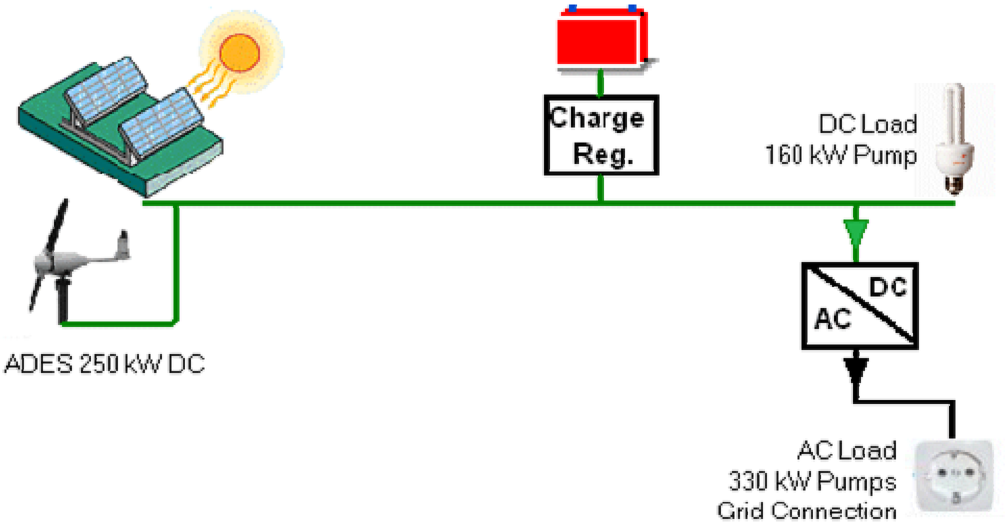

Fig. 4.15. System configuration of Valdabra irrigation pumping station in HOGA.

4.3.2 Simulation Scenarios

Results are presented for different scenarios. In the base case realistic values for electricity prices and investment for PV, Wind and Batteries are assumed. In a second scenario, PV prices are assumed to be reduced by a factor 0.5. In a third scenario, battery prices are at 25% and in a fourth scenario, both, PV and batteries are reduced.

Wind power cost is assumed to be fixed, as only one option is considered (ADES wind turbine) and energy from grid cannot be included in the analysis in HOGA. Therefore, a separated sensitivity analysis is carried out only with the HOMER model, where PV cost and grid prices are changed. PV cost is varied between 40-100% of base cost and grid prices between 0.10 – 0.25 €/kWh (67-133% of base price of 0.15 €/kWh).

Table 4.7. Scenarios for different PV and Battery costs.

Scenario	PV cost	Battery cost
1: base	2500 €/kWp	350 €/kWh
2: low PV	50%	100%
3: low battery	100%	25%
4: low PV + Battery	50%	25%

4.3.3 Results of 4 scenarios

In the following two tables, the system configurations proposed by HOMER and HOGA for the 4 scenarios are shown for the two cases (1: Pumping station, 2: Industrial area). In the table header, HMR stands for “HOMER” and HGA for “HOGA”.

4.3.3.1 Case 1: Pumping Station

For this case, results in terms of COE show that HOGA obtains sensibly lower energy costs compared to HOMER. Also system configurations change largely.

HOMER does not consider batteries in any case, while HOGA does it in scenario 4. Another difference is that HOMER considers always less PV power and wind capacity is reduced in scenarios 2 and 4 when large PV power is considered.

Table 4.8. System configurations proposed by HOMER and HOGA for case 1 (Pumping Station).

Scenario	1 base		2 low PV		3 low battery		4 low PV+Battery	
	HMR	HGA	HMR	HGA	HMR	HGA	HMR	HGA
Wind (kW)	500	500	250	500	500	500	250	500
PV (kW)	–	77	200	432	–	77	200	477
Battery (kWh)	–	–	–	–	–	–	–	912
Converter (kW)	250	500	250	500	250	500	250	500
Ren. Frac. (%)	49.0	49.6	48.0	59.4	49.0	49.6	49.0	70.5
COE (€/kWh)	0.104	0.070	0.108	0.060	0.104	0.070	0.108	0.070

Another observation is that HOGA always proposes a 500-kW-converter, while HOMER sees here an option to save money, reducing the size to 250 kW (by allowing some excess energy generation).

4.3.3.2 *Case 2: Industrial Area*

For this case, HOGA obtains values of COE sensibly higher than HOMER. A more detailed analysis of the differences in the calculation of COE in both simulation tools is needed in order to identify the reasons. As COE is an important selection parameter, it is likely that the differences in system configuration are widely due to the differences in the calculation of COE.

As in Case 1, HOMER does not consider batteries in any case, while HOGA does it in scenario 4. Again, HOMER considers always less PV power than HOGA. In this case, HOMER always proposes to install one turbine of 250 kW, while HOGA discards wind power at all. HOMER, again proposes always the 250-kW-converter. On the other side, HOGA proposes the installation of a 100-kW-converter in scenarios 1 and 3 (high PV cost) and a 250-kW-converter in scenarios 2 and 4 (low PV cost). It is especially interesting that in scenario 4, 540 kWp of PV power are installed, while the AC/DC converter is only rated at 250 kW. This can be explained by the large battery which is able to absorb excess solar production. As a result, a similar renewable fraction is obtained as in the case of HOMER.

Table 4.9. System configurations proposed by HOMER and HOGA for case 2 (Industrial area).

Scenario	1 base		2 low PV		3 low battery		4 low PV+Battery	
	HMR	HGA	HMR	HGA	HMR	HGA	HMR	HGA
Wind (kW)	250	–	250	–	250	–	250	–
PV (kW)	–	126	200	365	–	126	200	540
Battery (kWh)	–	–	–	–	–	–	–	1824
Converter (kW)	250	100	250	250	250	100	250	250
Ren. Frac. (%)	54	23.1	73	36.3	54	43.6	73	72.3
COE (€/kWh)	0.101	0.130	0.085	0.120	0.101	0.130	0.085	0.110

4.3.4 Results sensitivity analysis

In this section, results of the sensitivity analysis with HOMER are represented for the two cases under study. The main aim of this study was to find the conditions, where battery storage becomes profitable. Following the results obtained with HOGA, it is assumed that only a reduction of Battery capital cost of at least 75% can make batteries profitable (S4KS25P Capital Multiplier = 0.25 in Fig. 4.16). Keep in mind that this is the case if only energy management is considered, as HOMER and HOGA do not include auxiliary services in the cost analysis. It is also assumed that the profitability of the battery system will be strongly affected by the cost of installed PV power and purchase cost from the grid ("power price" in the figure).

Therefore, the sensitivity to PV cost and energy price from the grid has been evaluated here. It can be seen how PV power gains importance, as PV capital cost falls and grid price rises. In Fig. 4.16 it can be seen why HOMER did not include battery storage when a power price of 0.15 €/kWh is assumed. Battery systems are profitable only if solar-PV becomes cheaper and grid power prices rise at least above 0.18-0.20 €/kWh.

Case 1

Case 2

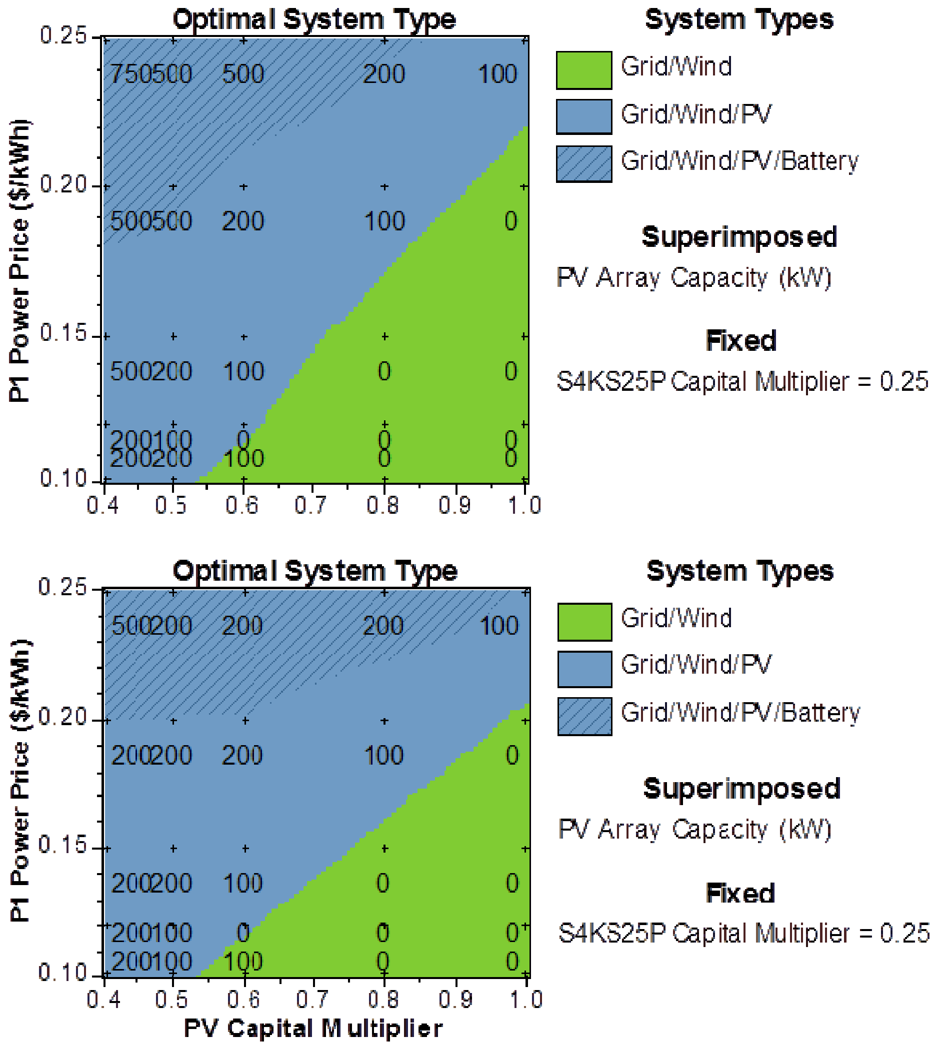

Fig. 4.16. Result of sensitivity analysis upon PV cost and electricity price from the grid, with reduction of battery capital cost of 75%; Installed PV power in kWp is superimposed.

Interestingly, the tendency is very similar for both study cases. PV-Systems are always profitable, if its cost falls below 1250 €/kWp (without considering the Inverter!). This is a very interesting result, as PV modules for prices below 1000 €/kWp can already be found on the market. Given that price (PV Capital Multiplier = 0.4), Battery systems become interesting when the power price rises above 0.18 – 0.20 €/kWh.

Finally, in Fig. 4.17 the same sensitivity screening is represented in terms of COE (Levelized Cost of Energy in €/kWh). Above, case 1 and below, case 2.

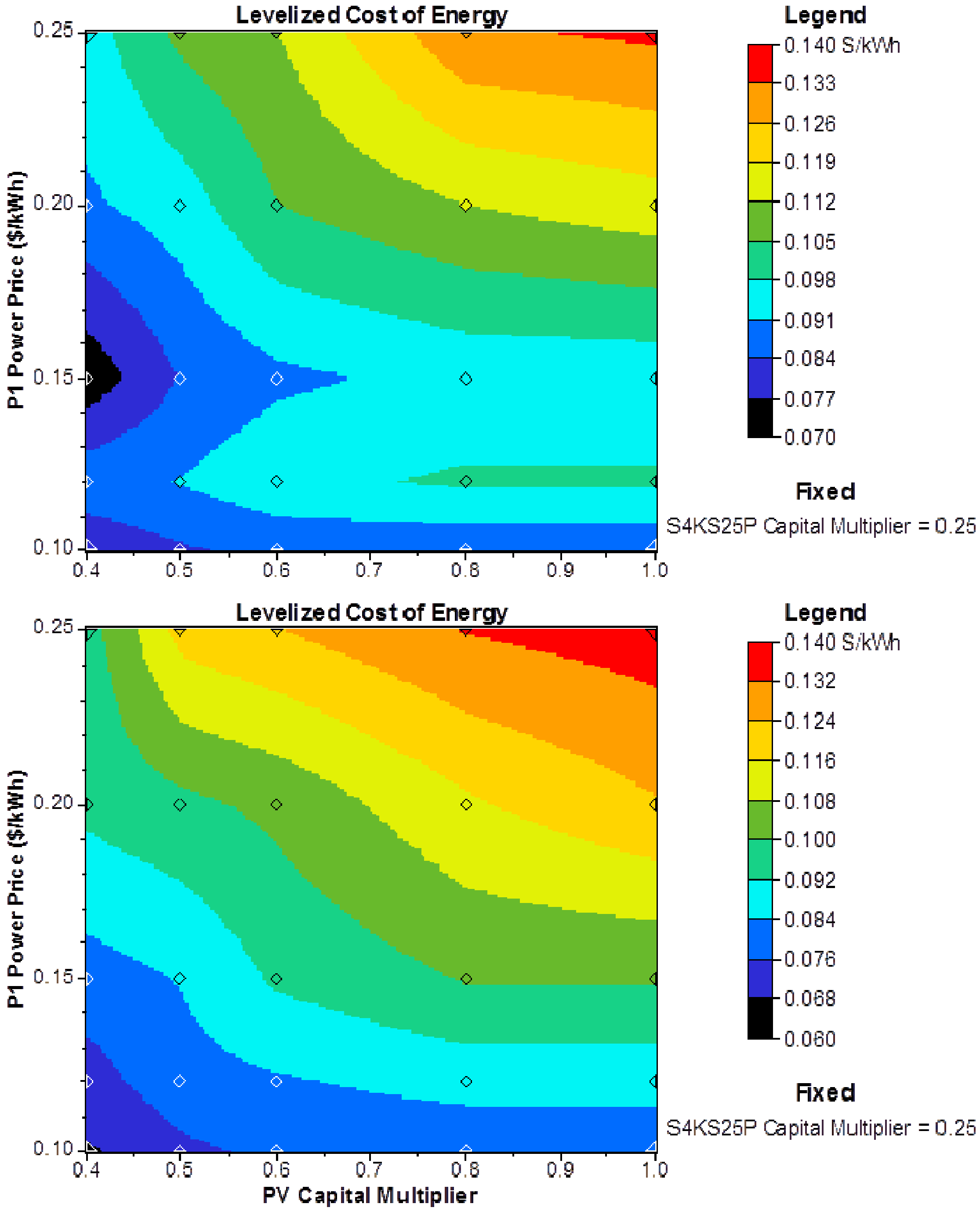

Fig. 4.17. COE in €/kWh as a result of sensitivity analysis upon PV cost and electricity price from the grid, assuming a reduction of battery capital cost of 75%.

In general, it is not surprising, that with lower power prices and lower PV installation costs, COE is lower. In any case, the integration of renewable energy sources reduces COE. In addition, with growing penetration of this distributed generation, the increase of power prices affects less the cost of the energy consumed.

4.3.5 Conclusions from HOMER and HOGA

The results of the sensitivity analysis at the same time provide the final conclusions:

- The integration of renewable energy sources reduces COE.

- Growing penetration of distributed generation reduces dependency of uncertain future of power prices
- Battery systems need to reduce costs below 100 €/kWh in order to be profitable for energy management

The reduction of 75% in these simulations means that the battery storage system would reduce its cost from 350 to 87.5 €/kWh storage capacity. This is a very tough goal to achieve, but probably the automotive industry will give the answer.

Finally, the results given by HOMER and HOGA differ widely. Some more investigation is needed to discover exactly the reasons for these differences. At least it shows that it is a good idea not to trust just one simulation tool.

4.4 Simulation results with Matlab/Simulink®

In this chapter, results are presented of the three active power control strategies, which were introduced in section 4.2.2. Two different cases are considered. In the first case (case A), a battery power of 100 kW is assumed, while in the second case (case B), this power is increased to 200 kW. The battery capacity in any case is assumed to be at 1 MWh. In addition to these cases, three subcases are considered: no distributed generation (DG), only wind (250 kW) and PV+wind (250 kW each).

- Case A: Battery with 100 kW / 1 MWh
- Case B: Battery with 200 kW / 1 MWh

The specific discharge time in the first case is 10h, while in the second case it is reduced to 5h. The second case gives to the system an increased margin of operation in terms of reactive and active power control, but also the battery can reach more rapidly its charge and discharge limits.

In the first sub-case (without DG), the nominal battery power is at the same time the nominal converter power. When wind and solar power is added, the converter power is increased at least up to 250 kVA, which is the nominal power of the considered installation of solar and wind generation (each). It is assumed that DG is integrated on the DC side of the converter, where also the battery is connected. In such a system, there is a DC/DC converter, controlling the battery charging and an AC/DC converter for grid connection. The battery power thus depends primarily on the rated power of the DC/DC converter, while the system power (available for P and Q control) depends on the rated power of the AC/DC converter. The described P control strategies directly act on the battery, as it is assumed that DG is not controllable. The only exception is that DG is limited to 250 kW in any case. This is an assumption derived from simulations with HOMER, where only 250 kW of converter power was proposed, while the joint installed power of DG (solar and wind) were 500 kW (250 kW each). In HOMER, the reason was that investment capital could be saved, while excess energy due to the reduced converter power was low. In our case, there is an additional motivation to limit DG power. As maximum demand was approximately 250 kVA, the existing infrastructure permits such power levels. But it is not guaranteed, if higher power levels would be possible without grid extension.

As DG is assumed to generate only active power, Q control becomes more important. As generated active power can reduce power demand down to zero, power factors can become very low, even with moderate reactive power consumption. Therefore, especially when DG is near nominal power, reactive power control must be guaranteed. Therefore, a 25% power reserve is added to the AC/DC converter, so that always 50 kvar of reactive power are available. Another possibility would be to give priority to Q control.

4.4.1 Simulation Parameters

Strategy 1: Peak shaving

In this control scenario, the following demand limits are established for discharge and recharge of the battery system (these parameters are maintained for cases A and B).

The initial value of SOC is set to 45%, so that the objective region is SOC = 40 … 50%. If SOC is outside that region and inside the power limits, the battery charging control will charge or discharge the battery at a 20% of nominal battery power, in order to return to the desired region of SOC.

Table 4.10. Control parameters for strategy 1 (peak shaving).

Parameter	No DG	250kW wind	250kW wind+pv
P_{max} [kW]	100	100	100
P_{min} [kW]	50	-100	-100

Strategy 2: Hourly program

In this control scenario, the following start times and durations are established for discharge and recharge of the battery system (these parameters are maintained for cases A and B and all sub-cases).

Table 4.11**.** Control parameters for strategy 2 (hourly program).

Parameter	Value
t_{ch}	21 h
t_{dch}	6 h
Δt_{ch}	8.5 h
Δt_{dch}	12 h

The limits of active power at PCC are calculated from the limits of strategy 1: Peak shaving as follows:

Table 4.12. Calculation of active power limits at PCC are from limits from strategy 1.

P_{max2} [kW] = $P_{max2} + 50$ kW

P_{min2} [kW] = $P_{min2} - 50$ kW

As a result, active power at PCC in case of no DG is restricted to 0 ... 150 kW and in case of DG present to -150 … 150 kW.

The initial value of SOC is set to 45%, although that value is not essential for this algorithm, as SOC is not monitored such as in strategy 1.

Strategy 3: Smoothing (with moving average)

In this control scenario, only the window width of the moving average needs to be defined. As smoothing capacity of the battery is directly related to its energy capacity, the same value of 12 h (24 time steps) is adopted.

Table 4.13**.** Control parameters for strategy 3 (smoothing).

Battery capacity	Parameter w (time steps)	Window width (duration T)
1 MWh	24	12 h

The initial value of SOC is set to 50%, although that value is not essential for this algorithm, as SOC is not monitored such as in Strategy 1.

Converter Model

The following parameters are introduced into the converter model mask:

Table 4.14. Converter Model parameters.

Parameter	No DG	250kW wind	250kW wind+pv
$S_{ren,max}$ [kVA]	0	250	250
$S_{c,margin}$ [kVA]	100 / 200	50	50
η_{conv} [%]	95	95	95
S_{cmax} [kVA]	100 / 200	300	300

Battery Model

The following parameters are introduced into the battery model mask. Values are maintained for all control strategies and sub cases (with or without DG).

Table 4.15. Battery model parameters.

Parameter	Value	Comment
P_{0bat}	100 / 200 kW	Case A / B
V_{0bat}	384 V	
C_{bat}	2760 Ah	→ E_{bat} = 1 MWh
SOC_{init}	45 / 50 %	Strategy 1+2 / 3
SOC_{min}	5 %	
SOC_{min2}	20 %	
SOC_{max}	100 %	
SOC_{max2}	80 %	

In order to understand the results, a code has been established for the representation of the different control strategies (1-3) and cases (A and B). Thus, a variable with the added code “2B” means that it was obtained with control strategy 2 and case B. In Table 4.16, possible options are summarized.

Table 4.16. Summary and codification of the different simulation options.

Option	Codification	Description
Strategy 1	1	Peak Shaving
Strategy 2	2	Hourly Program
Strategy 3	3	Smoothing
Case A	A	Storage at with 100 kW
Case B	B	Storage at with 200 kW

4.4.2 Statistical results: P Control

In the following tables several statistical parameters are presented which in part represent the performance of the different control strategies in combination with the two cases A and B and the sub-cases of distributed generation.

4.4.2.1 Microgrid without DG

First, the base case is analyzed, where no distributed generation (DG) is present. In Table 4.17 indicators are shown for active power control (P control). “Pload” represents the demand and “Pred” the active power flow at the point of common coupling (PCC), including all effects of the micro-grid (DG and storage). In the standard deviation, a slight reduction of variability can be observed in almost all cases. As could be expected, the larger battery system (case B) has a higher impact that the smaller one.

In the first place, it can be observed that the mean demand is higher in all scenarios. This reflects the losses in the storage system. While in control strategies 1 and 3 the deviation does not exceed 0.5 kW (0.7% of losses), in strategy 2 it is slightly higher.

Control strategy 1 (peak shaving) does not alter Mean and Median, but reduce STD considerably, although the system seems to be too small in order to deal with the overall maximum, which is almost the same.

Control strategy 2 (hourly program) cannot be recommended, as it increases STD heavily and extreme values are increased. It is also the case with the highest system losses.

Control strategy 3 (smoothing) reduces STD slightly and in this scenario it is the most effective strategy to reduce overall maximum values.

In general, differences between the cases A and B (50 and 100 kW battery) are minor.

Table 4.17**.** Statistical indicators of the impact of active power control.

Variable	Mean	Median	Standard Deviation	Minimum	Maximum	
Pload	77.0	74.3	26.9	0.0	246.5	kW
Pred1A	77.3	76.0	22.4	5.0	228.1	kW
Pred1B	77.4	75.6	22.6	5.0	230.5	kW
Pred2A	80.0	78.6	58.7	0.0	225.2	kW
Pred2B	80.0	78.5	58.7	0.0	225.2	kW
Pred3A	77.4	76.4	25.6	0.0	234.5	kW
Pred3B	77.4	76.4	25.6	0.0	234.5	kW

In Fig. 4.18 the histograms (empirical probability density function, pdf and cumulative distribution function, cdf) of active power are shown for all scenarios compared to the original demand (Pload). Control strategy 1 produces high peaks at the established limits of 50 and 100 kW respectively. Control strategy 2 (hourly program) shows similar behavior, but with peaks at 0 and 150 kW, according to the established power limits. Strategy 3 (smoothing) causes very little alteration of the power distribution. No apparent differences can be observed between case A (100 kW battery) and case B (200 kW battery).

As a summary, it can be observed that strategies 1 and 2 produce larger deviations from the original power distribution, while with strategy 3 almost the same distribution maintained.

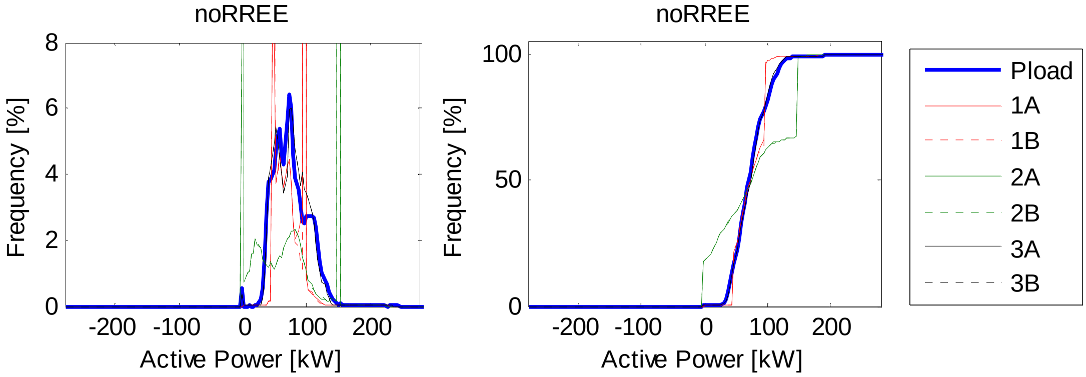

Fig. 4.18. Power distribution density (left) and cumulative (right) at PCC compared to original demand Pload, above case A (100 kW battery) and below case B (200 kW battery), without DG.

4.4.2.2 *Microgrid with DG*

The same evaluation has been done with renewable distributed generation in the system. In this case, solar PV and wind (250 kW installed power each). In Table 4.18 the statistical parameters are shown. In the first line, values of original active power demand Pload0 are shown.

It can be seen that DG reduces mean power. Negative values mean net generation instead of net consumption. In general, STD and extreme values increase due to DG. Only if solar PV and Wind power is installed, maximum consumption values are reduced in control strategies 1 and 3. Differences between cases A and B (100 and 200 kW battery system) are minor.

In Fig. 4.19 histograms (probability density) and cumulative distributions are shown for the three cases of DG.

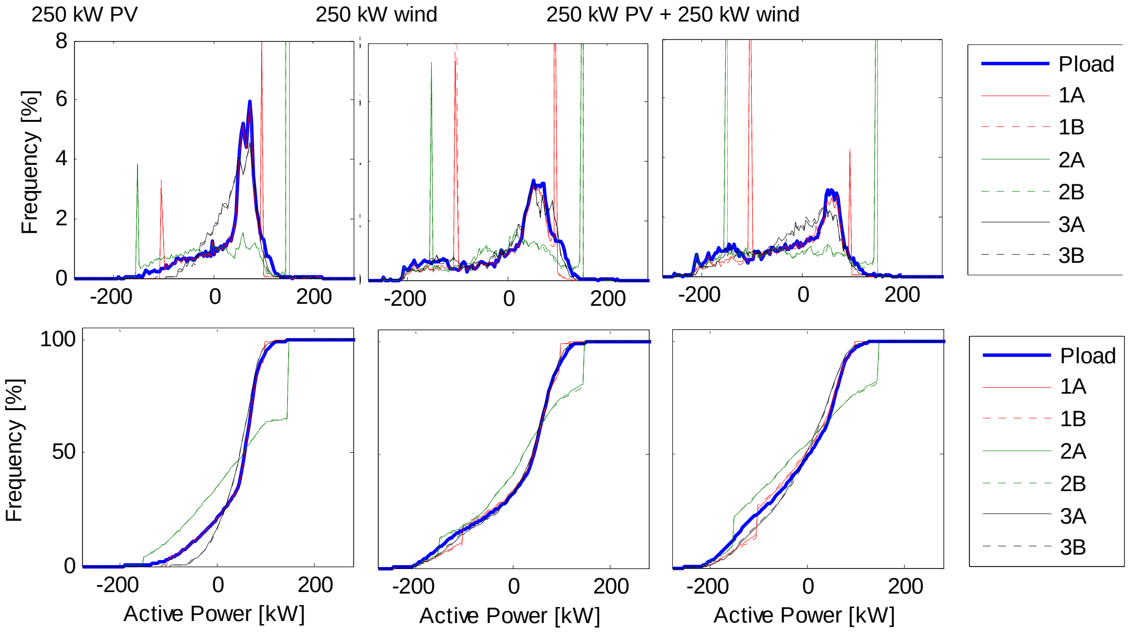

Fig. 4.19. Power distribution density (above) and cumulative (below) at PCC compared to original demand Pload minus DG, for only PV (left), only wind (center) and wind and solar PV (right).

Table 4.18**.** Statistical indicators of the impact of active power control.

Variable	Mean	Median	Standard Deviation	Minimum	Maximum	
Pload0	77.0	74.3	26.9	0.0	246.5	kW
250 kW solar pv						
Pload-DG	40.5	58.9	55.8	-189.7	217.4	kW
Pred1A	40.6	59.0	53.9	-100.0	215.0	kW
Pred1B	40.6	59.1	54.1	-100.0	214.7	kW
Pred2A	43.8	56.7	99.1	-189.7	185.8	kW
Pred2B	43.8	56.7	99.2	-189.7	185.8	kW
Pred3A	42.3	49.3	39.2	-93.4	201.5	kW
Pred3B	42.4	49.2	39.1	-111.6	202.6	kW
250 kW wind						
Pload-DG	11.1	45.1	88.7	-244.1	219.9	kW
Pred1A	11.5	43.7	82.9	-240.4	205.3	kW
Pred1B	11.5	44.4	83.0	-242.3	198.0	kW
Pred2A	14.2	23.5	104.6	-244.1	191.7	kW
Pred2B	14.2	23.1	105.7	-244.1	191.6	kW
Pred3A	12.5	41.2	82.2	-243.5	206.8	kW
Pred3B	12.6	41.7	82.8	-243.6	206.8	kW
250 kW solar pv + 250 kW wind						
Pload-DG	-18.7	5.4	91.0	-250.0	197.6	kW
Pred1A	-18.2	-2.6	83.0	-246.2	134.8	kW
Pred1B	-18.2	-4.2	82.9	-248.4	134.8	kW
Pred2A	-15.9	-22.9	116.6	-250.0	151.3	kW
Pred2B	-15.9	-23.4	117.5	-250.0	151.3	kW
Pred3A	-16.5	-1.4	77.9	-248.4	191.0	kW
Pred3B	-16.4	1.9	79.2	-249.3	189.0	kW

Another way to represent the same results is to arrange them by control strategies, rather than by DG penetration scenarios. In Fig. 4.20 for example Pload (without storage) is shown and it can be observed how DG extends the range of power into negative power (net generation) and values of positive power (consumption) are reduced.

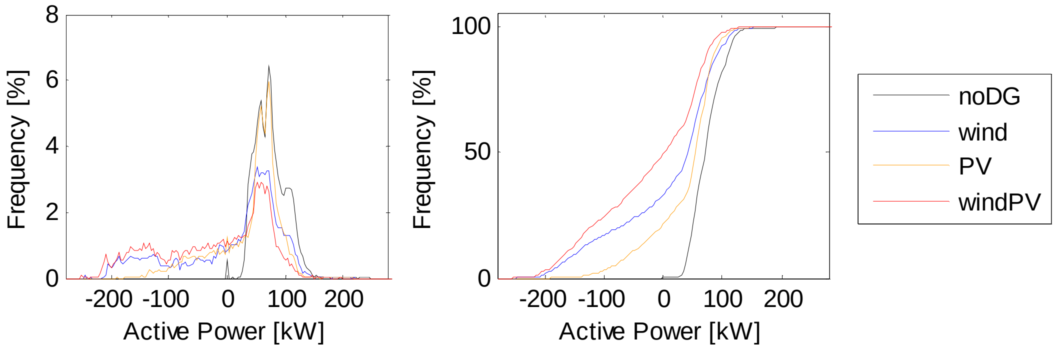

Fig. 4.20. Power distribution density (left) and cumulative (right) of Pload at PCC for no DG (black), 250 kW wind (blue), 250 kW PV (yellow) and 250 kW wind + 250 kW PV (red).

In Fig. 4.21 the impact of the different control strategies can be observed with DG penetration and battery power as parameters. Here, the power limiting properties of strategies 1 and 2 can be seen very well. Also the effectiveness depending on DG penetration becomes more visible.

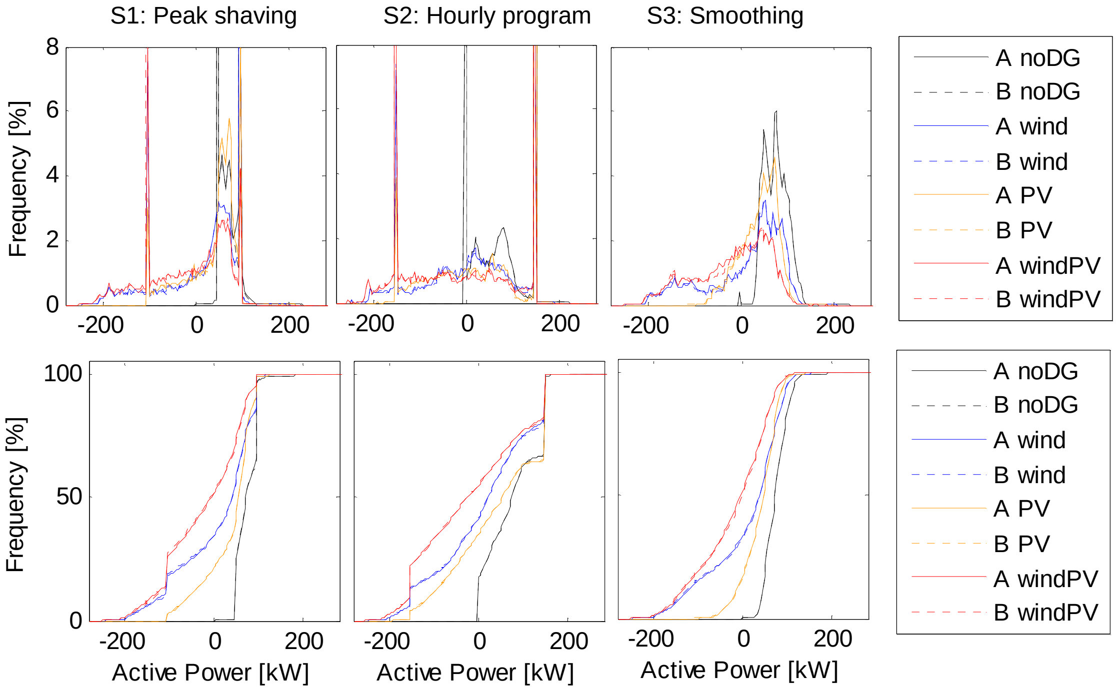

Fig. 4.21. Power distribution density (above) and cumulative (below) at PCC for the three control strategies, for no DG (black), only wind (blue), only PV (yellow) and wind and solar PV (red).

Peak power reduction

In order to illustrate the capacity of reducing demand peaks, in the following table relative values are shown comparing the original peak power with the one obtained with the introduction of energy storage and the different control strategies.

Table 4.19. Peak demand relative to the original value (without battery and P control).

Case	no DG	250 kW PV	250 kW wind	PV + Wind
1A	92.5%	98.9%	93.4%	68.2%
1B	93.5%	98.8%	90.1%	68.2%
2A	91.3%	85.5%	87.2%	76.6%
2B	91.3%	85.5%	87.1%	76.6%
3A	95.1%	92.7%	94.1%	96.7%
3B	95.1%	93.2%	94.1%	95.7%

In general it can be stated, that all control strategies are able to reduce maximum demand values. Interestingly, the daily program (control strategy 2) is more effective than peak shaving (strategy 1). Both strategies include power limitations, but while peak shaving only acts on power limits, the hourly program is based on a time schedule. If the time schedule is set in a convenient manner, the reduction potential of the battery can be exploited better. This is because extreme demand events may deplete the battery capacity even before reaching maximum demand.

A second general observation is that maximum power levels are reduced with increasing penetration of DG. But the reduction is not straight forward. The introduction of solar PV for example, increases maximum power demand for the peak shaving strategy, while for the others a reduction can be observed. Finally, largest peak power reduction ratios are obtained when wind and solar power is combined and strategy 1 is applied. In general, smoothing (strategy 3) has lowest impact on peak power reduction.

With the introduction of DG, not only peak demand, but also peak generation is an interesting point to observe. In Table 4.20 peak reduction effects of the different control strategies are shown. In general, the result is that peak generation is not limited except for the case of solar PV. Here, best results are obtained with peak shaving, but also with smoothing, reducing maximum peaks to half of the original values. In all other cases, reductions are below 2% and in the case of strategy 2 (hourly schedule), no reduction is observed.

Table 4.20. Peak generation relative to the original value (without battery and P control).

Case	250 kW PV	250 kW wind	PV + Wind
1A	52.7%	98.5%	98.5%
1B	52.7%	99.2%	99.4%
2A	100.0%	100.0%	100.0%
2B	100.0%	100.0%	100.0%
3A	49.3%	99.7%	99.4%
3B	58.8%	99.8%	99.7%

Examples of time series

In order to illustrate better the effect of the different control scenarios, several examples of the time series are shown in Fig. 4.22.

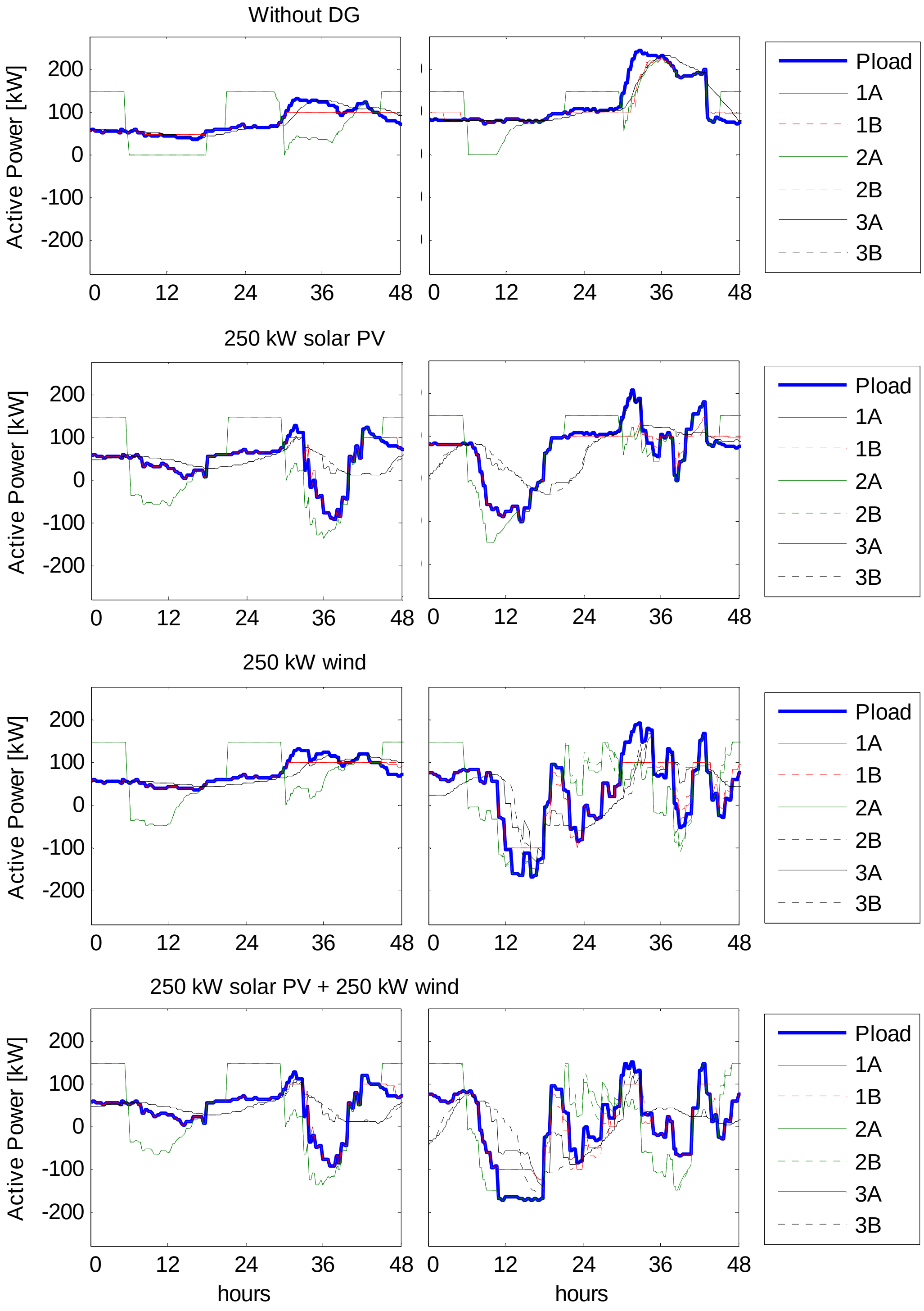

Fig. 4.22. Two typical sequences (48h each) of active power demand under different control scenarios compared to Pload, left: typical activity, right: high activity.

The same cases, but arranged in order to compare the effect of DG penetration for different control strategies is shown in Fig. 4.23

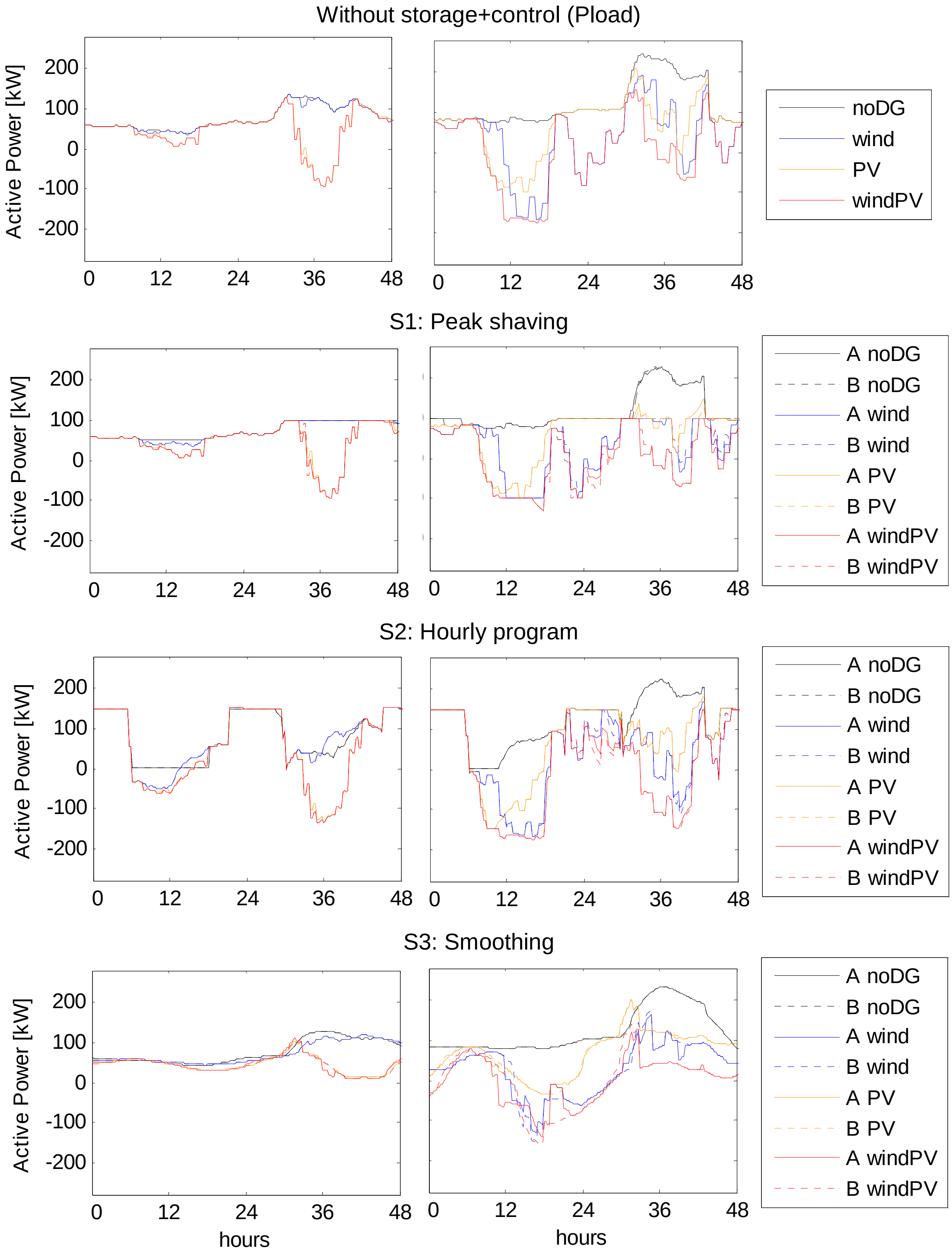

Fig. 4.23. Two typical sequences (48h each) of active power demand under different control scenarios comparing four levels of DG penetration, left: typical activity, right: high activity.

Therefore two sequences of 48 h each were chosen with typical power levels ("typical activity", left column) and with extremely high values ("high activity", right column). Each sequence starts at midnight and shows the load curve without storage (Pload) compared to the six control scenarios (A: 100 kW battery, B: 200 kW battery).

Results are presented for the 4 cases of distributed generation (DG) available: no DG, only solar pv, only wind and solar pv + wind.

It can be observed that control strategy 1 (peak shaving, red curve) is acting well, maintaining the limits, but in the case of high activity, without DG (right plot, first line) the battery is unable to serve the high demand. But with DG present, the peak is reduced and the battery can compensate it almost completely.

Control strategy 2 (hourly program, green curve) causes such large deviations from normal demand, that it becomes the dominant pattern. As the program is not sensible to available DG or extraordinary high demand peaks, the stress on distribution lines is increased due to elevated power flows. It also becomes clear that a power limitation is necessary, in order to avoid excessive power peaks. Especially when the battery is charged, the limit of 150 kW is reached often.

Finally the smoothing effect of strategy 3 becomes clear. The most interesting result of this strategy is the reduction of power ramps. It is also the strategy where an increased battery power rating (case B, 200 kW) leads to some visible improvement.

4.4.3 Statistical results: Q Control

In this section, statistical results of reactive power control (Q control) are presented. In Table 4.21, some statistical indicators are given for the situation without distributed generation. Values are compared to the case without storage (PFload0). It can be observed that in most cases a power factor of unity is attained, while the original power factor or 0.79 was quite low. The minimum of power factor at zero is due to a power shut down in the time series. In any cases there are outliers with minor importance.

The only exception, where the power factor is not compensated properly is in the case of scenario 2A (hourly time schedule of battery charging and discharging with 100 kW battery). In this case, it seems that active power reduction due to the discharge program lead to low power factors, which were not compensated due to the priority of active power control and limited converter power available.

Table 4.21**.** Statistical indicators of the impact of reactive power control, without DG.

Variable	Mean	Median	Standard Deviation	Minimum	Maximum	
PFload0	0.7891	0.7869	0.0680	0.0000	0.9851	p.u.
PFred1A	0.9966	1.0000	0.0174	0.4477	1.0000	p.u.
PFred1B	1.0000	1.0000	0.0018	0.8508	1.0000	p.u.
PFred2A	0.8829	1.0000	0.2644	0.0000	1.0000	p.u.
PFred2B	0.9992	1.0000	0.0283	0.0000	1.0000	p.u.
PFred3A	0.9967	1.0000	0.0198	0.0000	1.0000	p.u.
PFred3B	0.9998	1.0000	0.0142	0.0000	1.0000	p.u.

In Table 4.22 the same indicators are shown for different cases of installed renewable energy generation. In general it can be stated that the introduction of DG improves the possibilities of power factor compensation. This is due to the fact that the converter rated power is increased and a 25% oversizing was provided in order to enable reactive power compensation even when renewable power generation is at rated power. It the converter is only rated at maximum generation power, no reactive power compensation is possible, because active power control has priority in the presented case.

As mean and medians are all near unity, the only indicator where some differences can be seen is standard deviation (STD). For solar pv only, STD is extremely low in general and 0.013 for strategy 1 is the highest value. In the case of wind only, especially values for strategy 2 increase slightly, but are still very low with 0.014. Finally, if solar and wind are combined, all values increase further and highest numbers are observed again for strategy 2 with 0.022. In any case, the improvement compared to the situation without control (STD = 0.22 ... 0.25) is clearly visible.

Table 4.22. Statistical indicators of the impact of reactive power control.

Variable	Mean	Median	Standard Deviation	Minimum	Maximum	
PFload0	0.7891	0.7869	0.0680	0.0000	0.9851	p.u.
250 kW solar pv						
PFload	0.6831	0.7702	0.2270	0.0000	1.0000	p.u.
PFred1A	0.9998	1.0000	0.0131	0.0000	1.0000	p.u.
PFred1B	0.9998	1.0000	0.0131	0.0000	1.0000	p.u.
PFred2A	1.0000	1.0000	0.0003	0.9587	1.0000	p.u.
PFred2B	1.0000	1.0000	0.0003	0.9587	1.0000	p.u.
PFred3A	1.0000	1.0000	0.0000	1.0000	1.0000	p.u.
PFred3B	1.0000	1.0000	0.0000	1.0000	1.0000	p.u.
250 kW wind						
PFload	0.7059	0.7567	0.2202	0.0001	1.0000	p.u.
PFred1A	0.9999	1.0000	0.0097	0.0160	1.0000	p.u.
PFred1B	1.0000	1.0000	0.0005	0.9391	1.0000	p.u.
PFred2A	0.9996	1.0000	0.0142	0.2762	1.0000	p.u.
PFred2B	0.9995	1.0000	0.0147	0.2773	1.0000	p.u.
PFred3A	0.9999	1.0000	0.0017	0.9219	1.0000	p.u.
PFred3B	0.9999	1.0000	0.0017	0.9219	1.0000	p.u.
250 kW wind + 250 kW solar pv						
PFload	0.6832	0.7636	0.2553	0.0000	1.0000	p.u.
PFred1A	0.9996	1.0000	0.0168	0.1632	1.0000	p.u.
PFred1B	0.9998	1.0000	0.0102	0.2704	1.0000	p.u.
PFred2A	0.9989	1.0000	0.0210	0.2903	1.0000	p.u.
PFred2B	0.9989	1.0000	0.0217	0.2320	1.0000	p.u.
PFred3A	0.9999	1.0000	0.0019	0.9092	1.0000	p.u.
PFred3B	0.9999	1.0000	0.0019	0.9092	1.0000	p.u.

In order to illustrate the results graphically, cumulative distributions of the power factor are represented in Fig. 4.24 for original power factor of the demand PFload and in Fig. 4.25 for the different control strategies S1 – S3.

In Fig. 4.24 "noDG" (black curve) represents the power factor of the original load and the other curves refer to the resulting power factors with reduced active power due to DG. As active power is reduced down to zero and below (net generation), all power factors between zero and unity are possible if no reactive power compensation is introduced. This shows the importance, that DG needs to participate in reactive power control. Therefore nominal power of the converter needs to have some additional margin. In the presented simulations, converter power is assumed to be 25% (50 kVA) higher than the nominal installed power of DG. This enables reactive power compensation even if DG is injecting to the grid at nominal power.

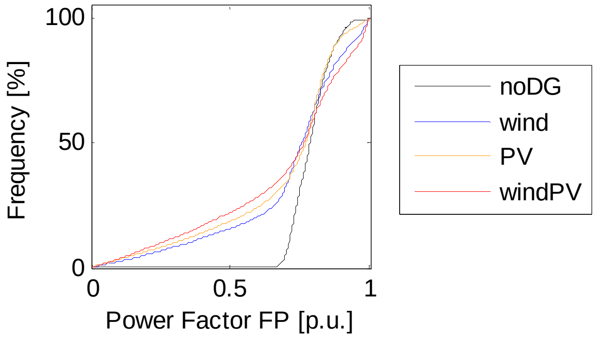

Fig. 4.24. Cumulative distribution of power factors of original demand FPload.

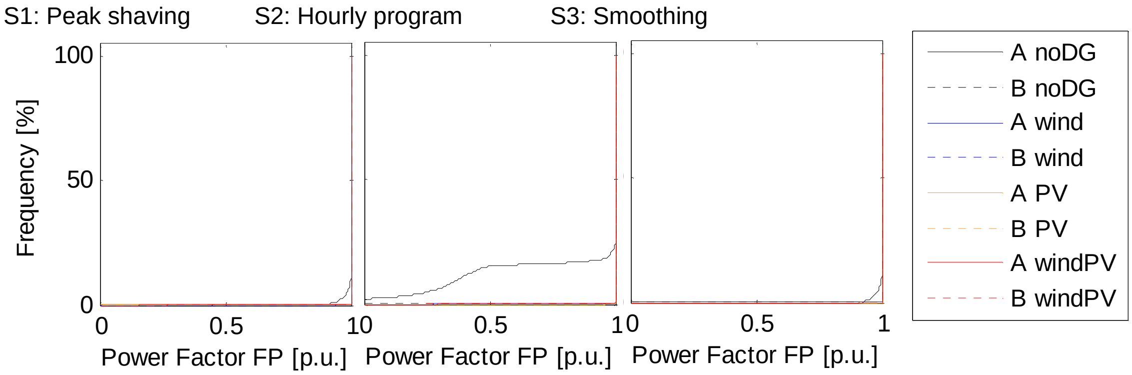

Fig. 4.25. Cumulative distribution of power factors for the three control strategies and battery sizes A: 100 kW and B: 200 kW.

In Fig. 4.25 the power factor at the connection point to the grid (PCC) is represented after the influence of the micro-grid (i.e. storage+control). It can be seen clearly that reactive power is compensated very well in all scenarios.

In the case “A noDG” (100 kW battery) the set-point of unity power factor is not always achieved. This is due to the fact that converter power is set equal to battery nominal power (see Table 4.14, p. 97). As reactive power control is subordinated to active power control and no additional power margin is added to the converter, it may occur that there is not enough converter power free for reactive power compensation. This becomes especially critical in the control scenario 2A (hourly program for battery charge and discharge with 100 kW battery). In this case, the hourly program causes often very low values of active power (reducing the power factor) and at the same time, the lower battery power does not leave enough margin for reactive power compensation. This problem is solved in case B with the 200 kW battery converter. In all other cases, reactive power control is very satisfactory, even with active power control having always priority.

4.4.4 Statistical results of SOC

In this section, the impact of distributed generation (DG) and control strategies on the state of charge (SOC) of the battery system is analysed. In Table 4.23 the statistical parameters, already presented in the preceding sections are shown here for the state of charge of the battery system. It may be mentioned, that the battery control algorithm includes a routine which establishes a preferred value of SOC near 50%. In addition, as described in section 4.2.2.6 (Battery Model), SOC is limited to a minimum and a maximum value are set to 5 and 100% respectively (see Table 4.15, p. 97). As a general tendency it can be observed that SOC is higher with increasing renewable generation.

In order to illustrate the results, in Fig. 4.26 the obtained data of SOC are represented using the cumulative distribution. It can be observed, how the different control strategies lead to different patterns of usage of the battery.

With control strategy 1 (peak shaving), the battery is almost always within the range defined for preferred SOC (in this case, 45% ± 5%). This effect is even reinforced with the introduction of solar pv. On the other side, wind power seems to reduce that effect, mainly increasing the percentage of time with SOC > 50%. In general, with this control strategy, the range of available battery capacity is not fully used.

On the other side, control strategies 2 and 3 cause a much more equilibrated use of the battery, showing a smooth distribution over the entire range of available battery capacity. Again, the introduction of solar pv reduces the range of used battery capacity, while with wind power and combined wind+pv, the curve is flattened, which means that values of SOC are distributed more uniformly in time.

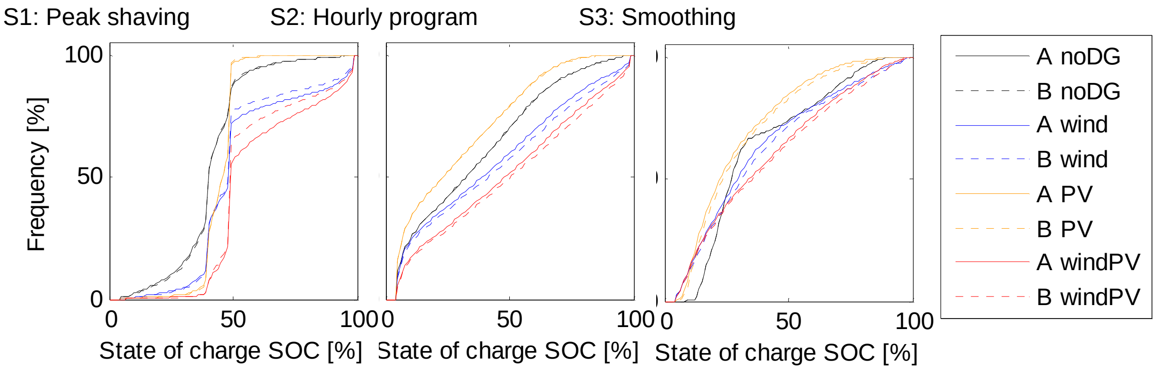

Fig. 4.26. Cumulative distribution of the state of charge (SOC) of the battery storage system for all simulation scenarios.

Table 4.23. Statistical indicators of the state of charge (SOC) of the battery system under different scenarios of distributed generation (DG) and control strategies.

Variable	Mean	Median	Standard Deviation	Minimum	Maximum	
Without DG						
SOC1A	41.4	40.1	12.9	5.0	98.1	%
SOC1B	41.5	40.1	12.5	5.0	98.1	%
SOC2A	35.7	33.3	25.0	5.0	98.8	%
SOC2B	35.7	33.4	25.0	5.0	98.8	%
SOC3A	36.7	27.9	21.2	9.8	91.6	%
SOC3B	36.7	27.9	21.2	9.8	91.6	%
250 kW solar pv						
SOC1A	45.2	46.6	6.2	5.0	69.6	%
SOC1B	45.3	46.6	5.9	5.0	69.6	%
SOC2A	29.0	23.8	21.9	5.0	93.3	%
SOC2B	29.0	23.9	22.0	5.0	93.5	%
SOC3A	29.2	23.2	18.6	5.4	97.1	%
SOC3B	30.7	24.3	19.5	5.5	98.5	%
250 kW wind						
SOC1A	53.6	50.0	20.6	5.0	100.0	%
SOC1B	52.2	49.4	19.3	5.0	100.0	%
SOC2A	42.4	39.8	30.1	5.1	100.0	%
SOC2B	44.4	42.2	31.0	5.1	100.0	%
SOC3A	36.9	30.3	25.1	5.0	99.7	%
SOC3B	38.5	32.0	25.7	5.0	99.7	%
250 kW wind + 250 kW solar pv						
SOC1A	60.9	50.0	19.8	7.9	100.0	%
SOC1B	58.4	50.0	18.6	7.9	100.0	%
SOC2A	49.1	48.9	30.8	5.1	100.0	%
SOC2B	50.9	51.2	31.3	5.1	100.0	%
SOC3A	39.8	35.1	25.9	5.0	99.2	%
SOC3B	41.0	36.2	26.7	5.0	99.7	%

4.4.5 Conclusions from Simulink simulation

Following the results of the simulations of HOMER and HOGA, a system configuration with 250 kW renewable power and 1 MWh of battery capacity is considered. In order to evaluate the impact of different levels of penetration of renewable generation (DG), four different scenarios are considered, including the base case without DG. Three control strategies are tested: 1: Peak shaving, 2: hourly profile and 3: Smoothing (with moving average) and two battery power capacities are assumed: A: 100 kW and B: 200 kW.

The following general conclusions can be drawn from the simulations:

- Control strategy 1, peak shaving is an effective strategy to reduce large demand peaks, but in combination with renewable generation, limits have to be chosen carefully.
- Only with peak shaving, the storage system is not fully used, as large peaks only occur a few times per year.

- Control strategy 2 (hourly programs) without taking into account actual demand and DG (only market prices for example) produce large deviations in consumption and power limits need to be established.
- If hourly programs are well designed, its effectiveness in peak shaving may be superior compared to a peak shaving strategy which is only based on threshold levels.
- Control strategy 3, smoothing with moving average is a very effective method in order to reduce power ramps, but only marginal effect is observed for reducing large power peaks.
- DG reduces active power consumption which makes reactive power control mandatory in order to avoid power factors near zero.
- With high penetration levels of DG, the limitation of generation peaks becomes more critical than the limitation of demand peaks.
- With adequate limitation of the generation, high penetration levels can be reached without the need of network reinforcement.
- Converter power needs to take into account reactive power control and a 25% oversizing seems to be a good orientation.
- For system operation, the combination of wind with solar pv is better than wind only.

4.5 Simulation results with GAMS

The model resolution is carried out using the GAMS programming software and the solver CPLEX.

In order to show the importance of storage for the improvement of self-consumption, two simulation cases are considered. In case A, it is assumed (such as in simulations with HOMER), that excess energy may be sold to the main grid at 0.05 €/kWh. In case B, the selling price is set to zero, which means no “export” of energy will take place.

4.5.1 Cost of energy (COE) and system cost

Fig. 4.27 shows the evolution of costs of energy (COE) over the planning horizon in for three scenarios. Here, COE is defined as total cost divided by total demand of energy. Exported energy is not included, but total cost is reduced by the income generated from the export.

In the base scenario (Conventional), the demand requirements are supplied solely by the distribution network. In this case, the energy cost is increasing from 0.10 to 0.25 €/kWh in 20 years, which means an annual elevation of electricity prices of 5%. With the introduction of distributed generation in the network (DG) COE is reduced to 0.07 €/kWh when considerable wind power is installed, and is maintained almost constant over the entire planning horizon. In the third scenario, when storage is considered (DG+ESS), from year 15 onwards COE decreases slightly more than without storage. The additional decrease is due to the fact that storage makes excess energy available which otherwise is dumped. It shall be mentioned, that a 20% annual decrease of installation costs has been considered here for storage, and after 15 years costs have fallen to 4,4% of the initial value.

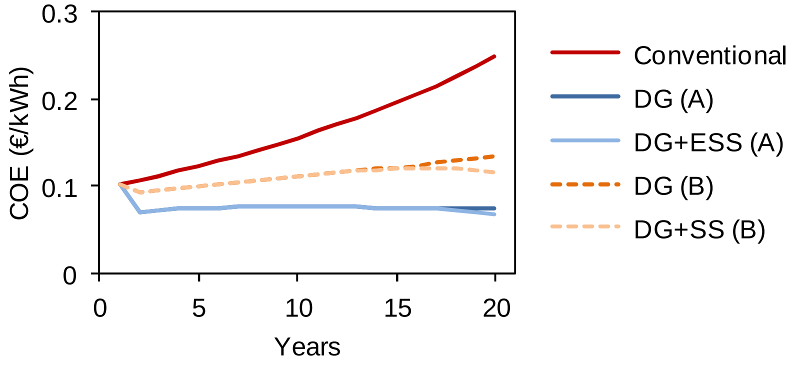

Fig. 4.27. Changes in the cost of energy during the planning period.

In Fig. 4.28 the distribution of annual costs is shown. In case A, the fact that there are negative cost values is again due to the assumption that energy can be sold to the grid at 0.05 €/kWh. Thus the surface in the negative region represents income from sold energy. In case A (left) it can be observed that absolute cost due to line losses (Lines) are actually increasing, but the percentage of total energy consumption and export to the grid is reduced, as shown in Fig. 4.29. In case B costs of line losses are reduced.

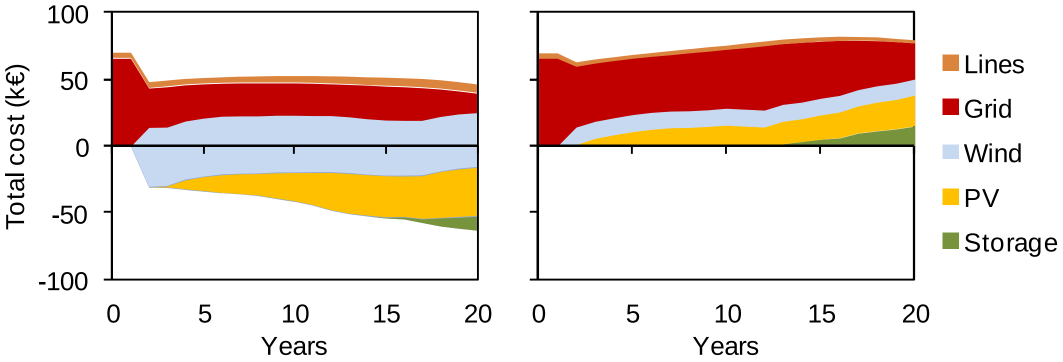

Fig. 4.28. Evolution of annual grid installation and operation cost by elements for case A with energy export (left) and case B without energy export (right).

4.5.2 Line losses

Fig. 4.29 shows line losses of the modelled distribution network as a percentage of total demand plus energy export for the three scenarios. In the first scenario (Conventional), losses are constant in p.u. throughout the planning period, which is due to the linearization of the losses, assumed in the model. In case A (export is possible) in the two scenarios (DG and DG+ESS), line losses fall after a slight increase in the first years. The initial increase is due to the installation of 400 kW of wind power, which often exceeds demand and needs to be evacuated to the main grid. The subsequent reduction in line losses is due to the increasing installation of solar power, which is better synchronized with demand and helps reducing flows within the distribution network. This effect in further reinforced, when storage starts to be implemented after 15 years. In case B (without export), line losses are reduced dramatically. As no energy can be exported, less renewable power is installed and no additional (inverted) power flows are generated.

The storage helps matching distributed renewable generation and demand and thus reduces power flows. The reduced loss contributes also to the decrease of the cost of energy, although the reduction of imported energy is more important.

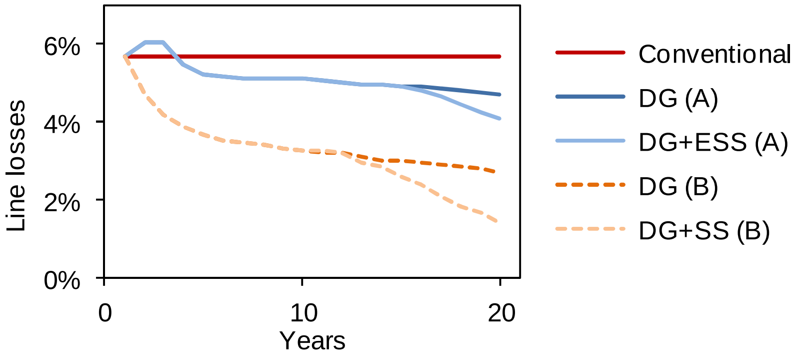

Fig. 4.29. Line losses as a percentage of total demand plus exported energy.

4.5.3 Installed power and generated energy

In Fig. 4.30 the evolution of installed power is represented. It can be observed, as in case A (with export option) much more power is installed. This means that even at only 0.05 €/kWh, it is profitable to sell energy to the grid. Installed power of "Grid" represents the maximum power flow of imported or exported power from or to the main grid. No transmission additional capacity is installed. The increase in grid power in case A is due to the fact that power lines are operated more at their limits. In case B, grid power is reduced slightly as demand power peaks are reduced by distributed generation. In the case of wind, the full power (case A: 402 kW, case B: 121 kW) is installed in year 2 and no more installations are foreseen. This is due to the assumption that installation costs for wind power will remain practically constant. Solar pv power installation sets in at year 3 and increases every year, as a 5% cost decrease is assumed every year, reducing pv installations costs to 38% of the initial cost after 20 years. Finals installed power in case A is 712 kW and in case B 444 kW. Finally, storage starts to be profitable in year 15 for case A and year 12 in case B. It can be seen as the installation of storage goes along with additional increase of solar pv. Final values of storage power and energy are 168 kW / 4.19 MWh in case A and 190 kW / 7.9 MWh in case B.

Fig. 4.31 shows the energy generated annually by each generation technology in the distribution system. Negative values of annual energy in case A represent energy sold to the grid.

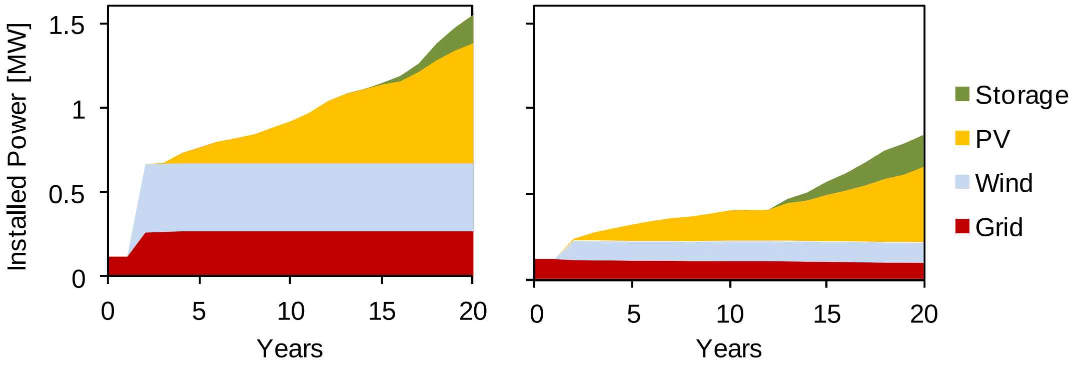

Fig. 4.30. Installed power by technology for case A with energy export (left) and case B without energy export (right).

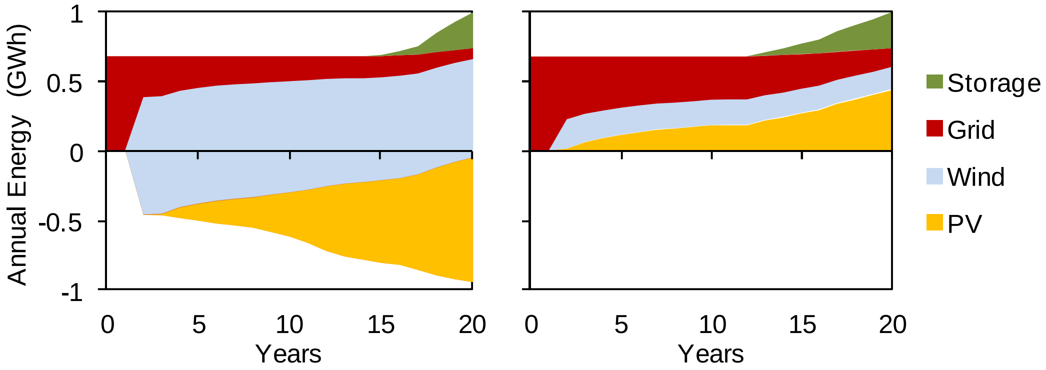

Fig. 4.31. Annual energy generates by each technology for case A with energy export (left) and case B without energy export (right).

Energy supplied by the main grid through the substation (Grid) tends to decrease from the second year and is gradually reduced further. Energy generated by wind sources starts participating in the second year and is maintained constant. Energy generated by the photovoltaic generators starts its participation in year 3 and has a significant increase until year 20. The energy exchanged with the storage system is represented together with the generation, although it is not additional available energy.

Fig. 4.32 shows the excess energy in the network as a percentage of total demand plus exported energy. In case A, excess energy is considerably lower than in case A. This is partly due to the possibility to sell the generated surplus to the grid, but the percentage also is lower because total amount of useful energy is larger.

In the scenario with distributed generation (DG), the excess energy reaches up to 14% of the demand (case A) and 55% (case B). When storage starts to be installed, the energy excess is reduced. The effect in case A is only small (reduction of 3 percentage points: 14 → 11%) but in case B the effect is large, as the excess is reduced to 31% (24 percentage points). On the other hand, storage losses only reach 1.7% (case A) and 3.9% (case B). This fact is responsible for the reduction of costs in the expansion of generation.

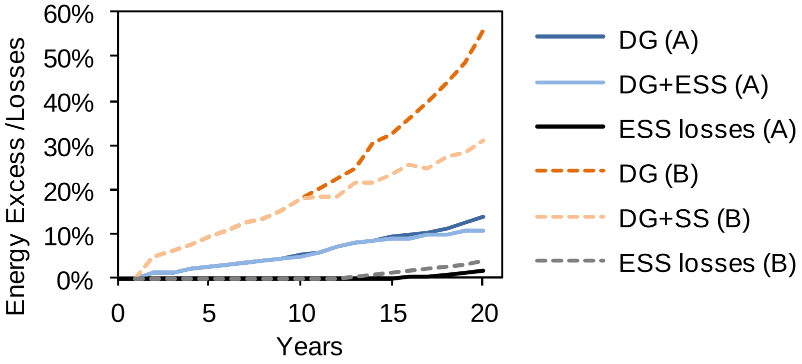

Fig. 4.32. Renewable excess energy generation and storage losses as a percentage of total demand plus exported energy.

4.5.4 Conclusions

Simulations show a considerable potential for profitably installing distributed renewable generation and storage in the modelled industrial area. Wind power is already profitable, and if the location is suitable, its immediate installation is suggested. Especially wind power would benefit from the possibility of selling energy to the grid, as the generation is not synchronized with the demand. Solar pv is also already an interesting option, but expected further installation cost reductions suggest a successive increase of installed power over the years. Finally, it is shown that energy storage enables even more profitable installation of solar pv and reduces line losses. It can become profitable because it makes excess energy available. Energy storage is not an immediate option, if no additional values such as power quality issued are included in the cost and benefit calculations. Storage needs to become much cheaper to be more profitable than allowing excess energy from cheap renewable sources. Especially if part of the excess energy can be sold to the grid, storage becomes less interesting, as the grid actually acts like a large storage. In the simulated case, the installation of storage only becomes profitable if installation costs are reduced by 96% case A or 93% in case B. Such huge cost reductions are only conceivable if used batteries from electric vehicles become available at a large scale and breakthroughs are obtained in storage technology. Recent research results are suggesting that in a horizon of less than 20 years such breakthroughs are probable. Energy densities may be more than 10 times higher than for present-day batteries. This combined with economics of scale may reduce the cost of suitable electrical storage solution by a factor 20, as assumed in this simulation.

5 HUELVA CHEMICAL PARK

5.1 Case without energy storage

5.1.1 Introduction

The aim of this document is to perform an analysis of the percentage of demand covered by renewable energy sources (wind and solar PV) in a micro-grid of a paper industry.

The paper is divided into three sections:

- First, a description of the electricity demand (section 2) and renewable resources linked to the geographical area (section 3) are done.
- Secondly, simulation results are shown, indicating the percentage of electric demand covered when wind power and photovoltaic power vary.

5.1.2 Electric demand description

Due to the inability to access to real (hour by hour) electric consumption data of the paper industry considered, the consumption profiles have been created using the only real electric data known, the annual consumption: 45.100 MWh. From this data, two possible hourly consumption profiles are implemented:

1) Constant all the year, assuming that the industry operates 24 hours a day, 365 days a year (5,4 MWh).
2) Variable, following the demand profile of REE. For its construction, the only condition is that the annual electric consumption must be equal to 45.100 MWh. Unlike the previous profile, which is constant, this reaches a maximum and minimum hourly consumption of 7,6 MWh to 3,2 MWh, respectively.

In Table 5.1, summarized electricity demand per months is shown. The first column contains the constant demand data, and second, the variable demand.

Table 5.1. Monthly electric demand.

MONTH	Constant Demand (MWh)	Variable Demand (MWh)
January	3.836,75	4.081,41
February	3.465,95	3.793,73
March	3.836,75	3.942,29
April	3.713,15	3.449,21
May	3.836,75	3.546,69
June	3.713,15	3.546,02
July	3.836,75	4.041,08
August	3.836,75	3.731,22
September	3.713,15	3.591,98
October	3.836,75	3.543,45
November	3.713,15	3.823,48
December	3.836,75	4.062,89
TOTAL	**45.100**	**45.100**

5.1.3 Renewable energy sources

The paper industry is located in a Chemical area in the province of Huelva (Spain). Renewable energies are considered in the analysis are: wind and solar (photovoltaic). Hourly data over a meteorological year are available of both sources.

To characterize the wind speed, Fig. 5.1 shows the distribution of wind speed throughout the year. As noted, the wind speed is focused on the interval between 2 and 9 m / s.

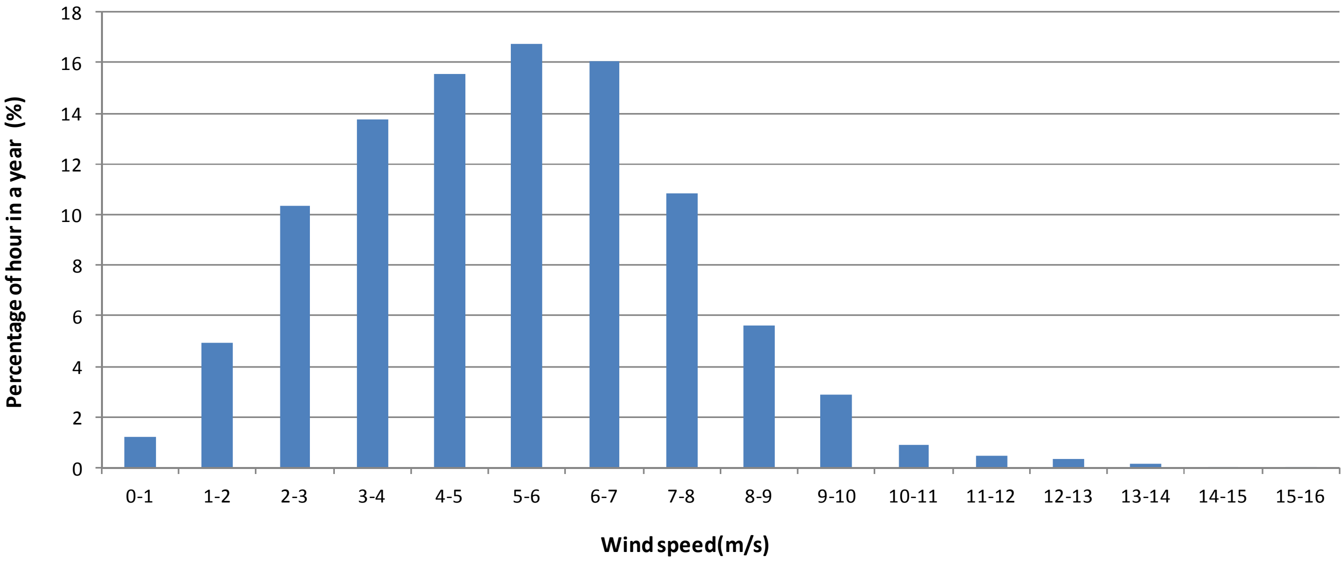

Fig. 5.1. Wind speed distribution.

Regarding solar energy, in simulations the photovoltaic panels are fixed, oriented to south with an inclination equal to the latitude (37° 15'). Table 5.2 shows the values of global solar insolation per month (at location) on a horizontal surface, and inclined at 37° 15'(south facing). This inclination is selected because it maximizes the irradiance at the location concerned.

Table 5.2. Monthly solar insolation.

MONTH	Solar insolation in horizontal surface (kWh/m^2)	Solar insolation in 37º sloped surface (kWh/m^2)
January	81	141,4
February	93	135,3
March	153	194,4
April	167	175,2
May	215	202,7
June	226	199,6
July	241	219,0
August	211	213,8
September	168	201,1
October	126	178,3
November	78	124,8
December	69	121,2
TOTAL	**1.827**	**2.107**

5.1.4 Simulations

For the simulations of this deliverable, it was considered a micro-grid without any electric storage system, and therefore, solar and wind technology have to supply every hourly electric demand.

The simulations have been performed varying the installed power of wind turbines and the electric peak power of the photovoltaic field, with a the range of variation of both technologies from 2 to 20 MW (with a step of 2 MW).

For wind technology, the Gamesa G80 wind turbine (2 MW rated power) has been used, whose characteristic curve (electric power versus wind speed) is shown in Fig. 5.2.

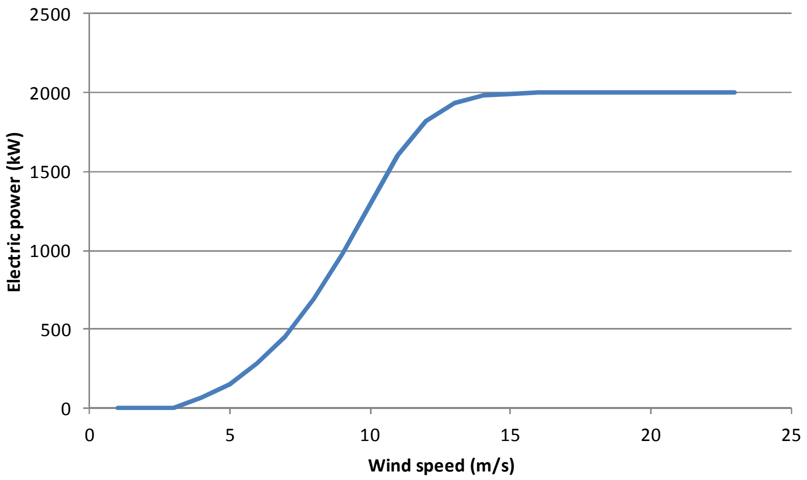

Fig. 5.2. Gamesa G80 power curve.

For photovoltaic technology, the photovoltaic panel considered is ISOFOTON I-106/12, with a peak power of 106 Wp per module. Its characteristic curve can be seen in Fig. 5.3.

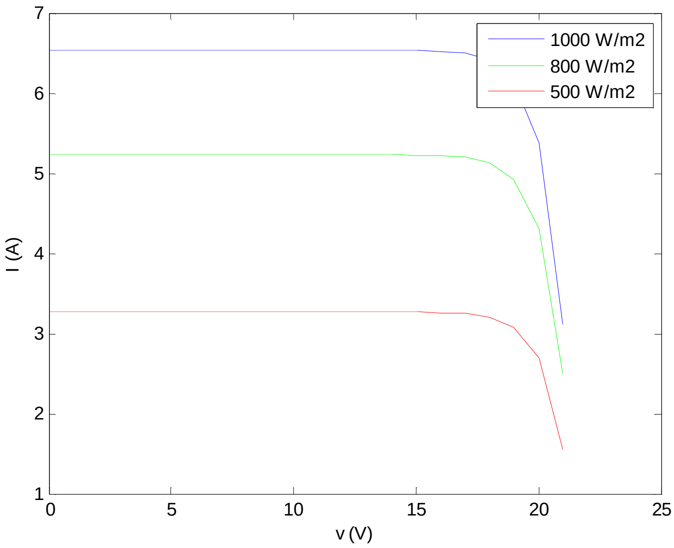

Fig. 5.3. Isofoton I-106 Photovoltaic panel intensity-voltage curve

The simulation scheme implemented realizes two considerations:

- If at the time step of simulation, the sum of the power produced by the photovoltaic field and the wind farm is greater (or equal) than the electric demand, this hour is taken into account on annual aggregate hours.

- On the contrary, if the sum of electric power of both technologies is lower than demand, that time step is not counted in the annual calculation.

Two cases are simulated, the first linked to the constant power demand and the second to the variable demand. In each case, a variation of electric demand percentage in each hour is done from 10 to 100% (with a step of 10%).

Below the simulations results are presented.

5.1.4.1 CASE 1: CONSTANT ELECTRIC DEMAND.

In Table 5.3 a summary of results is shown. In the axes are represented the wind power and solar power considered in each simulation, respectively. The values of table represent the percentage of hours during a year where production from renewable sources is higher than electric demand.

As shown, with higher combination of renewable sources simulated (a 20 MW wind farm and a 20 MW photovoltaic field) the percentage of hours during a year is 40,8%. This is poor value, because total electric power installed from renewable (40 MW) is 8 time higher than electric power demanded (5 MW).

Never, the demand of 100% of hours in the year will be covered by renewable sources, independently of wind farm and photovoltaic field sizes. There are hours in the year with a low speed of wind or no sun, where the electric production is 0 MWh.

Table 5.3. Percentage of electric demand covered by renewable sources. Case 1. 100% demand.

		Photovoltaic field power (MW)										
		0	**2**	**4**	**6**	**8**	**10**	**12**	**14**	**16**	**18**	**20**
Wind farm power (MW)	**0**	0,0	0,0	0,0	10,8	19,3	24,3	27,8	30,3	32,1	33,7	34,8
	2	0,0	0,0	0,7	12,4	20,3	25,1	28,5	30,8	32,7	34,2	35,3
	4	0,0	0,5	2,6	13,8	21,4	26,0	29,2	31,4	33,2	34,7	35,6
	6	1,3	2,4	4,8	15,4	22,7	27,1	30,1	32,2	34,0	35,4	36,3
	8	2,9	4,0	6,7	16,9	23,9	28,2	31,0	33,2	34,8	36,1	37,1
	10	4,1	5,4	8,1	18,1	24,9	28,9	31,8	33,9	35,5	36,7	37,7
	12	5,2	6,6	9,2	19,2	25,8	29,7	32,5	34,6	36,0	37,3	38,3
	14	6,4	7,8	10,6	20,3	26,7	30,4	33,3	35,2	36,7	38,0	38,9
	16	7,4	9,0	11,8	21,4	27,5	31,3	34,1	36,0	37,4	38,7	39,6
	18	8,3	10,0	12,9	22,3	28,3	32,0	34,8	36,7	38,1	39,3	40,2
	20	9,4	11,1	14,1	23,2	29,1	32,7	35,4	37,3	38,7	39,8	40,8

In Table 5.4 and Table 5.5 the same results are presented but considering a 50% and 10% of demand in each hour, respectively. As shown, with renewable source sizes selected the totally electric demand will be no covered, even if the demand considered is a 10% in each hour.

Table 5.4. Percentage of electric demand covered by renewable sources. Case 1. 50% demand.

		Photovoltaic field power (MW)										
		0	**2**	**4**	**6**	**8**	**10**	**12**	**14**	**16**	**18**	**20**
Wind farm power (MW)	**0**	0,0	0,0	19,3	27,8	32,1	34,8	36,6	38,3	39,6	40,4	40,9
	2	0,0	2,6	21,4	29,2	33,2	35,6	37,4	38,9	40,0	40,8	41,3
	4	2,9	6,7	23,9	31,0	34,8	37,1	38,7	40,2	41,3	42,0	42,5
	6	5,2	9,2	25,8	32,5	36,0	38,3	39,9	41,3	42,3	43,0	43,4
	8	7,4	11,8	27,5	34,1	37,4	39,6	41,1	42,4	43,4	44,1	44,5
	10	9,4	14,1	29,1	35,4	38,7	40,8	42,3	43,5	44,4	45,1	45,6
	12	11,3	16,0	30,5	36,6	39,9	41,9	43,3	44,5	45,4	46,0	46,5
	14	12,9	17,8	31,8	37,7	40,9	42,8	44,2	45,4	46,2	46,8	47,3
	16	14,6	19,4	33,0	38,8	41,8	43,7	45,0	46,2	47,0	47,6	48,2
	18	16,0	20,8	33,8	39,7	42,5	44,4	45,8	46,9	47,7	48,4	48,8
	20	17,2	22,1	34,8	40,4	43,2	45,0	46,4	47,5	48,3	48,9	49,3

Table 5.5. Percentage of electric demand covered by renewable sources. Case 1. 10% demand.

		Photovoltaic field power (MW)										
		0	**2**	**4**	**6**	**8**	**10**	**12**	**14**	**16**	**18**	**20**
Wind farm power (MW)	**0**	0,0	34,8	40,9	43,2	44,7	45,7	46,4	46,8	47,2	47,7	47,9
	2	9,4	40,8	45,6	47,6	48,7	49,5	50,1	50,6	50,9	51,3	51,6
	4	17,2	45,0	49,3	51,2	52,3	53,0	53,5	53,9	54,2	54,6	54,9
	6	22,4	47,9	51,8	53,7	54,6	55,4	55,9	56,2	56,5	56,8	57,1
	8	26,3	50,1	53,9	55,5	56,5	57,2	57,7	58,0	58,3	58,5	58,8
	10	28,7	51,5	55,2	56,8	57,7	58,4	58,9	59,2	59,5	59,7	60,1
	12	30,2	52,6	56,1	57,7	58,6	59,2	59,6	60,0	60,2	60,5	60,8
	14	32,7	53,9	57,3	58,8	59,7	60,3	60,8	61,1	61,3	61,7	61,9
	16	35,0	55,3	58,5	60,0	60,8	61,5	61,9	62,2	62,4	62,7	62,9
	18	36,4	56,0	59,2	60,6	61,5	62,1	62,4	62,8	63,0	63,3	63,5
	20	37,7	56,7	59,9	61,3	62,1	62,7	63,0	63,4	63,6	63,9	64,1

As shown, solar energy can supply more electric demand than wind energy, if no wind farm (0 – 20 MW photovoltaic field) and no photovoltaic field (0 – 20 MW wind farm) combinations are compared. Two reasons can be mentioned:

- Radiation conditions are ideal because location is in Southern Europe, so it has a greater value in most of sun light hours.
- Wind conditions are poor because the industrial area considered is located at sea level and out of the confluence of major currents of wind. Also, the wind turbine proposed works most of the time below its rated power.

Fig. 5.4 represents the percentage of hours during a year when the demand is covered by renewable technologies (20 MW of wind farm and 20 MW of photovoltaic field), varying the level of demand from 10 to 100%.

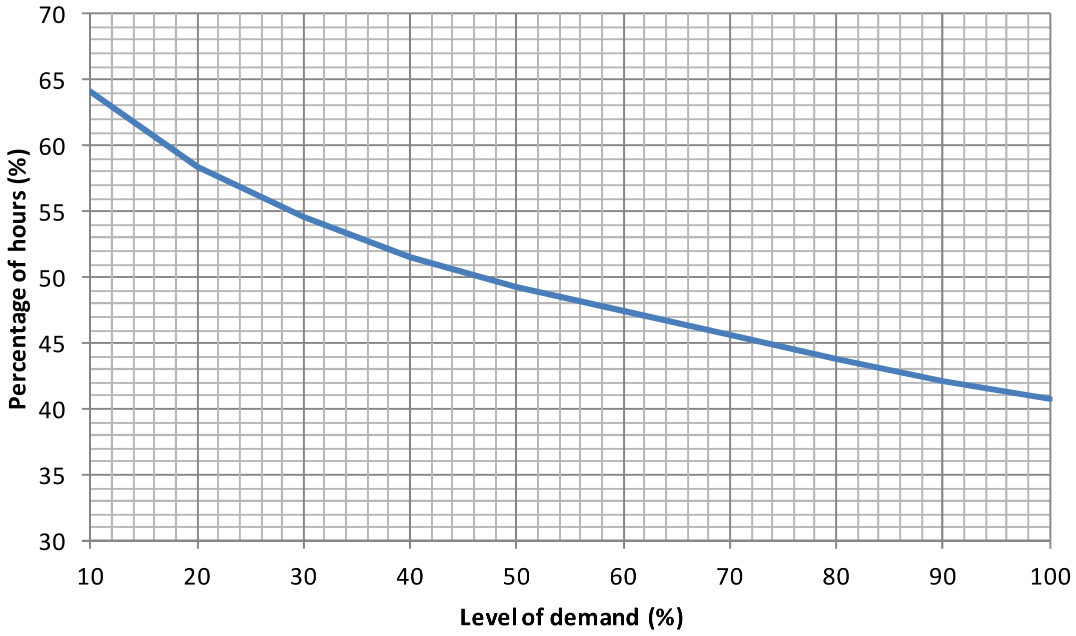

Fig. 5.4. Percentage of hours when demand is covered versus level of demand. Case 1.

5.1.4.2 CASE 2: VARIABLE ELECTRIC DEMAND.

Like the previous case, Table 5.6, Table 5.7 and Table 5.8, show the percentage of hours during a year when electric production from renewable sources is higher than electric demand, for a 100%, 50% and 10% of demand, respectively, when the demand is variable.

Table 5.6. Percentage of electric demand covered by renewable sources. Case 2. 100% demand.

		Photovoltaic field power (MW)										
		0	**2**	**4**	**6**	**8**	**10**	**12**	**14**	**16**	**18**	**20**
Wind farm power (MW)	**0**	0,0	0,0	0,1	7,3	16,8	22,6	26,5	29,3	31,1	32,9	34,2
	2	0,0	0,0	0,5	9,2	18,0	23,4	27,2	29,8	31,6	33,4	34,8
	4	0,0	0,3	2,1	10,9	19,3	24,3	28,0	30,5	32,3	33,9	35,2
	6	0,9	2,1	4,2	12,7	20,7	25,5	29,0	31,4	33,2	34,9	36,0
	8	2,7	3,9	6,2	14,0	21,9	26,6	30,0	32,4	34,1	35,7	36,8
	10	4,0	5,1	7,7	15,4	23,0	27,5	30,7	33,1	34,7	36,3	37,4
	12	5,2	6,3	8,9	16,4	23,9	28,2	31,5	33,7	35,3	36,8	38,0
	14	6,2	7,5	10,0	17,5	24,7	29,1	32,2	34,4	36,0	37,5	38,7
	16	7,2	8,6	11,1	18,5	25,6	29,9	33,0	35,1	36,7	38,1	39,2
	18	8,2	9,8	12,4	19,6	26,6	30,7	33,8	35,9	37,5	38,9	40,0
	20	9,2	10,7	13,4	20,6	27,4	31,4	34,3	36,5	38,1	39,5	40,5

Table 5.7. Percentage of electric demand covered by renewable sources. Case 2. 50% demand.

		Photovoltaic field power (MW)										
		0	**2**	**4**	**6**	**8**	**10**	**12**	**14**	**16**	**18**	**20**
Wind farm power (MW)	**0**	0,0	0,1	16,8	26,5	31,1	34,2	36,2	37,7	39,1	40,1	40,8
	2	0,0	2,1	19,3	28,0	32,3	35,2	36,9	38,5	39,7	40,5	41,2
	4	2,7	6,2	21,9	30,0	34,1	36,8	38,4	39,9	41,1	41,9	42,5
	6	5,2	8,9	23,9	31,5	35,3	38,0	39,5	40,9	42,1	42,8	43,4
	8	7,2	11,1	25,6	33,0	36,7	39,2	40,8	42,1	43,2	43,9	44,5
	10	9,2	13,4	27,4	34,3	38,1	40,5	42,0	43,2	44,3	45,1	45,6
	12	11,1	15,3	28,8	35,7	39,3	41,6	43,1	44,3	45,3	46,1	46,6
	14	12,8	17,1	30,3	36,9	40,4	42,6	44,1	45,3	46,3	46,9	47,4
	16	14,4	18,8	31,6	38,1	41,5	43,7	45,0	46,2	47,2	47,8	48,3
	18	16,0	20,3	32,8	39,1	42,4	44,6	45,9	47,1	48,0	48,7	49,2
	20	17,2	21,5	33,7	39,9	43,0	45,2	46,5	47,6	48,6	49,2	49,7

Table 5.8. Percentage of electric demand covered by renewable sources. Case 2. 10% demand.

		Photovoltaic field power (MW)										
		0	**2**	**4**	**6**	**8**	**10**	**12**	**14**	**16**	**18**	**20**
Wind farm power (MW)	**0**	0,0	34,2	40,8	43,2	44,5	45,6	46,3	46,9	47,2	47,6	48,0
	2	9,2	40,5	45,6	47,6	48,7	49,7	50,3	50,7	51,1	51,4	51,8
	4	17,2	45,2	49,7	51,5	52,6	53,5	54,0	54,4	54,7	55,1	55,4
	6	22,4	48,2	52,3	54,1	55,1	55,9	56,4	56,8	57,1	57,4	57,7
	8	26,3	50,3	54,3	56,0	56,8	57,6	58,1	58,5	58,8	59,1	59,4
	10	28,9	51,7	55,6	57,2	58,1	58,9	59,3	59,7	60,0	60,3	60,6
	12	31,1	53,2	57,0	58,5	59,4	60,1	60,6	61,0	61,3	61,5	61,7
	14	33,0	54,4	58,0	59,5	60,3	61,1	61,5	61,9	62,2	62,4	62,7
	16	34,8	55,4	58,9	60,4	61,2	61,9	62,4	62,8	63,0	63,2	63,5
	18	36,2	56,2	59,6	61,1	61,9	62,5	63,0	63,4	63,5	63,8	64,0
	20	37,7	57,0	60,3	61,9	62,6	63,3	63,7	64,1	64,2	64,4	64,6

Comparing the results obtained in this case with constant demand case, it is observed that the percentage of hours where demand is covered by the same combination of renewable technologies, agrees in most situations. So, it is possible to affirm that the demand profile does not have significantly influence in the sizing of wind and photovoltaic equipment.

5.2 Case with energy storage

5.2.1 Introduction

In this document, a micro-grid of a paper industry is simulated, focusing the analysis on the level of penetration of renewable energy sources into the micro-grid, when an electric storage system is considered.

For simulations, the renewable sources considered are: wind and solar photovoltaic. The size and type of equipment used are explained in the document of deriverable 9.

Also, in document of deliverable 9 the types of demand (constant and variable) are quantified.

The next section presents the operation mode of micro-grid, a summary of simulation results and some conclusions of analysis.

5.2.2 Simulations

The simulation scheme implemented realizes two considerations:

- If at the time step of simulation, production from renewable sources is higher than electric demand, excess of energy is sent to the storage system.
- On the contrary, if the sum of electric power of both technologies is lower than demand, the defect of energy is supplied by the storage system.

In simulations, first step is to determine the size of the wind farm and photovoltaic field that can supply all energy demand during a year. The only requisite for sizing is that the sum of all energy excess needs to be higher (or equal) than the sum of all energy defects during a year.

5.2.2.1 CASE 1: CONSTANT ELECTRIC DEMAND.

In case 1, the smallest combination of wind farm and photovoltaic field that can satisfy all electric demand during a year is: a wind farm of 8 MW and a photovoltaic field of 20 MW. With this combination, it is necessary a storage capacity of 26.374 MWh, that is the minimum size of storage needed.

Once the size of storage system is fixed, a simulation with all combination of renewable sources is done (in the same way of simulations performed in deliverable 9). In Table 5.9, the percentage of demand satisfied during a year is shown. As appear, with some combinations, it is possible to supply all electric demand.

Table 5.9. Percentage of electric demand covered by renewable sources. Case 1. 100% storage system.

		Photovoltaic field power (MW)										
		0	**2**	**4**	**6**	**8**	**10**	**12**	**14**	**16**	**18**	**20**
Wind farm power (MW)	**0**	53,1	59,0	66,4	74,2	79,1	82,5	85,0	86,9	88,5	89,8	90,9
	2	54,9	61,1	69,0	76,8	81,6	84,9	87,4	89,3	90,9	92,2	93,3
	4	56,7	63,4	71,5	79,2	84,0	87,3	89,8	91,7	93,3	94,6	95,7
	6	58,5	65,4	73,7	81,4	86,2	89,5	92,0	94,0	95,5	96,8	98,0
	8	60,1	67,2	75,6	83,3	88,1	91,5	94,0	95,9	97,5	98,9	100
	10	61,5	68,7	77,2	85,0	89,9	93,3	95,8	97,8	99,4	100	100
	12	62,8	70,2	78,8	86,6	91,5	94,9	97,5	99,5	100	100	100
	14	64,0	71,5	80,2	88,1	93,0	96,5	99,1	100	100	100	100
	16	65,1	72,8	81,6	89,5	94,4	97,9	100	100	100	100	100
	18	66,2	73,9	82,8	90,8	95,8	99,3	100	100	100	100	100
	20	67,2	75,0	84,0	92,0	97,0	100	100	100	100	100	100

In Fig. 5.5, it is possible to identify renewable sources combinations whose electric production is higher than demand, and therefore with the storage system selected can supply all the energy demanded.

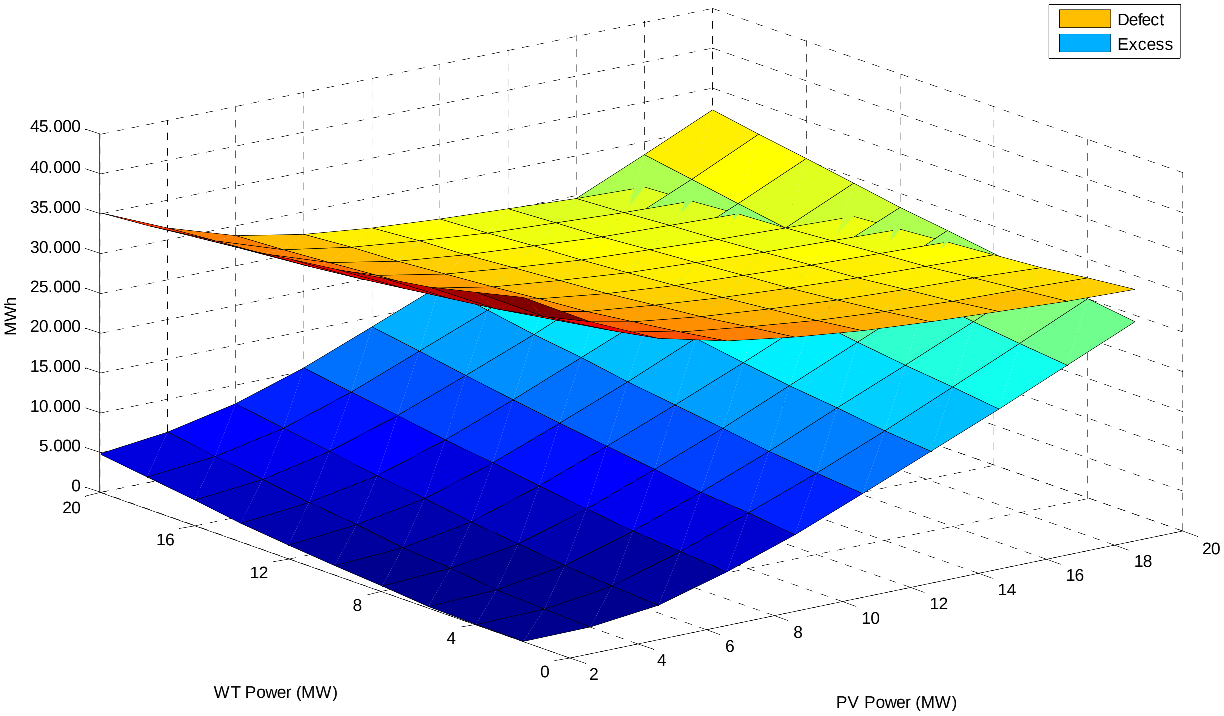

Fig. 5.5. Excess and defect of electric energy during a year. Case 1. 100 % storage system.

5.2.2.2 CASE 2: VARIABLE ELECTRIC DEMAND.

In Table 5.10, same results for variable demand are presented. In this case, optimum storage size is 24.861 MWh (lower than previous case), obtained with a combination of a 6 MW of wind farm and 20 MW of photovoltaic field.

Table 5.10. Percentage of electric demand covered by renewable sources. Case 2. 100% storage system.

		Photovoltaic field power (MW)										
		0	**2**	**4**	**6**	**8**	**10**	**12**	**14**	**16**	**18**	**20**
Wind farm power (MW)	**0**	50,1	55,7	62,6	70,5	76,3	80,3	83,3	85,6	87,5	89,1	90,4
	2	51,7	57,7	65,1	73,2	78,9	82,9	85,9	88,2	90,1	91,6	93,0
	4	53,4	59,8	67,6	75,7	81,4	85,4	88,4	90,7	92,6	94,2	95,5
	6	55,2	61,8	69,7	77,9	83,7	87,7	90,7	93,0	94,9	96,5	97,9
	8	56,7	63,5	71,6	79,8	85,6	89,7	92,8	95,1	97,0	98,7	100
	10	58,1	65,0	73,3	81,5	87,4	91,6	94,6	97,0	99,0	100	100
	12	59,3	66,4	74,8	83,2	89,1	93,3	96,4	98,8	100	100	100
	14	60,5	67,7	76,2	84,7	90,7	94,9	98,0	100	100	100	100
	16	61,6	68,9	77,6	86,1	92,2	96,4	99,6	100	100	100	100
	18	62,6	70,1	78,8	87,5	93,6	97,9	100,0	100	100	100	100
	20	63,6	71,2	80,0	88,7	94,9	99,2	100,0	100	100	100	100

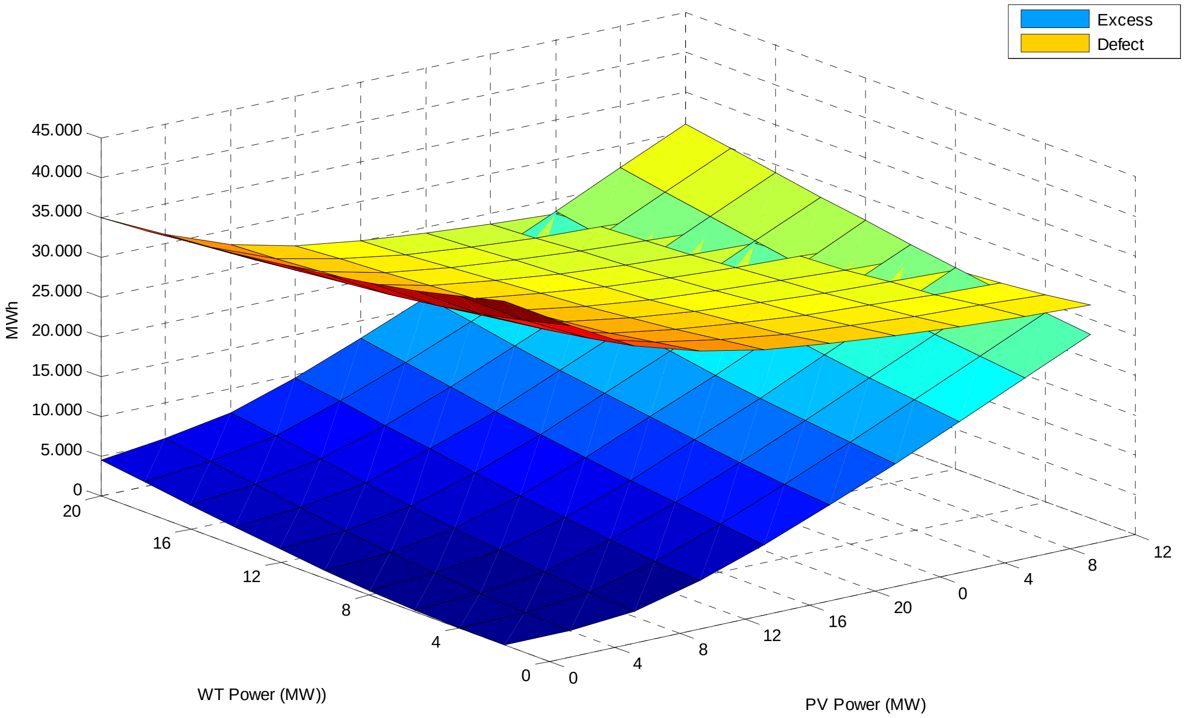

Fig. 5.6. Excess and defect of electric energy during a year. Case 2. 100 % storage system.

6 CONCLUSIONS

The results of the simulations with the models of the 5 case studies are presented in the report. Each of the case studies represents a particular industrial sector, with particular features, where a smart-grid could be installed. Different approaches have been taken for the studies, using a variety of simulation tools enabling the assessment of varied strategies. Besides, regarding the smart-grids there are simulations for grid connected systems but also for isolated systems.

According to the results of the simulations, the installation of renewable generation within the industrial areas is in many cases cost competitive against electricity prices from the grid. As explained in the report, the renewable resources vary deeply from one location to another, and a thorough study will have to be done to decide the optimal combination of renewable technologies before the installation of any smart-grid. Moreover, the specific characteristics of the local load demand will have to be taken into account in this kind of study, evaluating which renewable generation matches best with the demand. In principle, wind and PV power seem to be most feasible options for an industrial area regarding resource availability, but hydro and biomass power can be very interesting options in certain locations, providing different features. In any case, the installation of renewable energy systems is a good strategy to reduce dependency on future power prices.

In relation with energy storage, the analysis performed leave clear that with current investment costs and grid tariffs it is difficult to get profitability. Depending on the evolution of the prices of both storage technologies and grid electricity, the installation of such equipments can be cost-competitive in the future. It is worth mentioning that the profitability of an energy storage system will strongly depend on the number of operating hours of the system along the year, which depends on the strategy followed. Meanwhile, energy storage can be justified in cases where power quality is a key issue, in cases where a weak grid exists, and of course in isolated systems. Energy security issues also plays in favour of energy storage in cases where a backup is necessary, protecting the system from grid disturbances or even blackouts. Also, energy storage can help to avoid costly grid reinforcements. Today, it makes more sense to use the grid as the energy storage system where available, especially if a net-metering regulation exists.

Nevertheless, we must remember that energy storage is not the only tool for the energy management. Virtual storage is also a key actor for the control strategies within a micro-grid. Deferrable loads such as some refrigeration loads or electric vehicles recharging also serve to match generation with demand.

The present report shows that smart energy systems can be implemented at present in different industrial areas, providing interesting technical features. A high penetration of renewable energies together with an intelligent energy management system help industrial areas to reduce CO_2 emissions, also providing savings through a better energy efficiency. In this context, energy storage can play a key role within the control strategies when the necessary cost reduction takes place.

TITLE OF THE PROJECT: OPTIMAGRID SOE2/P2/E322

GT < 3 >: Implementation of micro-grids with high penetration of renewable energies

DELIVERABLE < 11 >: Validation of models with experimental data

ABSTRACT

Once several case studies were defined in GT2, an analysis of different scenarios has been developed in GT3. Within this deliverable, the focus is on the validation of the models developed for the available pilot microgrids.

The objective of these models is to follow in a reliable manner the performance of the microgrids presented as case studies. Thanks to these simulations, the implementation of different strategies can be tested from the technical point of view in order to assess its suitability for the real microgrids. Thus, these models can save time and cost when trying new control strategies for a specific installation.

The validation has been performed comparing the real behaviour of the plants with the results obtained from the simulation with the specific models developed.

Among others, the possible control strategies can be directed to the following targets:

- Maximum renewable consumption
- Reduction of emissions
- Minimum purchase from the grid
- Protection against disconnection from the grid (backup)
- Optimize grid purchases regarding tariff periods
- Price arbitrage (buy low, sell high)
- Reactive power compensation
- Take into account generation forecasts
- Take into account consumption forecasts or common patterns (daily, weekly…)

The models presented in this report have been developed in different software platforms.

CONTENTS

1 Ha - Walqa Technological Park 8
  1.1 Installation description 8
  1.2 Introduction of the system in Matlab program 14
  1.3 Data inputs 14
  1.4 Results 16
  1.5 Conclusions 18
2 AICIA - Laboratory Facilities 19
  2.1 Introduction 19
  2.2 Microgrid modelling 20
  2.3 Microgrid control strategies 35
  2.4 Experimental microgrid operation 36
3 ESTIA - HESS model validation 39
  3.1 Introduction 39
  3.2 Storage systems in microgrids 39
  3.3 Control of the HESS 43
  3.4 Experimental results 46
  3.5 Conclusions 52
  3.6 Bibliography 53
4 CENER - ATENEA Microgrid 54
  4.1 Installation description 54
  4.2 Microgrid modelling 55
  4.3 Model validation 57
  4.4 Control strategies 62
  4.5 Conclusions 64
5 CIRCE – GAMS and Simulink model validation 65
  5.1 Introduction 65
  5.2 Description of the validation case 65
  5.3 Validation of micro-grid planning tool with NEPLAN 66
  5.4 Validation of energy balance model with Micro-grid Emulator 74
6 Conclusion 85

LIST OF FIGURES

Fig. 1.1. Wind turbines........8

Fig. 1.2. Wind turbine locations in Walqa Technological Park........9

Fig. 1.3. Fixed installation in parking canopies of Walqa Technological Park........10

Fig. 1.4. DEGUER solar trackers and behind MECASOLAR solar tracker........10

Fig. 1.5. ADES solar tracker........11

Fig. 1.6. OX CTA building. www.oxcta.com........11

Fig. 1.7. Diagram of the Project ITHER........12

Fig. 1.8. Locations of distribution centers and evacuation........12

Fig. 1.9. Line diagram of the installation........13

Fig. 1.10. Diagram in Matlab........14

Fig. 1.11. Results........16

Fig. 1.12. Results........17

Fig. 2.1. Experimental plant configuration........19

Fig. 2.2. Five-parameter equivalent electrical circuit used to model a PV cell........21

Fig. 2.3. Inputs, outputs and parameters related to the PV array dynamical model........22

Fig. 2.4. (a) I-V and P-V curves for the ISOFOTON ISF-150 module. (b) radiation effects on the I-V curve and (c) ambient temperature effect on the I-V curve........23

Fig. 2.5. Comparison of the model and experimental electrolyzer voltage for different currents........25

Fig. 2.6. Measured and simulated hydrogen produced in electrolyzer........26

Fig. 2.7. Simulated and measured electrolyzer stack temperature........27

Fig. 2.8. (a) PEMFC polarization curve; (b) Oxygen pressure effects on the polarization curve; (c) stack temperature effects on the polarization curve........28

Fig. 2.9. (a) Comparison between model simulation and experimental absorption process at constant pressure (4.5 barg). (b) Model bed temperature and experimental during charging process........32

Fig. 2.10. (a) Comparison between model simulation and experimental desorption process at constant pressure demand (4.5 barg). (b) Model bed temperature and experimental measure during discharging process........33

Fig. 2.11. Comparison between battery experimental voltage and battery model voltage during a discharging test........34

Fig. 2.12. (a) PV array power supply. (b) first demand profile. (c) second demand profile........36

Fig. 2.13. (a) PEMFC operation. (b) electrolyzer operation. (c) hydrogen storage performance........37

Fig. 2.14. (a) Power exchanges with neighbor grids. (b) DC bus voltage........38

Fig. 3.1 Classification of different storage systems according to their specific energy and power........41

Fig. 3.2. Schematic representation of the 3LNPC topology. 43

Fig. 3.3. Control structure of the isolated case. 44

Fig. 3.4. Control structure of the grid-connected case. 45

Fig. 3.5. Control structure of the current of the VRB. 46

Fig. 3.6 Photograph of the experimental platform. 47

Fig. 3.7. Block diagram of the experimental tests in the isolated case study. 48

Fig. 3.8. Evolution of (a) P_{dc} and (b) $P_{vrb\ ref}$, P_{vrb}, P_{sc} variables during the variable DC power injection test..49

Fig. 3.9. Evolution of the offset during the variable DC power injection test. 49

Fig. 3.10. Evolution of the AC side variables during the variable DC power injection test. 49

Fig. 3.11. Block diagram of the experimental tests in the grid-connected case study. 50

Fig. 3.12. Evolution of (a) V_d, (b) I_d, (c) P and (d) Q variables during the disconnection from the main grid.51

Fig. 3.13. Evolution of (a) P_{vrb}, (b) P_{sc} and (c) P_{dc} variables during the disconnection from the main grid. ...52

Fig. 4.1. General view of the model in Simulink 56

Fig. 4.2. View of the tanks (left) and the stacks (right) of the flow battery 57

Fig. 4.3. Power loads fed by the microgrid 58

Fig. 4.4. Wind turbine power generation 59

Fig. 4.5. PV system power generation 59

Fig. 4.6. Power input/output of the Vanadium Redox Battery (positive-discharging / negative-charging) 60

Fig. 4.7. Representation of the SOC of the Vanadium Redox Battery 61

Fig. 4.8. Power exchange with the distribution power grid (positive-export / negative-import) 61

Fig. 4.9. Energy balance of the simulation 62

Fig. 5.1 Microgrid structure of assumed industrial area of 100 kW total mean power. 66

Fig. 5.2 Line losses for all combinations of solar PV and wind generation, without storage (above) and with up to 187 kW of storage power (below). 68

Fig. 5.3 Line losses as a percentage of total demand plus exported energy. 70

Fig. 5.4 Node voltages for different levels of solar PV generation assuming nominal wind power, without storage (above) and with up to 187 kW of storage power (below). 71

Fig. 5.5 Typical load profile (annual average) of the industrial area under study. 71

Fig. 5.6 Voltage at node N5 for all combinations of solar PV and wind generation, without storage (above) and with up to 187 kW of storage power (below). 72

Fig. 5.7 Schema of the Micro-grid Emulator. 75

Fig. 5.8 Vertical axis wind turbine from Kliux energies (http://www.kliux.com), at CIRCE. 76

Fig. 5.9 FIPA ContractNet interaction protocol. 79

Fig. 5.10 Comparison of distribution density (above) and cumulative (below) of active power at PCC for Peak Shaving control strategy, for Simulink and Multi-Agent model......81

Fig. 5.11 Two typical sequences (48h each) of active power demand with control scenario Peak Shaving from Emulator (Pcc Emul) and Simulink model (Pcc Simul) compared to Pload, left: typical activity, right: high activity......82

Fig. 5.12 Distribution density (above) and cumulative (below) of active power at PCC for Peak Shaving control strategy, Multi-Agent model with real wind generation data......83

Fig. 5.13 Sequence of 77 minutes of active power demand control (Peak Shaving) with real wind generation data. 83

LIST OF TABLES

Table 1.1. Wind turbine characteristics in Walqa Technological Park. 8
Table 1.2. Wind turbines characteristics. 9
Table 1.3. Characteristics of Photovoltaic installation. 9
Table 1.4. Technologies of photovoltaic electric power generation. 10
Table 1.5. Solar tracking technologies. 11
Table 1.6. Energy data 15
Table 2.1. Microgrid equipment 20
Table 2.2. Time constant orders of the microgrid equipment dominant dynamics. 21
Table 2.3. ISOFOTON ISF-150 data sheet and equivalent five model parameters. 23
Table 2.4. Model parameters for the PEM electrolyzer. 25
Table 2.5. PEMFC model parameters. 29
Table 2.6. Metal hydride tank model parameters. 31
Table 2.7. Battery model parameters. 34
Table 3.1 Parameters of the 3LNPC converter. 47
Table 4.1. Energy balance of the simulation 62
Table 5.1 Line losses for any combination of solar PV and wind generation, without storage. 69
Table 5.2 Line losses for any combination of solar PV and wind generation, with storage. 69
Table 5.3 Properties of Kliux wind turbine. 76
Table 5.4 Structure of Java classes of the multi-agent model. 77
Table 5.5 Control parameters for strategy 1 (peak shaving). 80
Table 5.6 Converter Model parameters for the case of 250kW wind+pv. 81

1 HA - WALQA TECHNOLOGICAL PARK

1.1 Installation description

ITHER Project is the development of infrastructure for hydrogen generation from renewable energies, belonging to Foundation for the development of new hydrogen technologies in Aragón. The ultimate aim of the project is to create a solid infrastructure for various renewable power generation technologies, allowing a laboratory feeding hydrogen production by electrolysis located in Hydrogen Foundation building.

The following section shows the different generation systems and management:

- Wind generation.
- Solar generation.
- Electrical switchgear and distribution connection.

Walqa Technological Park has 100 kW more of photovoltaic power in OX – CTA building.

1.1.1 Wind generation installation

The small wind farm owned by The Hydrogen Foundation is composed by three wind turbines with a combined output power of 635 kW. These machines are from "repowering" because it is difficult to find this low level of power in new machines and these are cheaper in terms of device acquisition. Specifically wind generators installed are:

Table 1.1. Wind turbine characteristics in Walqa Technological Park.

DENOMINATION	POWER (kW)
Vestas Turbine V29	**225 kW**
Enercon Turbine – 33	**330 kW**
Lagerway Turbine two bladed	**80 kW**

Fig. 1.1. Wind turbines.

Table 1.2. Wind turbines characteristics.

VESTAS	ENERCON	LAGERWAY
Power: 225 kW	Power: 330 kW	Power: 80 kW
Height: 30 m.	Height: 40 m.	Height: 40 m.
Technology: Doubly fed asynchronous.	Technology: Full converter synchronous.	Technology: Squirrel-cage asynchronous.
Diameter: 27 m.	Diameter: 33 m.	Diameter: 18 m.

Three very different turbines were chosen in order to enhance research orientation of facility, because it's possible to test different technologies allowing greater flexibility. The distribution of these turbines along Walqa Technological Park can be seen in the image below.

Fig. 1.2. Wind turbine locations in Walqa Technological Park.

1.1.2 Photovoltaic installation

The microgrid also includes photovoltaic generation with an installed peak power of 100 kW, divided as follows:

Table 1.3. Characteristics of Photovoltaic installation.

DENOMINATION	POWER (kW)
Fixed installation in parking canopies	60 kW
ADES solar tracker	20 kW
DEGUER solar tracker	5 kW
MECASOLAR solar tracker	10 kW

Fig. 1.3. Fixed installation in parking canopies of Walqa Technological Park.

Just as the wind farm, there are various tracking technologies as both of their own solar panel. This only reinforces the research orientation of ITHER project. There are three photovoltaic generation technologies and two tracking technologies:

Table 1.4. Technologies of photovoltaic electric power generation.

TECHNOLOGY	EFFICIENCY
Polycrystalline	12%
Monocrystalline	14%
Heterogeneous Union	17%

Fig. 1.4. DEGUER solar trackers and behind MECASOLAR solar tracker.

Fig. 1.5. ADES solar tracker.

Table 1.5. Solar tracking technologies.

SOLAR TRACKING TECHNOLOGIES
Tracking by calendar or astronomical calendar
Tracking by maximum brightness point

Walqa Technological Park has 100 kW more of photovoltaic power in OX – CTA building. This installation is included in our analysis.

Fig. 1.6. OX CTA building. www.oxcta.com

1.1.3 Interconnection center

Finally, the Project has a central interconnection with medium voltage cells motorized automated, which by means of a PLC and SCADA, you can choose at any time whether to sell generated electricity as a generator attached to the special regime or the energy is sent to the Hydrogen Foundation laboratory to generate hydrogen by electrolysis. Below are some general diagrams of the facility, its location and interconnection of the different generators:

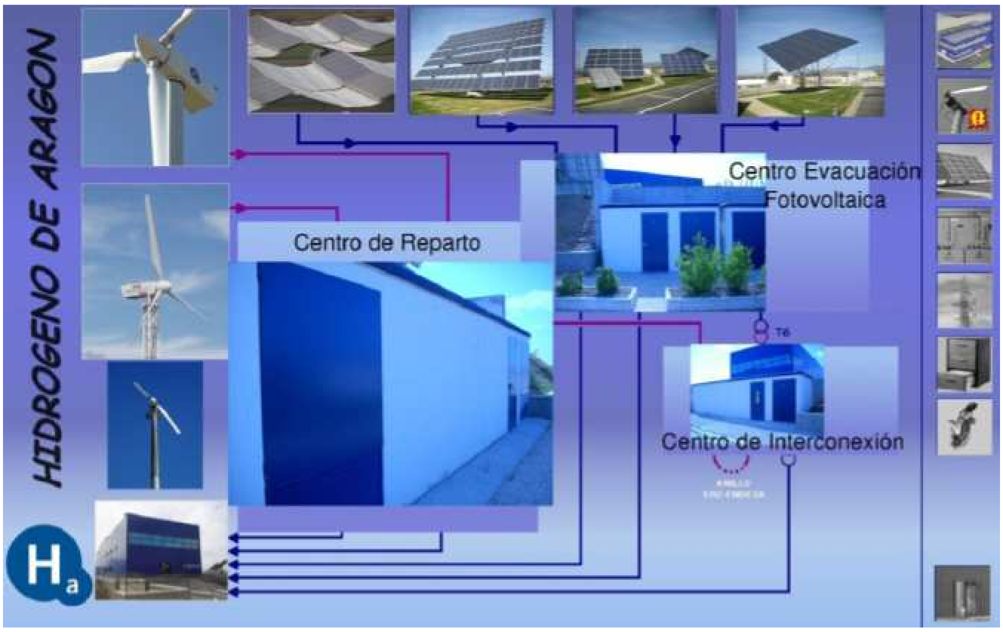

Fig. 1.7. Diagram of the Project ITHER.

Fig. 1.8. Locations of distribution centers and evacuation.

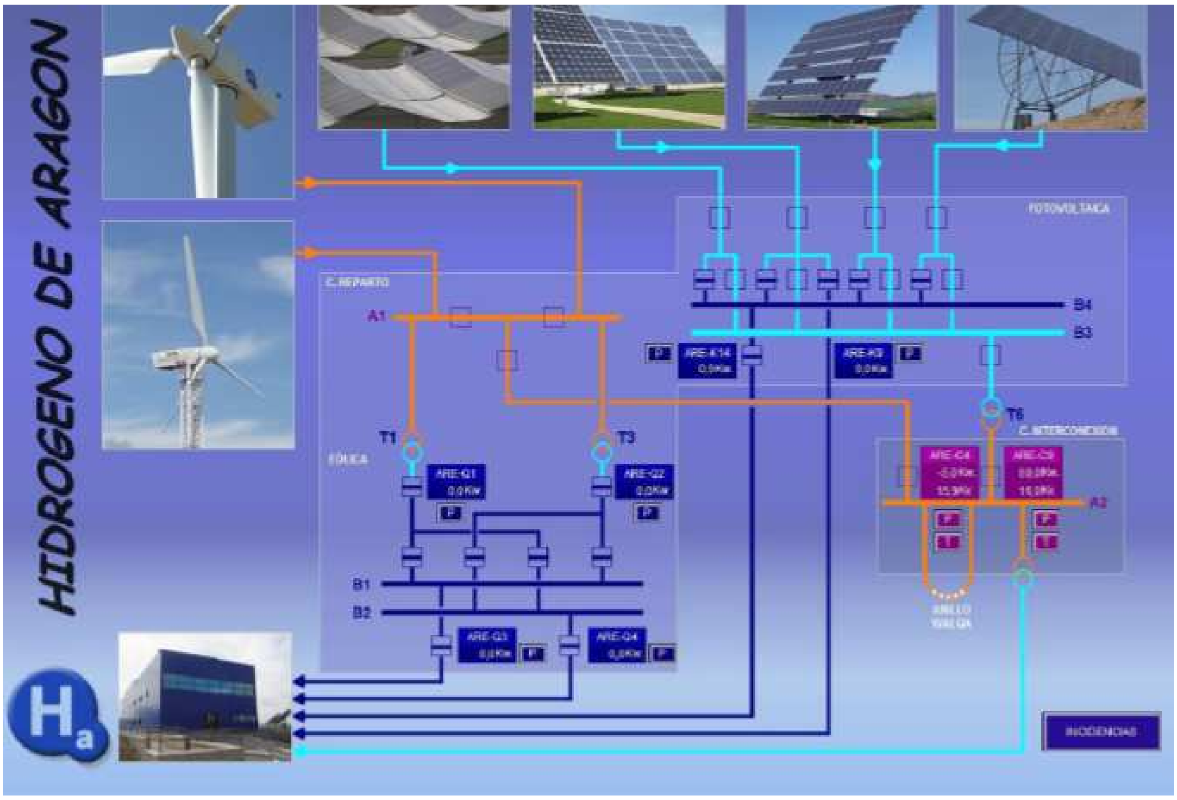

Fig. 1.9. Line diagram of the installation.

1.2 Introduction of the system in Matlab program

Walqa Technological Park electric consumption is defined in Matlab program. Some assumptions have been taken into account:

- Maximum consumption: 2400 kW.

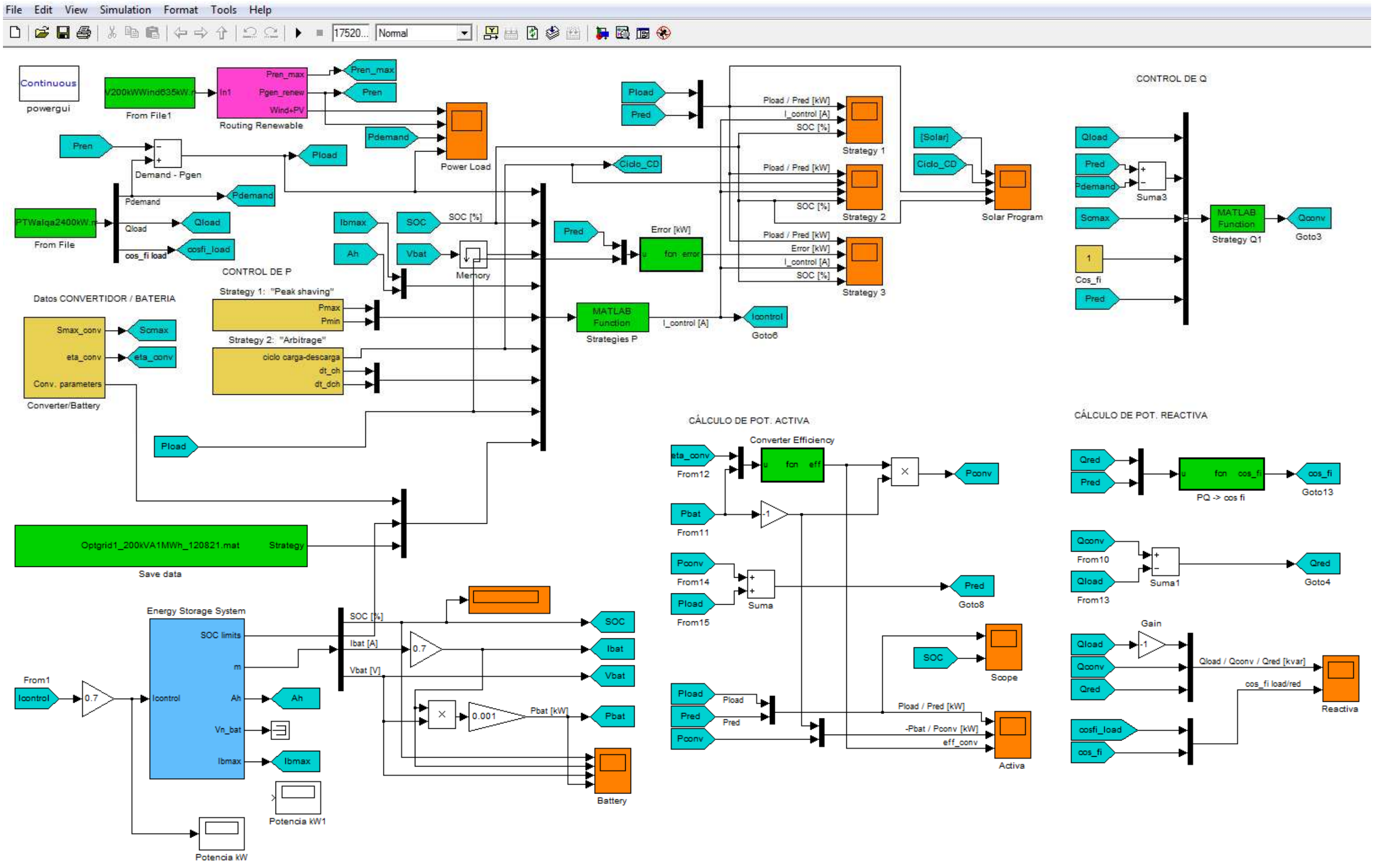

Fig. 1.10. Diagram in Matlab.

1.3 Data inputs

- PV and wind electric production, provided by San Jorge University.
- Walqa Technological Park electric consumption, provided by San Jorge University.
- Energy Storage System (hydrogen) with 65 kW of power and 25% of total efficiency.

The global results of Walqa Technological Park are in the next schedule:

Table 1.6. Energy data

Fecha	Generación eólica (kWh)	Generación fotovoltaica (kWh)	Generación térmica (kWh)	Generación aislada (kWh)	Producción de H_2 (kg)	Consumo eléctrico (kWh)	Consumo térmico (kWh)	Consumo eléctrico P.T. Walqa (kWh)	Huella de CO_2 (kg)	Balance EERR edificio FHA (%)	Aportaciones P.T. Walqa (kWh)
dic-11	61242.0	4618.0	930.0	0.0	4.2	6074.0	1740.0	214957.0	7.469.866	11.902	69.535.928
nov-11	18009.0	14429.0	490.0	0.0	6.2	6209.0	1440.0	222398.0	7.224.924	6.406	43.923.484
oct-11	38933.0	13073.0	830.0	0.0	3.5	6370.0	170.0	231890.0	4.906.276	12.691	62.412.108
sep-11	22786.0	17935.0	0.0	0.0	2.1	7324.0	0.0	258127.0	4.924.354	0.0	54997.26
ago-11	16682.0	22975.0	0.0	0.0	21.5	7350.0	0.0	279126.0	4.242.177	0.0	57945.1
jul-11	22795.0	19890.0	0.0	0.0	6.2	7440.0	0.0	255061.0	5.441.743	0.0	58517.44
jun-11	19922.0	15252.0	0.0	0.0	4.2	8375.0	0.0	231107.0	7.036.759	0.0	47.314.592
may-11	12770.0	15936.0	620.0	0.0	3.1	6755.0	270.0	185128.0	5.862.261	8.826	41.391.056
abr-11	15006.0	6895.0	1360.0	0.0	5.8	5904.0	310.0	196728.0	7.480.467	21.886	27389.42
mar-11	24112.0	7427.0	2150.0	0.0	4.2	6756.0	2960.0	216988.0	7.441.441	22.128	37.450.892
feb-11	50427.0	9277.0	1760.0	0.0	3.7	8435.0	2430.0	216988.0	7.815.261	16.199	67.088.492
ene-11	17188.0	8020.0	830.0	0.0	2.4	7024.0	2720.0	221146.0	6.821.669	8.518	31591.92

1.4 Results

We use different approaches for the strategy of our minigrids, using some of the following ideas:

- Maximum renewable consumption.

The load in our microgrid is always bigger than our renewable production. Then, we consumed all our renewable production.

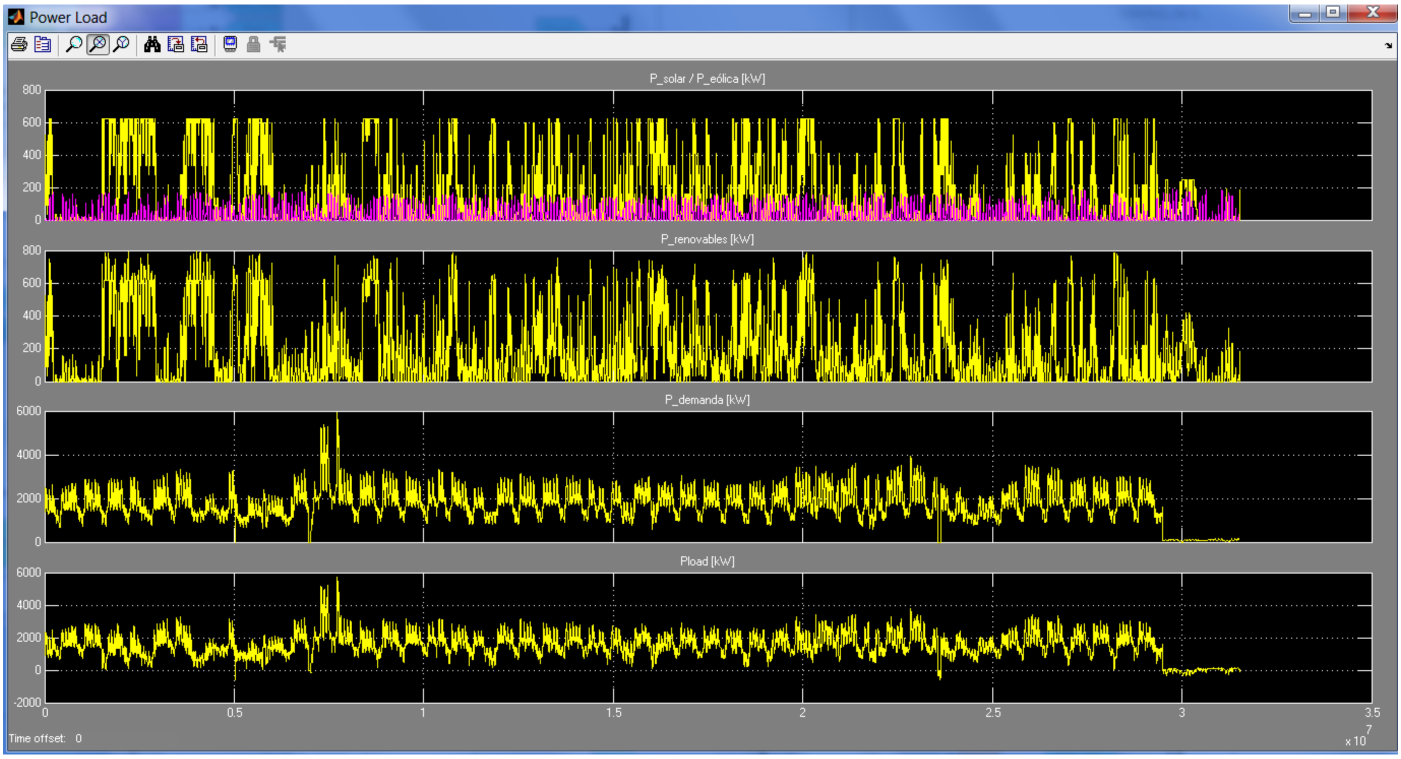

Fig. 1.11. Results.

In this diagram we could see our renewable production (power) of PV solar and wind in the first chart. In the second one, it is shown the total renewable production (PV + wind). In the third one, we could see the total electricity demand of Walqa Technological Park and in the last one appear the load that is not cover by renewable production.

The fact that we consumed directly all the renewable energy we produced in each moment causes that it is not useful to have an Energy Storage System. To profit an energy storage system we should increase renewable generation power.

- Reduction of emissions.

The reduction of emissions is directly proportional to the renewable energy production.

In one year, the PV solar energy production is 244489,521 kWh. Then, using IDAE constant 0,34 kg CO_2 emissions avoided/kWh. We have avoided the emission of ***83126,44 kg CO_2***.

In one year, the wind energy production is 1376415,96 kWh. Then, using IDAE constant 0,34 kg/CO_2 emissions avoided/kWh. We have avoided the emission of ***467981,42 kg CO_2***.

We consumed all the renewable energy in the moment is produced. Then, we purchase the minimum power from the grid.

- Minimum purchase from the grid.

We consumed all the renewable energy in the moment is produced. Then, we purchase the minimum power from the grid.

- Protection against disconnection from the grid (backup).

We don't have capability in this moment to be protected against disconnection from the grid (Back up). To allow that, we need a continuous power from our Energy Storage System of **6000 kW**. Other possibility is to have a first back up system of **4000 kW** output and an additional back up generator system of 2000 kW that only connect in extreme situations.

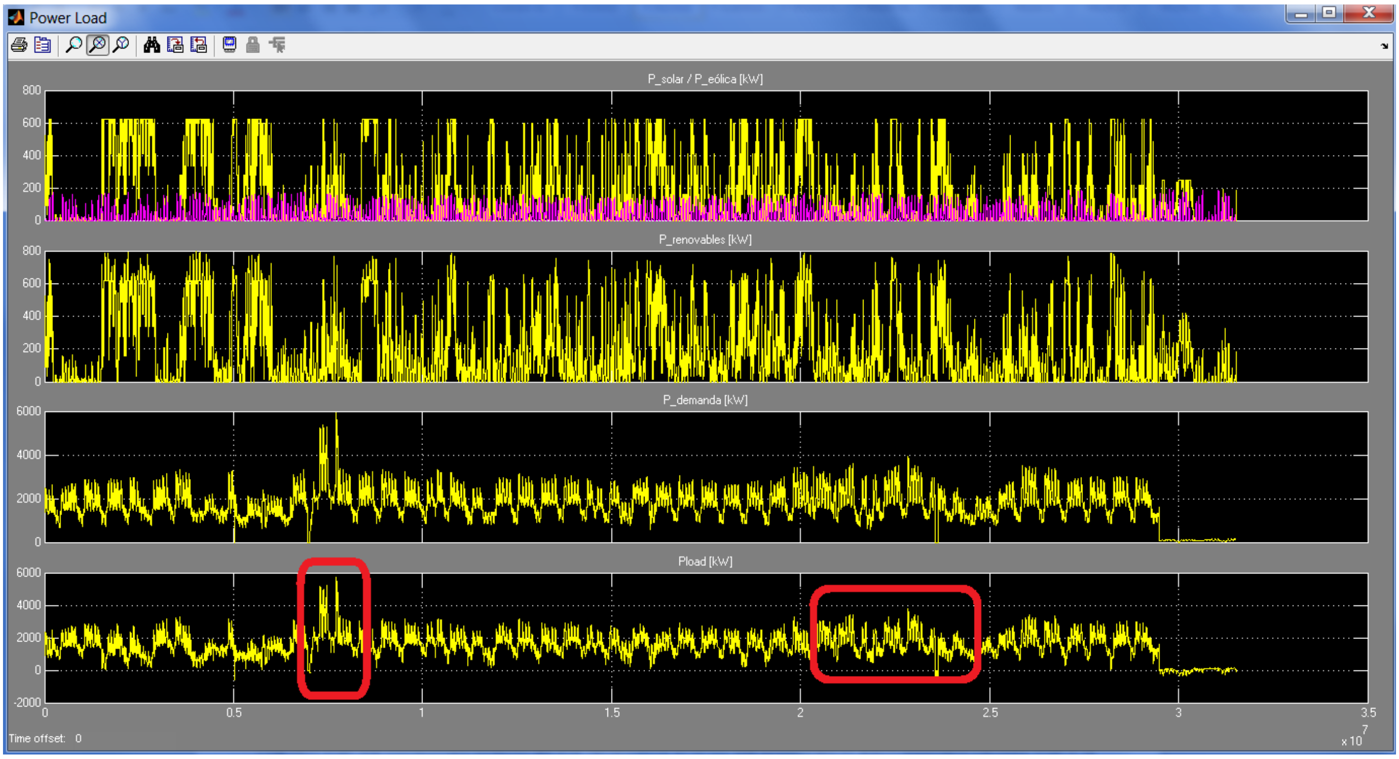

Fig. 1.12. Results.

It's possible depending the system we add in our microgrid, that we choose like primary power our energy storage system and like back up system the grid. It will depend on the cost of the kWh of energy of the system added in comparison with the cost of grid electricity.

If we choose the grid like primary power and we want to be protected against disconnection from the grid during 4 hours, we will need an increased energy storage system with 16000 kWh of capacity and 4000 kW of output power. Using hydrogen, considering 50% of efficiency in the fuel cell system, we will need 32000 kWh or **969,7** kg of H_2. Nowadays, we have 34,5 kg H_2 of storage.

To be able to do net balance with the grid, we need to increase our renewable power. We have to have **1509,2 kW** of generation solar power capacity considerating 1430 equivalent hours of solar and 900 equivalent hours of wind production. Then we will need to install **1309,2 kW** of new PV panels. We do not consider to increase wind power because we don't have enough hours of wind production per year.

- Optimize grid purchases regarding tariff periods.

Increase generation solar power like we propose in the last point, allow us to feed our power electricity consumption with renewable energy in net balance. We do not consider to increase our hydrogen energy storage system because nowadays is not economically viable. Then, we don't use grid purchases regarding tariff periods.

- Price arbitrage (buy low, sell high).

Solar energy production is higher (9h – 18h) in the time that our consumption is higher and the price of electricity is high too.

We have other advantage with the system proposed. Solar energy production is lower in winter like the electricity demand, because heating systems are based on propane. On the other hand, we have a high solar production between May and November. The Walqa Tecnological Park consumption is higher in summer time because of cooling building electricity consumption systems.

1.5 Conclusions

- Walqa Technological Park consumed instantly all its renewable energy production.
- The fact that we consumed directly all the renewable energy we produced in each moment causes that it is not useful to have an Energy Storage System. To profit an energy storage system we should increase renewable generation power.
- In one year, Walqa Technological Park renewable energy production avoided the emission of **551107,86 kg CO_2**.
- To be protected against disconnection from the grid, Walqa Technological Park will need a continuous power from our Energy Storage System of **6000 kW**. Other possibility is to have a first back up system of **4000 kW** output and an additional back up generator system of 2000 kW that only connect in extreme situations.
- To be able to do net balance with the grid, we need to increase our renewable power. We have to have **1509,2 kW** of generation solar power capacity considering 1430 equivalent hours of solar and 900 equivalent hours of wind production. Then we will need to install **1309,2 kW** of new PV panels. We do not consider increasing wind power because we don't have enough hours of wind production per year.
- Solar energy production is higher (9h – 18h) in the time that our consumption is higher and the price of electricity is high too.
- Solar energy production is lower in winter like the electricity demand, because heating systems are based on propane. On the other hand, we have a high solar production between May and November. The Walqa Tecnological Park consumption is higher in summer time because of cooling building electricity consumption systems.

2 AICIA - LABORATORY FACILITIES

2.1 Introduction

The document is divided in three main parts. First of all, a description of mathematical models of principal components of the microgrid of AICIA is done. Also, a model validation with experimental data is performed. In second section, different control strategies of microgrid are defined. Finally, in last section, complete mathematical model of microgrid is simulated considering one of the operation modes described in section 2.3, the experimental plant operates using the same control strategy, and a comparison of model results and experimental data is done.

The microgrid under study is schematized in Fig. 2.1. The proposed system is primarily powered by a photovoltaic array. In order to avoid power interruptions caused by the intermittency of the solar resource, an electrolyzer is placed in the main power distribution line. Then, when there is a power excess, electricity is used to produce and store hydrogen. On the contrary, a fuel cell generates electricity by using the stored hydrogen when it is required. A battery pack is also incorporated in the main power distribution line in order to maintain a fixed voltage on the line and thus simplifying the converters design. Then, the designed system includes five different converters: a DC/AC converter which connects appliances and neighbouring grids, a bidirectional DC/DC converter to provide and obtain power from an electric vehicle and three unidirectional DC/DC converters to adapt the photovoltaic array power, the electrolyzer power and the fuel cell power requirements respectively. Moreover, the aforementioned microgrid is connected to other neighbouring grids to exchange energy with the demand.

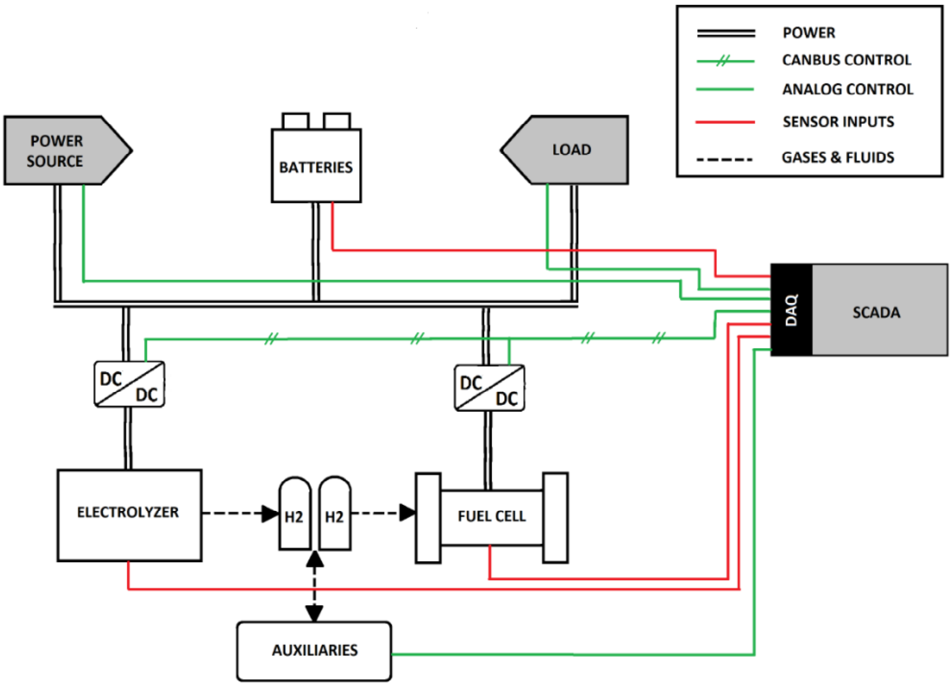

Fig. 2.1. Experimental plant configuration.

The experimental set-up is shown in Fig. 2.1 and is located at AICIA laboratory facilities. The main characteristics of the pilot plant devices are listed in Table 2.1.

Table 2.1. Microgrid equipment

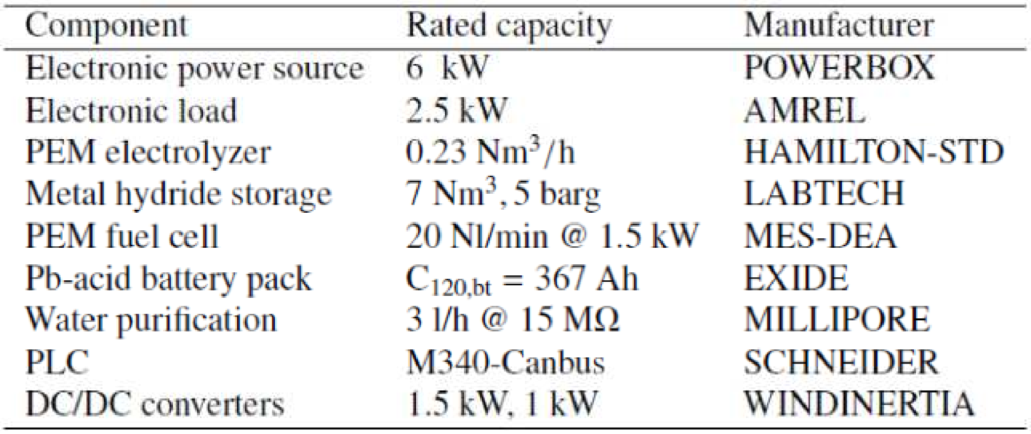

Component	Rated capacity	Manufacturer
Electronic power source	6 kW	POWERBOX
Electronic load	2.5 kW	AMREL
PEM electrolyzer	$0.23\ Nm^3/h$	HAMILTON-STD
Metal hydride storage	$7\ Nm^3$, 5 barg	LABTECH
PEM fuel cell	20 Nl/min @ 1.5 kW	MES-DEA
Pb-acid battery pack	$C_{120,bt} = 367$ Ah	EXIDE
Water purification	3 l/h @ 15 MΩ	MILLIPORE
PLC	M340-Canbus	SCHNEIDER
DC/DC converters	1.5 kW, 1 kW	WINDINERTIA

The photovoltaic array is emulated by a programmable electronic power source which permits to simulate the behavior of the system under different weather conditions. Analogously, another programmable electronic load simulates the domestic power demand. Other possible loads and the interconnection among other grids are also simulated by combining both programmable power source and load. This configuration makes flexible the simulation of different power inputs and outputs.

The hydrogen installation is composed by a 1 kW PEM electrolyzer, a metal hydride storage tank and a PEM fuel cell system. Hydrogen purification systems are not required since the electrolyzer produces high purity hydrogen. The hydrogen is stored on a $LaNi_5$ metal hydrides alloy storage tank with a 7 Nm^3 storage capacity. Since heat is required to release the hydrogen storage content, a cooling/heating system is incorporated to the test bench. Finally, a 1.5 kW PEM fuel cell completes the hydrogen installation. As auxiliary devices the system comprises electrovalves and a safety nitrogen circuit.

All the electronic devices are connected to a 48-V_{DC} bus supported by a 24-monoblock battery pack of advanced lead-acid batteries with a $C_{120,bt} = 367$ Ah capacity. For the sake of simplicity, the performance of the DC/DC converter which connects the photovoltaic array to the main 48-V_{DC} bus is emulated by the programmable power source and the DC/DC and DC/AC converters which connect the electric vehicle, domestic loads and external grids to the bus are mimicked by the programmable power load.

Regarding the microgrid Supervisory Control and Data Acquisition (SCADA) system, a M-340 programmable logic control (PLC) is installed as the main plant control platform. The controller is provided with data acquisition cards in order to communicate with the programmable load and power source, the plant devices and sensors. The communication between the DC/DC converters and the PCL is performed by Canbus communication protocol.

2.2 Microgrid modelling

A practical and accurate dynamic model of the complete domestic microgrid is developed and presented in this section. Avoiding modelling ancillary devices (such as the security–related nitrogen circuit), the proposed interconnected model comprises the following devices: photovoltaic (PV) array, battery pack, electrolyzer, metal hydride storage tank, PEM fuel cell, neighbour grids and electric vehicle. This kind of system represents multi–physic domains whose dominant characteristic times are shown in Table 2.2.

Electrical dynamics, which are various orders of magnitude lower than the dominant dynamics, will thus be neglected.

Table 2.2. Time constant orders of the microgrid equipment dominant dynamics.

Dynamic effect	Characteristic time
PV-field temperature	O(10^3) s
PEM Electrolyser temperature	O(10^2) s
Metal hydride temperature	O(10^3) s
PEM fuel cell temperature	O(10^2) s
Battery time response	O(10^1) s

2.2.1 Photovoltaic array model

The electric circuit models for a PV array consider solar cells as an equivalent electric circuit with radiation and temperature dependent components as seen in Fig. 2.2. The most widely used equivalent circuit is composed of five parameters. For convenience, this formulation is adopted in this model resulting the following relationship:

$$I_{PV} = I_L - I_{diode} \cdot \left(e^{\left(\frac{V_{PV}+I_{PV}\cdot R_S}{a_{PV}}\right)} - 1 \right) - \frac{V_{PV}+I_{PV}\cdot R_S}{R_{SH}} \qquad [1]$$

where I_{PV} is the PV cell current, V_{PV} is the PV cell voltage, I_L is the photocurrent, I_{diode} the diode reverse saturation current, a_{PV} the modified ideality factor, RS the series loss resistance and R_{SH} the shunt loss resistance. The factor a_{PV} can be expressed for one individual cell as:

$$a_{PV} = \frac{n_{diode}\cdot k\cdot T_{PV}}{q} \qquad [2]$$

where n_{diode} is the diode ideality factor, k the Boltzmann constant ($1.3806\cdot10^{-23}$ J/K), T_{PV} the cell temperature (Kelvin) and q the electron charge (C).

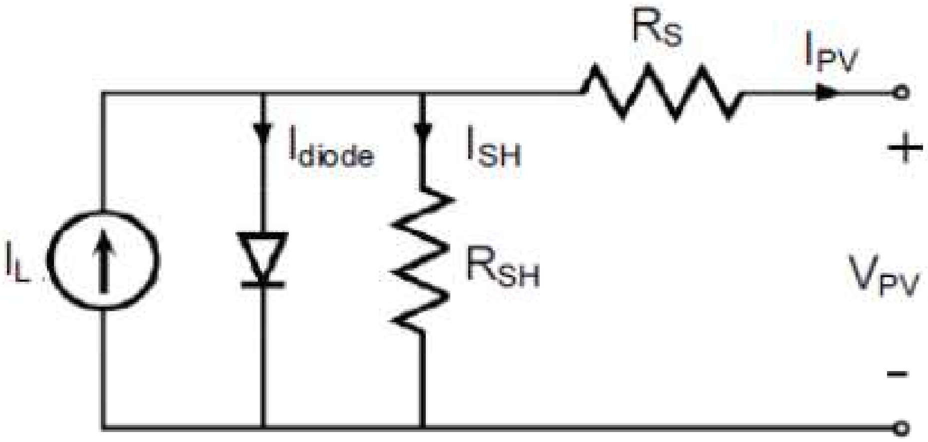

Fig. 2.2. Five-parameter equivalent electrical circuit used to model a PV cell.

Despite the fact that the five PV model parameters (a_{PV}, I_L, I_0, R_S and R_{SH}) are not provided by manufacturers, there are currently different methods to estimate such parameters from those commonly provided in PV datasheets, which are: maximum power voltage, $V_{PV,max}$, maximum power current, $I_{PV,max}$, open–circuit voltage, $V_{PV,0}$, short–circuit current, I_{SC}, short–circuit current temperature coefficient, $\alpha_{I,SC}$, and open–circuit voltage temperature coefficient, $\beta_{VPV,0}$. Again, the simplest methods are based on parameter reduction resulting in poor accuracy while methods that give accurate results imply the solution of highly non-linear system equations. There exist some iterative methods to estimate these parameters from the manufacturer's data using simplifications in the equation solving procedure [1]. Although the description of this method is out of the scope of this document, inputs and outputs of the parameter estimation block are shown in Fig. 2.3 together with the main inputs and outputs of the PV model.

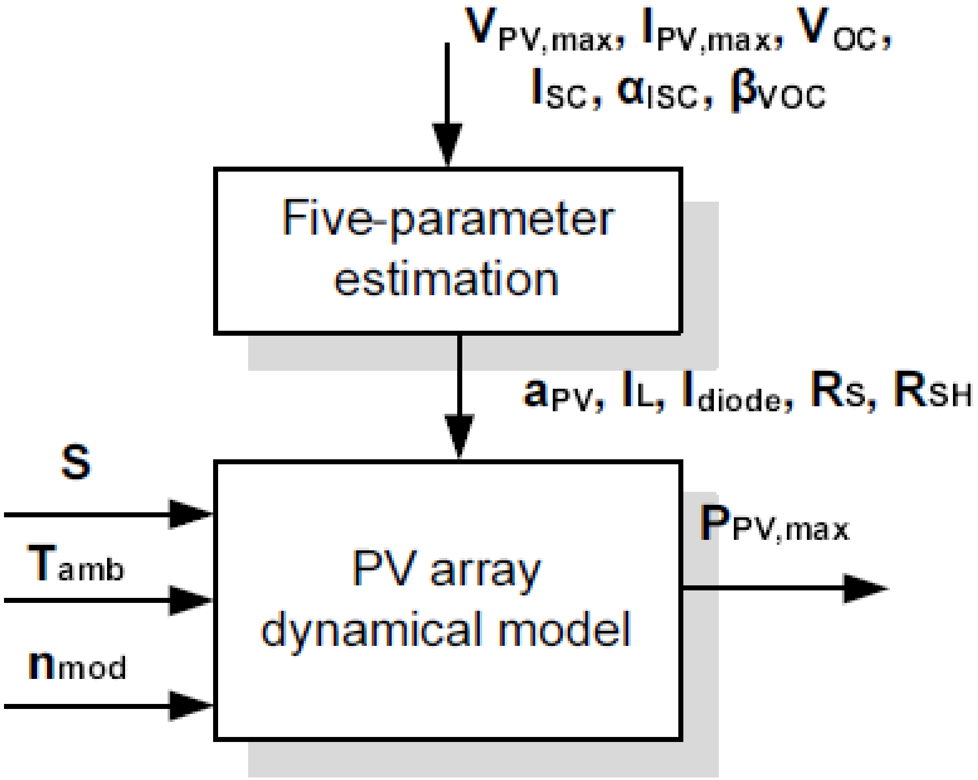

Fig. 2.3. Inputs, outputs and parameters related to the PV array dynamical model.

The PV array herein modelled is composed by 20 ISF-150 modules manufactured by ISOFOTON. The corresponding data provided by the manufacturer is presented in Table 2.3 as well as the calculated five parameters given by the fast convergence method. Fig. 2.4 (a) shows the representative I-V and P-V curves for a single module at a given absorbed radiation and module temperature. The power delivered by the PV array is calculated as:

$$P_{PV} = n_{mod} \cdot I_{PV} \cdot I_{PV} \qquad [3]$$

---

[1] C. Carrero, D. Ramirez, J. Rodríguez, C. Platero, Accurate and fast convergence method for parameter estimation of PV generators based on three main points of the I-V curve, Renewable Energy 36 (2011) 2972-2997.

Table 2.3. ISOFOTON ISF-150 data sheet and equivalent five model parameters.

Datasheet parameter	Value
$V_{PV,max}$	18.5 (V)
$I_{PV,max}$	8.12 (A)
V_{OC}	22.6 (V)
I_{SC}	8.70 (A)
$\alpha_{I_{SC}}$	0.003654 (A/K)
$\beta_{V_{OC}}$	-0.072998 (V/K)
Five model parameters	**Value**
a_{PV}	0.6326
I_L	8.7324
I_{diode}	$2.5642 \cdot 10^{-15}$
R_S	0.2458
R_{SH}	65.9544

As can be seen in Fig. 2.4 (a), there is a power maximum value for the PV module, $P_{PV,max}$. Power electronic devices are designed to run PV systems around this value, $P_{PV,max}$. Fig. 2.4 (b) and (c) depict the effect of different absorbed radiation and ambient temperature on the module I-V curve.

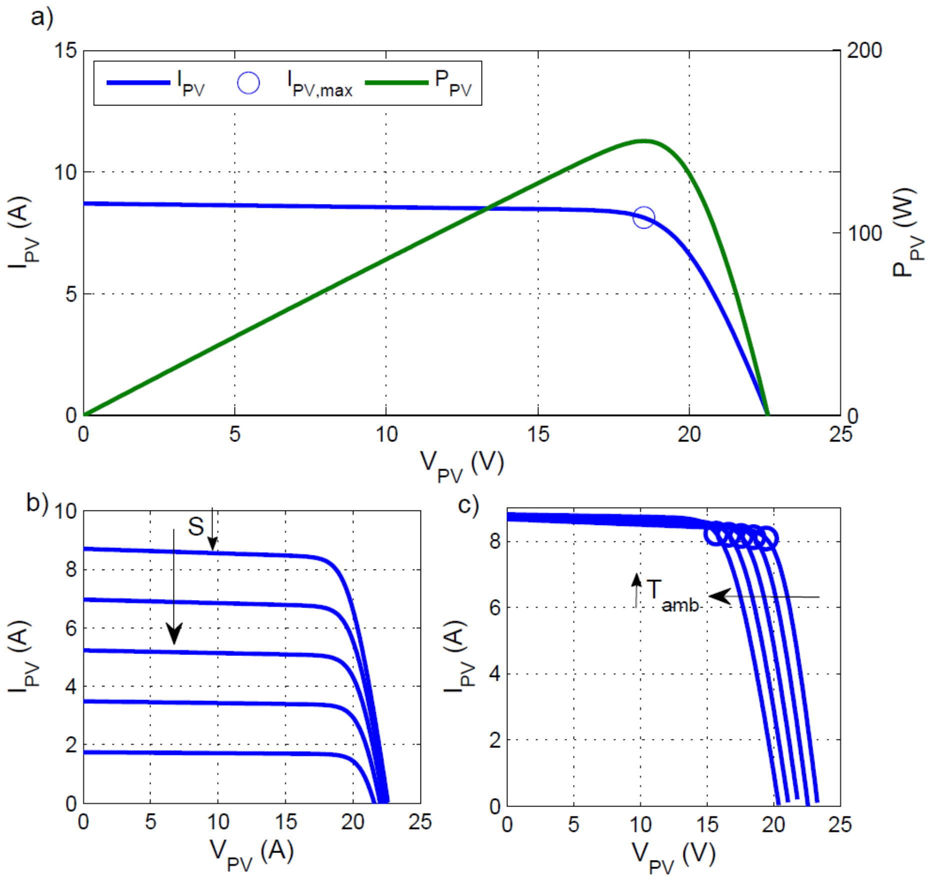

Fig. 2.4. (a) I-V and P-V curves for the ISOFOTON ISF-150 module. (b) radiation effects on the I-V curve and (c) ambient temperature effect on the I-V curve.

2.2.2 Electrolyzer model

An electrolyzer uses the electrolysis principle to split water into hydrogen and oxygen applying a high current through two electrodes separated by an electrolyte. In the pilot plant, the electrolyte is a proton exchange membrane.

The electrolyzer modelled is operated in current mode. This means that a current is applied to the stack and then a differential of potential, V_{ez}, is reached according to the next expression:

$$V_{ez} = V_{ez,0} + V_{etd} + V_{ez,ohm} + V_{ion} \qquad [4]$$

where $V_{ez,0}$ is the reversible potential, V_{etd} is the electrodes overpotential, $V_{ez,ohm}$ is the ohmic overvoltage and V_{ion} is the ionic overpotential. Hence, the voltage drop is a sum of four terms that can be drawn through the following expressions:

$$V_{ez,0} = 1.23 - 0.3 \cdot 10^{-3}(T_{ez} - 298) + 2.3\frac{R \cdot T_{ez}}{4\,F}\,ln\left(p_{H2,oz}^{2} \cdot p_{O2,oz}\right) \qquad [5]$$

$$V_{etd} = \frac{R \cdot T_{ez}}{F}\,sinh^{-1}\left(\frac{1}{2}\,\frac{i_{ez}}{i_{ao}}\right) + \left(\frac{\delta_B}{\sigma_B} i_{ez}\right) + R_I \cdot i_{ez} \qquad [6]$$

$$\sigma_B = (0.005139\lambda - 0.00326)e^{128\left(\frac{1}{303} - \frac{1}{T_{ez}}\right)} \qquad [7]$$

where T_{ez} is the electrolyzer stack temperature, R is the ideal gas constant, F is the Faraday's constant, $p_{H2,ez}$ is the hydrogen partial pressure, $p_{O2,ez}$ is the oxygen partial pressure, i_{ez} is the electrolyzer current density, i_{ao} is the anode current density, i_{co} is the cathode current density, δ_B and σ_B are the thickness and conductivity of Nafion® 117 electrolyte and λ is the membrane water content. The last two terms of Equation [4] can be grouped as:

$$V_{ez,ohm} + V_{ion} = \frac{\delta_B \cdot I_{ez}}{A_{ez} \cdot \sigma_B} \qquad [8]$$

where A_{ez} is the electrolyzer effective area. Equation [6]-[8] are related to the electrolyzer polarization curve. The real coefficients presented in these equations were obtained from technical brochure and by fitting experimental data from the electrolyzer SPE HAMILTON-STD. Parameters are summarized in Table 2.4. Fig. 2.5 shows a comparison between the voltage measured in the plant and the simulated voltage varying the current.

Table 2.4. Model parameters for the PEM electrolyzer.

Param.	Comments	Value
A_{ez}	Stack area	212.5 cm^2
$p_{H_2,ez}$	Partial pressure	6.9 bar
$p_{O_2,ez}$	Partial pressure	1.3 bar
i_{ao}	Anode current density	1.0631^{-6} A/cm^2
i_{co}	Cathode current density	1^{-3} A/cm^2
δ_B	Membrane thickness	178 μm
σ_B	Membrane conductivity	0.14 S/cm
λ	Membrane water content	21 $molH_2/molSO_3$
$C_{ez,t}$	Thermal capacity	402400 J/K

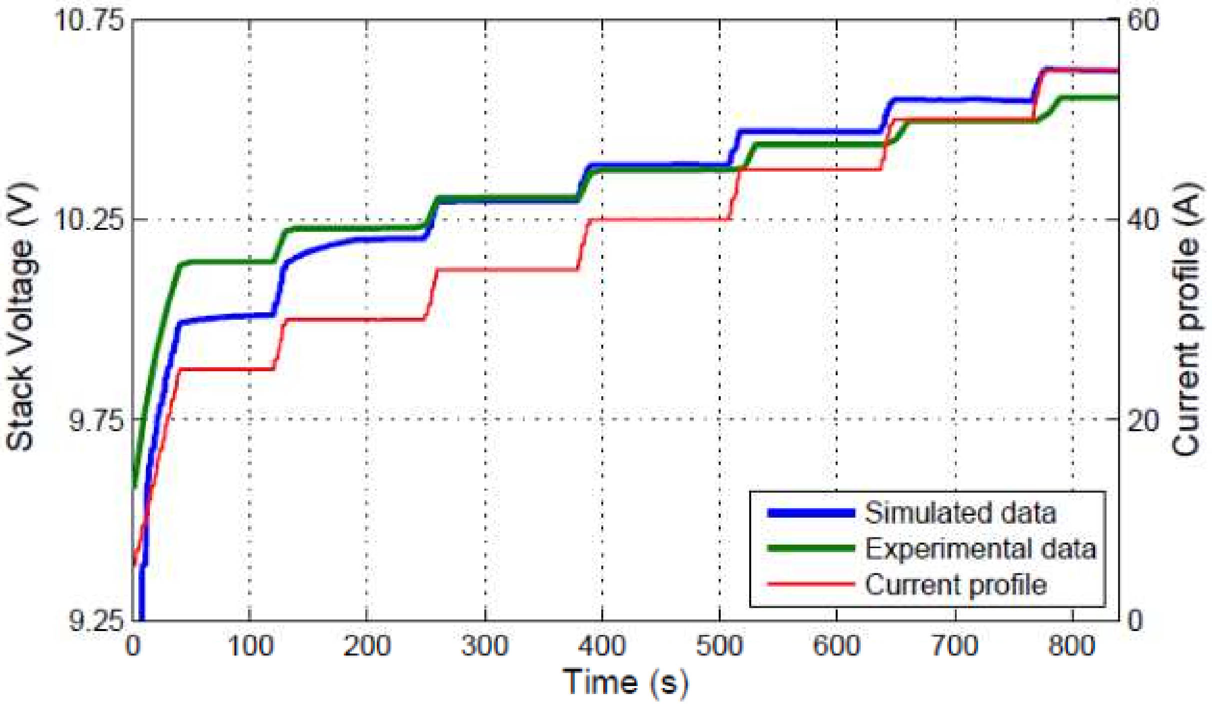

Fig. 2.5. Comparison of the model and experimental electrolyzer voltage for different currents.

The hydrogen flow rate produced by the electrolyzer, $m_{H2,ez}$, can be directly obtained from the electrolyzer current as:

$$\dot{m}_{H2,ez} = n_{ez}\frac{I_{ez}}{F} \qquad [9]$$

where I_{ez} is the stack current, n_{ez} is the number of electrolyzer cells and F is the Faraday constant. The validation of this equation with experimental data is presented in Fig. 2.6. A lumped capacitance thermal dynamic model is used to predict the electrolyzer temperature. Next equations can be obtained from the overall energy balance:

$$C_{ez,t}\frac{dT_{ez}}{dt} = \dot{Q}_{gen} - \dot{Q}_{loss} - \dot{Q}_{cool} \qquad [9]$$

where $C_{ez,t}$ is the overall thermal capacity of the electrolyzer, Q_{gen} is the heat produced by the stack, Q_{loss} is the heat delivered to the environment and Q_{cool} is the heat removed by the cooling system. The heat generated in the stack is due to the thermodynamic irreversibility in the electrolysis process and can be approximated by:

$$\dot{Q}_{gen} = \dot{W}_T(1 - V_{tm}) \qquad [10]$$

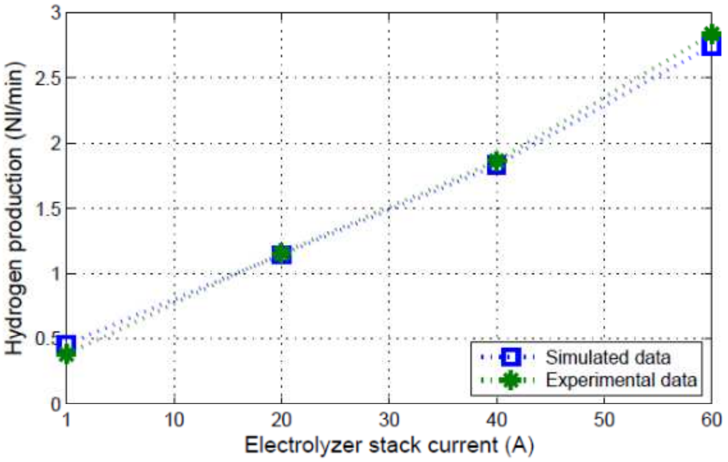

Fig. 2.6. Measured and simulated hydrogen produced in electrolyzer.

The heat generated depends on the electrolyzer power consumption, W_T, and on the so-called thermoneutral potential, V_{tn}, which is a point when the electrolysis reaction becomes an exothermic reaction. The following expressions are used to calculate the thermoneutral potential:

$$V_{tm} = V_{hv} + \frac{1.5}{2\,F}\frac{p_{sat}}{p_{ez}-p_{sat}}\left(4.29\cdot 10^4 + 40.76\,(T_{ez}-273) - 0.066\,(T_{ez}-273)^2\right) \qquad [11]$$

$$V_{hv} = 1.4756 + 2.252\cdot 10^{-4}\,(T_{ez}-273) - 1.52\cdot 10^{-8}\,(T_{ez}-273)^2 \qquad [12]$$

$$p_{sat} = e^{13.669-\frac{8096.23}{T_{ez}}} \qquad [13]$$

where V_{hv} is the higher-high-value voltage, p_{sat} is the vapor partial pressure, p_{ez} is the electrolyzer pressure and T_{ez} is the electrolyzer temperature. The wasted heat is a sum of the effects of radiation and convection losses. Heat losses can be expressed as:

$$\dot{Q}_{loss} = UA_{ez,t}(T_{ez} - T_{amb}) \qquad [14]$$

where $UA_{ez,t}$ is the overall heat transfer coefficient. Regarding the cooling heat, the hypothesis of an ideal cooling system coupled with the electrolyzer is adopted herein. Thus, the system is able to remove any excess of heat avoiding overheating.

Fig. 2.7 shows the thermal dynamic validation for a current profile.

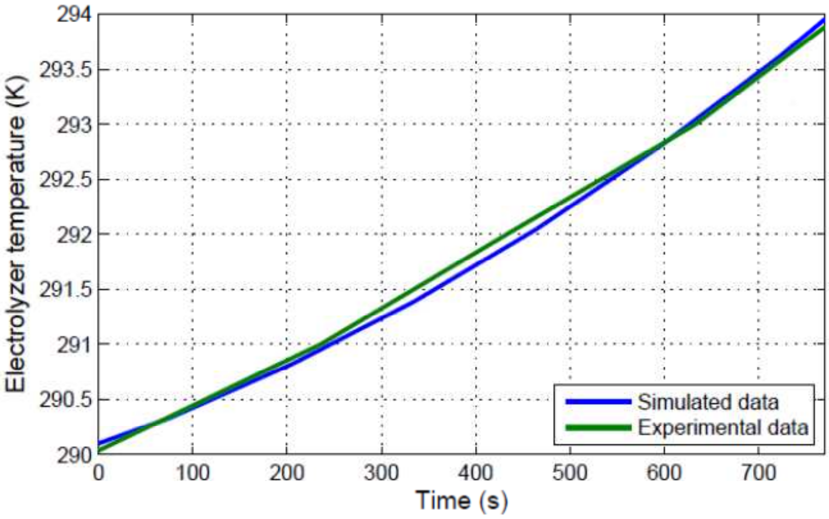

Fig. 2.7. Simulated and measured electrolyzer stack temperature.

2.2.3 Fuel cell model

For PEM fuel cell model, simplified one dimensional time dependent models are more suitable for control purposes and long term simulations. Such simplified dynamic models are mainly composed of three modules: electrochemical static relations (since these dynamics can be neglected), fluid dynamics and thermal dynamics.

With respect to the electrochemical static model, the voltage supplied by a fuel cell is evaluated by curves that present the cell voltages, V_{fc}, versus the current density:

$$V_{fc} = V_{fc,0} - V_{act} - V_{fc,ohm} - V_{conc} \qquad [15]$$

$$V_{fc,0} = 1.046 + 0.003\,(T_{st} - T_{st}^{0}) + 0.244\left(\frac{1}{2}ln\left(p_{O2,fc}\right) + ln\left(p_{H2,fc}\right)\right) \qquad [16]$$

$$V_{act} = 0.066\left(1 - e^{\frac{-i_{st}}{0.013}}\right) \qquad [17]$$

$$V_{fc,ohm} = 0.299\, i_{fc} \qquad [18]$$

$$V_{conc} = 0.028\, i_{fc}^{(1+8.001)} \qquad [19]$$

where $i_{fc}=I_{fc}/A_{fc}$ denotes the current density, A_{fc} = 61 cm^2 being the effective membrane area of each cell which composed the stack modelled in this paper and T_{st}^{0} = 296 K being the nominal operating temperature. Fig. 2.8 shows the polarization (I-V) curve corresponding to the PEMFC as well as the dependence of this curve with the oxygen pressure inside the stack and with the stack temperature. As mentioned in [2] hydrogen pressure can be assumed constant.

---

[2] A.J. del Real, A. Arce, C. Bordons, Development and experimental validation of a PEM fuel cell dynamic model, J. Power Sources 173/1 (2007) 310-324.

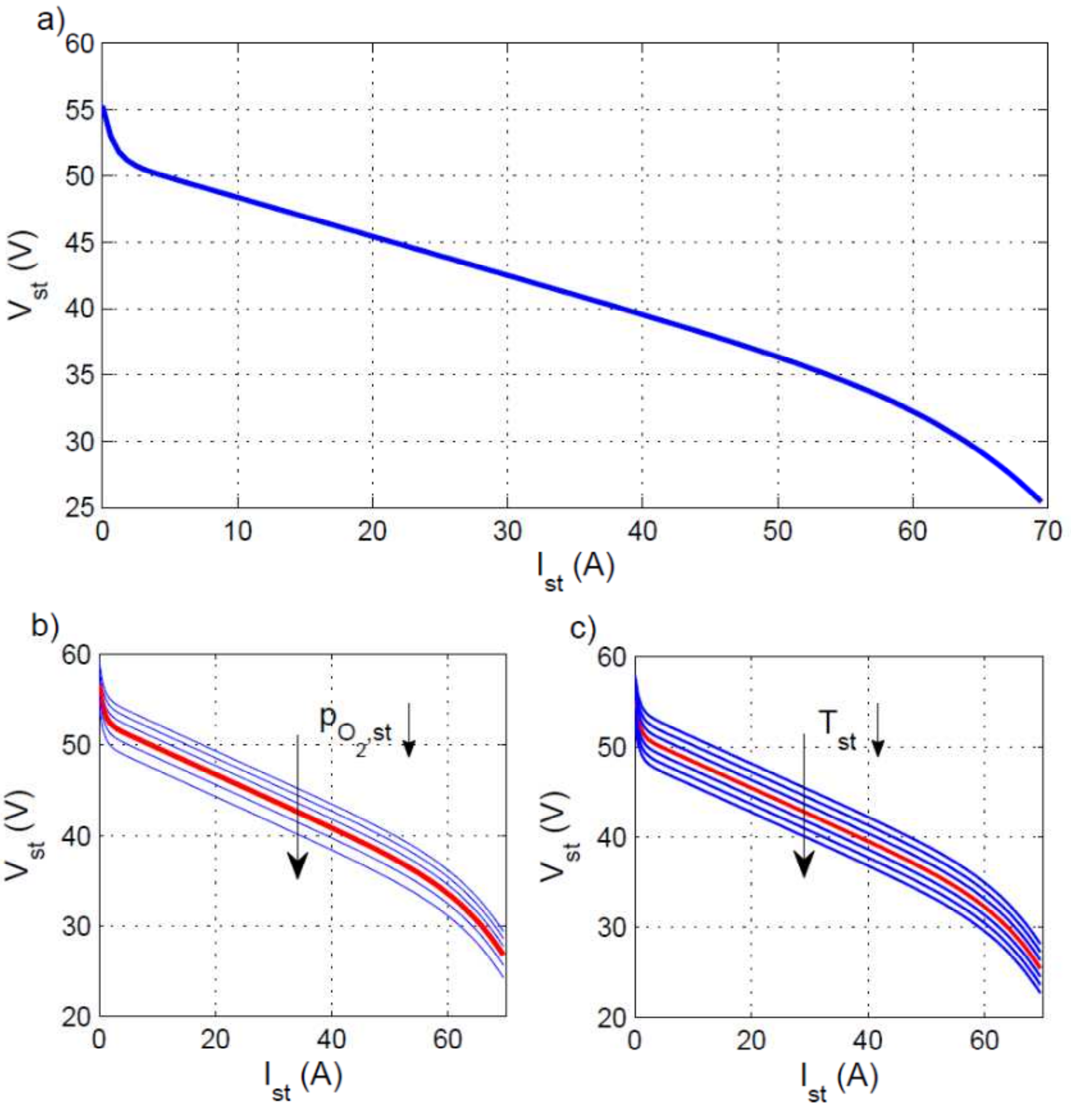

Fig. 2.8. (a) PEMFC polarization curve; (b) Oxygen pressure effects on the polarization curve; (c) stack temperature effects on the polarization curve.

The thermal dynamics are formulated through an energy balance accounting for the energy produced by the water formation reaction, $\dot{H}_{reac}$, the energy supplied in the form of electricity, P_{elec}, the amount of heat evacuated by radiation, $\dot{Q}_{rad}$, and both natural and forced convection, $\dot{Q}_{conv}$:

$$m_{st}\, C_{st} \frac{dT_{st}}{dt} = \dot{H}_{reac} - P_{elec} - \dot{Q}_{rad} - \dot{Q}_{conv} \qquad [20]$$

where m_{st} is the fuel cell stack mass and C_{st} is the average heat capacity of the system. The enthalpy flow rate, H_{reac}, is calculated as:

$$\dot{H}_{reac} = \dot{m}_{H2}\, \Delta h_{H2} + \dot{m}_{O2}\, \Delta h_{O2} - \dot{m}_{H2O}\, \Delta h_{H2O} \qquad [21]$$

$$\Delta h_{H2} = Cp_{H2}(T_{st} - T^{0}) \qquad [22]$$

$$\Delta h_{O2} = Cp_{O2}(T_{st} - T^{0}) \qquad [23]$$

$$\Delta h_{H2O} = h_{f,H2O}^{0} + Cp_{H2O}(T_{st} - T^{0}) \qquad [24]$$

where $h_{f,H2O}^{0}$ is the mass specific enthalpy of vapour formation and Cp_{H2} , Cp_{O2} and Cp_{H2O} are the specific heats of hydrogen, oxygen and vapour respectively, T^{0} is the reference temperature for the enthalpy. The hydrogen consumption can be calculated from the next stoichiometric balance:

$$I_{st} = I_{fc} \qquad [25]$$

$$\dot{m}_{H2,fc,cons} = \frac{I_{st}}{2\,F\,A_{fc}} \qquad [26]$$

Energy yielded in the form of electricity is:

$$V_{st} = n_{st}\,V_{fc} \qquad [27]$$

$$P_{st} = V_{st}\,I_{st} \qquad [28]$$

being P_{st} the stack power, V_{st} the stack voltage and Ist the stack current.

Radiation heat exchanged is modelled as shown below, where ε_{st} is the emissivity, σ is the Stefan-Boltmann constant and Arad is the radiation exchange area:

$$\dot{Q}_{rad} = \varepsilon_{st}\,A_{st}\,\sigma\left(T_{st}^{4} - T_{amb}^{4}\right) \qquad [29]$$

The convective term is composed by two others, one of them corresponding to the natural convection heat, Q_{nat}, and the other, to the forced convection heat, Q_{forc}. In each case, the convective heat transfer coefficients (h_{nat} and h_{forc}) are different, just as the exchange areas A_{nat} and A_{forc} are, since natural convection takes place in the fuel cell lateral walls and forced convection occurs across the internal cell walls due to the installed fan.

$$\dot{Q}_{conv} = \dot{Q}_{nat} + \dot{Q}_{forc} = h_{nat}\,A_{nat}(T_{st} - T_{amb}) + h_{forc}\,A_{forc}(T_{st} - T_{amb}) \qquad [30]$$

Finally, Table 2.5 includes the parameter values for the PEMFC under study:

Table 2.5. PEMFC model parameters.

Parameter	Value	Dimension
m_{st}	5	kg
C_{st}	1100	$\mathrm{Jkg^{-1}K^{-1}}$
ε_{st}	0.9	–
A_{rad}	0.1410	$\mathrm{m^{2}}$
A_{nat}	0.0720	$\mathrm{m^{2}}$
A_{forc}	1.2696	$\mathrm{m^{2}}$
h_{nat}	14	$\mathrm{WK^{-1}m^{-2}}$
h_{forc}	19.65	$\mathrm{WK^{-1}m^{-2}}$

2.2.4 Metal hydrure tank model

Metal Hydride (MH) tanks are a very suitable solution for hydrogen storage in stationary power plants achieving high energy storage densities. A simplified model of a $LaNi_5$ alloy of 7 Nm^3 capacity is used to analyze the cyclic processes for absorption-desorption. The metal hydrides hydrogen absorption, also referred to as refueling process, is governed by an exothermic reaction. The heat released causes an increase of the bed temperature and a reduction of the absorption rate. The inverse process, desorption process, needs a heating fluid to maintain the reaction.

The MH bed has been modelled as a zero-dimensional system to allow a realistic but simplified description of the complex reactions inside this alloy. The model includes two separate blocks for absorption and desorption processes. Thus, the equations must be separately tailored for each process. The mass balance for the refueling process is:

$$\dot{m}_{H2,in} = \varepsilon_{MH}\, f\, v_{bed}\,\frac{d\rho}{dt} + (1-\varepsilon_{MH}) f\, \rho_s\, v_{bed}\,\frac{dq_{H2,a}}{dt} \qquad [31]$$

where ε_{MH} is the porosity of MH powder, f is the volume ratio of the heat transfer equipment volume to the total bed volume, v_{bed} is the bed volume, ρ is the hydrogen gas density, ρ_s is the MH density and $q_{H2,a}$ is the absorbed hydrogen weight fraction. In our system, the hydrogen absorbed in the MH is equal to the hydrogen produced by the electrolyzer. The refuelling process produces heat removed by a cooling fluid. This heat can be calculated through the next energy balance:

$$\left(\rho\, Cv_g + \frac{1-\varepsilon_{MH}}{\varepsilon_{MH}}\; q_{H2,a}\, \rho_s\, Cp_s + \frac{1-\varepsilon_{MH}}{\varepsilon_{MH}}\;\rho_s\, Cp_s\right)\frac{dT_{MH}}{dt} = -\frac{1-\varepsilon_{MH}}{\varepsilon_{MH}}\rho_s \Delta H_a\,\frac{dq_{H2,a}}{dt} - U_a\,\frac{A_{cs}}{\varepsilon_{MH}\, f\, v_{bed}}(T_{MH}-T_c) + \frac{p_{MH}}{\rho}\,\frac{\dot{m}_{H2,in}}{\varepsilon_{MH}\, f\, v_{bed}} \qquad [32]$$

where C_{vg} is the specific heat of H_2 gas at constant volume, Cp_s is the MH specific heat at constant volume, U_a is the overall heat transfer coefficient for absorption, A_{cs} is the heat transfer area, T_{MH} is the MH temperature, T_c is the cooling water temperature and $m_{H2,in}$ is the hydrogen supply mass flow rate.

The hydrogen desorbed in the process is calculated from the mass conservation balance. For our system the hydrogen desorbed is equal to the the hydrogen injected to the fuel cell:

$$\dot{m}_{H2,out} = -\varepsilon_{MH}\, f\, v_{bed}\,\frac{d\rho}{dt} - (1-\varepsilon_{MH}) f\, \rho_s\, v_{bed}\,\frac{dq_{H2,d}}{dt} \qquad [33]$$

being $q_{H2,d}$ the desorbed hydrogen weight fraction. The hydride cools down during the desorption process. Thus, the system is heated in order to maintain the appropriate conditions for the desorption process. The energy balance for the desorption case can be evaluated as:

$$\left(\rho\, Cv_g + \frac{1-\varepsilon_{MH}}{\varepsilon_{MH}}\; q_{H2,d}\, \rho_s\, Cp_s + \frac{1-\varepsilon_{MH}}{\varepsilon_{MH}}\;\rho_s\, Cp_s\right)\frac{dT_{MH}}{dt} = -\frac{1-\varepsilon_{MH}}{\varepsilon_{MH}}\rho_s \Delta H_d\,\frac{dq_{H2,d}}{dt} - U_d\,\frac{A_{cs}}{\varepsilon_{MH}\, f\, v_{bed}}(T_{MH}-T_h) + \frac{p_{MH}}{\rho}\,\frac{\dot{m}_{H2,out}}{\varepsilon_{MH}\, f\, v_{bed}} \qquad [34]$$

where U_d is the overall heat transfer coefficient for desorption, T_h is the water heating temperature and $m_{H2,out}$ is the hydrogen output flow rate.

The hydrogen content in the MH alloy at equilibrium conditions can be drawn from the equilibrium pressure on a Pressure-Composition-Temperature (PCT) curve (or Pressure-Composition-Isotherm (PCI) curve). Note that the equilibrium pressure is highly dependent on temperature as given by the Van't Hoff law. Absorption reaction kinetics for $LaNi_5$-H_2 hydrides are accepted to be described by the next expression:

$$\frac{dq_{H2,a}}{dt} = C_a e^{\left(\frac{-E_a}{R\,T_{MH}}\right)}\, ln\left(\frac{p_{MH}-p^{*}_{MH}}{p_{MH}}\right)\left(q_{H2,a,max} - q_{H2,a}\right) \qquad [35]$$

Analogously, the desorption case results in:

$$\frac{dq_{H2,d}}{dt} = C_a e^{\left(\frac{-E_a}{R\,T_{MH}}\right)} ln\left(\frac{p_{MH}-p^*_{MH}}{p_{MH}}\right)\left(q_{H2,d,max} - q_{H2,d}\right) \qquad [36]$$

where p_{MH} is the pressure in the metal hydride bed, p^*_{MH} represents the equilibrium pressure, C_a is the Arrhenius rate constant and E_a is the activation energy. Table 2.6 shows the parameters for the metal hydride tank.

Table 2.6. Metal hydride tank model parameters.

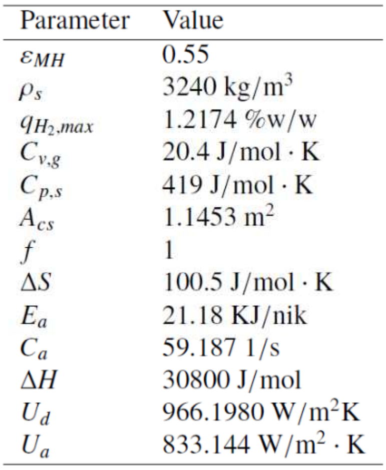

Parameter	Value
ε_{MH}	0.55
ρ_s	3240 kg/m^3
$q_{H_2,max}$	1.2174 %w/w
$C_{v,g}$	20.4 J/mol · K
$C_{p,s}$	419 J/mol · K
A_{cs}	1.1453 m^2
f	1
ΔS	100.5 J/mol · K
E_a	21.18 KJ/nik
C_a	59.187 1/s
ΔH	30800 J/mol
U_d	966.1980 W/m^2K
U_a	833.144 $W/m^2 \cdot K$

Experimental and simulation results are compared for the absorption and desorption processes. Specifically, Fig. 2.9 (a) illustrates the storage system response for the absorption mode with a constant pressure. The hydrogen content on the metal hydride tank rises very fast at the beginning of the process which results in a rapid temperature increment and a reduction of the hydrogen absorption rate as seen in Fig. 2.9 (b).

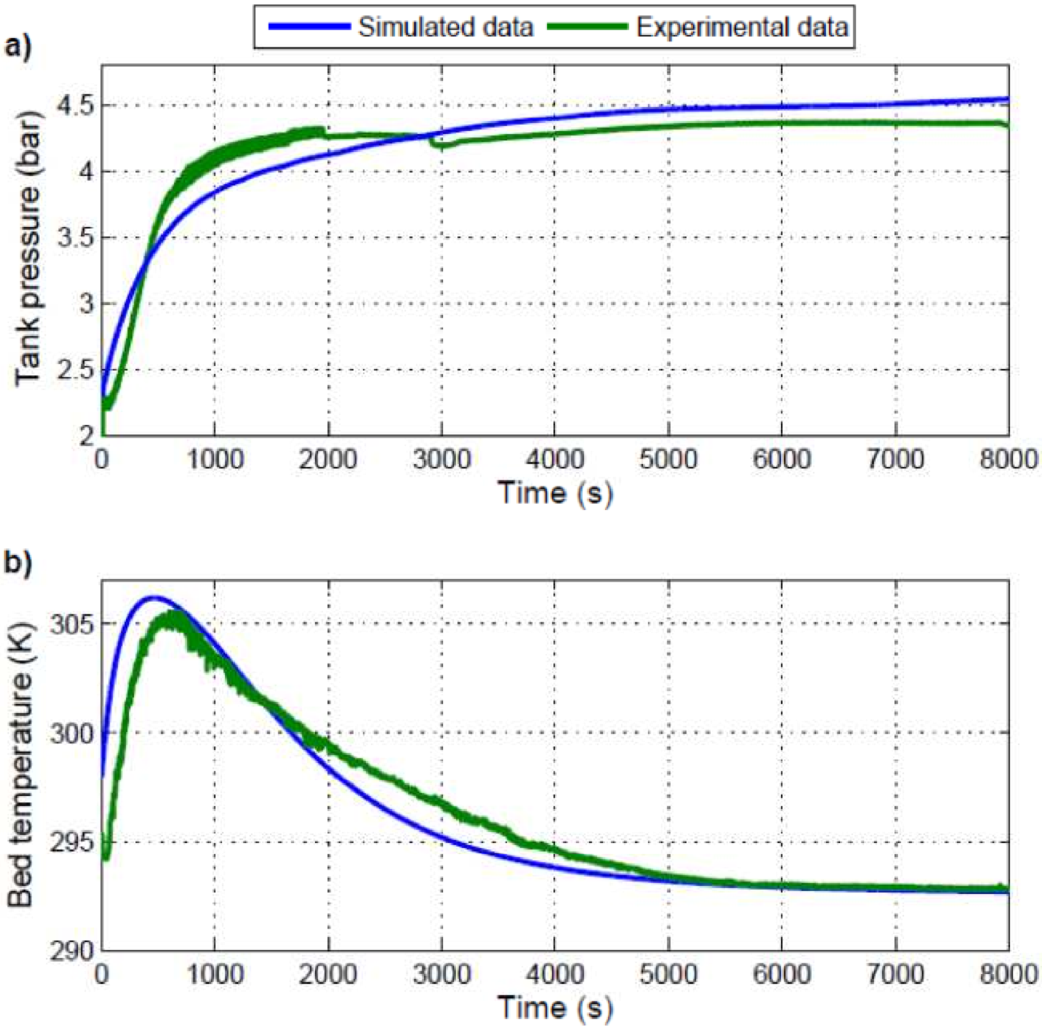

Fig. 2.9. (a) Comparison between model simulation and experimental absorption process at constant pressure (4.5 barg). (b) Model bed temperature and experimental during charging process.

On the other hand, the desorption model is validated by performing a constant hydrogen demand from the fuel cell. The auxiliary heating system heats the hydride with hot water (40-70 ºC) in order to enhance the desorption process. The strong dependence on hot water inlet temperature should be highlighted here. The effect of increasing the fluid temperature and desorption flow rate is represented in Fig. 2.10 (a), while the thermal dynamic validation for such a desorption case is shown in Fig. 2.10 (b).

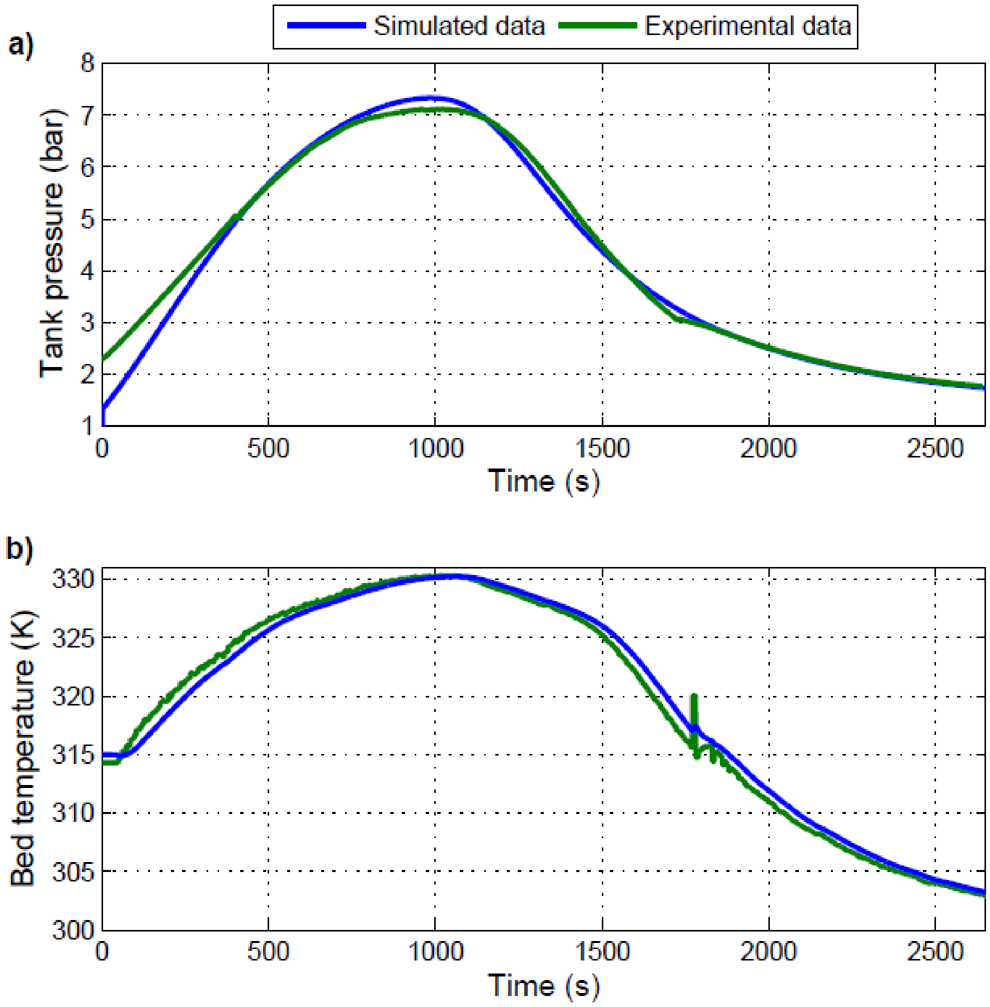

Fig. 2.10. (a) Comparison between model simulation and experimental desorption process at constant pressure demand (4.5 barg). (b) Model bed temperature and experimental measure during discharging process.

2.2.5 Battery bank model

The model for battery bank uses an internal resistance, R_i, and a controlled voltage source to undertake the battery exponential behaviour. The battery voltage is expressed as:

$$V_{bt} = V_{bt,int} + R_i\, I_{bt} \qquad [37]$$

being V_{bt} the battery voltage, $V_{bt,int}$ the battery internal voltage and I_{bt} is the battery current. The internal voltage for the battery charging process is:

$$V_{bt,int} = V_{bt,0} + K_{bt}\,\frac{C_{120,bt}}{C_{120,bt}-C_{out,t}}\left(I_{bt}^{*} - C_{out,t}\right) + A_{bt}e^{B_{bt}\,C_{out,t}} \qquad [38]$$

$$C_{out,t} = \int_0^t I_{bt}\,dt \qquad [39]$$

Analogously, for the discharging process the internal voltage is:

$$V_{bt,int} = V_{bt,0} - K_{bt} \frac{C_{120,bt}}{C_{out,t}+0.1\, C_{120,bt}} I^{*}_{bt} - K_{bt} \frac{C_{120,bt}}{C_{120,bt}-C_{out,t}} C_{out,t} + A_{bt} e^{B_{bt}\, C_{out,t}} \qquad [40]$$

where $V_{bt,0}$ is a constant voltage, I^*_{bt} is the battery current filtered by a first-order filter, A_{bt} is the exponential zone amplitude, B_{bt} represents the exponential zone inverse time constant, K_{bt} is the polarization constant, $C_{out,t}$ is the extracted capacity and $C_{120,bt}$ is the maximum battery capacity. The model parameters are obtained through the experimental test shown in Fig. 2.11 and listed in Table 2.7. The battery response time is estimated to be 31 seconds.

Table 2.7. Battery model parameters.

Parameter	Value
$C_{120,bt}$	367 Ah
$V_{bt,0}$	51.58 V
K_{bt}	0.006215 V
A_{bt}	11.053 V
B_{bt}	2.452 Ah^{-1}

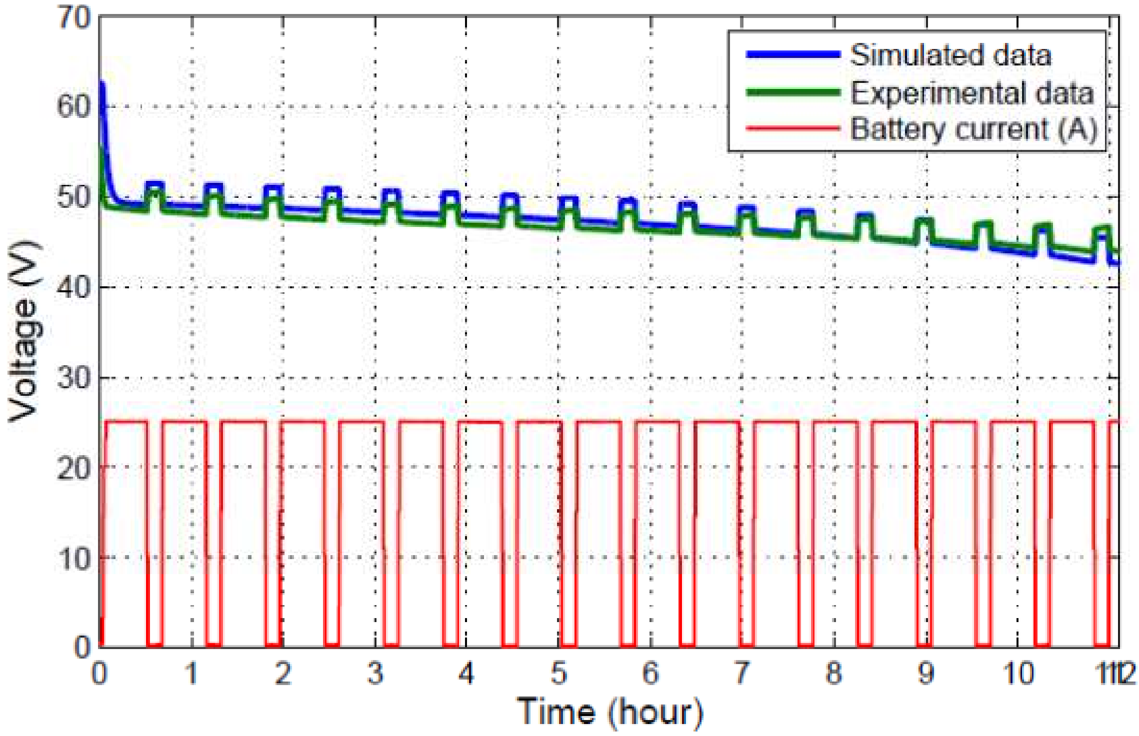

Fig. 2.11. Comparison between battery experimental voltage and battery model voltage during a discharging test.

2.3 Microgrid control strategies

This section aims to define and describe the different operation modes of a microgrid existing in the state of art. These operation modes are considered to be simulated and tested in the experimental facility. Five operation modes are defined:

- Mode 1. Satisfaction of electricity demand.
- Mode 2. Maximization of hydrogen production.
- Mode 3. Constant operation of electrolyzer and fuel cell.
- Mode 4. Extension of battery bank life.
- Mode 5. Maximization of economic benefits.

2.3.1 Satisfaction of electricity demand

This mode aims to minimize the loss of energy from renewable sources, when demand and generation differ. The objective of this mode is satisfying in each moment the electricity demand.

In this way, the control relax all restrictions on the equipment concerning an efficiency operation, economic or otherwise, and always prioritize the demand satisfaction, thus leading to the plant in order to minimize energy profiles generated and defendant.

It is a characteristic mode of isolated systems: hospitals, telecommunication facilities and military applications.

2.3.2 Maximization of hydrogen production

The control system optimizes the operation of the electrolyzer, managing the energy supplied in order to maximize hydrogen production, hurting overall system efficiency and individual equipment focusing in increasing the hydrogen production.

It is based on modifying the profile of energy that is supplied to the electrolyser aided by secondary system management storage batteries and associated power converter electrolyzer.

This mode of operation seeks to maximize hydrogen reserves. This operation mode is more appropriated for energy storage facilities which also need to supply vehicles powered by hydrogen or hydrogen for other commercial applications.

2.3.3 Constant operation of electrolyzer and fuel cell

Within the operating modes on economic criteria, the first criterion is to increase life of equipment. Such criteria can be conjugated or applied individually.

It is demonstrated that the variable power operation of electrolyzer or fuel cell has influence in the life of equipment, decreasing it, because it have been designed for operating at constant power. The idea is liberate batteries operation in order to absorb variable power operation and let the electrolyzer and fuel cell operate at constant power.

2.3.4 Extension of battery bank life

An operation mode opposite to the above; in this case, battery bank operates at constant power, and electrolyzer and fuell cell operate at variable power. The idea is to increase battery life.

2.3.5 Maximization of economic benefits

This operation mode is more complex to be implemented in the control system of a microgrid, due to a quantity of information needed concerning purchase and sale of electric energy. Taking into account the price of energy, maximize the energy production of microgrid when selling price is high and storage energy from renewables when selling price is low. To perform this control, it is necessary to know the variation of prices of electricity during a day.

2.4 Experimental microgrid operation

The microgrid mathematical description is validated through this section with the experimental results gathered from the microgrid facility. The microgrid operated considering the operation mode 1, defined in section before. The experiment comprises 8 hours of continuous operation. Two different power demands are coupled during operation time (Fig. 2.12 (b) and (c)). As seen, the power demand is mainly concentrated on two periods (midday and late afternoon). The power supplied from the photovoltaic array is concentrated on the first half of the day and with some variability. Finally, the second demand consumes power from the microgrid in the last middle of the simulated day.

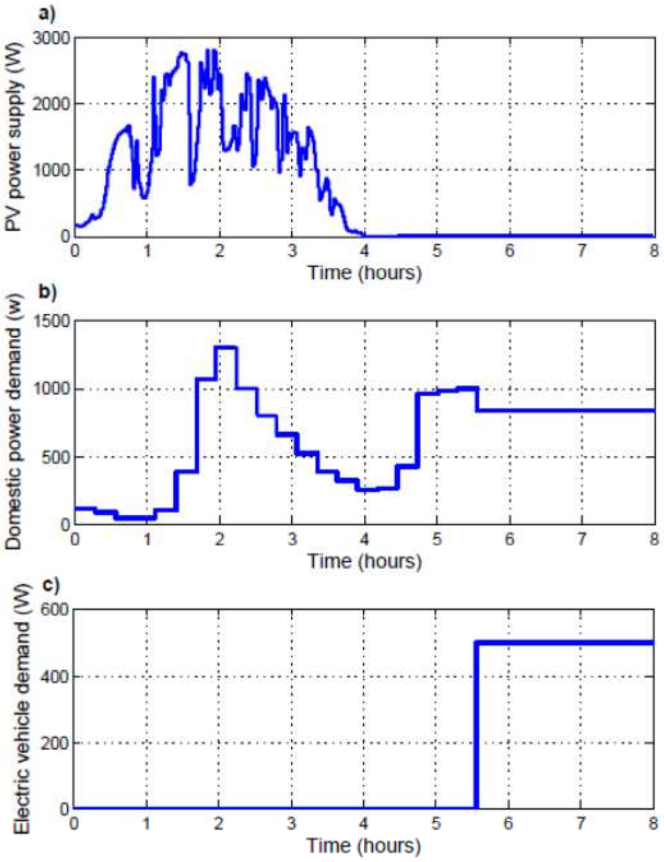

Fig. 2.12. (a) PV array power supply. (b) first demand profile. (c) second demand profile.

The plant power generators track the power profile with the support of the fuel cell. Hydrogen is generated by the electrolyzer when power surplus exceeds. The hydrogen stock is the result of both processes: stored hydrogen is reduced when the fuel cell operates and increased when the electrolyzer is utilized. Fig. 2.13 (c) compares the experimental and simulated hydrogen stock while Fig. 2.13 (a) and (b) show the fuel cell and the electrolyzer utilization respectively. The comparison exhibits a good fitting between experiment and simulated data.

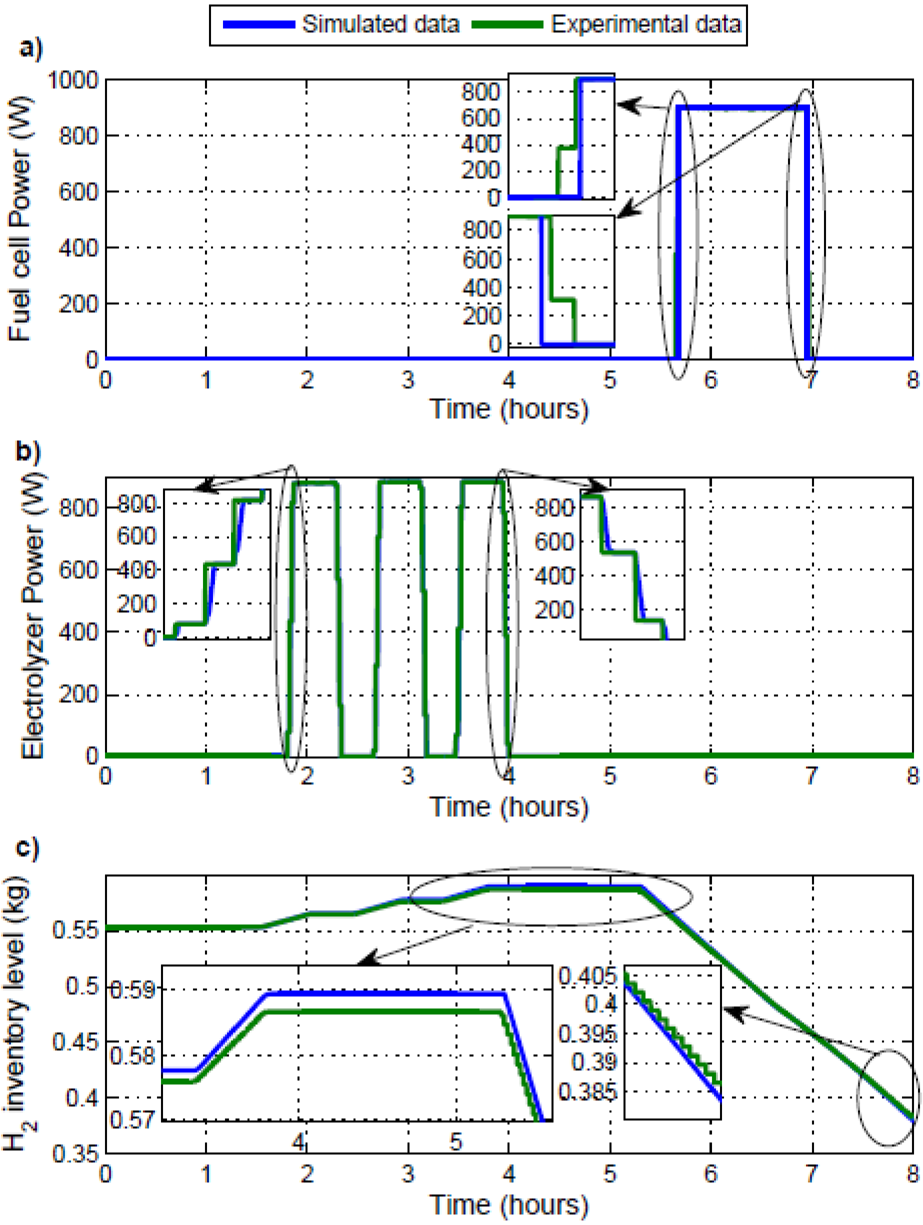

Fig. 2.13. (a) PEMFC operation. (b) electrolyzer operation. (c) hydrogen storage performance.

Since power exchanges with neighbour grids are allowed, the proposed domestic microgrid imports power when its own sources are not capable to track its demands (mainly, the first consumption and the second demand). Contrarily, power export occurs when there is an energy excess. Both cases occur in the implemented experiment as observed in Fig. 2.14 (a). The exported power has positive sign while imported power has negative values. Fig. 2.14 (b) shows the resulting voltage of the DC bus. The DC voltage varies notably during the first stage when the battery exchanges power and remains constant after the 5.6 hours of the test since the battery does not work. This is explained by the availability of the solar resource on the first stage of the day and the lack of PV power on the second stage while the power demand is still present. This leads the battery discharging till the minimum limit. Note that, at this time the FC and the grid starting to supply power in order to satisfy the loads and avoid the battery under-discharging.

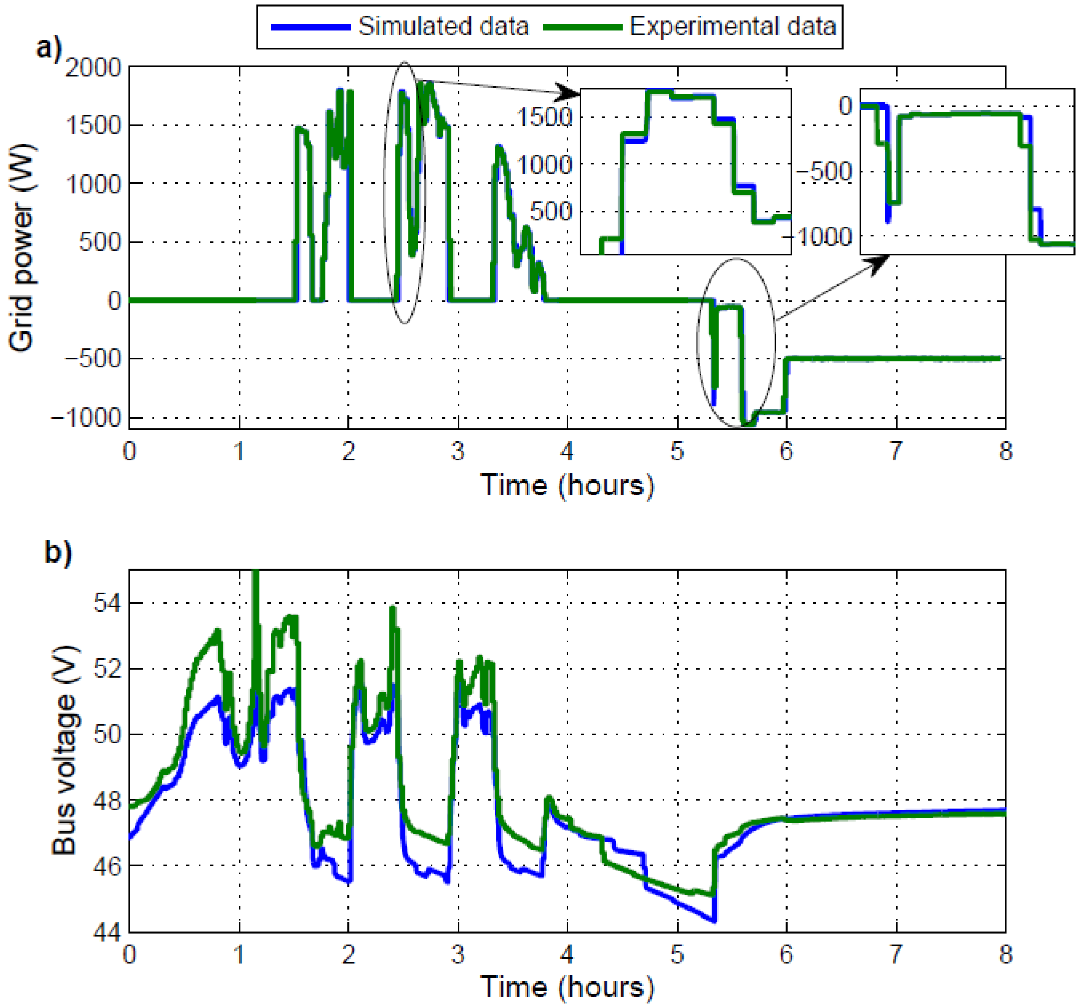

Fig. 2.14. (a) Power exchanges with neighbor grids. (b) DC bus voltage.

3 ESTIA - HESS MODEL VALIDATION

3.1 Introduction

The increasing penetration of Distributed Generation systems based on Renewable Energy Sources is introducing new challenges in the current centralised electric grid. The microgrid is one of the alternatives that is being analysed in order to increase the penetration level of renewable energy sources in electrical grids and improve the power quality.

The microgrid stability is highly sensitive to power variations coming from the energy sources or loads. In this context, an energy storage system is essential and it must satisfy two criteria: to have a high storage capacity to adapt the generation to the demand and to be able to supply fast power variations to overcome the power quality problems that may arise.

In this work the association of a SuperCapacitor bank and a Vanadium Redox Battery is used to satisfy the mentioned requirements. A novel power conversion topology to control and interface the selected hybrid storage system with the rest of the microgrid has been used in this work. A Three-Level Neutral Point Clamped converter has been used to control at the same time the two storage systems, due to the reduced power losses and harmonic distortion that it is able to offer. This topology could be used in a back-to-back topology to smooth the power generated by a wind turbine, among other applications.

The operation of the selected storage system and power conversion topology has been validated in different case studies both in simulations and in the experimental platform. The experimental results carried out in the microgrid installed in ESTIA have proved the validity of the proposed storage system and control algorithm of the three level converter.

3.2 Storage systems in microgrids

3.2.1 Distributed Generation

The traditional grid has become old and unreliable in unpredicted events due to several problems [1]. One of the existing issues is the saturation of distribution and transmission lines in some points of the grid. In other cases the lines must be changed as they have been damaged by time. Furthermore, the energetic crisis created by the limited existence of fossil fuels is increasing the necessity of using generation systems that are not based in this energy source. Moreover, many countries have taken policies at different levels in order to reduce the emission of greenhouse gases, which includes a minimal use of RES [2]. Furthermore, the past few years and especially Post-Fukushima, for the first time in history many countries with a nuclear past considered the level of future demand for electricity being unclear.

Under such circumstances, the advantages of renewable and distributed energy generation offer an attractive alternative for power supply. This, in parallel to the increasing social awareness about the climate change, has increased the importance of the RES as an alternative to the fossil fuel based energy sources.

On the other hand, the power market liberalisation has permitted customers not only to consume electricity, but also to generate and sell it. As a consequence, the number of small generation systems that are connected at the distribution line level is continuously increasing [3]. These generation systems are called Distributed Generation (DG) due to their physical distributed nature. The increasing penetration of DG sources is changing the perspective of the grid from centralised to decentralised [2].

3.2.2 Microgrid

The continuously higher penetration of DG in the distribution grid is replacing a part of the power supplied by the centralised power generators, which creates several challenges that must be carefully addressed in order to keep the proper operation of the electric grid. The microgrid (MG) is being analysed as a solution to these issues [4].

A MG is generally defined as a weak electric grid based on localised grouping of electricity DG (with a rated power smaller than 100kW [5]), loads and storage systems that normally operates connected to the Low Voltage or Medium Voltage distribution network in a unique point called Point of Common Coupling (PCC) [1]. One of the essential characteristics of the MG is its ability to operate connected or disconnected from the main grid as physical and economic conditions dictate [5]. From the grid's point of view a MG can be regarded as a controlled entity that can be operated as a single aggregated load or even as a small power source or ancillary service supporting the network [6]. From the customer's point of view, a MG provides enhanced Power Quality and Reliability (PQR) energy supply [7].

In a MG the use of storage systems plays a vital role in order to ensure energy balance, power balance and also allowing to maintain a high power quality [8].

3.2.3 Benefits of using storage systems

The benefits introduced by an Energy Storage System (ESS) in the operation of a network can be classified in two main groups: ancillary services and power quality and reliability.

3.2.3.1 Ancillary services

Ancillary services are those services necessary to support the delivery of electricity from seller to purchaser while maintaining the integrity and reliability of the interconnected transmission system. Some of the ancillary services that an ESS can provide are the reactive power supply and voltage control, area regulation, spinning reserve, load following, network stability and backup supply [9].

3.2.3.2 Power quality and reliability

For the end-use customer highly reliable electric energy with the highest possible power quality has to be supplied. Storage systems play a vital role to provide these requirements [10].

Reliability is related to the complete loss of voltage of a grid. It can be defined as the degree to which the performance of the elements in a bulk system results in electricity being delivered to customers within accepted standards and in the amount desired [11]. Storage systems can be used to provide ride through capability when outages of extended duration occur. They can be used to substitute the power supply for a certain period of time or for middle-time power supply, to maintain power until another on-site generation system is started [12, 13].

On the other hand, storage systems can also be used to face different issues that affect power quality. Usually two power quality problems are considered to be important: transient voltage events (typically voltage dips) and harmonic distortion. Other power quality problems include frequency variations and low power factor. Storage systems controlled with power converters can be used to mitigate harmonics as well as to avoid frequency variations and transient voltage variations improving the power quality of the grid [14–16].

3.2.4 Renewable Energy Sources Integration

The output variations of the Renewable Energy Sources (RES) that are most used in the MG context, i.e. wind turbines (WT) and photovoltaic (PV) panels, are classified as short-duration and slow duration or diurnal. The effect of clouds in case of PV and wind gusts in case of WT can create fast power variations and consequently power generation systems that can react at the same speed should be used to keep the operation of the network under standard conditions. As the classical generators are not able to face those variations, the use of storage systems is necessary.

An energy storage device offers the possibility of storing the surplus energy generated by RES when the generation is higher than the demand and then giving the stored energy back to the grid when the generation is lower than the demand [17]. This way, the energy generated by RES is better harnessed and at the same time the power injected in the grid is smoothed, reducing the negative impact of RES. The use of a storage system in parallel to a RES allows to keep the output power of the system at constant level [12].

3.2.5 Hybrid Energy Storage System

An energy storage system used in a microgrid application must satisfy different specifications. A high life expectancy is necessary to support the large amount of charge-discharge cycles that the ESS will have. A high efficiency would minimise the energy lost in each of those cycles. A high power rating is required to be able to absorb/supply a high input and output power. Finally, the ESS should also have a fast response to face fast power variations. On the other hand, from the energy point of view, the selected storage system needs a high storage capacity and very low self-discharge which will allow to store energy for periods of time of hours-days, allowing the MG to operate autonomously.

The specific power and specific energy are two of the most important characteristics to determine the validity of a storage system for the MG application. These characteristics determine the energy storage capacity per mass unit, measured in Wh/kg, and the maximum power capacity per mass unit, measured in W/kg, respectively. Fig. 3.1 shows the classification of some of the currently available storage technologies according to their specific energy and power.

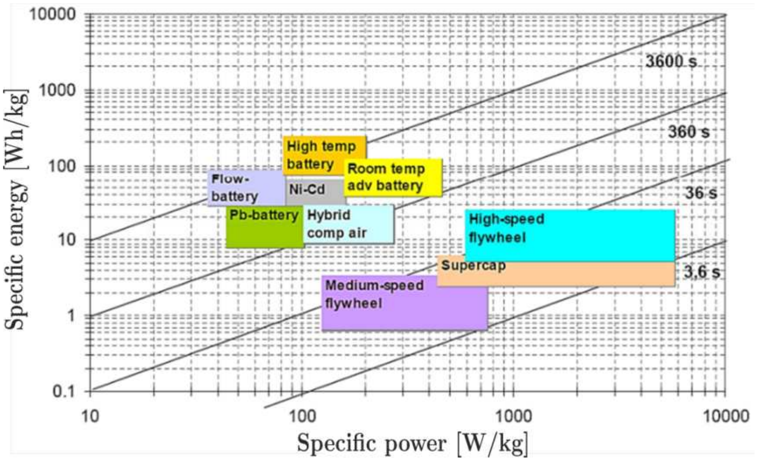

Fig. 3.1 Classification of different storage systems according to their specific energy and power.

As it can be seen from Fig. 3.1, nowadays there is not any storage technology capable of offering at the same time a high specific energy and specific power.

The different types of batteries (Lead-acid, NiCd, Li-ion, NaS and the flow batteries) have a relatively high specific energy but a low specific power. On the other hand, the storage technologies of high specific power (SC, Flywheels and SMES) have low specific energy comparing with the batteries. Consequently, if only one storage technology is used, it must be oversized in power or in energy in order to satisfy all the requirements. A battery should be oversized from the point of view of the power rating, which will lead to a physically big and economically costly storage system. On the other hand, the storage technologies of high specific power need to be oversized from the energy capacity point of view to satisfy the storage capability requirement [18], leading to a high cost ESS as well. Furthermore, even if a storage system is able to satisfy both energy and power rating requirements, it should also satisfy the response time specification.

Consequently, it is necessary to associate more than one storage technology in parallel to satisfy the requirements of the MG application. This association between two different storage technologies is called Hybrid Energy Storage System and it is usually formed by a high specific power storage device and a high specific energy storage device.

Li-ion batteries have a high efficiency and a relatively small self-discharge. However, their depth-of-discharge (DOD) rate highly dependant cycle life is a factor that limits their usability as long-term storage devices. The operation constraint related to the limited DOD rate is especially important in a MG application, as the storage will suffer many charge-discharge cycles with high DOD rates. Lead-acid batteries have the same DOD constraint and furthermore contain environmentally unfriendly materials. Their low life expectancy comparing to other types of batteries and the necessity of periodical water maintenance are other disadvantages for the use of this type of battery in a MG application. In the case of NiCd, their environmentally harmful materials are limiting factors for their use. The new directives that have been approved concerning recycling targets for this type of battery make their future uncertain [19]. NaS batteries are well adapted for high energy rating applications, they have a negligible self discharge and contain environmentally friendly materials. However, the necessity to externally heat the batteries to keep the operational temperature in the required range is their most important disadvantage. In the case of flow batteries, the possibility of easily increasing the storage capacity using higher tanks and more electrolyte make them highly interesting from the MG application’s point of view. Furthermore, their self-discharge is negligible and the efficiency is similar to the one of other types of batteries, which make them interesting for long-term storage applications [20]. In addition, they can be fully discharged with no life expectancy reduction [19]. One of the most important disadvantages of flow batteries is the necessity of pumps to move the electrolytes and the consequent loss of energy. Among the flow batteries, VRB has the highest efficiency and cycle life, and it is considered to be a promising storage technology for RES integration [21, 22].

Taking into account that the life expectancy of the batteries Lead-acid, NiCd, NaS and Li-ion is several times smaller than the cycle life of the flow batteries, that they have higher self-discharge rates as well as DOD rate limitations and other operational constraints, in this thesis a VRB flow battery has been selected as long-term storage device.

On the other hand, among the different high specific power and fast response time storage technologies, the SC has been selected. SMES technology has the disadvantage of having to maintain at a low temperature the superconducting coil and the use of a strong magnetic field, which can be harmful for human health. Comparing to flywheels, SC offers an easier installation, no security issues created by a rotating mass, no maintenance costs and much smaller self-discharge.

3.3 Control of the HESS

The control of the power flow of an ESS is carried out using power converters, which are used as interfaces between the storage systems and the MG.

In this work a Three-Level Neutral Point Clamped (3LNPC) converter has been used to control the power flow of the selected HESS and at the same time to interconnect it with the rest of the MG. Both storage devices are used as the two input voltage sources of the converter, as it is shown in Fig. 3.2.

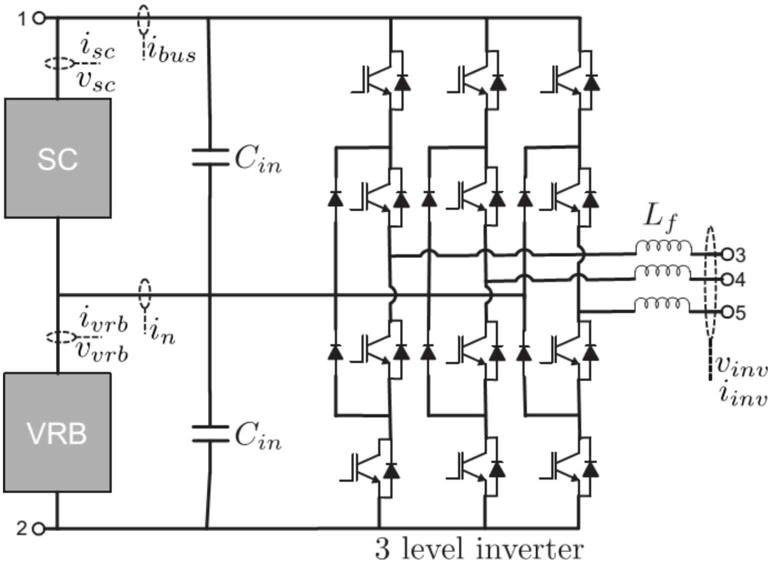

Fig. 3.2. Schematic representation of the 3LNPC topology.

The most important advantage of this topology is its ability to control the power flow of a HESS through just one power converter. From the point of view of the DG applications, the fact of having an integral solution of the power conversion system of the HESS is especially interesting as the system will need to be installed in several locations. This novel topology takes advantage of the possibilities of a three-level converter to reduce the power losses and increase the THD comparing to the systems where a typical two-level inverter is used. As for the same DC bus voltage the voltage applied to each semiconductor device in a 3LNPC converter is the half of the voltage applied in a two-level inverter, the power losses obtained by a 3LNPC converter are smaller for the same switching frequency and operating conditions. At the same time, as the three-level converter uses three DC bus voltage levels, the output AC signals have a better THD [23].

3.3.1 Control of a 3LNPC converter

The control of the AC side variables and the DC side variables has been carried out by separated algorithms in order to emphasize the possibility of using a 3LNPC converter to control the DC power flow. For the sake of simplicity, the AC side variables have been controlled using the well known PI algorithm in the dq0 reference frame. Typical linear control algorithms that work in parallel with PWM modulation strategies are able to satisfy the steady state and transitory requirements that have been fixed in this work.

The second part of the control system of the 3LNPC converter is the one related to the zero-sequence injection control. This algorithm focuses on the DC power division between the input ESS, and it is based on a PI regulator and a current reference generator. The current reference generator selects the value of the current reference of the VRB according to the state of the HESS and to the operational limits of the 3LNPC converter. The PI controller receives the error of the current of the VRB and generates the necessary zero-sequence component to make this error null.

3.3.1.1 AC variables control system design

The control of the AC side variables has been designed taking into account that the 3LNPC converter will have two different operation modes: the isolated operation and the grid-connected operation.

In the isolated case, the objective is to fix the frequency and the voltage of the AC side, as the inverter is the element that will fix those variables. Consequently, according to the power required by the loads connected to the AC bus, the power given by the inverter will be different. The power supplied by the inverter will be defined by the loads and is not a user-selectable parameter. In this operation mode the control algorithm is formed by two loops. An inner loop for the dq current components regulation, and an outer loop for the dq voltage components regulation. The inner current PI controller has been designed to have a settling time of 10 ms and no overshoot. On the other hand, the outer voltage PI controller has been designed to have an overshoot of 3% and a settling time of 25 ms. The value of the load RL that has been employed to calculate the controllers has been 9.2 Ω. Fig. 3.3 shows the structure of the control algorithm in the isolated case.

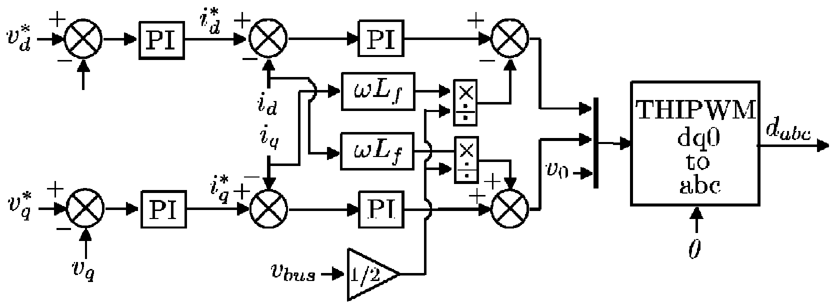

Fig. 3.3. Control structure of the isolated case.

In the grid-connected operation, the inverter works connected to an external voltage source that fixes the voltage of the AC side. The first consequence is that the inverter will need a synchronisation method to connect to the AC bus in a safe mode. The second consequence is that the inverter is not the responsible of fixing the AC variables any more. In the grid-connected mode the controlled variables are the active power and the reactive power supplied/absorbed by the converter to/from the AC bus. The active and reactive powers can be controlled through the i_d and i_q components respectively. Therefore, in this operation mode the control algorithm only needs one control loop, the one of the current, and it will be the same of the isolated case. However, in this case the current reference values will be calculated according to the P and Q reference values. From the HESS power management point of view, those power variables can be selected to improve the operation of the HESS according to the needs of the system. Fig. 3.4 shows the structure of the control algorithm in the grid-connected case.

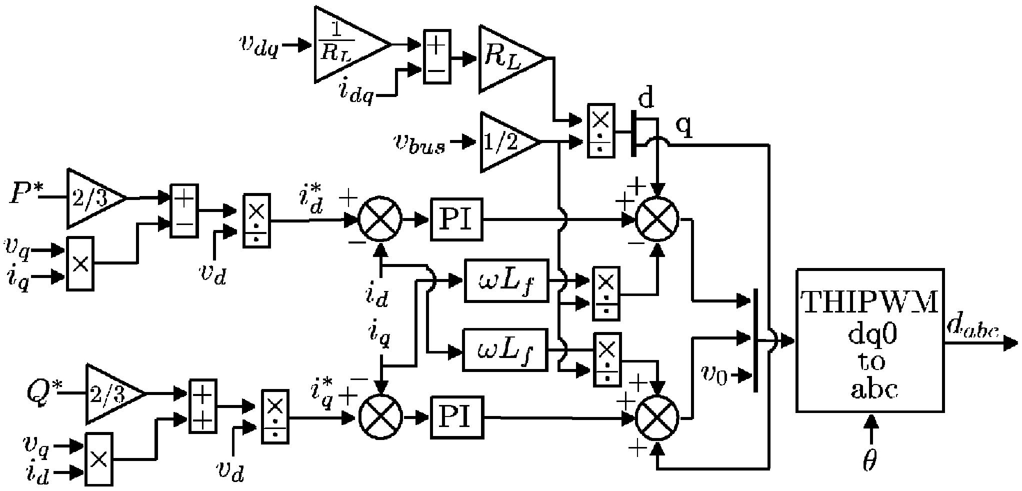

Fig. 3.4. Control structure of the grid-connected case.

The transition from one operation mode to the other is carried out smoothly resetting and initialising the PI controllers.

3.3.1.2 VRB current controller design

The zero-sequence component is used to control the power flow of the HESS. The power division between the SC and VRB must be carried out according to the frequency: fast power variations must be absorbed or supplied by the SC and the low frequency part by the VRB. The injection of the zero-sequence can be selected with the objective of controlling the current of the VRB. Therefore, the power of the VRB will be directly controlled, while the remaining power will be absorbed or supplied by the SC. The power control of the SC is carried out indirectly, thus.

The dynamics of the DC currents of the 3LNPC converter are defined by the d_{abc} duty cycles and the i_{abc} currents of the AC side. The duty cycle signals include the zero-sequence. On the other hand, the AC side currents are determined by the PI-based control system designed in the dq0 reference system. Furthermore, the switching frequency and the DC capacitors have a direct effect on the high frequency component of the DC currents, which limits the proportional parameter of the zero-sequence controller. The PI control system of the current of the VRB has been designed by trial and error using the Simulink simulation model.

The reference signal of the PI controller of the zero-sequence is generated by a rule-based algorithm according to the operational limits of the 3LNPC converter. Those limits establish the maximum/minimum accessible VRB and SC currents according to 5 variables: the modulation index, the DC voltage unbalance, the phase difference between AC voltages and currents, the injected zero-sequence and the received DC current. The operational limits of the 3LNPC converter can be calculated from its average model. Fig. 3.5 shows the structure of the control of the current of the VRB.

The i_{vrb} reference generation must be carried out according to the operational limits of the 3LNPC in each operation point, but also according to the SOC of the storage systems. Therefore, the reference generation is based on two parts:

1. State manager: it is the responsible of defining the state of each storage system according to their SOC.

2. Reference definer: it is the responsible of defining the reference of the current of the VRB according to the operational limits and the state of each ESS.

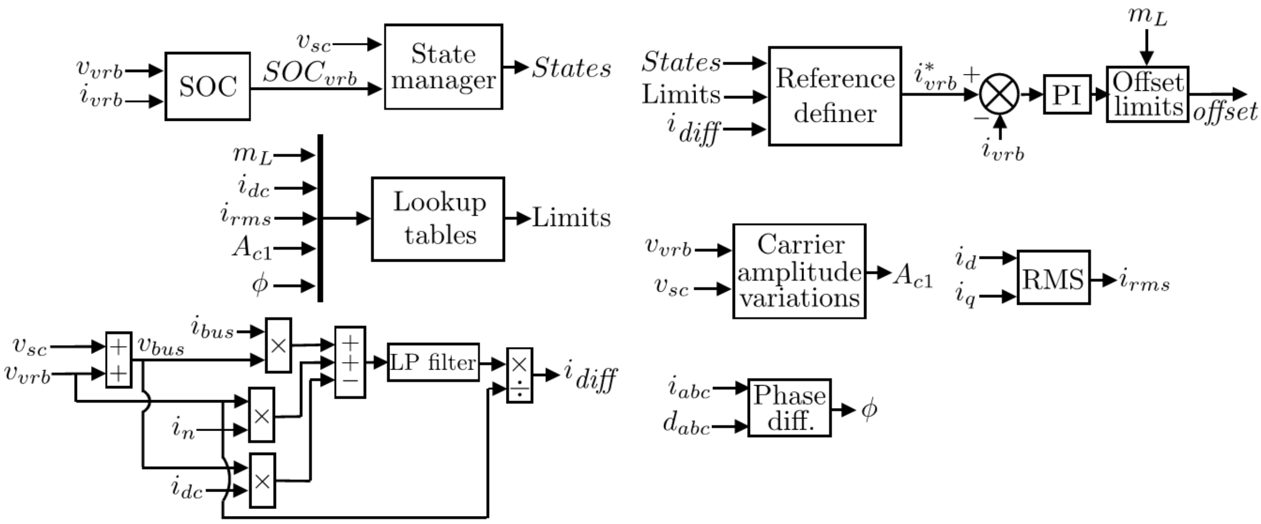

Fig. 3.5. Control structure of the current of the VRB.

Three different ranges (upper, middle and lower) have been defined for each ESS in order to determine their charge level (1 for the upper, 2 for middle and 3 for lower). The voltage and currents limits of each ESS have been also taken into account in order to ensure a safe operation and stop the execution if the safety limits are exceeded. Each range contains an hysteresis in order to avoid fast transitions from one state to the other.

The selection of the reference current of the VRB must take into account several aspects. Firstly, the charge level of the ESS, which represent their SOC. Secondly, the relation among the power received from RES in the DC side and the power required by the load. Finally, the ability of the 3LNPC to face increasing or decreasing power variations, which is defined by the injected zero-sequence.

The reference defined by the reference selector is filtered to avoid the possible fast variations introduced by the state variable. The cut-off frequency of this filter has been selected to be at 10 rad/s, but as it will be explained later, in some experimental tests it has been reduced in order to be able to show the desired results.

Once the reference is generated, the VRB current error is calculated and used by the previously mentioned PI in order to modify the injected zero-sequence and to keep the current of the VRB at the reference level. However, the 3LNPC converter is not supposed to work in overmodulation in this work. Consequently, it has been necessary to limit the zero-sequence generated by the PI to avoid that.

3.4 Experimental results

3.4.1 3LNPC converter experimental unit

A custom made 3LNPC converter constructed by Arcel enterprise has been used to experimentally validate the designed and previously introduced control system.

Even if the converter was sized to work at 1200 V/50 A maximum values, the tests that have been carried out in this thesis were of low voltage values, around $60\,V_{dc}/11\,V_{rms}$, due to the limitation of the characteristics of the used storage devices: the maximum voltage levels of the used storage devices are 48.6 V for the SC and 32 V for the VRB. Consequently, small-scale tests have been carried out. Even if the tests were performed in non-conventional voltage levels, the tests are completely representative of what would happen at higher voltage levels.

Two printed circuit boards have been designed and constructed in order to sense, scale and filter the measured signals, i.e. the voltages and currents of the DC and the AC sides. 11 signals have been measured, two DC bus voltages, three DC currents and the voltages and currents of each of the three phases. A second order filter with a cut-off frequency of 3 kH z has been selected to eliminate the effect of the switching frequency (15 kH z) and to avoid the aliasing effect. Table 3.1 summarised the most important characteristics of the 3LNPC converter.

Table 3.1 Parameters of the 3LNPC converter.

Parameter	Value
C_1C_2	3.3 mF
L_{filter}	3 mH
V_{dc}	60 V
V_{rms}	11 V
f_{fund}	50 Hz
f_s	15 kHz
$f_{c\ filter}$	3 kHz

Fig. 3.6 shows the picture of the different elements that have been used to experimentally validate the solution proposed in this thesis. A commercial SC of the Maxwell manufacturer, a custom-made VRB, different loads, the mentioned 3LNPC converter and a Hardware-in-the-loop system (the unit OP5600 of Opal-RT manufacturer) have been used in the experimental validation.

Fig. 3.6 Photograph of the experimental platform.

3.4.2 Isolated case study

The operation of the proposed control system has been tested when the HESS is supplying power to an AC resistive and balanced load. The AC load is kept constant while a variable current is injected in the DC bus. In this case, due to the long execution time, it has not been possible to compare the obtained results with simulation results and consequently only the experimental part is shown.

Fig. 3.7 shows the general block diagram of the configuration of the system that has been used to carry out the above mentioned tests.

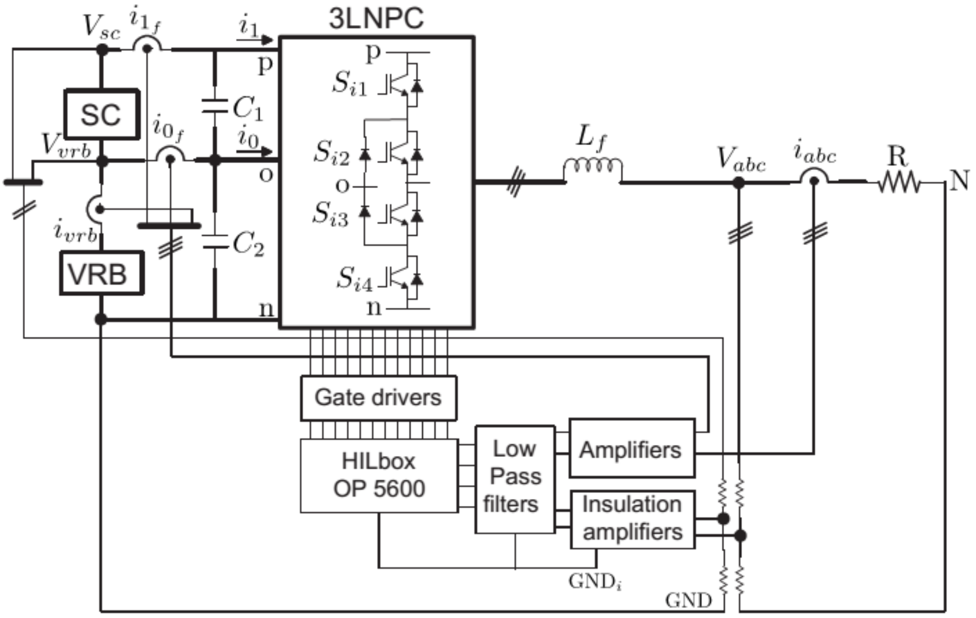

Fig. 3.7. Block diagram of the experimental tests in the isolated case study.

3.4.2.1 Variable DC power injection

In this case study a variable i_{dc} current has been injected in the DC bus while the AC load has been kept constant at 9.2 Ω. The objective of this case study has been to show the ability of the proposed control structure to divide the power between the SC and the VRB according to the frequency, when the variation comes from the DC side. This DC side current represents the power variations generated by different RES.

The i_{dc} variations have been manually generated by a voltage source. Therefore, the variations of the current profile were limited in frequency and it has been necessary to reduce the cut-off frequency of the filter of the current reference of the VRB from 10 rad/s to 1.25 rad/s. Due to the long execution time, it has not been possible to simulate the experimental tests in Matlab/Simulink. Consequently, only experimental results are shown. It has been taken into account also that both ESS are in the state 2 during the entire test.

Fig. 3.8a shows the power that is injected in the DC bus using the voltage source, while Fig. 3.8b shows the evolution of the power of the VRB, its reference and the power of the SC. In the range [0, 4] s the injected power is higher than the power required by the load (around 40 W). Consequently, the rule-based algorithm starts to decrease the power reference of the VRB. While the power supplied by the VRB is being reduced, the power difference between the input DC power and the power required by the load is absorbed by the SC. The power division is carried out following the fixed requirements, as the SC faces the fast power variations. On the other hand, from the instant 4 s till the end of the test the power received from the voltage source is not enough to satisfy the power requirement of the load. Thus, the power supplied by the VRB is increased. The algorithm tends to supply the same power in order to keep the offset around 0 level and increase the capacity of the HESS to face increasing or decreasing power variations.

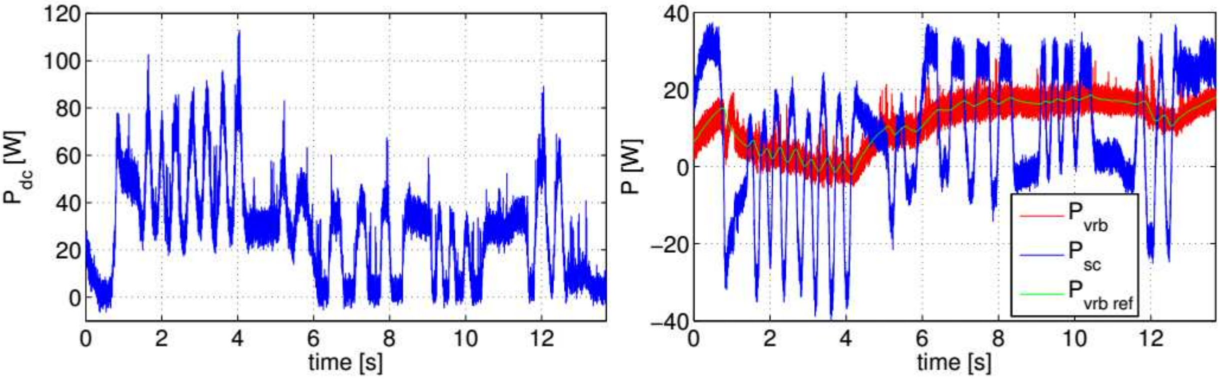

(a) (b)

Fig. 3.8. Evolution of (a) P_{dc} and (b) $P_{vrb\ ref}$, P_{vrb}, P_{sc} variables during the variable DC power injection test.

Fig. 3.9 shows the evolution of the zero-sequence injected to the modulating signals in order to control the power flow of the HESS. It can be seen that the rule-based algorithm is able to keep the offset around 0 value, and also to divide the power according to its frequency between the SC and the VRB.

Fig. 3.10 shows the main variables of the AC side of the 3LNPC converter. This figure shows that the zero-sequence injection has no effect on the AC side and therefore the variables remain constant during the entire test as the AC load does not have any variation.

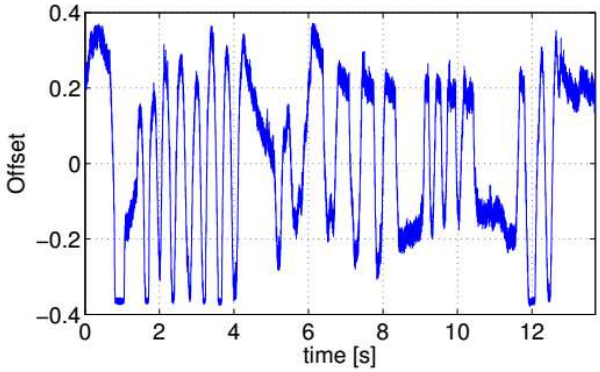

Fig. 3.9. Evolution of the offset during the variable DC power injection test.

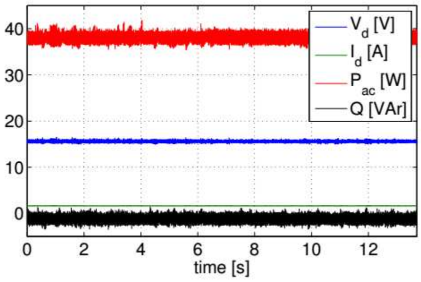

Fig. 3.10. Evolution of the AC side variables during the variable DC power injection test.

3.4.3 Grid-connected case study

This case study analyses the behaviour of the 3LNPC converter when the disconnection from the main grid occurs. The results obtained from this case study show that the presented multilevel inverter can divide the power between the SC and the VRB according to its frequency when the islanding transition occurs.

Fig. 3.11 schematically shows the configuration of the system that has been used during these tests.

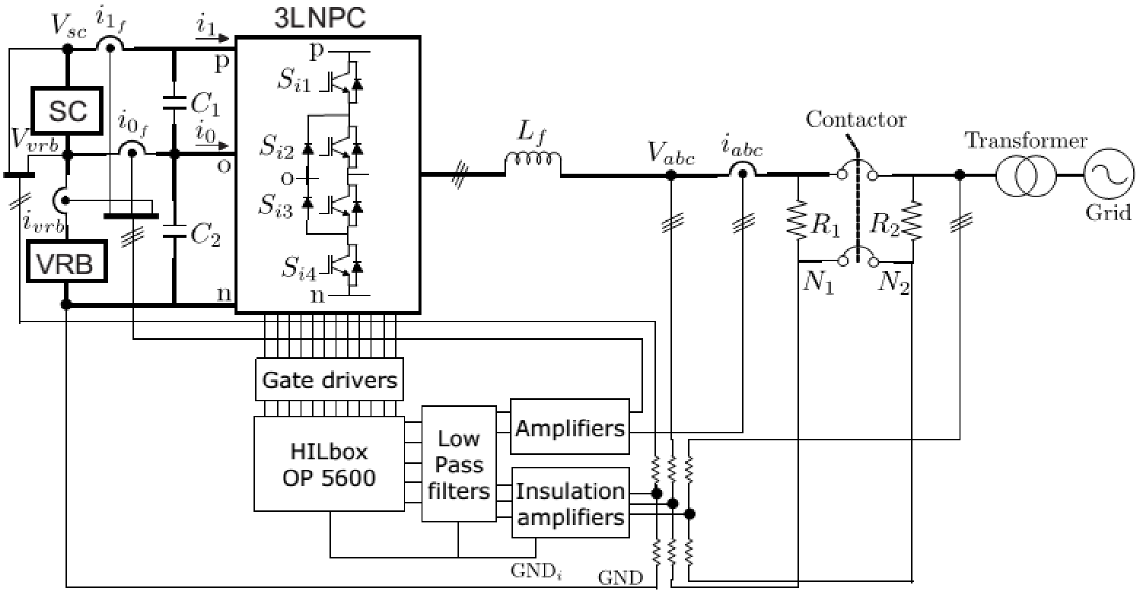

Fig. 3.11. Block diagram of the experimental tests in the grid-connected case study.

The 3LNPC converter is connected to the main grid through a step-down transformer (230 V_{rms}/12 V_{rms}). The converter feeds a three-phase resistive balanced load (R_1) of 1.8 Ω, while the grid feeds another resistive load (R_2) of 4.7 Ω in the secondary of the step-down transformer. A contactor is used to connect or disconnect the converter from the main grid.

The active power required by the resistive load of the converter is 240 W . Once the grid-connection is done, the active power supplied by the converter is reduced to 100 W in order to create a power difference that the converter will have to face once the disconnection occurs. This way, the converter needs to face a power step of 140 W , which must be supplied by the SC. The grid-disconnection is done to show that the 3LNPC converter is able to face this event, while the power division between the SC and the VRB is carried out according to the defined requirements. Therefore, no fault detection algorithm has been implemented, the disconnection has been done directly by the user.

The same case study has been analysed experimentally and by means of simulations using Matlab/Simulink and the SimPowerSystems toolbox. The simulation and experimental results are compared in Fig. 3.12 and Fig. 3.13.

Fig. 3.12 shows the variables of the AC side of the 3LNPC converter. Fig. 3.12a and Fig. 3.12b represent the evolution of the d component of the AC voltage and current respectively. In both cases the simulation and experimental results show a similar evolution.

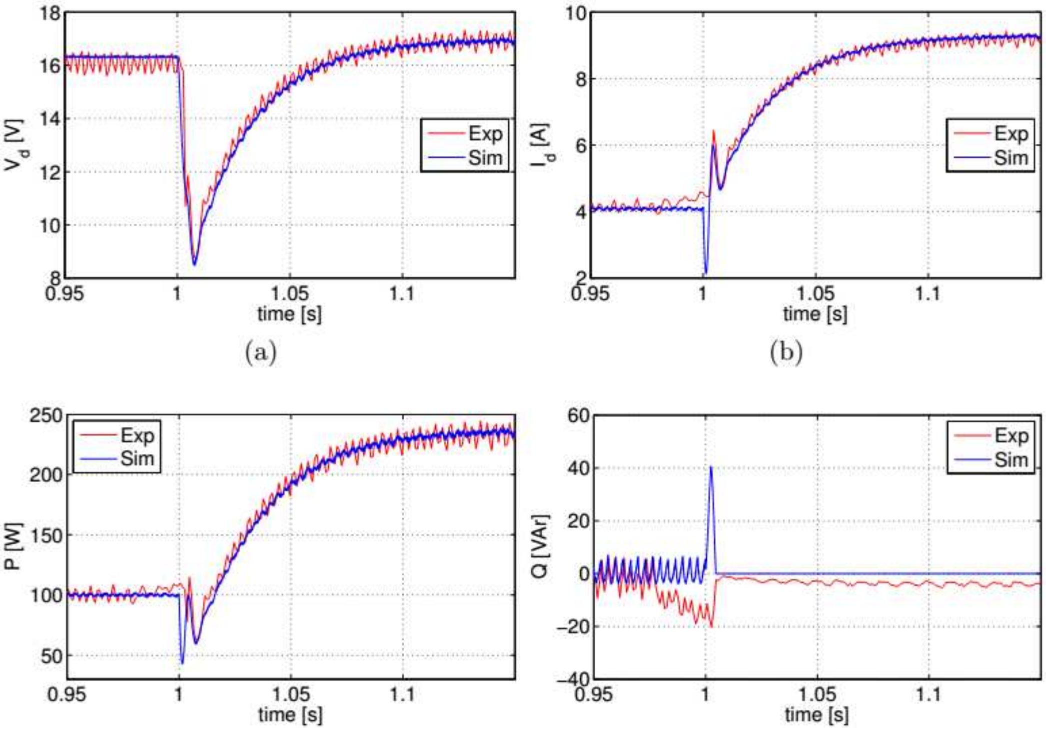

(a) (b)

Fig. 3.12. Evolution of (a) V_d, (b) I_d, (c) P and (d) Q variables during the disconnection from the main grid.

When the converter operates connected to the grid, the voltage is smaller than 12 V_{rms} due to the effect of the lines used to connect the different elements. When the disconnection occurs at 1 s instant, the control mode switches from grid-connected to the isolated mode. Thus, after the disconnection the voltage is kept at the reference 12 V_{rms}. Fig. 3.12c shows the evolution of the active power, where the mentioned variation from 100 W to 240 W is shown. On the other hand, the evolution of the reactive power of the converter is shown in Fig. 3.12d. A non-zero value is detected in the experimental results due to the effect of the filtering and the digitalisation.

Fig. 3.13a, Fig. 3.13b and Fig. 3.13c show the evolution of the power of the VRB, SC and the addition of both respectively. A difference between experimental and simulation results can be noticed due to the impossibility of properly simulating the power losses in Simulink. However, the dynamics of the power of the SC and the VRB show a good agreement between simulations and experimental results. These dynamics show how the power step is completely supplied by the SC and then how the control algorithm varies the current of the VRB in order to adapt it to the new operation point according to the rules defined in the designed algorithm.

The shown results prove that the converter and the presented control algorithm are able to divide the power between the SC and the VRB when the disconnection occurs. The results also show that the transition from the grid-connected operation mode to the isolated operation mode is carried out smoothly, resetting and initialising the controllers and the phase detection according to the previous values.

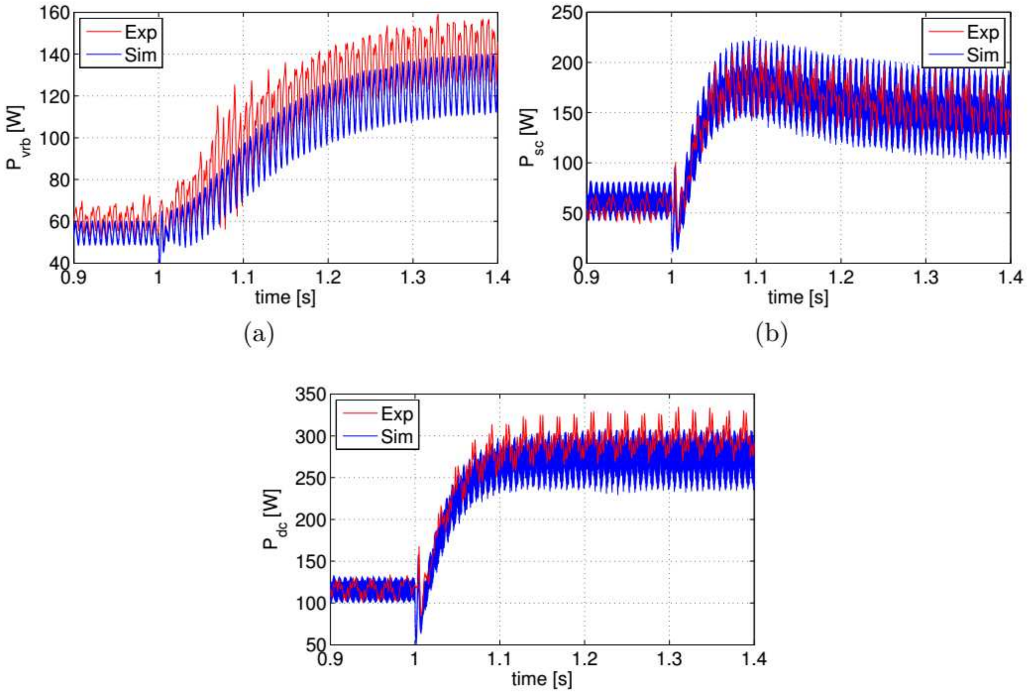

Fig. 3.13. Evolution of (a) P_{vrb}, (b) P_{sc} and (c) P_{dc} variables during the disconnection from the main grid.

3.5 Conclusions

The power conversion topology that has been used in this work allows to reduce the power losses and number of power converters used to control and interconnect a HESS with the rest of the microgrid. A control algorithm that takes into account the operational limits of the selected power conversion interface has been designed.

The presented control algorithm has been validated by simulations and also experimentally. The simulation results show that the control algorithm operates as expected. The good agreement between experimental and simulation results prove the validity of the used simulation environment, which could therefore be used to analyse the operation of the system in different case studies.

The employed power converter allows to easily introduce a HESS for example in a back-to-back converter of a wind turbine, reducing the variability of the wind power and improving its grid integration. The HESS and the 3LNPC converter will be used as the grid side converter and they would allow to smooth the power generated by the wind turbine reducing the negative impact on the operation of the grid. It could be installed for example in the wind turbines that can be installed in the harbour of Bayonne.

3.6 Bibliography

[1] J. Driesen and F. Katiraei, “Design for distributed energy resources,” IEEE Power and Energy Magazine, vol. 6, pp. 30–40, May 2008.

[2] A. Ipakchi and F. Albuyeh, “Grid of the future,” IEEE Power and Energy Magazine, vol. 7, pp. 52–62, Apr. 2009.

[3] A. Hajizadeh and M. A. Golkar, “Control of hybrid fuel cell/energy storage distributed generation system against voltage sag,” Int. J. Electrical Power & Energy Systems, vol. 32, pp. 488–497, June 2010.

[4] N. Hatziargyriou, H. Asano, R. Iravani, and C. Marnay, “Microgrids,” IEEE Power and Energy Magazine, vol. 5, pp. 78–94, Aug. 2007.

[5] R. H. Lasseter, “MicroGrids,” in IEEE PES Winter Meeting, 2002, vol. 1, pp. 305–308, 2002.

[6] A. Tsikalakis and N. Hatziargyriou, “Centralized control for optimizing microgrids operation,” IEEE Trans. Energy Conversion, vol. 23, pp. 241–248, Mar. 2008.

[7] F. D. Kanellos, A. I. Tsouchnikas, and N. D. Hatziargyriou, “Micro-grid simulation during grid-connected and islanded modes of operation,” in Proc. Int. Conf. Power Systems Transients (IPST’05), 2005.

[8] S. Abu-Sharkh, R. Li, T. Markvart, N. Ross, P. Wilson, R. Yao, K. Steemers, J. Kohler, and R. Arnold, “Microgrids: Distributed on-site generation,” tech. rep., Tyndall research centre, University of Southampton, 2005.

[9] J. M. Eyer, J. J. Iannucci, and P. C. Garth, “Energy storage benefits and market analysis handbook,” Tech. Rep. SAND2004-6177, Sandia National Laboratories, Dec. 2004.

[10] D. Sutanto, “Energy storage system to improve power quality and system reliability,” in Student Conf. Research and Development SCOReD, pp. 8–11, 2002.

[11] J. Kueck, B. Kirby, P. Overholt, and M. Lawrence, “Measurement practices for reliability and power Quality-A toolkit of reliability measurement practices,” Tech. Rep. ORNL/TM-2004/91, Oak Ridge National Laboratory, June 2004.

[12] J. Eyer and G. Corey, “Energy storage for the electricity grid: Benefits and market potential assessment guide,” Sandia Report SAND2010-0815, Feb. 2010.

[13] H. Chen, T. N. Cong, W. Yang, C. Tan, Y. Li, and Y. Ding, “Progress in electrical energy storage system: A critical review,” Progress in Natural Science, vol. 19, pp. 291–312, Mar. 2009.

[14] G. Rodriguez, “A utility perspective of the role of energy storage in the smart grid,” in Proc. IEEE PES General Meeting, 2010.

[15] D. Casadei, G. Grandi, and C. Rossi, “Power quality and reliability supply improvement using a power conditioning system with energy storage capability,” in IEEE Int. Symposium Ind. Electron., vol. 2, pp. 1135 –1140, May 2004.

[16] J. Barrado, R. Grino, and H. Valderrama-Blavi, “Power-Quality improvement of a Stand-Alone induction generator using a STATCOM with battery energy storage system,” IEEE Trans. Power Delivery, vol. 25, pp. 2734 –2741, Oct. 2010.

[17] D. Conolly, The Integration of Fluctuating Renewable Energy Storage. Ph.D. dissertation, University of Limerick, Dec. 2010.

[18] H. Zhou, T. Bhattacharya, D. Tran, T. Siew, and A. Khambadkone, “Composite energy storage system involving battery and ultracapacitor with dynamic energy management in microgrid applications,” IEEE Trans. Power Electron., vol. 26, pp. 923–930, Mar. 2011.

[19] F. Díaz-Gonzalez, A. Sumper, O. Gomis-Bellmunt, and R. Villafáfila-Robles, “A review of energy storage technologies for wind power applications,” Renewable and Sustainable Energy Reviews, vol. 16, pp. 2154–2171, May 2012.

[20] K. Divya and J. Østergaard, “Battery energy storage technology for power systems-an overview,” Electric Power Systems Research, vol. 79, pp. 511–520, Apr. 2009.

[21] W. Li, G. Joos, and J. Belanger, “Real-Time simulation of a wind turbine generator coupled with a battery supercapacitor energy storage system,” IEEE Trans. Ind. Electron., vol. 57, pp. 1137–1145, Apr. 2010.

[22] A. Testa, S. De Caro, and T. Scimone, “Analysis of a VRB energy storage system for a tidal turbine generator,” in 13th European Conf. EPE, pp. 1–10, 2009.

[23] L. Clotea, A. Forcos, C. Marinescu, and M. Georgescu, “Power losses analysis of two-level and three-level neutral clamped inverters for a wind pump storage system,” in Proc. 12th Int. Conf. Optimization of Electrical and Electronic Equipment, pp. 1174–1179, 2010.

4 CENER - ATENEA MICROGRID

4.1 Installation description

The facility is located on the premises of the Wind Turbine Test Laboratory (LEA) of CENER, in the industrial estate of Rocaforte in Sangüesa (Navarra) and it has been developed by the Renewable Energy Grid Integration Department.

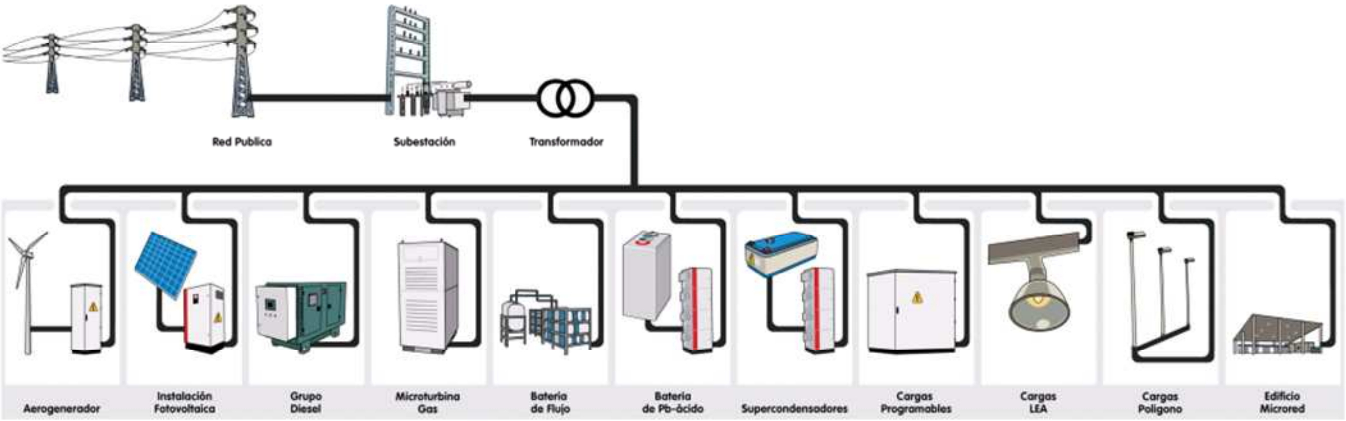

The microgrid is comprised of the following elements:

- A low voltage distribution network, where a series of distributed energy sources are interconnected to provide electricity and heat for a group of consumers.
- A local communication infrastructure
- A hierarchical control and management system
- Energy storage systems
- Smart consumption and load controllers
- A central controller that manages the microgrid, which gives the set point to the controllers of all the other equipment, such as the generation sources, the energy storage systems and smart loads.

This is a microgrid for industrial application, designed to supply part of the electrical loads of the specific facilities of the LEA as well as part of the public lighting of the industrial estate. It was built under AC type architecture, that is, all the elements are connected to the same AC bus for the mutual exchange of energy. This AC bus is connected to the electrical grid at one single point, which permits interaction with it.

The main targets of the installation are the following:

- To manage the available generated power at every moment so the supply to the loads is always guaranteed
- To optimize the use of renewable energies to cover the loads, promoting the energy independence of LEA
- To protect the existing equipments from faults coming either from the grid or from the microgrid itself
- To be able to send the energy excess to the main grid, so the microgrid does not operate as an independent entity but as an active part of the grid

- To be used as a test bench for new equipments, generation systems, energy storage and strategies for microgrid control and protection

4.2 Microgrid modelling

The tool described in this report comprises a combination of mathematical and electrical models simulating the behaviour of each of the components installed in the microgrid, and hence, the microgrid. The platform used to model these systems was Matlab/Simulink.

This simulation platform allows forecasting the behaviour of the system. At the same time, it enables to analyze the system response after the implementation of new generation or storage systems, as well as to define the overall control system and management strategy.

This model of the CENER microgrid in Sangüesa consists of the following equipments:

- Energy storage systems
    - Lead-acid battery bank
    - Flow battery
- Power generation systems
    - Wind turbine
    - Photovoltaic system
    - Diesel power generator
- Loads supplied by the microgrid
    - Lighting of one of CENER's buildings
    - Public lighting in the industrial area of Rocaforte
    - Ancillary consumptions in the microgrid
    - Programmable loads bank
- Electric system
    - Electric grid
    - Power transformer
    - Connection to the grid
    - Switches
    - Wattmeters
- Control systems
    - Management system of the microgrid
    - Control panel for the switches

The Fig. 4.1 shows a general scheme of the overall model.

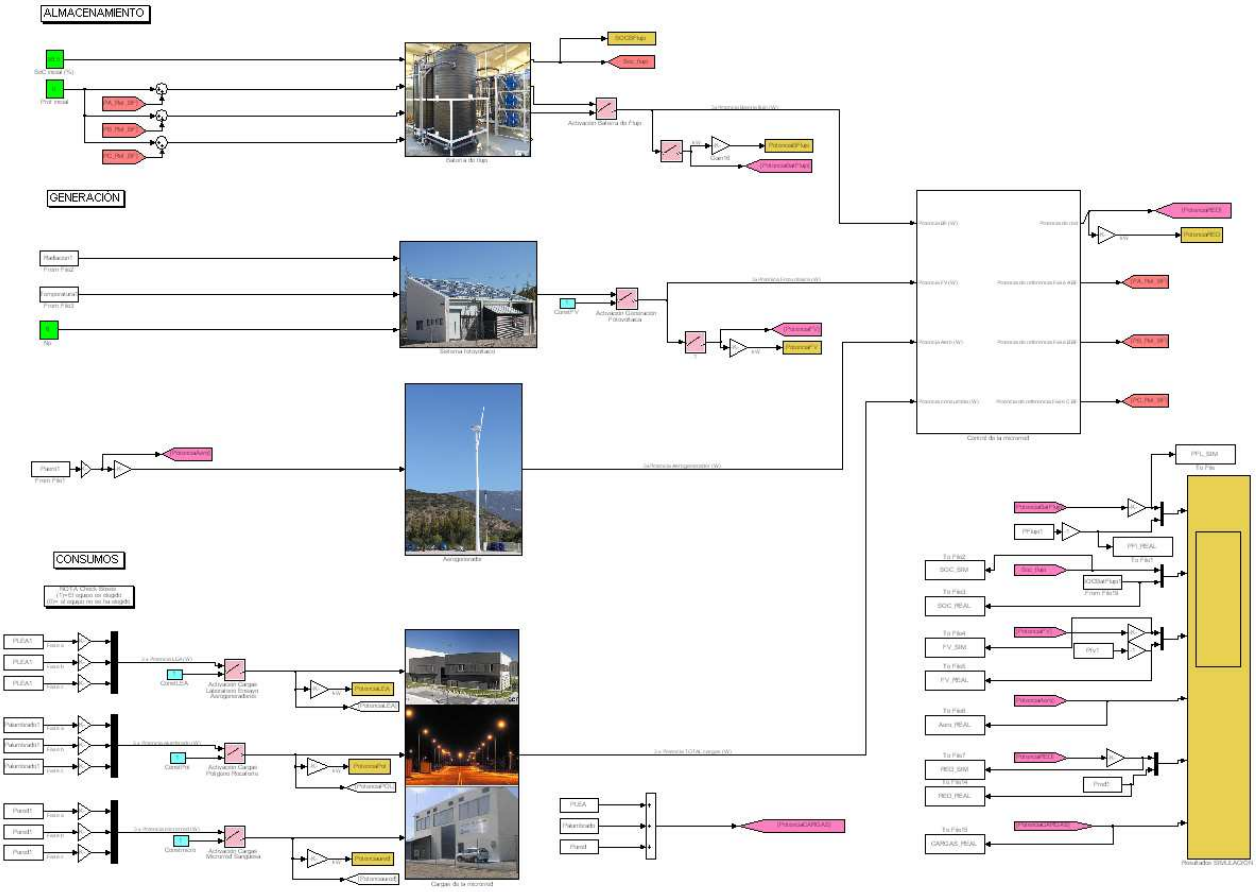

Fig. 4.1. General view of the model in Simulink

4.2.1 Model strategy

Now, the logic used for the management of the system is detailed. There are two working modes available for the system: the first one considers the microgrid connected to the external electric grid through the power transformer (Connected mode), and the other one consists on working isolated from the electric grid, while one of the energy storage systems generates its own grid (Island mode).

In this report, the validation of the connected mode is performed. Broadly speaking, while the microgrid remains connected to the external grid (Connected mode), the performance for every *t* instant is the following:

- If the generation from the renewable systems is greater than the consumption of the loads, the exceeding energy will be absorbed by the energy storage systems provided that they have enough available capacity. Otherwise, this energy will be delivered to the grid so it can be used by other consumers.
- If the generation from the renewable systems is lower than the consumption of the loads, this part will be supplied by the energy storage systems provided that their SOC (state of charge) is within the acceptable range. Otherwise, the electric grid will meet the loads.

- All in all, the main target is that the consumption of the loads is met by the elements within the microgrid, avoiding the consumption from the external electric grid if possible.
- It is worth mentioning that the management strategy is not the same for all of the storage systems in the microgrid. It will depend on their skills and on the priority set in the strategy.

4.3 Model validation

4.3.1 Introduction

The multiple technologies available in ATENEA microgrid allow testing different configurations of microgrids. Generally, it makes no sense to use all the equipments at the same time, but to choose the ones that would be installed within one specific microgrid architecture. That way, the elements included in the model for this validation are listed below:

- Generation
    - Wind turbine
    - PV system
- Storage
    - Vanadium redox flow battery

Fig. 4.2. View of the tanks (left) and the stacks (right) of the flow battery

- Loads
    - Lighting at LEA building
    - Lighting at the industrial area
    - Load from microgrid building
- Connection to the distribution power grid

The block on the top-right in Fig. 4.1 comprises the control system of the microgrid. It gathers all the data related to power generation and consumption, and according to the strategy implemented in the system, it calculates and sends the setpoint for charging/discharging the storage. Although there are many elements in the system, the only one receiving continuous inputs from the control system is the storage system. In principle, decisions regarding the rest of elements could only be to be connected or disconnected.

In this case, the main objective is to minimize the energy exchange through the connection with the grid. Thus, whenever possible, the existing loads are met by the renewable generation and the energy stored.

4.3.2 Methodology

The aim of the validation is to compare the performance of the real microgrid with the one of the model, checking that it follows the real behaviour of the installation. A well developed and tuned model is a strong management tool in order to try different strategies and architectures in a microgrid.

The validation started registering all the data from the meteorological station, the generation, the loads and the performance of the energy storage. These tests took place during 5 days, from 18th to 22nd of April 2013. Once this data is collected, it was used as an input for the model (i.e. loads, meteorological data) and also as a reference for the validation (i.e. management of the energy storage, energy exchange with the grid).

4.3.3 Results

The time-step used in the simulations is 10 minutes, so in the figures in X axis we can see 144, 288, etc. that corresponds with 1 day, 2 days, etc.

In Fig. 4.3 the power loads connected to the microgrid are shown. It is worth noting the load increase during the nights due to the lighting in the industrial area. Also, at the end of the graph a high consumption above 10 kW appears. The load in this graph corresponds to the real measurements taken in the installation, and it is used as an input for the model validation.

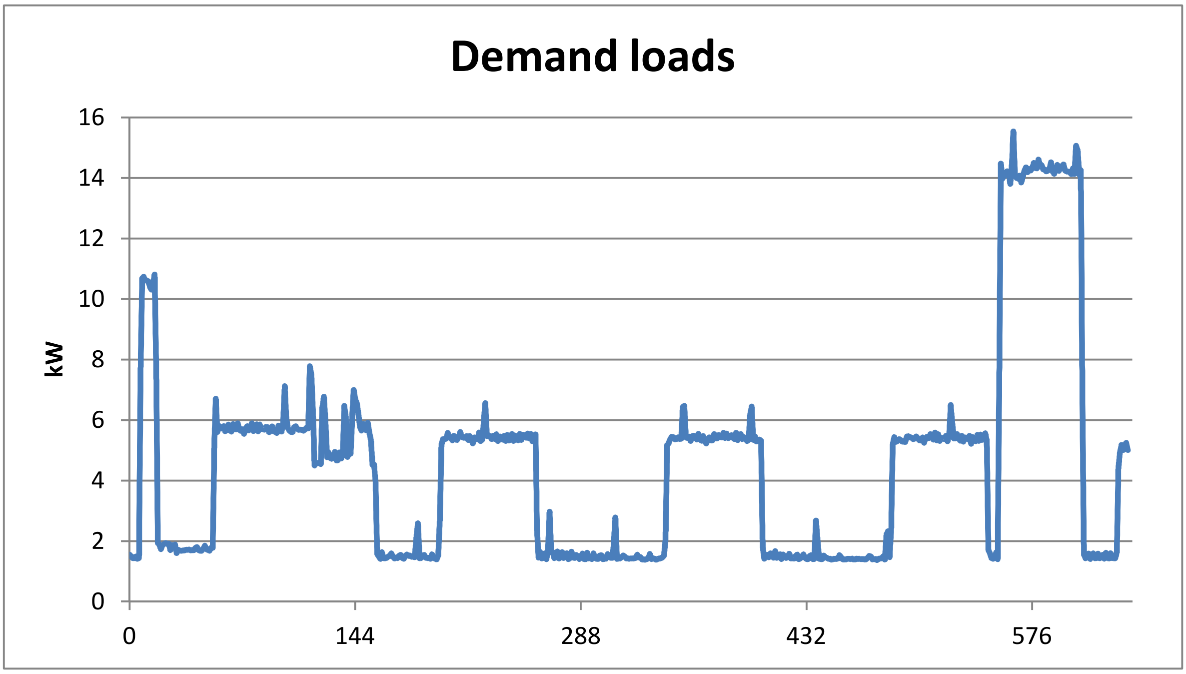

Fig. 4.3. Power loads fed by the microgrid

Regarding power generation, in first place we can see the production of the wind turbine in Fig. 4.4. This data comes from the measurement of the generation of the real wind turbine, which also enters the model as it is.

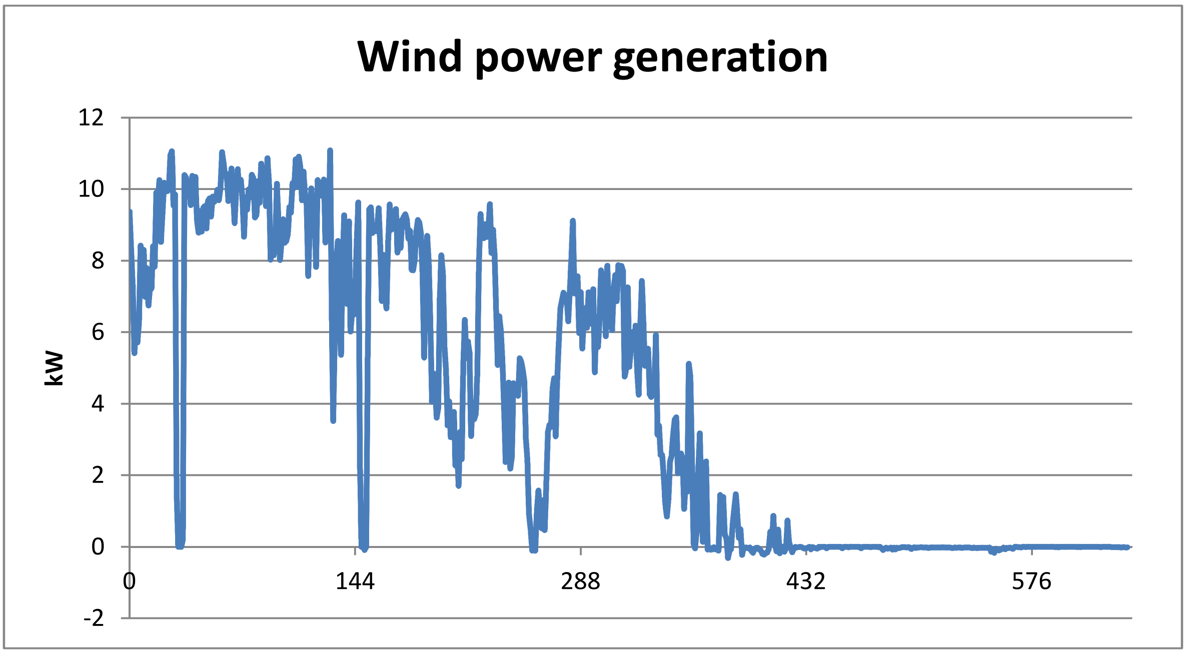

Fig. 4.4. Wind turbine power generation

In second place, the power generation of the PV system is depicted in Fig. 4.5. In this case, the inputs for the model are the real measurements of solar radiation and ambient temperature. Thus, the model box of the PV system uses these inputs to calculate the power generation of the system. In the figure, the output from the model box can be compared with the corresponding measured generation.

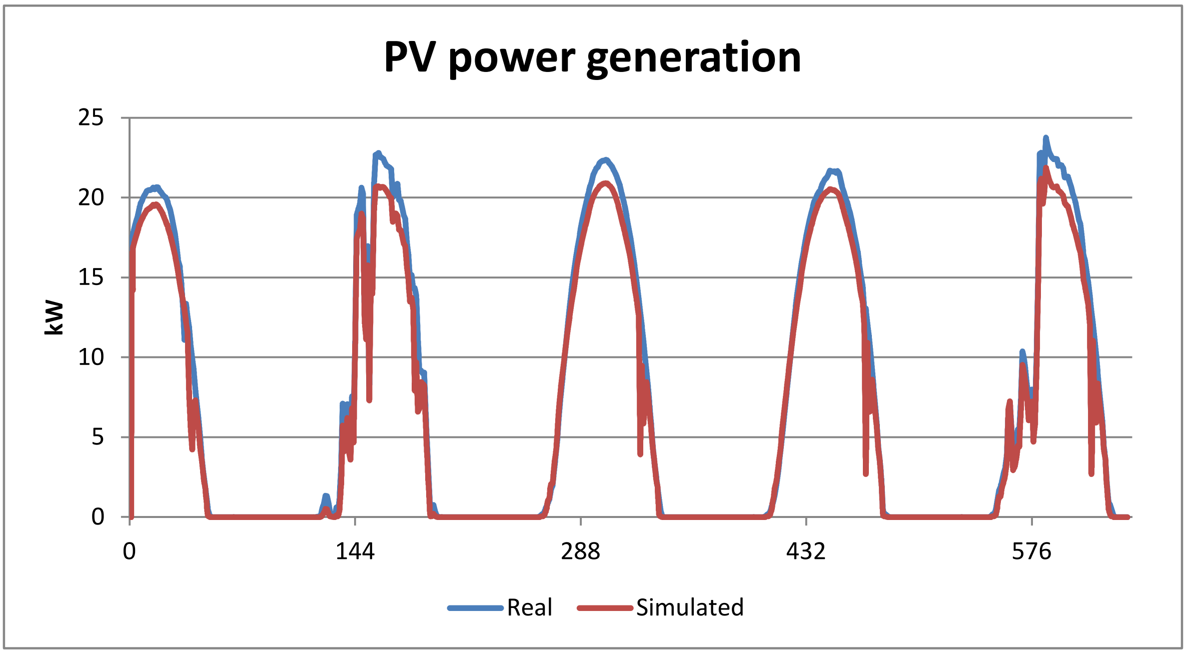

Fig. 4.5. PV system power generation

According to the strategy implemented in the control system, the energy storage is charged and discharged at every moment in order to minimize the energy exchange with the distribution grid. In Fig. 4.6 the power delivered or absorbed by the battery is detailed. It can be noted that the power calculated by the model follows the behaviour of the vanadium redox flow battery in the real system accurately. Of course, some disturbances exist due to different reasons but the general performance of the energy storage is nicely represented in the simulation.

On the right side of the figure, a high power charge is shown. This happens when the system falls below the minimum acceptable SOC, and the control starts charging the battery taking energy from the grid.

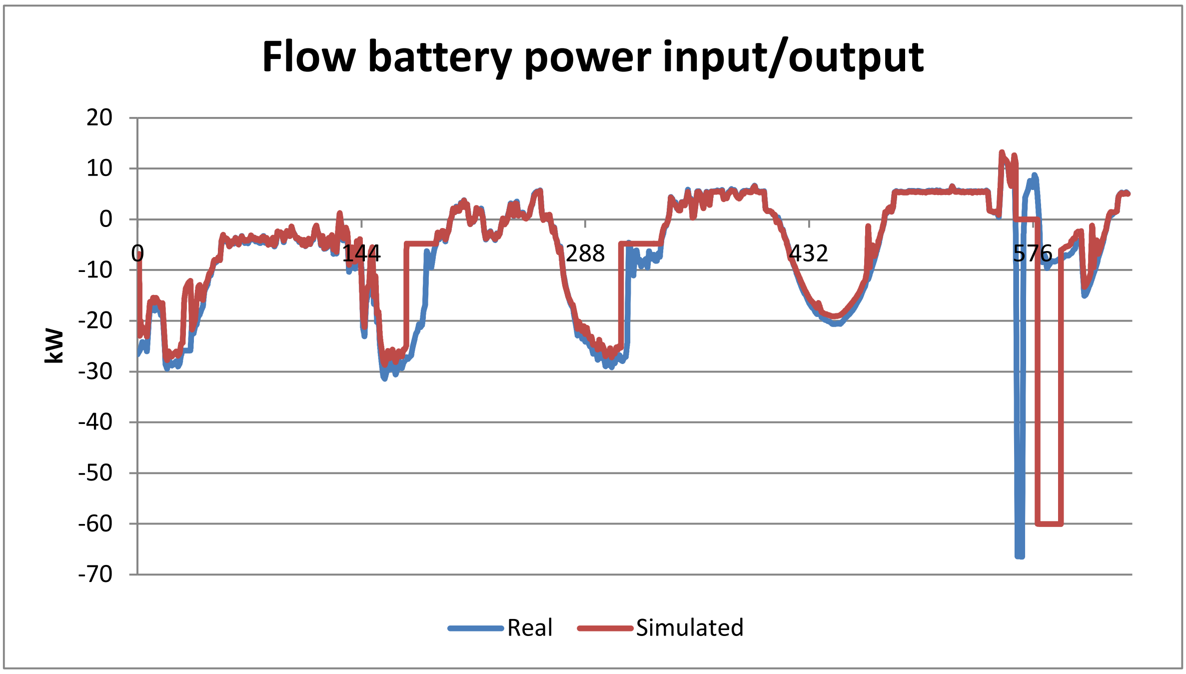

Fig. 4.6. Power input/output of the Vanadium Redox Battery (positive-discharging / negative-charging)

In the same way, in Fig. 4.7 a comparison of the real and simulated SOC is presented. This is one of the key parameters of the model when running for long simulations of several days. It indicates the availability of stored energy which is a key factor regarding strategy, and it can differ importantly from the real situation when accumulating a little error for some days. Moreover, stratification of electrolyte in the tanks can cause a wrong measure of the SOC until it becomes homogeneous. This is not simulated in the model so in the first day (0-144) a strong inconsistence in shown for the SOC data.

Last, the power exchange with the distribution network is shown in Fig. 4.8. As mentioned before, one of the targets of the control strategy is to minimize this power exchange with the grid, avoiding the purchase of electricity if possible. At the same time, storing energy is preferred to selling electricity. Nevertheless, as energy storage is a limited resource, some moments there exist when some electricity has to be taken or delivered to the grid. When a SOC of 100% is reached, energy can no longer be stored and, contrarily, when a SOC of 0% is reached, no more energy can be delivered by the battery. This can be seen in Fig. 4.7 and Fig. 4.8.

Regarding the accuracy of the simulation, in Fig. 4.8 a little mismatch is shown due to the above mentioned simulation error for the SOC. That way, the model reaches 100% SOC slightly before than the real case and the same occurs for 0% SOC.

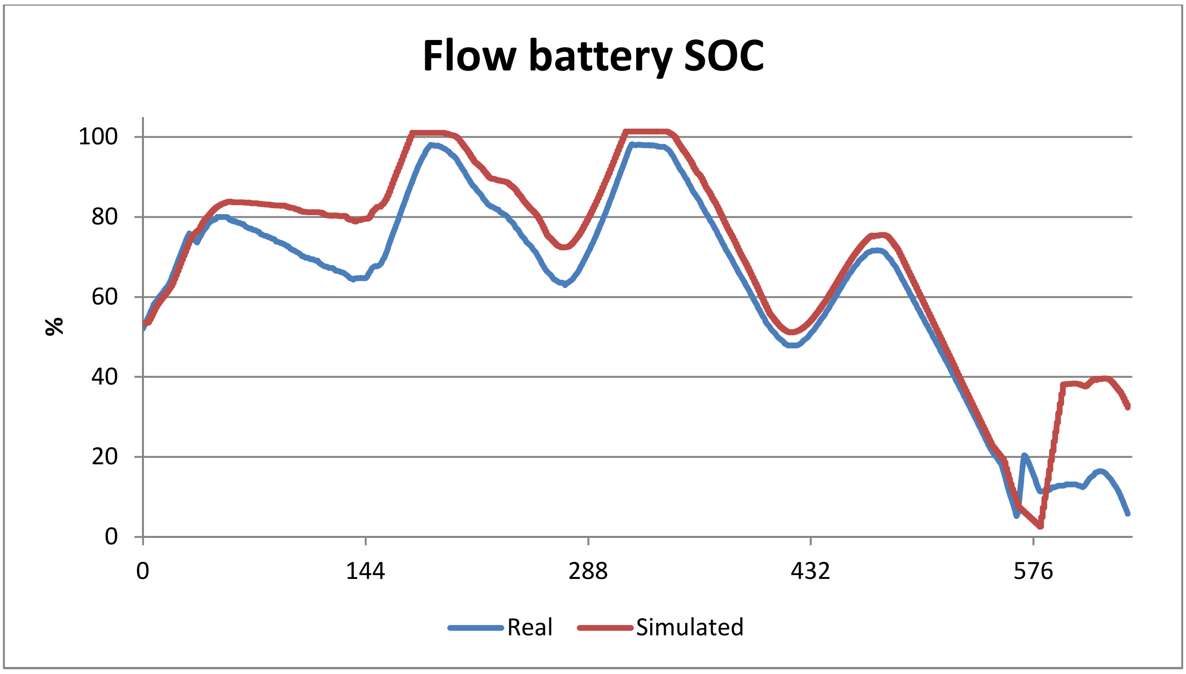

Fig. 4.7. Representation of the SOC of the Vanadium Redox Battery

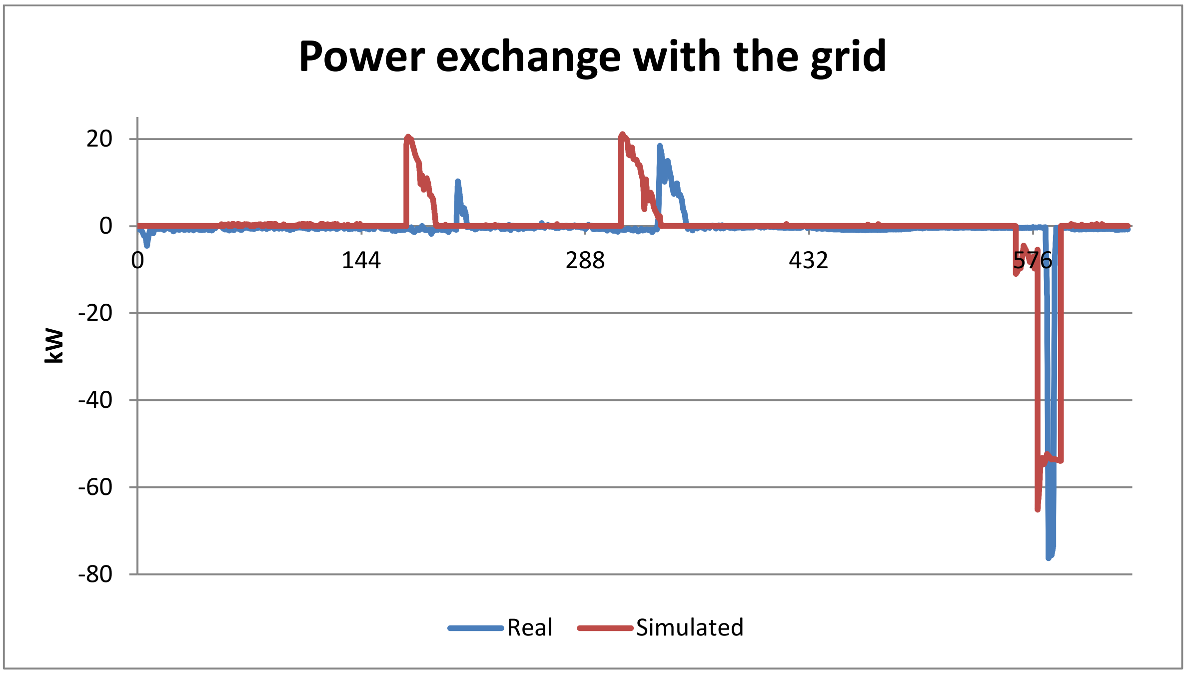

Fig. 4.8. Power exchange with the distribution power grid (positive-export / negative-import)

Finally, the energy balance of the simulation is detailed in Table 4.1. First, we can see that there is no simulated value for *Demand loads* and *Wind generation*, given that these are inputs for the model and no simulation is carried out. For the rest of values, *PV generation*, *Flow battery balance* and *Grid exchange balance*, there is some error that has to be accepted for long duration simulations.

Table 4.1. Energy balance of the simulation

	Real (kWh)	Simulated (kWh)
Demand loads	4,858.1	
Wind generation	4,118.5	
PV generation	7,693.1	6,993.0
Flow Battery balance	-7,353.0	-6,881.0
Grid Exchange balance	-701.5	-627.6

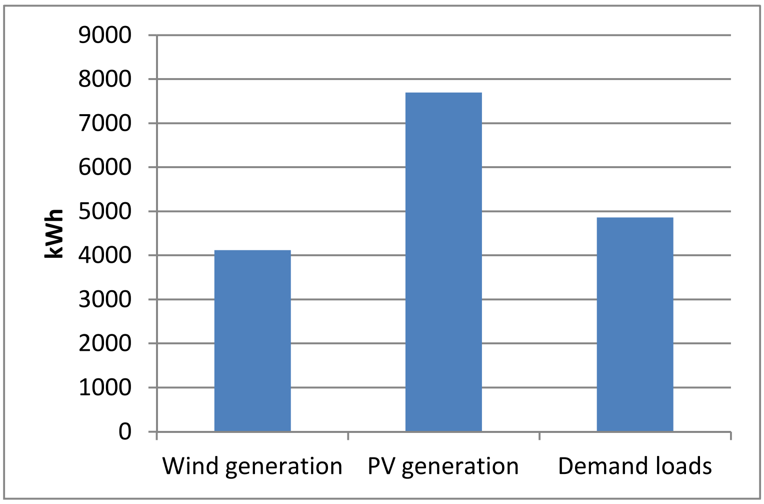

Fig. 4.9. Energy balance of the simulation

4.4 Control strategies

In this section, different possible strategies that can be tried or implemented in the control of the microgrid are presented and discussed.

4.4.1 Protection against power outages

Different strategies exist in order to protect your system against power failures. This event can be solved by energy storage systems or by generation systems. In any case, the response time of each equipment is the key factor for the process of grid isolation when an unexpected failure occurs.

When the generation systems (diesel generator, gas microturbine, etc.) are in charge of maintaining the microgrid in case of an event, the response of the system presents a delay corresponding to the starting time of the generator. This delay of about 30 seconds will occur unless the generator is already running but, of course, generally it is not an acceptable strategy to maintain this equipments running in order to avoid the delay.

Instead, the energy storage systems can take this responsibility when the distribution network presents a failure. In this case, the response can occur immediately if the converter is correctly designed for this purpose, and that way the transition between connected and isolated mode can be done without zero crossing. The energy storage systems contribute to the correct performance of the microgrid either in connected or isolated mode, and consequently all their functionalities remain always available given that the system is always running.

4.4.2 Optimization regarding tariff schedule

A microgrid that never purchases energy from the grid would be ideal, but this is not generally the case. However, if avoiding grid purchases is not possible, at least a strategy can be implemented to lower the cost as much as possible. Thus, the control system can decide to charge the energy storage systems during the night with a lower tariff if an energy deficit is expected for the next day. In the same way, a load can be served directly from the grid without relying on the generation systems or the energy storage existing within the microgrid.

This is the case in ATENEA microgrid, where one of the connected loads is the nocturnal lighting of the industrial area. If the control system decides that there is not enough energy in the storage systems or a low renewable generation is expected for the next day, the lighting load can be directly covered with energy from the grid. That way the existing stored energy can be better used during high tariff periods, avoiding expensive purchases.

4.4.3 Price arbitrage

In some cases, high differences appear in the wholesale market for electricity that can trigger a strategy like this one. It consists on purchasing electricity during low tariff periods for selling it during high tariff periods, which is also known as “buy low, sell high” strategy. Of course, the difference in price has to be enough to compensate grid taxes, amortization of equipment and energy efficiency losses. Today, in SUDOE region the current price levels do not justify the installation of an energy storage system for that purpose. Nevertheless, an existing energy storage system can be eventually be used under this strategy during certain moments.

4.4.4 Reactive compensation

Through the energy storage systems, reactive energy absorbed or delivered to the grid by the loads can be compensated, whenever the existing converters allow it. In some cases, this possibility can avoid the installation of specific infrastructure to compensate this reactive power.

4.4.5 Generation and consumption forecasts or patterns

Usually, the control system of a microgrid makes its decisions based on the data acquired in the present moment. That way, the state of charge of an energy storage system, the power generated by the renewable systems and so on, are the ingredients to make the decision of charging/discharging storage, switching on/off backup power systems, etc. Here, we are introducing a new factor in the strategy by including “future” data.

For instance, if a very sunny and windy day is expected where a generation excess will have to be stored, it is possible to leave space for it avoiding a 100% SOC. Contrarily, if an energy deficit is expected maybe it is a good idea of charging the storage during low tariff periods. In the same way, sometimes there is available data about consumption patterns, with a periodic profile or not, that can also help with decision making.

In our case, we know the schedule of the industrial area lighting during the night so a strategy like this could also be implemented in our control system.

4.5 Conclusions

The validation of CENER's microgrid model has been detailed and discussed. In the future, the general microgrid model will be completed with the models of new equipment being installed in the system.

Some differences exist due to different reasons between the simulation and the real case, but the model has proven to be useful. This model is a strong tool in order to try different microgrid architectures and strategies for any specific microgrid design. Thanks to this model, the real performance of a determined microgrid with a specific generation and energy storage portfolio can be forecasted facilitating the role of decision making regarding architecture. Also, the different strategies mentioned above can prove their usability by means of this model for a specific microgrid design, giving and added value to the future infrastructure.

5 CIRCE – GAMS AND SIMULINK MODEL VALIDATION

5.1 Introduction

In WG3, in deliverables D9/10, CIRCE presented several simulations considering two cases of micro grids:

Micro-grid 1: Rural micro-grid for irrigation pumping

Micro-grid 2: Industrial area with small workshops and industrial stores

The simulations carried out and presented in D9/10 were the following:

- Sizing: Comparison of HOGA and HOMER (Micro-grids 1 and 2)
- Energy balance: Simulink model (Micro-grid 2)
- Planning: GAMS optimization (Micro-grid 2)

In order to validate the models, the models in Simulink and GAMS have been selected, because those are the models which actually contribute to the project with valuable results. Therefore, two different studies have been carried out.

Firstly, in order to validate the planning tool, developed in GAMS, the simplified load flow calculations have been validated with another software called NEPLAN. As the simplified model in GAMS does not include voltages within the microgrid, with NEPLAN, optimization results have been simulated in order to identify possible problems of over and under voltage in the micro-grid under study.

Secondly, the Simulink model has been validated with experimental data. The most contribution of this model is the development of operational strategies, in order to improve load flows in the micro grid with storage capacity available. As it is not possible to operate in a real industrial area, the Simulink model has been validated with a Micro-grid Emulator. This emulator is a kind of “Power Hardware in the Loop” (PHIL), where a hardware component (such as a wind generator) is connected to a simulation software in real-time.

5.2 Description of the validation case

Although this micro-grid has been presented in previous reports of this project, is seems convenient to remind this case again.

The generic case describes typical industrial areas where the activity is dominated by small workshops, small factories and industrial stores. This type of industrial areas is very common in the entire zone of SUDOE (Portugal, Spain and south-west France).

5.2.1 Optimization model

In this case, no renewable energy generation is present and the aim of the model is twofold. First, a possible development of distributed generation is simulated as an optimised planning problem with a planning horizon of 20 years. In a second step, the operation of a developed micro-grid after 20 years is simulated. It is assumed that solar pv and wind power resources are available. The topology of such a micro-grid is basically linear, as these industrial areas are distributed along a road. In Fig. 5.1, the assumed grid structure is depicted. In this example, the wind generator is connected to node 3 while solar pv is assumed to be possible at all nodes with consumption (2, 3, 4 and 5).

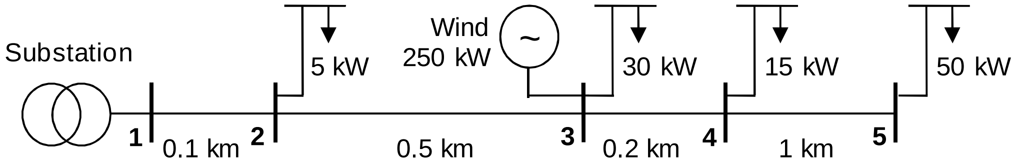

Fig. 5.1 Microgrid structure of assumed industrial area of 100 kW total mean power.

In the planning tool, several scenarios where considered:

- Case A: energy export at 0.05 €/kWh is possible
- Case B: no energy export (selling price set at 0 €/kWh)

In both cases, two sub-scenarios are considered: including or not storage facilities.

For the validation, only one scenario has been selected, which is Case A, with storage. This case has been selected for validation, as it represents the case where the planned installed power of distributed generation is highest. Thus, problems of over-voltages are expected to be most severe. The model parameters, obtained at the end of the planning horizon (after 20 years) are the following:

- **Wind power**: P_{wind} = 372 kW
- **PV power**: P_{PV} = 697 kW
- **Storage**: P_{SS} = 187 kW, E_{SS} = 4954 kWh

5.2.2 Operational model

In a second step, the simulated operation of a developed micro-grid is validated with the emulator tool. In order to facilitate the comparison of results, the same parameters are used as for the simulation in Simulink:

- **Wind power**: P_{wind} = 250 kW
- **PV power**: P_{PV} = 250 kW
- **Storage**: P_{SS} = 200 kW, E_{SS} = 1000 kWh

As the emulator has limited power (2.5 kW wind generator), the input from the wind generator is scaled by a factor 100, before it is incorporated in the network model.

As shown in Fig. 5.1, there is only one wind generator installed (i.e. one injection node). On the other side, solar PV and storage is assumed to be installed at all 4 consumption nodes. Thus, the installed PV power is distributed in the micro-grid according to the consumption levels. The same way, storage is also distributed.

5.3 Validation of micro-grid planning tool with NEPLAN

5.3.1 Description of the model to be validated

The first validation has been carried out for the planning tool, developed using GAMS as software platform. In this model, a timeline of 20 years is assessed. Results show that in a beginning, no energy storage is installed, because it is still very costly, but at a certain moment in the future, it will become interesting to install such systems, because they make excess energy generation useful and thus directly lower the overall cost of energy. Detailed results have been presented in deliverables D9/10 (WP3) of this project.

The optimization algorithm is applied to Micro-grid 2 (Industrial area with small workshops and industrial stores), as mentioned before. The micro-grid in Fig. 5.1 is implemented in detail, in order to consider losses in distribution lines and thermal limits of the existing installation. It is assumed that any installation of renewable energy is limited to the energy evacuation capacity of the existing distribution lines.

The optimization model has one important limitation, because node voltages are not included. As a results, possible under- or over-voltages, caused by high demand or high distributed generation are not detected. Another limitation is that only active power flows are considered. Therefore, in order to study the implications of these limitations, load flows of the distribution grid under study are calculated with commercial network analysis software (NEPLAN). The model setup is described in the next section.

5.3.2 Description of the validation model

In the optimisation model actually 840 different load flows were preformed, in order to capture all possible combinations of consumption, generation and energy prices. For validation, only a few load flows are calculated in order to demonstrate the tendencies of voltage levels and line losses as a function of installed distributed generation and storage capacity.

The following scenarios were analysed:

1. Basic: Passive network (only loads, no DG, no storage)
2. DG: Loads and distributed generation (no storage)
3. DG+SS: Loads, DG and storage

5.3.2.1 Model parameters

Loads

Loads are modelled with their mean apparent power (active and reactive), which sums up to 100 kVA in the entire micro-grid.

5.3.3 Validation results

5.3.3.1 Validation of distribution line losses

In order to obtain a critical evaluation of the results of the simplified optimization model regarding line losses, all combinations of solar PV and wind generation have been tested with and without storage. As with NEPLAN power flows are performed without any reference of time, no direct comparison is possible with the results from the optimization tool which gives the result for annual energy balances. Nevertheless, tendencies can be outlined and possible sources of error may be identified.

In the figure below, results of NEPLAN simulations are shown for the study cases of no storage (above) and available storage power of 187 kW.

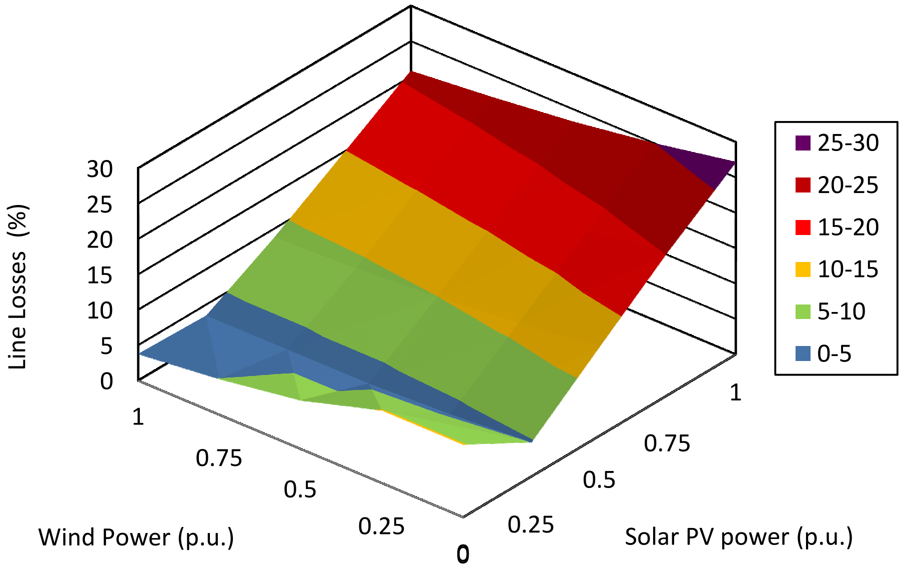

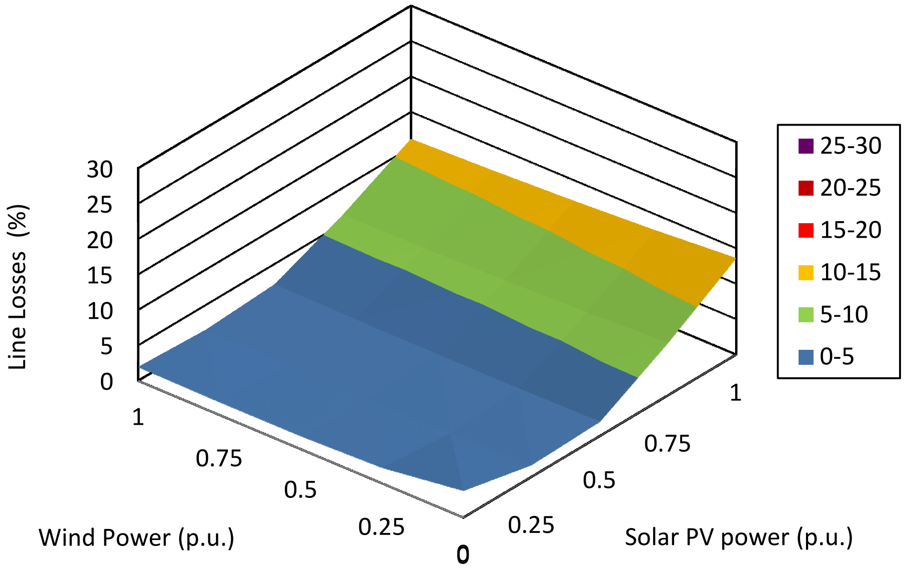

Fig. 5.2 Line losses for all combinations of solar PV and wind generation, without storage (above) and with up to 187 kW of storage power (below).

In the following tables, results are represented again. Notice, that for the no-storage scenario, the optimization model proposes the installation of 15% less solar PV power, while wind power is almost the same. This is a sign that the optimization reduces PV power also due to excessive line losses.

Table 5.1 Line losses for any combination of solar PV and wind generation, without storage.

Wind PV	**0.00**	**0.25**	**0.50**	**0.75**	**1.00**
0.00	**10.3**	10.3	6.8	5.0	3.7
0.25	4.8	3.9	3.5	3.4	3.4
0.50	12.6	11.1	10.0	9.2	8.7
0.75	20.2	18.2	16.8	15.6	14.7
1.00	27.2	25.0	23.2	21.9	20.8

Table 5.2 Line losses for any combination of solar PV and wind generation, with storage.

Wind PV	**0.00**	**0.25**	**0.50**	**0.75**	**1.00**
0.00	3.8	2.2	1.8	1.8	3.8
0.25	1.7	1.3	1.2	1.3	1.7
0.50	2.0	1.9	1.9	2.0	2.0
0.75	7.4	6.9	6.5	6.3	7.4
1.00	13.6	12.7	12.1	11.6	13.6

Anyway, the drastic reduction of line losses due to storage is confirmed with the NEPLAN model. Notice that the NEPLAN model includes losses due to reactive power flows, which are neglected in the simplified optimization model.

Comparison with GAMS

In order to compare the results, the reference case (no DG, no storage) is a good indicator. While in the simplified optimization model line losses of 5.7% were calculated (see Fig. 5.3), with the more realistic model of NEPLAN, over 10% are obtained (see Table 5.1).

Fig. 5.3 shows line losses of the modelled distribution network as a percentage of total demand plus energy export for the three scenarios. In the first scenario (Conventional), losses are constant in p.u. throughout the planning period, which is due to the linearization of the losses, assumed in the model. In case A (export is possible) in the two scenarios (DG and DG+ESS), line losses fall after a slight increase in the first years. The initial increase is due to the installation of 400 kW of wind power, which often exceeds demand and needs to be evacuated to the main grid. The subsequent reduction in line losses is due to the increasing installation of solar power, which is better synchronized with demand and helps reducing flows within the distribution network. This effect in further reinforced, when storage starts to be implemented after 15 years. In case B (without export), line losses are reduced dramatically. As no energy can be exported, less renewable power is installed and no additional (inverted) power flows are generated.

Storage helps matching distributed renewable generation and demand and thus reduces power flows. The reduced loss contributes also to the decrease of the cost of energy, although the reduction of imported energy is more important.

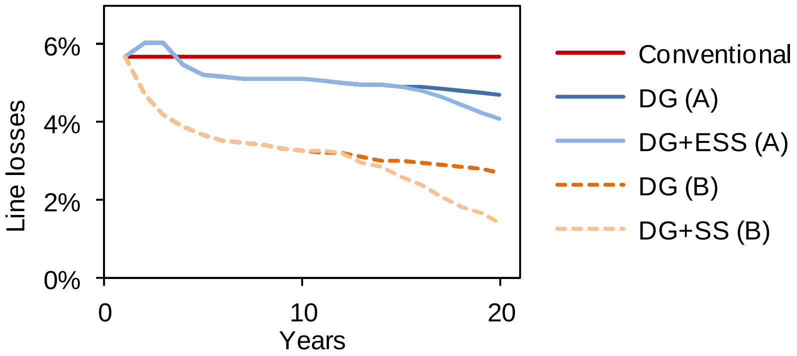

Fig. 5.3 Line losses as a percentage of total demand plus exported energy.

It is difficult to compare the results presented in Fig. 5.2 and Fig. 5.3. There even seems to be a contradiction, as losses are reduced with PV power in the optimization model, while in NEPLAN, losses increase with increased PV power. Here the difference of load flow analysis (instantaneous evaluation) and energy balance for planning becomes visible. In NEPLAN, results would suggest that a large amount of installed PV power would increase overall line losses. But if an energy balance over the whole year is performed, the opposite conclusion can be drawn. The reason for this difference is that solar PV power seldom actually generated 100% of nominal power. Thus, there is a high frequency of lower power levels, which match very well with consumption and thus, reduce line losses.

On the other hand, the large potential of loss reduction due to energy storage could be confirmed very well with NEPLAN.

It may be noticed, that reactive power compensation was not included in the NEPLAN model. This means that further loss reduction can be obtained if the capability of DG to perform reactive power compensation is included.

5.3.3.2 Evaluation of node voltages in the low voltage grid

The second objective of this validation procedure was to evaluate the importance of voltage levels in the simulation model. In the simplified optimization model, node voltages were not calculated.

Therefore, again different combinations of solar PV and wind generation are considered with and without storage. In Fig. 5.4, results are presented for some selected cases, assuming always that the wind generator is running at nominal power. In the upper graph, the situation without storage is shown. In the case that there is no solar PV power available, it can be observed that at node N5 a severe under-voltage is present. The reason is the large demand at that point which is situated just at the end of the distribution line. On the other hand, with increasing PV power, over-voltages start to be a problem. In any case, node N5 is the most problematic point in that grid, presenting the largest deviations from nominal voltage.

In the lower graph of Fig. 5.4, the impact of storage is shown. It can be observed, that under-voltages can be mitigated completely. This is due to the fact that the storage system can cover the load, being sized at 187 kW, while mean demand only reaches 87 kW of active power. In this example, only 42% of storage power is needed in order to maintain nominal node voltage. This way, storage is able to maintain node voltages in a corridor of ±5% of nominal voltage, if solar PV generation does not surpass 50% of its nominal power. Keep in mind that for demand, average power has been assumed for the load flow, while at noon, when solar power is highest, also demand may be up to 170% of its average value (see Fig. 5.5). Nevertheless, an important result of this study is that over-voltages may occur during peak generation periods which cannot be compensated by the storage system.

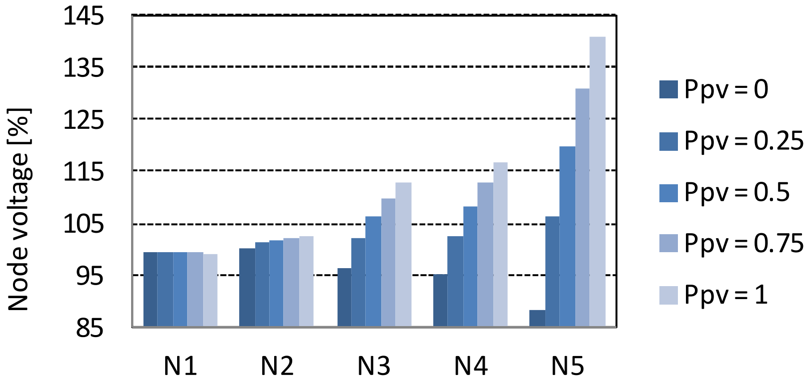

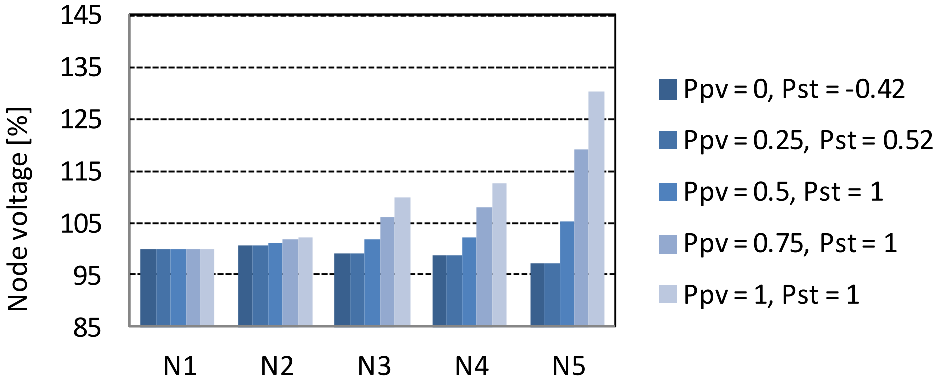

Fig. 5.4 Node voltages for different levels of solar PV generation assuming nominal wind power, without storage (above) and with up to 187 kW of storage power (below).

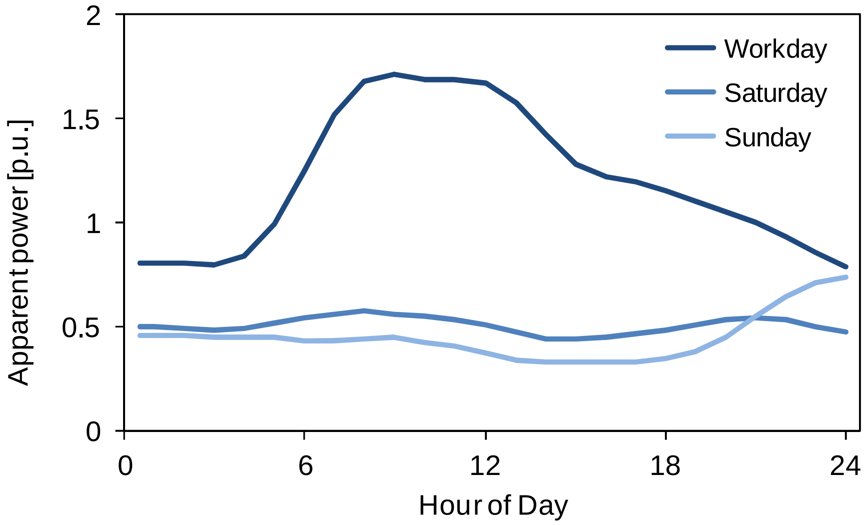

Fig. 5.5 Typical load profile (annual average) of the industrial area under study.

As especially node N5 suffers severe over- and under voltage, another representation of this situation has been chosen in Fig. 5.6, in order to represent all combinations of wind and solar PV power. It can be observed, that there is almost no visible impact of the wind generator on the voltage at node N5. This can be explained by the topology of the radial distribution grid. Wind power is evacuated without any problems from node N3 towards the transformer station. To achieve that, voltage at node N3 is only elevated very slightly from 95% to 96.6% of nominal (in the case of zero solar PV power). On the other hand, over-voltages due to large solar PV power injection elevated voltage at N3 from 95% up to 112%.

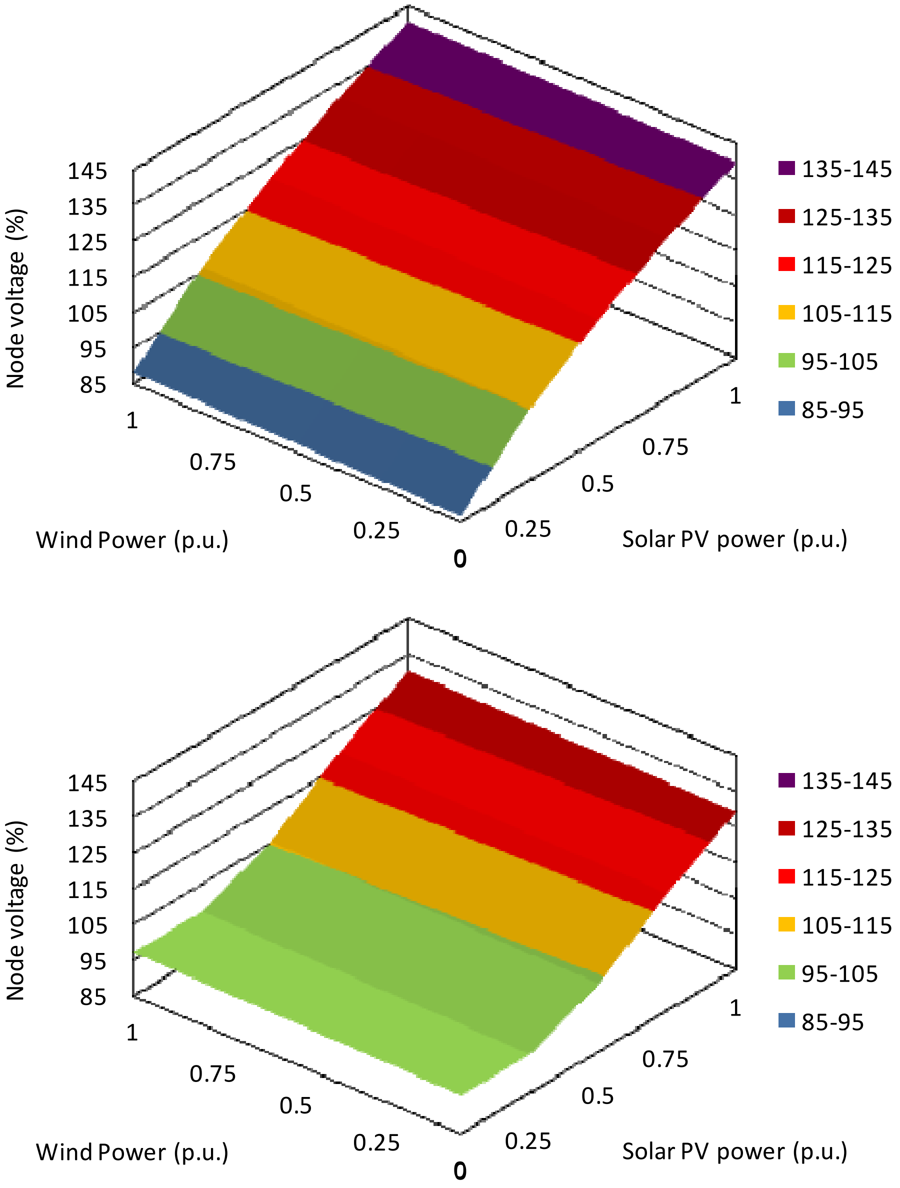

Fig. 5.6 Voltage at node N5 for all combinations of solar PV and wind generation, without storage (above) and with up to 187 kW of storage power (below).

5.3.4 Conclusions

Results of a planning tool with a simplified model of the electrical network have been evaluated with power flow analysis software (NEPLAN). In a first step, network losses have been studied. It has been shown that with power factors of 0.8 and lower, losses due to reactive power flows need to be included in the planning tool, as line losses are underestimated in a large extent. While only 5% of losses were calculated in the planning tool, with NEPLAN 10% are obtained. As a result, the large potential of cost reductions due to reactive power compensation was not taken into account in the optimization process. The capability of storage to reduce line losses has been confirmed with the NEPLAN model, as only active power flows are influenced here, which were modelled correctly in the planning model.

A second issue to be evaluated in this validation was the node voltage which was not considered in the planning tool. Results from NEPLAN show that in this example, the farthest node presents sever problems of under-voltage when no DG is present. On the other hand, it is the most vulnerable point for over-voltage, due to excessive injection of renewable power. Storage can mitigate this problem only in part, as installed solar PV power is much larger than storage power. But the problem of over-voltage is less severe as it seems, as solar generation is very well synchronised with the typical load curves.

Line losses:

- Reactive power flows cause large losses
    - Must be included in the optimization model
    - Opportunities of loss reductions with Q compensation are important
- Properly sized storage can reduce line losses dramatically
    - DC model is adequate here, as mainly active power flows are affected

Node voltages:

- Voltage levels are an important issue and need to be included in a planning tool
- Without DG: under-voltage at farthest nodes
- With DG: over voltage at maximal generation of solar PV
- Good synchronisation of demand and solar resource reduces the problem
- Storage can mitigate under-voltages completely and over-voltages only in part

Conclusions for planning tool (GAMS model):

- Possible DG to be installed in the grid may have been over-estimated
- Additional constraints due to voltage limits reduce amount of renewable energy which may be absorbed by the system
- Profitability of storage systems may be under-estimated as voltage control can be an additional service
- Reactive power compensation may reduce line losses by 50%, which is an additional benefit from DG
- Load flow tools such as NEPLAN cannot give estimates on annual energy balances and cannot be used for planning

5.4 Validation of energy balance model with Micro-grid Emulator

5.4.1 Description of the model to be validated

The model to be validated in this case was implemented with Matlab/Simulink®. The objective here was to show the usefulness of different control strategies, using an approach of energy balances. The model contained the following features:

- Renewable generation (wind, solar pv), 1 year, 30 min timestep
- Demand (P,Q), 1 year, 30 min timestep
- Converter model with Q (reactive) control
- Battery model with P (active power) control, three strategies:
    - Peak shaving
    - Hourly program (schedule)
    - Demand curve smoothing (with moving average)
- P/Q at PCC (at connection to main grid)

The simulation includes control of active and reactive power using converters and a battery storage system (BSS). As input, several time series are possible. In the first place, the demand with active and reactive power (P_{load} and Q_{load}) with a time step of 30 min. In addition, time series of renewable sources such as wind (P_{genw}) and solar pv (P_{genpv}) are considered. In this case, time series are adopted from HOMER simulations (but with 30-min time step).

The output of the model is the power flow at the point of common coupling (PCC), which are active and reactive power P_{red} and Q_{red}. Secondary results are the state of charge of the battery (SOC) and the power factor (PF) of the mini-grid.

5.4.2 Description of the validation model

As no renewable energy and battery systems, installed in a real-world environment were available, the validation has been carried out with a micro-grid emulator. A schema of the emulator is shown in Fig. 5.7.

This emulator consists of two parts: 1) power electronics and 2) micro-grid simulator. Therefore, is can be said that this is an example of Power Hardware in the Loop (PHIL). The power electronics permits the emulation of any generator or load, but also the connection of a real power element such as a wind generator or a battery for example. The micro-grid simulator is a cluster of computers which performs a distributed power flow calculus, simulating the distribution grid. Thus, the distributed character of the generators and loads in the micro-grid can be reproduced in the simulator. At the same time, also a distributed control paradigm based on a multi agent system is implemented.

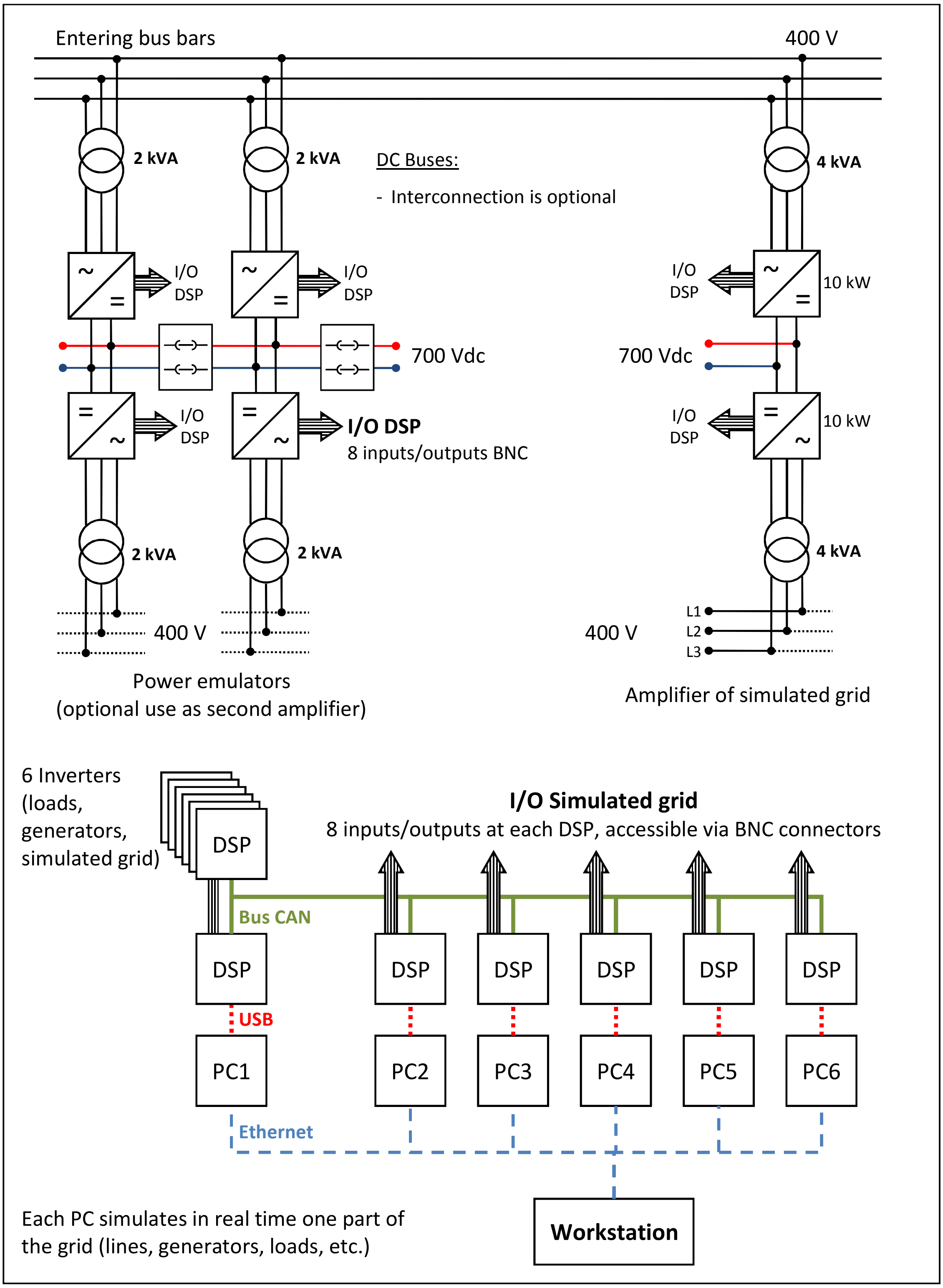

Fig. 5.7 Schema of the Micro-grid Emulator.

5.4.2.1 PHIL: Power Hardware

In the presented case, the real experimental data for validation is obtained from a 2-kW vertical axis mini wind turbine from Kliux energies (see Fig. 5.8). All remaining parts of the micro-grid are modeled within the agent-based micro-grid simulator.

Fig. 5.8 Vertical axis wind turbine from Kliux energies (http://www.kliux.com), at CIRCE.

Some technical data of the wind turbine are summarized in the following table.

Table 5.3 Properties of Kliux wind turbine.

Wind turbine components	Vertical axis rotor (Kliux Geo1800) Gear box Permanent magnet generator Converter: Etesian Mini 2600, 2 kW, 230 Vac, 50 Hz (Santerno) Steel tower GSM Communication module (optional) Meteorological station (optional)
Dimensions and weights	Rotor + Generator + Gearbox: 117 kg + 120 kg = 237 kg Tower: minimum 233 kg Rotor diameter: 2.36 m Rotor height: 3m Gearbox height: 0.83 m Tower height: min. 6 m
Performance	Nominal power: 1800 W Cut-in wind speed: 3.5 m/s Cut-out wind speed: not necessary due to areodynamic breaking Max. Rotor speed: 106 rpm. Noise at 10m distance: 32.6 dBA Durability: 25 years
Other	Blade material: Expanded polyurethane Nominal output voltage: 230Vac Certificates: ISO: 9001, 14001 y CE Certificates in progress: IEC 61400 -2/ -11/ -12, AWEA 9.1, BWEA 2009 Standard

5.4.2.2 PHIL: Micro-Grid simulator

Apart from the power hardware, the mirco-grid simulator is a very important component of the emulator, as it enables the evaluation of the interaction of the power elements with any desired grid configuration.

The simulation of the micro-grid is implemented with a multi-agent system, based on JADE (Java Agent DEvelopment Framework, http://jade.tilab.com/). This approach has been chosen due to its simplicity and clarity. The distributed modelling approach permits the construction of a complex system based on simple elements which communicate with each other, following the rules established in the multi agent system.

In the following paragraphs, the architecture of the multi-agent system is described.

It is possible to implement the Simulink model in a fairly straight forward manner. The java classes written for this specific case are following the structure shown below:

Table 5.4 Structure of Java classes of the multi-agent model.

Element Category	Superclass	Class
Agents	DG (Distributed Generation)	Wind
		Solar PV
		Storage
	Consumption	Load Agents
		Main Grid
	Control	RealPowerManager
		ReactivePowerManager
		Node
Physical Elements		Battery
		Converter
		Lines
Auxiliary classes		Constants
		ReadExcel
		SerialPort

Agents

In a multi-agent system (MAS), all information is exchanged via asynchronous messages. Therefore, any element in the micro-grid is able to receive input data, process it and send results as output to other agents.

The MAS has two operating modes: *simulation* and *monitoring*. In simulation mode, generation and demand data are read periodically from input files (such as Excel for example). In monitoring mode, a power flow is performed, reading data measurements from physical elements (such as a wind turbine) in real-time.

The “agent” classes are classified according to their function: generation, consumption and control. Any agent is programmed as an extension of the *Agent* class in the JADE library. There is no limit in Java, how many times the *Agent* class can be extended.

DG:

As a consequence, the classes *Wind*, *PV* and *Storage* (or any other type of distributed generation) are derived from the superclass *DG*, which in turn is an extension of *Agent*.

Consumption:

The consumption agents are managing the demand in the grid. *LoadAgent* is in charge of al consumption elements (with the option of disconnecting not priority loads in case of an emergency). The agent *Grid* is dedicated to the interconnection (PCC) of the micro-grid with the main grid.

Control:

The control section contains the “brain” of the micro-grid, where the power flows are managed. In this superclass are located the agents *RealPowerManager* and *ReactivePowerManager*. Both agents receive information via messages in ACL (Agent Communication Language) format. Inputs are processed following the established control strategies and setpoints are generated for other agents.

The *Node* agent is not implemented yet, but its function will be to change the configuration (physical topography) of the micro-grid, without the need of any change in the coding. This agent will read power flow data from a node and send them to the control agents.

All agents are able to take actions, according to their properties defined in their “behaviour”, which is an extension of superclass *Behaviour*. In order to maintain clarity in the code, the behaviour has been embedded in each agent class file. All agents have at least the behaviour “MailBox”, which is responsible for reception, processing and sending of ACL messages.

The JADE framework adopts the communication conventions, established by FIPA (Foundation for Intelligent Physical Agents). FIPA has established several well defined communication protocols. After a bibliographical review, the protocol “FIPA-ContractNet” has been chosen for this application. As a result, the control agent plays the role of an *initiator* and all other agents are *participants*. The communication process, which is very similar to an auction, is illustrated in Fig. 5.9.

Physical elements

In this category, the physical generation elements and lines are modelled.

Converter:

The *Converter* agent models a voltage source converter (VSC), which is able to control active (P) and reactive (Q) power output, modifying phase angle and amplitude of its output voltage.

Modelling parameters: efficiency, apparent power and current limits.

Storage:

The agent of type *Storage* establishes an instance of the class *Battery* which models the behaviour of the battery storage.

Modelling parameters: efficiency, nominal power, storage capacity, nominal voltage

Other elements such as lines, breakers, etc. are still under development.

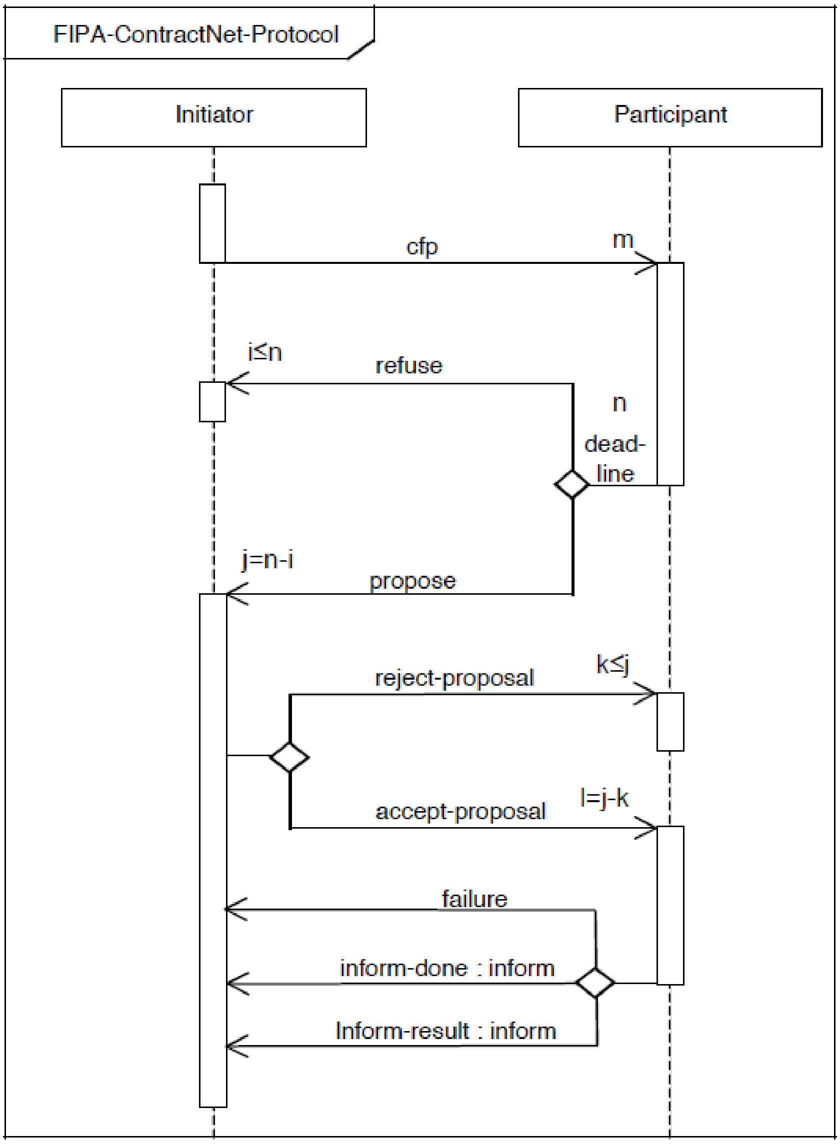

Fig. 5.9 FIPA ContractNet interaction protocol.

Auxiliary classes

This third category contains all classes which do not fit in the others. At this stage of development, only two classes are present here: *Constants* and *ReadExcel*.

Constants:

The first one, called *Constants*, is not exactly a class, but rather an interface which collects all constants which are common to the micro-grid and subject to be used by the other classes. In order to have access to these constants, any class can simply implement *Constants*.

ReadExcel:

This class only works in simulation mode and reads generation and consumption data from an Excel file when it is required by an agent.

SerialPort:

This class is the pendent to *ReadExcel*, but in monitoring mode. It is dedicated to manage the communication in real-time with physical (power) elements, such as a wind generator or a battery, which may be connected to the emulator.

5.4.3 Validation Results

5.4.3.1 Parameters of the validation model

The validation of the Simulink model is carried out in two steps:

- Emulation with input variables from Simulink model
- Emulation with real data from Kliux wind turbine

Strategy 1: Peak shaving

In this control scenario, the following demand limits are established for discharge and recharge of the battery system.

Table 5.5 Control parameters for strategy 1 (peak shaving).

Parameter	No DG	250kW wind	250kW wind+pv
P_{max} [kW]	100	100	100
P_{min} [kW]	50	-100	-100

Strategies 2 and 3 (hourly program and smoothing) are not implemented at the moment, but will be available until the end of the project.

Converter Model

In the emulator, a more realistic converter model has been implemented. Instead of assuming only one converter, distributed converters are considered. Thus, every generator (solar PV, wind) is associated to a converter with its nominal power. In addition, every storage unit has its converter. As a result, much more converter power is available for reactive power compensation.

In the Simulink model with DG, the combined renewable power was limited to 250 kVA plus an additional margin of 50 kVA was considered. In the multi-agent model of the emulator, converter power of DG is limited to 200 kVA individually for solar PV and wind, and in addition, battery power of 200 kVA is available. As a result, the installed converter power in the emulator model is with 600 kVA two time the power considered in the Simulink model. In Table 5.6 the two cases are compared.

Table 5.6 Converter Model parameters for the case of 250kW wind+pv.

Parameter	Simulink	Multi-agent Emulator
$S_{ren,max}$ [kVA]	250	400
$S_{c,margin}$ [kVA]	50	0
$S_{c,battery}$ [kVA]	0	200
η_{conv} [%]	95	95
S_{cmax} [kVA]	300	600

5.4.3.2 Results of the validation model

First validation: Emulator with data from Simulink model

In Fig. 5.10, probability distributions are shown, in order to compare the time series from the Simulink model and the Multi-Agent model of the micro-grid emulator. In the upper plot, probability density is shown and in the lower cumulative probability. Resulting active power demand (Pload1 for Simulink and Pload2 for emulator), shows some differences on the left-hand side. The difference consists in the fact that distributed generation is limited in a different way in the multi-agent model. As a result, total DG can reach up to 400 kW, while in the Simulink model the combined power was limited to 250 kW.

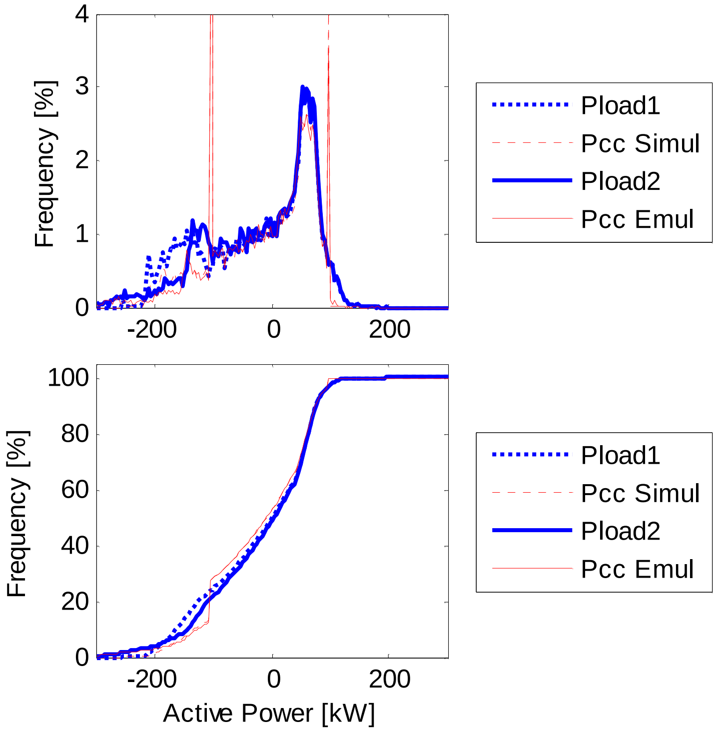

Fig. 5.10 Comparison of distribution density (above) and cumulative (below) of active power at PCC for Peak Shaving control strategy, for Simulink and Multi-Agent model.

In Fig. 5.11 time series from the Simulink model and the multi-agent model are compared. In the left plot (typical activity), no significant differences can be observed, while in the right plot (high activity), some clear differences can be seen. Again, this is due to the differences in the limitation of distributed generation.

Therefore, in the right plot of Fig. 5.11 Pload2 (from multi-agent model), shows some larger generation peaks (negative values).

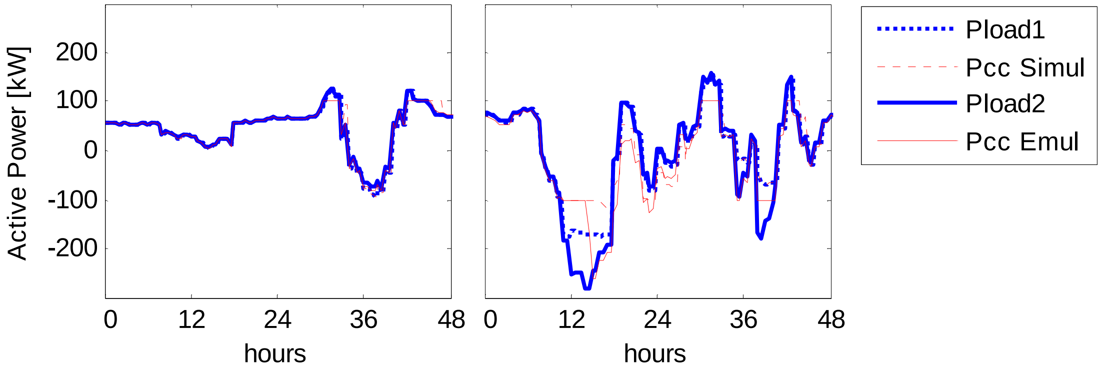

Fig. 5.11 Two typical sequences (48h each) of active power demand with control scenario Peak Shaving from Emulator (Pcc Emul) and Simulink model (Pcc Simul) compared to Pload, left: typical activity, right: high activity.

Second validation: Emulator with real measured data

In this second validation phase, the peak shaving control strategy is applied to real measured data with a time step of one second. This is at the same time the demonstration of the capability of the emulator to operate in real-time conditions.

Similar to the first validation step, in Fig. 5.12 probability distributions are shown, in order to illustrate the effect of the control strategy. In the upper plot, probability density is shown and in the lower cumulative probability. It can be observed, that the power limits of ±30 kW are perfectly maintained.

In Fig. 5.13, the entire time series is shown. The time period are almost 77 minutes, with a sampling rate of one second. While wind generation comes from the Kluix turbine, all other parameters are simulated within the multi-agent simulation system. Four different demand levels have been simulated and solar PV power is assumed to be constant over the whole time interval.

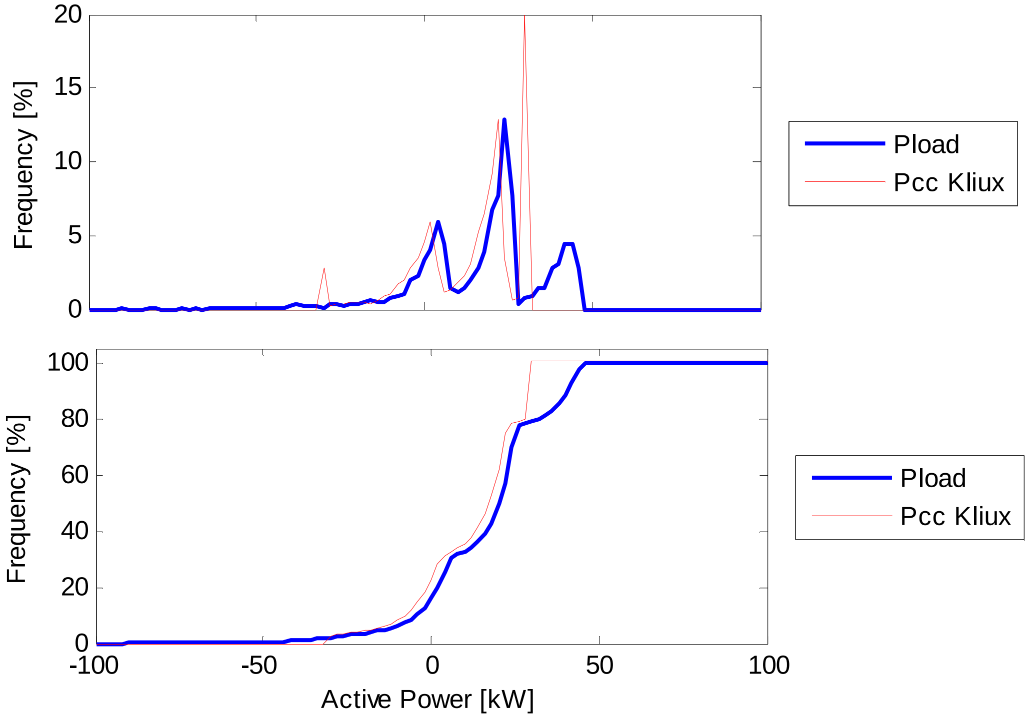

Fig. 5.12 Distribution density (above) and cumulative (below) of active power at PCC for Peak Shaving control strategy, Multi-Agent model with real wind generation data.

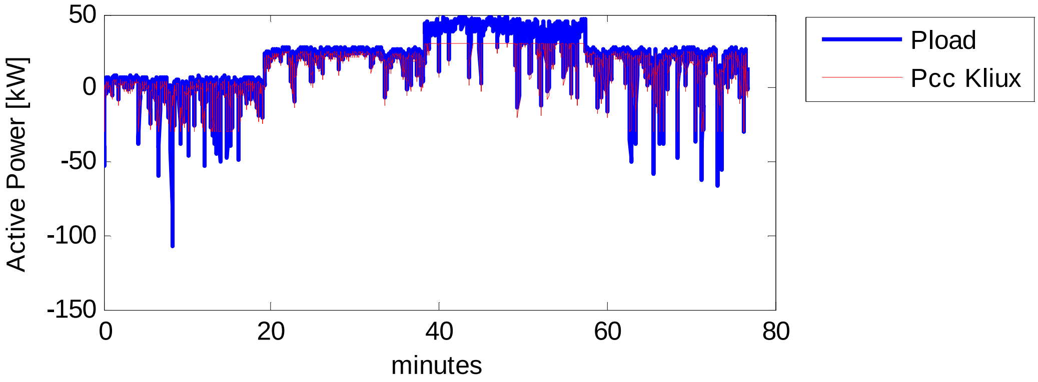

Fig. 5.13 Sequence of 77 minutes of active power demand control (Peak Shaving) with real wind generation data.

5.4.4 Conclusions

In this section, a Simulink model of an industrial area has been validated with a micro-grid emulator, based on power hardware in the loop (PHILP) system. The emulator consists of one part with power electronics and a second part with a cluster of desktop computers, where the micro-grid is simulated with an asynchronous distributed computation model, based on multi-agents.

In a first step, the Simulink model is reproduced with the emulator. Very similar results are obtained, but some shortcomings of the Simulink model are shown. The most important difference is that the emulator represents better the distributed nature of the micro-grid. The peak shaving control strategy is implemented in the emulator and its viability is validated.

In a second step, simulated wind power data is replaced by real-time data from a wind turbine. The same peak shaving strategy is applied without any problems, although the time step in this case is only one second. Thus, the capability of real-time operation of the emulator has been demonstrated successfully.

The following general conclusions can be drawn from the simulations:

- The Simulink model could be implemented in the more realistic environment of a multi-agent platform (JADE)
- With distributed converters, a large unused capacity (mainly from solar PCV) facilitates reactive power control and oversizing seems to be unnecessary.
- Control strategy “peak shaving” is working properly for 30-min time steps as well as 1-s time steps
- The communication system of the JADE platform proves to be suitable for micro-grid applications in real-time (sample times of one second or less)
- The micro-grid emulator is a valuable tool in order to test distributed control strategies with direct application in real world conditions

6 CONCLUSION

Five validations have been presented and discussed in this report. Each model focuses the simulation on different issues of the system, and each of them is designed for a different objective.

The model presented by FHa for the Walqa Technological Park enables an overall look of the installed microgrid. Thus, it is possible to estimate the required sizing of the equipments for the implementation of a specific control strategy. Moreover, this model is capable of performing long term simulations of several months for the infrastructure located at the technological park.

In relation with AICIA Laboratory, a practical and accurate dynamic model of the complete domestic microgrid is developed and presented. Avoiding modelling ancillary devices the proposed interconnected model comprises generation, load and storage components. The comparison exhibits a good fitting between experimental and simulated data.

Regarding the validation from ESTIA, a novel power conversion topology to control and interface the selected hybrid storage system with the rest of the microgrid has been used. The operation of the selected topology has been validated in different case studies (grid connected and isolated) both in simulations and in the experimental platform. The proposed system could work connected to a wind turbine smoothing the power generated and reducing the negative impact of the operation on the grid.

The tool described in the report from CENER comprises a combination of mathematical and electrical models simulating the behaviour of each of the components installed in ATENEA microgrid. This model is a strong tool in order to try different microgrid architectures and strategies for any specific microgrid design. Thanks to this model, the real performance of a determined microgrid with a specific generation and energy storage portfolio can be forecasted facilitating the role of decision making regarding architecture.

Within the part from CIRCE, two different studies have been carried out. Firstly, in order to validate the planning tool developed in GAMS, a timeline of 20 years is assessed. This model studies the suitability of storage in a specific microgrid from the cost-effectiveness point of view. Secondly, the Simulink model has been validated. The contribution of this model is the development of operational strategies, in order to improve load flows in the micro grid with storage capacity available.